THERMODYNAMICS-BASED OPTIMIZATION AND CONTROL OF INTEGRATED ENERGY SYSTEMS

BY

NEERA JAIN

DISSERTATION

Submitted in partial fulfillment of the requirements
for the degree of Doctor of Philosophy in Mechanical Engineering
in the Graduate College of the
University of Illinois at Urbana-Champaign, 2013

Urbana, Illinois

Doctoral Committee:

Professor Andrew Alleyne, Chair
Assistant Professor Alejandro Domínguez-García
Associate Professor Dimitrios Kyritsis
Associate Professor Srinivasa Salapaka
Professor Jakob Stoustrup, Aalborg University

Abstract

With increasing worldwide demand for energy comes the need to both generate and consume energy more efficiently. Integrated energy systems (IESs) combine power generation technologies, such as internal combustion engines or fuel cells, with other technologies which directly utilize the power produced by the generator and/or utilize the thermal energy otherwise wasted in the production of power. IESs are becoming more prevalent because of their environmental, economic, and reliability benefits. However, to fully realize these benefits, effective optimization and control of IESs is required. In turn, this requires a function which can accurately capture the objectives (performance, efficiency, etc.) for the system in terms of desired decision variables.

The aim of this research is to develop a systematic methodology for developing objective functions to be used in conjunction with optimal control algorithms for improving operational efficiency and performance of IESs. This is accomplished through the use of a thermodynamics-based minimization metric, exergy destruction, which is used as the foundation for deriving objective functions which are 1) physics-based, 2) generalizable to a wide class of IESs, and 3) modular with the ability to characterize not only an entire IES but also specific subsystems of a larger IES. Exergy destruction can be used to characterize irreversibilities across multiple energy domains (chemical, electrical, mechanical, and thermal) making it a particularly suitable metric for IESs.

The generalizability and modularity of the optimization framework is demonstrated through static setpoint optimization of a combined heating, cooling, and power (CCHP) system with time-varying performance demands. It was shown that minimizing exergy destruction increases exergetic efficiency at some expense of energy consumption, but that the decrease in exergy destruction can possibly outweigh the increases in energy consumption. An additional

layer of flexibility was introduced as the "interchangeability" between power minimization and exergy destruction rate minimization for those subsystems in which the reversible power is constant with respect to the decision variables. Interchangeability allows the user to only derive the exergy destruction rate for those systems in which the equivalence does not hold and construct an objective function which would result in the same solution as minimizing the rate of exergy destruction in every subsystem.

Exergy analyses have long been used to better understand the behavior of a variety of thermodynamic systems, primarily from a static design and operation point of view. However, as the complexity of integrated energy systems grows, for example as a result of intermittent grid power from renewable energy technologies such as wind and solar, an understanding of transient behavior is needed. As a case study, the dynamic exergy destruction rate was derived for the refrigerant-side dynamics of a vapor-compression cycle system and then used in formulating an exergy destruction minimization (EDM) optimal control problem for the system with full actuation capabilities. The results highlighted how time-varying control decisions can affect the distribution of irreversibilities throughout the overall system. Moreover, it was shown that EDM has the potential to uncover a different set of solutions than those produced by an energy or power minimization and is therefore a valuable tool for operational optimization of IESs.

To all of my teachers.

Acknowledgements

First and foremost, I would like to thank my advisor, Prof. Andrew Alleyne, for his mentorship and advice throughout the duration of my graduate career. I owe much of my success in graduate school to him. For 7 years he has provided me with guidance and support as I navigated through research, and life, and I have learned so much in what feels like a very short time. I look forward to continuing to learn from him in the years ahead as I progress through my career. I would also like to acknowledge the members of my doctoral examination committee – Alejandro Domínguez-García, Dimitrios Kyritsis, Srinivasa Salapaka, and Jakob Stoustrup – who have helped guide and strengthen my research with their own expertise. In particular, I would like to thank Prof. Salapaka and Prof. Carolyn Beck who wrote letters of recommendation on numerous occasions for me, and I thank them for their part in my success in securing valuable fellowships throughout my graduate career.

I have been extremely fortunate to work in the Alleyne Research Group (ARG). My peers in the ARG are among the most intelligent and kind people I have ever known. I want to thank present and past members of the ARG who conduct research in the thermal systems area – Vikas, Tim, Joey, Megan, Justin, Rich, and Matt – for many valuable discussions which contributed to the work contained in this thesis. I would like to especially thank Vikas for his help with the modeling of the CCHP system which was critical to the results presented in Chapter 3. With respect to the results presented in Chapter 5, I want to extend a special thanks to Bin and Joey for their expertise in the dynamic modeling of VCC systems as well as to Justin for his help in formulating the MPC-based optimal control problem.

To the aforementioned members of the ARG as well as Kira, Dave, Nanjun, Sarah, Sandipan, Erick, and Yangmin – thank you all for your friendship and countless hours of fun and laughter both inside and outside of the lab. You have all been an important part of my

experience at Illinois, and I hope we remain friends for many years to come. I would like to particularly acknowledge Kira, Dave, Tim, and Vikas, with whom I have grown very close and whose advice, both personal and professional, I have sought on many occasions. I am looking forward to many years of friendship ahead with each of them.

Beyond research, my passion for promoting women in engineering is something that has defined me in graduate school. I want to thank Jennifer, Helen, and Serena, who joined me in 2007 to form the first executive board of MechSE Graduate Women. I want to thank Jessie and Sam who have each led the group as president since then, and for strengthening an organization which continues to play an important role in the MechSE Department.

There are also many others (too many to mention) outside of the ARG who have made my experience in graduate school more rewarding and enjoyable. Here I acknowledge three in particular. To my friend Gayathri – thank you for your friendship and support; it has been invaluable to share such similar experiences with one another throughout our graduate careers. To my roommate Cathy, thank you for being the best roommate anyone could ask for, and for being a very constant and present friend. To my husband Shreyas, thank you for your endless encouragement, particularly through the most difficult moments in my research.

Last but not least, I want to thank my parents who have exemplified the value of hard work and discipline throughout my life. To my siblings Bhavana and Ankush – thank you for reminding me how to enjoy life and for your continued love and support through all of my endeavors.

Table of Contents

List of Tables

List of Figures

List of Symbols

A	area	m^2
a	aperture	% of maximum
C	cooling capacity	kW
c_p	specific heat capacity (at constant pressure)	$kJ \cdot (kg \cdot K)^{-1}$
$\mathbf{d}$	disturbance vector	--
E	energy	kJ
F	fraction of	dimensionless
h	specific enthalpy	$kJ \cdot kg^{-1}$
J	objective function	--
k	conductivity	$kW \cdot (m \cdot K)^{-1}$
L	length	m
m	mass	kg
$\dot{m}$	mass flow rate	$kg \cdot s^{-1}$
P	pressure	kPa
$\dot{Q}$	heat transfer rate	kW
S	entropy	$kJ \cdot K^{-1}$
s	specific entropy	$kJ \cdot (kg \cdot K)^{-1}$
T	temperature	K
t	time	s
u	control input	--
$\mathbf{u}$	control input vector	--
UA	overall heat transfer coefficient	$kJ \cdot (s \cdot K)^{-1}$
V	volume	m^3

v	velocity	$m \cdot s^{-1}$
$\mathbf{v}$	vector of decision variables for setpoint optimization	--
$\dot{W}$	work transfer rate (i.e. power)	kW
X	exergy	kJ
$\dot{X}$	exergy transfer rate	kW
$\overline{x}$	mean quality	dimensionless
$\mathbf{x}$	dynamic state vector	--
α	heat transfer coefficient	$kW \cdot (m^2 \cdot K)^{-1}$
$\overline{\gamma}$	mean void fraction	dimensionless
ε	HX effectiveness	dimensionless
ζ	normalized zone length	dimensionless
η	efficiency	dimensionless
ρ	density	$kg \cdot m^{-3}$
ψ	specific flow exergy	$kJ \cdot kg^{-1}$
ω	rotational speed	rpm

List of Subscripts

a	air
ach	achieved
c	condenser (in VCC system)
C	cooling demand
*c*1	superheated fluid region in condenser
*c*2	two-phase fluid region in condenser
*c*3	subcooled fluid region in condenser
CHW	chiller
CHWR	chiller return
CHWS	chiller supply
comb	combustor (inside gas turbine)
comp	air compressor (inside gas turbine)
comp,ref	refrigerant compressor in electric chiller
cond	condenser (in steam loop)
CR	cross-sectional
cv	control volume
DAE	deaerator
des	desired
dest	destroyed
e	evaporator
*e*1	two-phase fluid region in evaporator
*e*2	superheated fluid region in evaporator
f	fuel, fan

g	exhaust gas, saturated vapor
g,exhaust	exhaust gas exiting HRSG
gen	generated
GT	gas turbine
H	heating demand (in CCHP system), high temperature reservoir
HWR	hot water return line
i	in (inlet)
k	compressor (in VCC system)
L	low temperature reservoir
l	saturated liquid
o	outlet
p	pump
p	prediction
r,R	refrigerant
rev	reversible
s	steam
sat	saturated
SL	steam loop
ST	steam turbine
turb	turbine (inside gas turbine)
u	control
v	EEV
w	water, tube wall
FF	feedforward
y	output
0	reference environment
12	between the first and second fluid regions (of a heat exchanger)
23	between the second and third fluid regions (of a heat exchanger)

List of Abbreviations

CCHP	combined cooling, heating, and power
CHP	combined heat and power
COP	coefficient of performance
CRC	Carnot refrigeration cycle
DOF	degree of freedom
EDM	exergy destruction minimization
EEV	electronic expansion valve
HRSG	heat recovery steam generator
HVAC	heating, ventilation, and air-conditioning
IC	internal combustion
IES	integrated energy system
TEV	thermostatic expansion valve
VCC	vapor-compression cycle

Chapter 1
Introduction

This thesis investigates the use of exergy destruction as a minimization metric in the optimization and control of integrated energy systems (IESs). More broadly, this thesis seeks to define a systematic methodology for developing objective functions for a wide class of energy systems that is versatile enough to accommodate the growing diversity of IESs. In addition, the proposed methodology offers some potential advantages, based on designer tradeoffs, over current approaches. Section 1.1 provides a general overview of the class of IESs, and Section 1.2 describes the current state of optimization and control of these systems. The latter will be used to identify specific characteristics needed in an optimization framework in order for it to be suitable for most IESs.

In this thesis, an emphasis is specifically placed on the operation of IESs as opposed to the design of these systems. As electrification of energy systems continues to increase, the need for model-based optimal control strategies for these systems will grow. The approach taken here is to understand and utilize tools from the thermodynamics community in conjunction with existing control methodologies to develop a suitable framework. Accordingly, thermodynamic fundamentals will be discussed in detail in Chapter 2 to familiarize the reader before these ideas are used in the context of setpoint optimization and control later in the thesis.

1.1 Integrated Energy Systems

Integrated energy systems (IESs) combine prime-mover technologies, such as internal combustion (IC) engines, and/or fuel cells, with other technologies which directly utilize the power produced by the prime-mover and/or utilize the thermal energy otherwise wasted in the production of power. IESs can be thought of as complex systems comprised of many

interconnected heterogeneous subsystems such as the prime-movers listed above, thermally-activated heating systems, desiccant dehumidifiers, vapor-compression refrigeration systems, and/or energy storage systems [1]. One of the most common types of IESs are combined heat and power (CHP) systems in which waste heat generated as a byproduct of power generation, typically with a gas turbine, is then used to provide heating to buildings and/or for other end uses. Another example is an electric-hybrid automobile wherein an internal combustion engine generates mechanical power to move the vehicle and simultaneously power the HVAC (heating, ventilation, and air-conditioning) system on board while storing excess energy as chemical energy in a battery. IESs are becoming more prevalent because of their environmental, reliability, economic, and efficiency benefits [1] [2] [3]. A number of government initiatives, including the Combined Heat and Power Partnership, have been created to improve the CHP capacity of the U.S. [2]. In 2012 an executive order was signed by President Barack Obama setting "a national goal of 40GW of new CHP installation" in the U.S. by 2020 [4]. Along with the increase in installed capacity, it will be critical that the new capabilities are utilized in the most effective manner possible where the term 'effective' will depend on the end goal of the system operator.

A key feature of the IES heterogeneity is that it typically spans multiple energy domains - chemical, electrical, mechanical and thermal - as evidenced by the examples of subsystems which comprise IESs. Figure 1.1 visualizes this diversity by highlighting how energy generation, transmission, and consumption/storage can be realized with different forms of energy. For example, rather than a gas turbine being utilized as the prime mover, a photovoltaic solar array or fuel cell, or combination thereof, might be used instead as the primary power generation technology [5]. Moreover, energy storage technologies, such as chilled water tanks or advanced batteries, are also being used to further improve the efficiency of IESs [6].

The diversity of IESs is also seen in their performance capacity. CHP systems are often built at a large scale to support energy-intensive manufacturing facilities and for large districts of buildings, such as college campuses and hospitals [5] [7]. However, similar types of systems are being developed at a smaller scale for the residential building sector [6]. In summary, the class of IESs is not only hugely diverse with respect to type of system and scale, but we expect to see this class of systems continue to grow in the future.

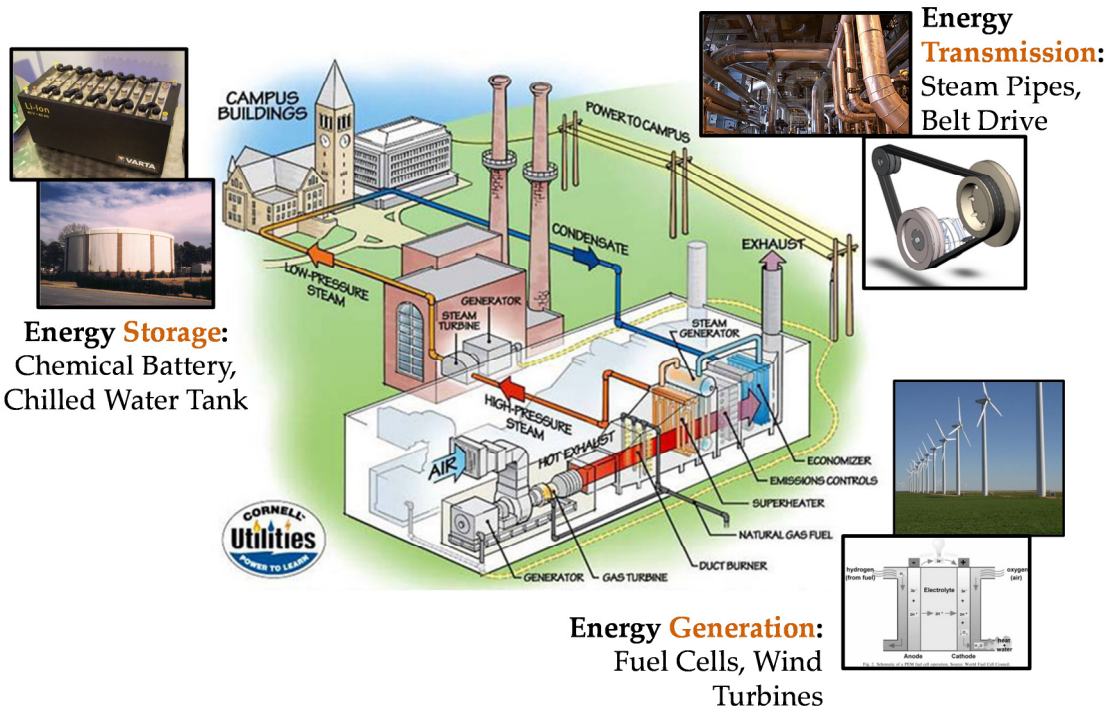

Figure 1.1: Diversity of integrated energy systems.

1.2 Optimization and Control of IESs

To fully realize the benefits of IESs, effective control of these systems is required. Through online optimization and control, IESs can effectively respond to disturbances such as variations in weather or energy loads that cannot be accounted for at the design stage [8] [9] [10] [11] [12]. Although outside the scope of the current work, it is also possible to utilize anticipated information, based on predictions of weather and loads, to balance the operation of the IESs in an optimal fashion. While many different optimization algorithms have been developed for a wide range of systems, their effectiveness depends largely on the formulation of the optimization problem to be solved, specifically how well the objective function is defined. A common minimization metric for IESs is operational cost (in dollars) [12] [13] [14] [15]; sometimes this is referred to as 'economic optimization'. However, this metric does not explicitly consider the efficiency of the IES which is heavily dependent on the level of irreversibility in the system (which in turn also has environmental implications). Moreover, economic metrics do not accurately capture the underlying physics which govern the behavior of the system, particularly because such metrics are typically empirically derived. In [9], the authors advocate the

consideration of different minimization metrics, but the proposed objective functions for energy and CO_2 emissions are empirically-based modifications of an objective function again based on electricity and fuel costs. In [8] an objective function is proposed which minimizes the daily operation cost of a micro combined heat and power (μCHP) system and is generalizable for various systems within the class of μCHP systems. However, the optimization variables are only the electrical and thermal inputs/outputs of various subsystems such as the energy input to a thermal storage device; the operation of the thermal storage device itself is not optimized with respect to the amount of thermal energy it must store.

What is lacking among these examples is an objective function that is *physics-based*, *generalizable*, and *modular*. Let us describe these attributes in greater detail.

1. Physics-based. As mentioned in the previous section, commonly used minimization metrics are typically empirically derived. There are two major disadvantages to this approach. First, these metrics do not necessarily capture the underlying physics of the IES subsystems which may result in missed opportunities to further improve efficiency (and/or other objectives) when such metrics are minimized. Secondly, empirically derived metrics cannot easily be extrapolated if or when a system changes, thereby making them less modular. A physics-based metric has the potential to overcome these disadvantages.

2. Generalizable. IESs are often comprised of a diverse set of subsystems arranged in different architectures or configurations and therefore, generalizability in the methodology for designing an appropriate objective function is necessary [1] [8]. Unfortunately, a major challenge in accomplishing this comes from the fact that the individual subsystems which comprise IESs are heterogeneous and typically characterized using different efficiency metrics. For example, internal combustion engines are often characterized in terms of their fuel efficiency whereas heat and cooling systems are typically characterized in terms of coefficient of performance (COP). It is difficult to combine these metrics in a meaningful way that preserves the physics of the system.

3. Modular. In addition to having a metric that is generalizable to different types of systems, it may be desirable to quickly modify an objective function to include or exclude

specific subsystems in a particular IES. Therefore, an objective function which can be easily modified for different systems in a systematic way is desirable.

The scope of this thesis is to develop a systematic methodology for deriving objective functions to be used in conjunction with optimization and optimal control algorithms for improving operational efficiency and performance of IESs. In the following chapters, a thermodynamics-based minimization metric, exergy destruction, will be described and formulated as the foundation for deriving appropriate objective functions. The exergy destruction minimization (EDM) objective will be constructed as the sum of the exergy destruction in each subsystem of the IES. This will provide a common and modular metric for evaluating the efficiency of the complete system since exergy destruction can be used to characterize irreversibilities across multiple energy domains (chemical, electrical, mechanical, thermal). The merits of the framework will be demonstrated through various case studies.

1.3 Organization of Thesis

The thesis is organized as follows. Chapter 2 introduces the concept of exergy and outlines the exergy-based optimization framework. In Chapter 3, the generalizability and modularity of the optimization framework is demonstrated through static setpoint optimization of a combined heating, cooling, and power (CCHP) system with varying performance demands over a 24-hour period. Moreover, the benefits of the physics-based metric are highlighted in a comparison between EDM and conventional energy minimization of the CCHP system. In Chapters 4 and 5, the EDM framework is applied to an individual energy system, specifically a vapor-compression cycle (VCC) system. Here the emphasis is extended beyond setpoint optimization to include control of the physical system itself for setpoint regulation. In Chapter 4, a static setpoint optimization of a VCC system conducted using EDM is augmented with a feedforward plus feedback control framework designed to operate the system at the optimal operation setpoints. Experimental results are provided to validate the approach. In Chapter 5, the dynamic rate of exergy destruction is derived for the VCC system so that transient, rather than steady-state, operation of the system can be considered. A finite-horizon optimal control problem is then formulated and solved offline to yield the optimal control input sequences for tracking a desired cooling capacity profile. The results are validated on a nonlinear simulation

model. Again, the benefits of the EDM metric, now in the context of transient operation, are highlighted in a comparison between EDM and energy consumption minimization of the VCC system. The thesis concludes in Chapter 6 with a summary of research contributions as well as directions for future work.

Chapter 2

Exergy-Based Optimization Framework

2.1 Thermodynamic Fundamentals

The first law of thermodynamics is a statement of energy conservation. That is to say, energy can never be destroyed. The second law introduces the notion of entropy and connects it to the irreversibility that is observed in natural phenomena by postulating that a process can only proceed in "the direction that causes the total entropy of the system plus surroundings to increase" [16]. It distinguishes between spontaneously feasible and infeasible processes.

It is the combination of the first and second laws of thermodynamics that is particularly powerful. Exergy (also referred to as "availability") is defined as the maximum reversible work that can be extracted from a substance at a given state during its interaction with a given environment. Thermomechanical exergy is defined mathematically as

$$\frac{dX_{cv}}{dt} = \frac{dE_{cv}}{dt} - T_0 \frac{dS_{cv}}{dt} \qquad (2.1)$$

where

$$\frac{dE_{cv}}{dt} = \dot{Q} - \dot{W} + \sum_i \dot{m}_i \left(h_i + \frac{v_i^2}{2} + g z_i \right) - \sum_o \dot{m}_o \left(h_o + \frac{v_o^2}{2} + g z_o \right) \qquad (2.2)$$

and

$$\frac{dS_{cv}}{dt} = \sum_j \frac{\dot{Q}_j}{T_j} + \sum_i \dot{m}_i s_i - \sum_o \dot{m}_o s_o + \dot{S}_{gen} \,. \qquad (2.3)$$

In both the energy and entropy rate balances, *i* denotes inlets and *o* denotes outlets. In Eq. 2.3, $\dot{Q}_j$ is the heat transfer rate at the location on the control volume boundary where the instantaneous temperature is T_j.

Whereas energy is always conserved, exergy is not. Similarly to energy, exergy can be transferred in three ways: by heat transfer, work, or through mass exchange with the environment. However, contrary to energy, exergy is destroyed during irreversible phenomena such as chemical reactions, mixing, and viscous dissipation. The amount of exergy destroyed in a system or through a process is a measure of the loss of potential to do work and is proportional to the amount of entropy generated in the system; this is described by the Gouy-Stodola theorem [17]:

$$\dot{X}_{dest} = T_0 \dot{S}_{gen} \geq 0 . \qquad (2.4)$$

Therefore, exergy destruction is a useful quantity to consider when characterizing the efficiency of thermodynamic systems. Specifically, the exergetic (second-law) efficiency, η_{II}, is defined as [18]

$$\eta_{II} = 1 - \frac{\text{Exergy destroyed}}{\text{Exergy supplied}} . \qquad (2.5)$$

The total exergy rate balance for a control volume is given by

$$\frac{dX_{cv}}{dt} = \underbrace{\sum_j \left(1 - \frac{T_0}{T_j}\right)\dot{Q}_j}_{\substack{\text{exergy transfer}\\ \text{accompanying}\\ \text{heat transfer}}} - \underbrace{\left(\dot{W}_{cv} - P_0 \frac{dV_{cv}}{dt}\right)}_{\substack{\text{exergy transfer}\\ \text{accompanying}\\ \text{work transfer}}} + \underbrace{\left(\sum_i \dot{m}_i \psi_i - \sum_o \dot{m}_o \psi_o\right)}_{\substack{\text{exergy transfer accompanying}\\ \text{mass transfer}}} - \dot{X}_{dest} \qquad (2.6)$$

where the specific flow exergy, ψ, is defined as

$$\psi = (h - h_0) - T_0 (s - s_0) + \frac{v^2}{2} + gz + \psi^{\text{ch}} . \qquad (2.7)$$

The quantities T_0, P_0, h_0, and s_0 are the temperature, pressure, specific enthalpy, and specific entropy, respectively, of the reference environment. The reference environment is typically chosen as an infinite reservoir with which the system is interacting, such as the ambient

environment. The use of a reference environment for defining exergy is consistent with the way in which all forms of potential energy are defined.

In addition to characterizing thermal and mechanical potential, exergy can also characterize chemical potential. This is represented by the term ψ^{ch} in Eq. 2.7 which is the chemical contribution to the total specific flow of exergy entering and leaving a control volume. For example, in the case of combustion, the chemical exergy is the maximum reversible work that can be extracted through the reaction of the fuel with environmental components [16].

2.2 Exergy-Based Analysis and Optimization

2.2.1 Exergy Analysis

Like the first and second laws of thermodynamics, exergy can be used to analyze systems and understand their behavior. Exergy analysis has been used extensively in the thermodynamics community to understand which subsystems and/or components are responsible for the greatest irreversibilities in the overall system, thereby influencing design changes at the system and/or component level [19]. In the context of individual thermal systems, [20] provides an extensive review of exergy analyses that have been conducted on vapor-compression cycle (VCC) systems, particularly highlighting the effect of different refrigerants, as well as key parameters such as evaporating temperature, on the exergetic efficiency of the system. More recently, [21] uses exergy analysis to evaluate the better of two designs of expander cycles used in a refrigeration system. For integrated energy systems (IESs), [22] analyzes each component in a combined-cycle power plant and highlights the heat recovery steam generator as the one with the lowest exergetic efficiency. It is suggested in [22] that operating parameters be optimized in order to improve performance.

Exergy analysis has also played a significant role in the area of thermoeconomics, also called exergoeconomics, which is a methodology for calculating the monetary costs associated with the design and operation of a thermal system, particularly by assigning monetary costs to the various exergy flows in a system [23] [24] [25]. More recently, Lazaretto and Tsatsaronis presented a general approach for evaluating exergy-based efficiencies and costs in thermal systems [26].

2.2.2 Exergy Destruction Minimization

In addition to exergy analysis, researchers have used exergy destruction minimization (EDM), also known as entropy generation minimization or thermodynamic optimization [27], to optimize design and operational parameters in many thermal systems [28] [29]. In particular, design parameters, such as heat exchanger geometry, have been optimized using EDM [30] [31] [32]. However, while exergy destruction minimization (EDM) has been used to determine design and nominal operational parameters, to the knowledge of the authors, exergy destruction minimization (EDM) has not been used as a metric in optimal control of energy systems. We believe EDM is particularly suitable for the optimization of IESs because of two features of exergy destruction:

1.) *Exergy destruction can be used to characterize irreversible losses across multiple energy domains.* Therefore, exergy destruction provides us with a common metric to describe the efficiency of different components or subsystems which are typically defined using different efficiency metrics. Consider an engine-driven VCC system: internal combustion (IC) engines are often characterized in terms of their fuel efficiency whereas heating and cooling systems are typically characterized in terms of coefficient of performance (COP). It is difficult to combine these metrics in a meaningful way that preserves the physics of the system. Describing the efficiency of the IC engine and VCC system in terms of exergy destruction would overcome this hurdle [33].

2.) Total exergy destruction for a given system can simply be expressed as the sum of the exergy destroyed in its components and/or subsystems. This modularity is particularly useful when considering complex systems such as IESs because the objective function can be easily modified to include/exclude individual subsystems as desired by the engineer.

2.2.3 Relationship Between EDM and Power Minimization

In the context of optimization, it is common for the amount of power consumed (generated) in a system to be minimized (maximized). The relationship between exergy destruction rate minimization and power minimization is characterized by the Gouy-Stodola theorem (Eq. 2.4) which can be equivalently expressed [27] as

$$\dot{X}_{dest} = \dot{W} - \dot{W}_{rev}. \quad (2.8)$$

The reversible rate of change of work, $\dot{W}_{rev}$, also called *reversible power*, refers to the amount of power that the system would consume (or produce) if there were no irreversibilities in the system. Let us define two objective functions, J_1 and J_2, where J_1 is equal to the rate of exergy destruction and J_2 is equal to the actual power consumed (or produced).

$$J_1 = \dot{X}_{dest} = \dot{W} - \dot{W}_{rev} \quad (2.9)$$

$$J_2 = \dot{W} \quad (2.10)$$

Equation 2.8 implies that if the quantity $\dot{W}_{rev}$ is constant with respect to the decision variables of an optimization problem, then the minimizations of J_1 and J_2 are equivalent [27], i.e.

$$\min_{\dot{W}_{rev}=C}\left(J_1\right) = \min\left(J_2\right). \quad (2.11)$$

Examples of when the reversible work/power is, and is not, constant with respect to the decision variables of an optimization problem will be discussed in Chapter 3. Of particular interest is when the equivalence between exergy destruction rate minimization and power minimization *does not* exist which will be explored throughout this thesis.

2.3 EDM Framework for Integrated Energy Systems

While exergy destruction minimization (EDM) has been used to determine design and nominal operational parameters, exergy destruction minimization (EDM) has not been used to optimize IESs over varying load profiles nor in conjunction with optimal controllers such as model predictive control. In this thesis EDM is applied as an optimization metric in the context of real-time operation of energy systems.

Optimization of IESs can be characterized by multiple (competing) objectives such as meeting specified performance demands, maximizing system efficiency, and/or minimizing wear on physical components. It is necessary to define a mathematical function that captures the objectives for a given IES and can be minimized or maximized to yield an optimal solution.

In this optimization framework, we will focus on two primary objectives: 1) meet specified performance demand, and 2) maximize system efficiency. The first objective will be

enforced as a constraint. Therefore, we seek an objective function which captures the second objective of maximizing system efficiency. Given the attributes of exergy destruction highlighted in Section 2.2.2, exergy destruction is an appropriate *physics-based*, *generalizable*, and *modular* metric to be used for the optimization of IESs. This optimization framework can be applied using the following procedure:

1. Define the objective function to minimize the total exergy destroyed over a specified time horizon. For example:

$$J_{EDM} = \sum_{k=1}^{N} \dot{X}_{dest,total}[k] \cdot Ts \qquad (2.12)$$

   where *Ts* is the discrete sample time.
2. Determine the decision variables based on modeling assumptions and available degrees of freedom (DOFs).
3. Derive an expression for the rate of exergy destruction, $\dot{X}_{dest}$, in each subsystem of the overall system (or in each component of a single system).
4. Define the total exergy destruction rate for the system by summing together the exergy destruction rates of each subsystem:

$$\dot{X}_{dest,total} = \dot{X}_{subsystem,1} + \dot{X}_{subsystem,2} + \cdots + \dot{X}_{subsystem,n}. \qquad (2.13)$$

5. Define constraints for the optimization problem.

This procedure is intentionally generalized to highlight the modularity of this approach. Noteworthy is the fact that it is not necessary to introduce constant weights on the individual subsystem rates of exergy destruction in Eq. 2.13 because in this objective function, the same quantity (exergy destruction rate in units of power) is being summed for every subsystem. Therefore, if one individual subsystem destroys more exergy than others, it will inherently be penalized more than the other subsystems in the optimization. This highlights a major advantage of this approach since tuning weightings in an objective function comprised of terms in different units would become increasingly difficult as the complexity of the system increases.

In the next chapter, the optimization framework outlined here will be applied to a combined cooling, heating, and power (CCHP) system for the purpose of setpoint optimization. When the equivalence between exergy destruction rate minimization and power minimization exists, it will be shown that power and exergy destruction rate can be interchanged in a larger objective function. When equivalence does not exist, it will be shown that the EDM provides a solution which destroys less exergy than an energy consumption minimization of the same system while also favoring those subsystems with higher isentropic efficiencies. In Chapter 5, this framework will be used with an optimal control algorithm to control a vapor-compression cycle (VCC) system.

Chapter 3
Setpoint Optimization of a CCHP System

A combined cooling, heating, and power (CCHP) system is a common type of integrated energy system (IES). In this chapter the exergy destruction minimization (EDM) framework outlined in Chapter 2 is applied to a CCHP system. The results will highlight the modularity of the EDM framework in describing irreversibilities across multiple energy domains. In particular, the notion of interchangeability will be introduced wherein exergy destruction rate and power consumption can be interchanged for particular subsystems in the overall objective function to yield the same solution as in EDM. Finally, the advantages of EDM as compared to energy consumption minimization will be explored.

The CCHP system considered in this chapter is shown schematically in Figure 3.1 and is modeled after an existing system at the University of California, Irvine [34]. It is comprised of four major subsystems: a gas turbine, a heat recovery steam generator (HRSG), a steam loop, and an electric chiller bank. The goal of this case study is to find the optimal operation setpoints for the CCHP system at each hour for 24 hours of operation. The problem will be posed as a static optimization problem, and the system will be described using static models of the four subsystems. The decision variables in the optimization problem will be chosen as independent operational parameters for which setpoint values can be assigned. Based on the optimization framework outlined in Chapter 2, the objective function for minimizing exergy destruction, J_{EDM}, is defined as

$$J_{EDM} = \sum_{k=1}^{24} \dot{X}_{dest,CCHP}[k] \cdot Ts \qquad (3.1)$$

where the sample time, *Ts*, is 3600 seconds. However, since *Ts* is a constant, it can be removed from the summation and J_{EDM} can be redefined as

$$J_{EDM} = \sum_{k=1}^{24} \dot{X}_{dest,CCHP}[k]. \qquad (3.2)$$

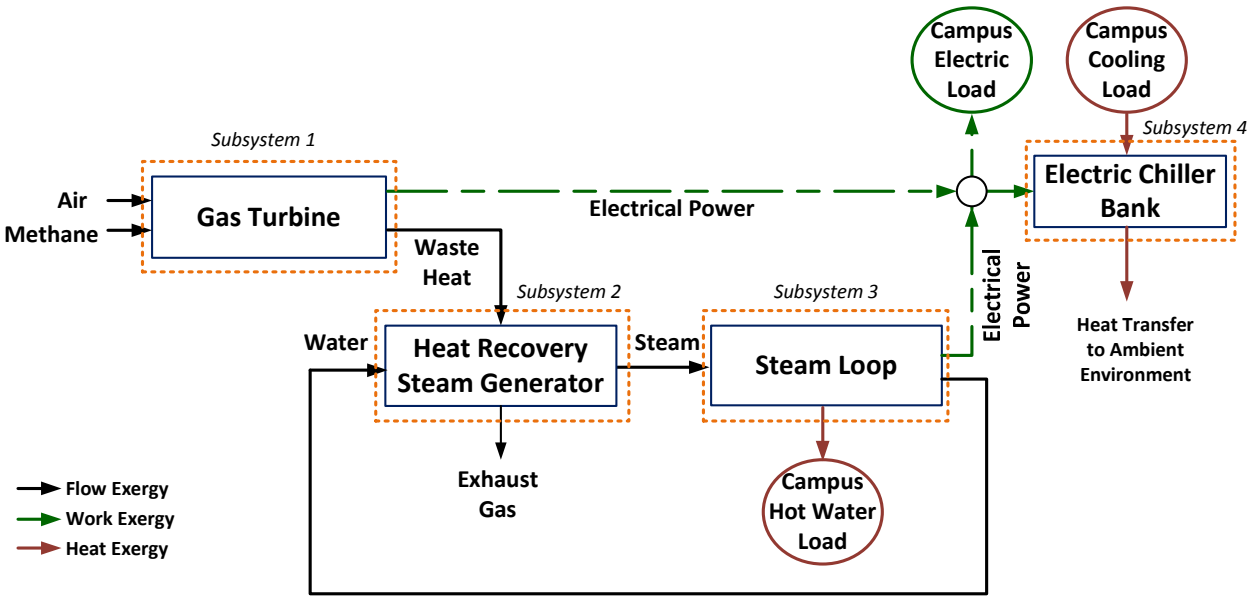

Figure 3.1: Schematic of CCHP system.

In the next section, static models for each of the subsystems will be presented and then used to obtain an expression for the total rate of exergy destruction in the CCHP system.

3.1 Determining the Decision Variables

In the following subsections, modeling assumptions and equations for each of the four CCHP subsystems are given. The model equations, which are largely based on [35] with some modifications, have generally been derived using first-principles. However, in the case of some subsystems, empirically-derived models originally developed for the actual CCHP system at UC Irvine will be used. Based on these subsystem model descriptions, a set of decision variables will be defined for the setpoint optimization problem.

As will be highlighted again later in this chapter, this optimization framework gives the user flexibility to use a combination of physics-based and data-based models in the exergy-based optimization framework. Additionally, more detailed models can be used to describe certain subsystems if desired. Depending upon the modeling assumptions that are made, as well as the

actuation capability of the actual system under consideration, different decision variables will be available for optimization.

3.1.1 Subsystem 1: Gas Turbine

The gas turbine consists of three standard components: an air compressor, a combustor, and a turbine. To model the gas turbine, the following assumptions are made:

1. the compressor pressure ratio is constant,
2. the specific heat capacities of air and exhaust gas are constant,
3. air and combustion exhaust gas behave as ideal gases,
4. the isentropic efficiencies of both the compressor, η_{comp}, and turbine, η_{turb}, are constant values between 0 and 1,
5. the fuel for the gas turbine is methane,
6. combustion is adiabatic and isobaric.

The individual equations for the compressor, combustor, and turbine are described in the following subsections. The decision variables for the gas turbine subsystem are the fuel mass flow rate, $\dot{m}_f$, and the net power produced by the gas turbine, $\dot{W}_{GT} = \dot{W}_{turb} - \dot{W}_{comp}$.

3.1.1.1 Compressor

The compressor is used to compress air to a higher temperature and pressure before it is combusted with methane. The pressure of the air exiting the compressor is given by

$$P_{comp,out} = Pr \cdot P_{comp,in} \tag{3.3}$$

where *Pr* is the pressure ratio across the compressor. The temperature of the compressor outlet air is

$$T_{comp,out} = T_{a,in}\left[1 + \frac{1}{\eta_{comp}}\left(Pr^{0.4/1.4} - 1\right)\right]. \tag{3.4}$$

The power consumed by the compressor can then be determined by evaluating

$$\dot{W}_{comp} = \dot{m}_{a,in} c_{p,a}\left(T_{comp,out} - T_{a,in}\right) \tag{3.5}$$

where it is assumed that η_{comp}, the isentropic efficiency of the compressor, is a constant value between 0 and 1 and is specified in the optimization problem.

3.1.1.2 Combustor

The stoichiometric chemical reaction between methane (CH_4) and the compressed air which takes place in the combustor is described by

$$0.5\mathrm{CH_4} + 3.76\mathrm{N_2} + \mathrm{O_2} \rightarrow 0.5\mathrm{CO_2} + \mathrm{H_2O} + 3.76\mathrm{N_2}. \quad (3.6)$$

However, in actuality, the combustion reaction in gas turbines is typically characterized by an equivalence ratio less than one, where [16] defines the equivalence ratio as

$$\phi = \frac{(FA)_{actual}}{(FA)_{stoichiometric}}. \quad (3.7)$$

Here we assume an air-fuel ratio of 22.0, which is characterized by the following chemical reaction:

$$0.5\mathrm{CH_4} + 4.82\mathrm{N_2} + 1.2826\mathrm{O_2} \rightarrow 0.5\mathrm{CO_2} + \mathrm{H_2O} + 4.82\mathrm{N_2} + 0.2826\mathrm{O_2}. \quad (3.8)$$

Based on Eq. 3.8, the mass flow rates of fuel (methane), air, and combustion products are related to one another as shown in Eq. 3.9 and Eq. 3.10.

$$\dot{m}_g = 1.02\dot{m}_{a,in} \quad (3.9)$$

$$\frac{\dot{m}_{a,in}}{\dot{m}_f} = 22.0 \quad (3.10)$$

The temperature of the combustion products leaving the combustor can be obtained by evaluating the following energy balance:

$$T_{comb,out} = \frac{\dot{m}_f}{\dot{m}_{a,in} c_{p,a}} \mathrm{LHV_{CH_4}} + T_{comp,out} \quad (3.11)$$

where $\mathrm{LHV_{CH_4}}$ is the lower heating value of methane [16]. The combustion process is assumed to be isobaric so that $P_{comb,out} = P_{comb,in}$.

3.1.1.3 Turbine

After exiting the combustor, the combustion products, modeled as an ideal gas, enter the turbine. The temperature of the exhaust gas as it leaves the turbine is given by

$$T_{turb,out} = T_{comb,out}\left[1-\eta_{turb}\left(1-\left(\frac{P_{turb,out}}{P_{comb,out}}\right)^{0.4/1.4}\right)\right] \quad (3.12)$$

where η_{turb}, the isentropic efficiency of the turbine, is a constant between 0 and 1 and is specified in the optimization problem. The power produced by the turbine is then evaluated using the equation

$$\dot{W}_{turb} = \dot{m}_g c_{p,a}\left(T_{out,comb} - T_{turb,out}\right). \quad (3.13)$$

3.1.2 Subsystem 2: Heat Recovery Steam Generator

The heat recovery steam generator (HRSG) is used to generate steam from the exhaust gas exiting the gas turbine. For simplicity, it is modeled here as a counter-flow heat exchanger although in general, it contains many individual components such as boilers and an economizer. The effect of the unmodeled components is captured using a lumped heat exchanger effectiveness, ε, which is taken to be constant in the optimization problem. However, with more detailed models, the effectiveness could be expressed in terms of operational parameters thereby creating an additional optimization degree of freedom (DOF). To model the HRSG, the following assumptions are made:

1. the HRSG can be modeled as a counter-flow heat exchanger with constant effectiveness, ε,
2. the pressure in the water/steam mass stream drops by a constant factor, $f_{p,w}^{HRSG}$, between the inlet and outlet of the HRSG,
3. the specific heat capacities of water and exhaust gas are assumed to be constant,
4. the mass flow rate of the steam exiting the HRSG is equal to the mass flow rate of water entering the HRSG: $\dot{m}_w = \dot{m}_s$.

There are no decision variables specifically associated with the HRSG; once $\dot{m}_f$ and $\dot{W}_{GT}$ have been determined for Subsystem 1, Eqs. 3.14 – 3.17 can be evaluated.

Based on Assumption 2, the pressure of the steam exiting the HRSG is

$$P_{w,out} = f_{p,w}^{HRSG} P_{w,in} \quad (3.14)$$

where $f_{p,w}^{HRSG}$ is the pressure loss factor in the water/steam mass stream, and $P_{w,in}$ is specified as a constant in the optimization problem. The heat exchanger effectiveness is described by

$$T_{g,in} - T_{g,out} = \epsilon\left(T_{g,in} - T_{w,in}\right) \quad (3.15)$$

where $T_{w,in}$ and ε are specified as constants in the optimization problem. In order to compute the temperature at which steam exits the HRSG, the following energy balance is first used to find the enthalpy at which the steam exits the HRSG:

$$\dot{m}_g c_{p,g}\left(T_{g,in} - T_{g,out}\right) = \dot{m}_w\left(h_{s,out} - h_{w,in}\right). \quad (3.16)$$

Then the approximated linear relationship, shown in Eq. 3.17, between superheated water vapor enthalpy and temperature is used to determine $T_{s,out}$.

$$T_{s,out} = \theta_{h,1} h_{s,out} + \theta_{h,2} \quad (3.17)$$

Equation 3.16 assumes that there is enough potential in the exhaust gas to generate steam. The numerical values for the regression coefficients, $\theta_{h,1}$ and $\theta_{h,2}$, are provided in Table 3.1 and were obtained using fluid property tables provided in [36].

Table 3.1 Linear Regression Coefficients for $T_{s,out}$

Coefficient	Value
$\theta_{h,1}$	0.4445
$\theta_{h,2}$	1314.75

3.1.3 Subsystem 3: Steam Loop

The steam generated in the HRSG is used for two purposes upon entering the steam loop: generating electricity via a steam turbine and meeting the campus hot water demand. To model the steam loop, the following assumptions are made:

1. there is no leakage of water/steam anywhere in the steam loop,
2. the deaerator and condenser are regulated at specified constant pressures, P_{DAE} and $P_{cond,1}$, respectively,
3. steam behaves like an ideal gas

4. in the range of operation under consideration, the specific heat capacity of steam, $c_{p,s}$, varies linearly with temperature,
5. in the range of operation under consideration, the saturation temperature of water, $T_{w,sat}$, is linearly dependent on the inlet water pressure, $P_{w,out}$,
6. steam is in a gaseous state upon exiting the steam turbine
7. steam is in a gaseous state upon exiting the heat exchanger with the hot water circuit
8. the isentropic efficiency of the steam turbine, η_{ST}, is a constant between 0 and 1,
9. and the water pumps have 100% mechanical efficiency.

The inlet steam mass flow rate, $\dot{m}_{s,in}$, is divided into two mass flow rates, determined by f_1^s, the fraction of steam diverted towards the steam turbine:

$$\dot{m}_{s,1} = f_1^s \dot{m}_{s,in}, \tag{3.18}$$

$$\dot{m}_{s,2} = \left(1 - f_1^s\right) \dot{m}_{s,in}. \tag{3.19}$$

The electrical power generated by the steam turbine is then evaluated using the expression

$$\dot{W}_{ST} = \dot{m}_{s,1} c_{p,s} \eta_{ST} T_{s,in} \left[1 - \left(\frac{P_{cond,1}}{P_{s,in}} \right)^{0.25} \right] \tag{3.20}$$

where a linear relationship between $T_{s,in}$ and $c_{p,s}$ is approximated as shown in Eq. 3.21. The numerical values for $\theta_{cp,1}$ and $\theta_{cp,2}$ are provided in Table 3.2.

$$c_{p,s} = \theta_{cp,1} T_{s,in} + \theta_{cp,2} \tag{3.21}$$

Table 3.2 Linear Regression Coefficients for $c_{p,s}$

Coefficient	Value
$\theta_{cp,1}$	0.0006
$\theta_{cp,2}$	1.6599

The remaining steam is used to meet the campus hot water demand by exchanging thermal energy with the campus hot water circuit. The amount of heat delivered to the hot water return line is

$$\dot{Q}_H = \dot{m}_s c_{p,s} \left(T_{s,in} - T_{w,sat} \right) \quad (3.22)$$

where the saturated water temperature, $T_{w,sat}$, is evaluated at the pressure of the steam as it exchanges heat with the hot water line, $P_{w,out}$, using the approximated linear relationship

$$T_{w,sat} = \theta_{T,1} P_{w,out} + \theta_{T,2} . \quad (3.23)$$

The numerical values for the regression coefficients are provided in Table 3.3.

Table 3.3 Linear Regression Coefficients for $T_{w,sat}$

Coefficient	Value
$\theta_{T,1}$	0.0249
$\theta_{T,2}$	435.47

The steam exiting the steam turbine is pumped through the condenser towards the deaerator. The steam exiting the heat exchanger with the hot water circuit passes through a second condenser and then the two streams of water combine as they flow through the deaerator and are pumped back towards the HRSG. The power consumed by each of the pumps is

$$\dot{W}_{p,1} = \frac{\dot{m}_{s,1}}{\rho_w} \left(P_{DAE} - P_{cond,1} \right) \quad (3.24)$$

and

$$\dot{W}_{p,2} = \frac{\dot{m}_{s,in}}{\rho_w} \left(P_{w,out} - P_{DAE} \right) . \quad (3.25)$$

The decision variable associated with the steam loop is f_1^s.

3.1.4 Subsystem 4: Electric Chiller Bank

The electric chiller bank consists of seven individual chillers. Auxiliary equipment such as cooling towers and pumps are omitted from this analysis. The rate of cooling provided by the *i*th chiller is given by

$$\dot{Q}_{c,i} = \dot{m}_{CHW,i} c_{p,w} \left(T_{CHWR} - T_{CHWS,i} \right). \quad (3.26)$$

The chiller water return temperature T_{CHWR} is assumed to be the same for each chiller and is specified as a constant in the optimization problem. Moreover, $c_{p,w}$, the specific heat of water, is a known constant. However, the water mass flow rates, $m_{CHW,i}$, $i \in \{1,2,...,7\}$, and the supply water temperatures, $T_{CHWS,i}$, $i \in \{1,2,...,7\}$, for the individual chillers are not fixed and therefore are decision variables in the optimization problem.

The power consumed by the *i*th chiller, $\dot{W}_{CHW,i}$, is described using an empirical model developed in [34] which is a linear function of the cooling capacity provided by that chiller:

$$\dot{W}_{CHW,i} = \alpha_i \dot{Q}_{c,i} + \beta_i . \quad (3.27)$$

The regression coefficients α and β for each chiller are given in Table 3.4. Note that Chiller 5 is the most efficient chiller for variations in cooling capacity. This feature will be highlighted in the results presented in Section 3.4.

Table 3.4 Linear Regression Parameters for Chiller Power Consumption

	α	β
Chiller 1	0.1357	204.91
Chiller 2	0.1357	204.91
Chiller 3	0.1716	99.453
Chiller 4	0.1604	686.29
Chiller 5	0.1213	454.94
Chiller 6	0.3683	151.29
Chiller 7	0.3127	427.63

3.1.5 Summary of Decision Variables

There are a total of 17 decision variables to be optimized for the CCHP system. These are depicted visually in Figure 3.2 to give the reader a better understanding of what the decision variables are in the context of the overall system.

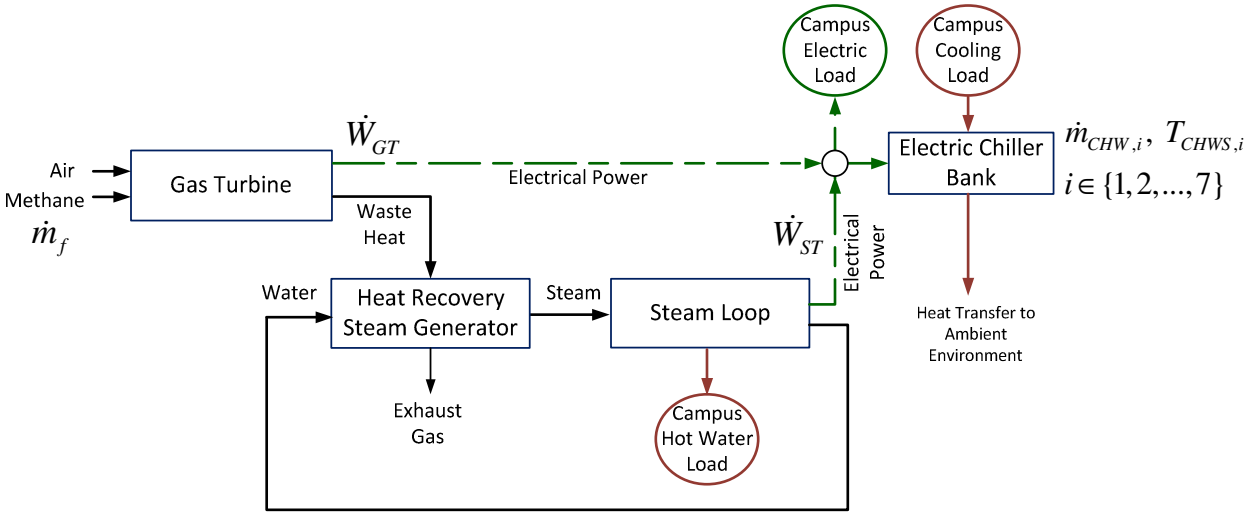

Figure 3.2: CCHP system schematic highlighting decision variables.

3.2 Derivation of the Exergy Destruction Rate

In order to derive an expression for the total rate of exergy destruction (at steady-state) in the CCHP system, each of the aforementioned subsystems is analyzed individually. The exergy rate balance for a control volume is given by

$$\frac{dX_{cv}}{dt} = \sum_j \left(1 - \frac{T_0}{T_j}\right)\dot{Q}_j - \left(\dot{W}_{cv} - P_0 \frac{dV_{cv}}{dt}\right) + \sum_i \dot{m}_i \psi_i - \sum_o \dot{m}_o \psi_o - \dot{X}_{dest} \qquad (3.28)$$

where the flow exergy, ψ, is defined as

$$\psi = h - h_0 - T_0(s - s_0) + \frac{v^2}{2} + gz + \psi^{ch}. \qquad (3.29)$$

The exergy rate balance for a control mass (i.e. closed system) is

$$\frac{dX}{dt} = \sum_j \left(1 - \frac{T_0}{T_j}\right)\dot{Q}_j - \left(\dot{W} - P_0 \frac{dV}{dt}\right) + \dot{X}^{ch} - \dot{X}_{dest}. \qquad (3.30)$$

The reference state is chosen to be the ambient environment and is described by T_0 and P_0 where T_0 will be specified at each hour and P_0 = 101.325 kPa is atmospheric pressure. The reference temperature is updated at each hour based on a typical 24-hour ambient temperature profile for summer months [37] in Southern California, shown in Figure 3.3.

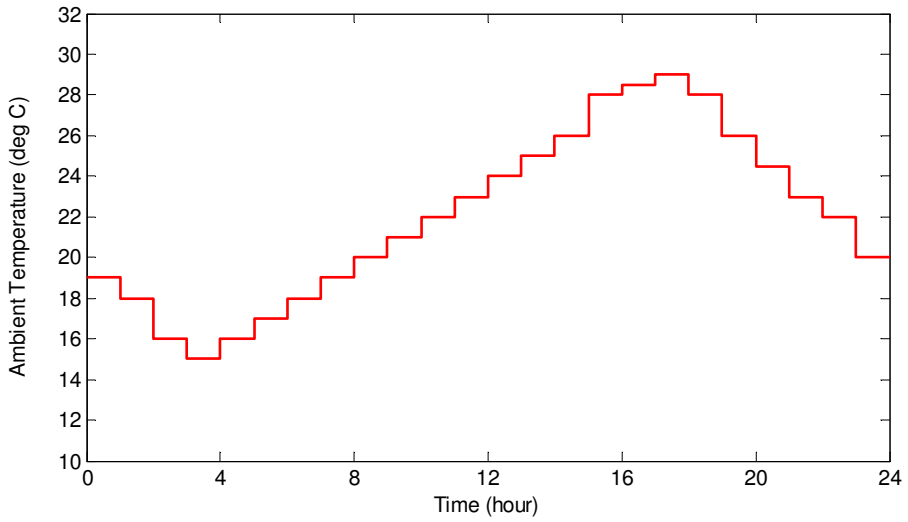

Figure 3.3: Ambient temperature profile over 24-hour prediction horizon.

3.2.1 Subsystem 1: Gas Turbine

The first control volume is drawn around the gas turbine as shown in Figure 3.1. We apply Eq. 3.28 to this control volume and make the following simplifications based on the fact that the gas turbine is operating at steady-state at each hour and there is no heat transfer across the boundary of the control volume:

$$\frac{dX_{cv}}{dt} = \sum \left(1 - \frac{T_0}{T_j}\right)\dot{Q}_j - \left(\dot{W}_{cv} - P_0 \frac{dV_{cv}}{dt}\right) + \sum_i \dot{m}_i \psi_i - \sum_o \dot{m}_o \psi_o - \dot{X}_{dest} . \qquad (3.31)$$

The expression for the rate of exergy destruction in the gas turbine is

$$\dot{X}_{dest,GT} = \dot{W}_{comp} - \dot{W}_{turb} + \dot{m}_f \psi_f^{ch} + \dot{m}_{a,in}\psi_{a,in} - \dot{m}_{g,out}\psi_{g,out} . \qquad (3.32)$$

Note that the flow exergy of air, $\dot{m}_{a,in}\psi_{a,in}$ is zero in this analysis because the air enters the compressor at the reference state.

3.2.2 Subsystem 2:HRSG

The second control volume is drawn around the heat recovery steam generator (HRSG) as shown in Figure 3.1. Subsystem 2 is assumed to be operating at steady state and there is no exergy transfer by work or heat across the boundary of the control volume. Therefore, the expression for the rate of exergy destruction in the HRSG is given by Eq. 3.34.

$$\cancel{\frac{dX_{cv}}{dt}} = \sum \left(1 - \frac{T_0}{T_j}\right) \cancel{\dot{Q}_j} - \left(\cancel{\dot{W}_{cv}} - P_0 \cancel{\frac{dV_{cv}}{dt}}\right) + \sum_{in} \dot{m}\psi - \sum_{out} \dot{m}\psi - \dot{X}_{dest} \qquad (3.33)$$

$$\dot{X}_{dest,HRSG} = \dot{m}_g \left(\psi_{g,in} - \psi_{g,exhaust}\right) + \left(\dot{m}_w \psi_{w,in} - \dot{m}_s \psi_{s,out}\right) \qquad (3.34)$$

3.2.3 Subsystem 3: Steam Loop

The third control volume is drawn around the steam loop as shown in Figure 3.1. Subsystem 3 is assumed to be operating at steady-state so the differential terms in Eq. 3.35 are zero. In this control volume, the exergy transferred from the steam to meet the hot water load is modeled as $\dot{Q}_H$. There is exergy transfer by work due to the power generated by the steam and the power consumed by the two water pumps. Finally, the steam entering, and the water exiting, the steam loop contain flow exergy.

$$\cancel{\frac{dX_{cv}}{dt}} = \sum \left(1 - \frac{T_0}{T_j}\right) \dot{Q}_j - \left(\dot{W}_{cv} - P_0 \cancel{\frac{dV_{cv}}{dt}}\right) + \sum_{in} \dot{m}\psi - \sum_{out} \dot{m}\psi - \dot{X}_{dest} \qquad (3.35)$$

The final expression for the rate of exergy destruction in the steam loop is

$$\dot{X}_{dest,SL} = \left(1 - \frac{T_o}{T_{HWR}}\right)\left(-\dot{Q}_H\right) - \left(-\dot{W}_{p,1} - \dot{W}_{p,1} + \dot{W}_{ST}\right) + \left(\dot{m}_s \psi_{s,in} - \dot{m}_w \psi_{w,out}\right). \qquad (3.36)$$

Note that the flow exergy terms in Eq. 3.34 will cancel out with the flow exergy terms in Eq. 3.36 because they represent a closed circuit of water which circulates through Subsystems 2 and 3 and repeatedly changes phase between steam and water.

3.2.4 Subsystem 4: Electric Chiller Bank

The fourth and final control volume is drawn around the electric chiller bank as shown in Figure 3.1. Subsystem 4 is assumed to be operating at steady-state. Since there is no mass transfer across the boundary of the control volume, though, the electric chiller bank can be treated as a closed system. Therefore, Eq. 3.30 is used to derive the rate of exergy destruction in the electric chiller bank:

$$\cancel{\frac{dX}{dt}} = \sum \left(1 - \frac{T_0}{T_j}\right) \dot{Q}_j - \left(\dot{W} - P_0 \cancel{\frac{dV}{dt}}\right) + \cancel{\dot{X}^{ch}} - \dot{X}_{dest}. \qquad (3.37)$$

The rate of exergy destruction for the entire electric chiller bank is given by the summation

$$\dot{X}_{dest,CHW} = \sum_{i=1}^{7}\left(\left(1-\frac{T_0}{T_{CHWR}}\right)\dot{Q}_{C,i} + \dot{W}_{comp,ref,i}\right). \quad (3.38)$$

3.2.5 Expression for Total Exergy Destruction Rate

An expression for the total rate of exergy destruction in the complete CCHP system can be obtained by summing the expressions for $\dot{X}_{dest}$ given in Eqs. 3.32, 3.34, 3.36, and 3.38. After some cancellations, this yields

$$\begin{aligned}\dot{X}_{dest,CCHP} = \dot{W}_{comp} - \dot{W}_{turb} + \dot{m}_f \psi_f^{ch} - \dot{m}_{g,exhaust}\psi_{g,exhaust} + \left(1-\frac{T_0}{T_{HWR}}\right)\left(-\dot{Q}_H\right) \\ + \dot{W}_{p,1} + \dot{W}_{p,2} - \dot{W}_{ST} + \sum_{i=1}^{7}\left(\left(1-\frac{T_0}{T_{CHWR}}\right)\dot{Q}_{C,i} + \dot{W}_{comp,ref,i}\right)\end{aligned} \quad (3.39)$$

where $\psi_f^{ch} = 51.849$ MJ/kg for methane (CH_4) at the standard reference state [16] and

$$\psi_{g,exhaust} = \left(c_{p,g}\left(T_{g,exhaust} - T_0\right) - T_0\left(c_{p,g}\ln\left(\frac{T_{g,exhaust}}{T_0}\right) - R_g \ln\left(\frac{P_{g,exhaust}}{P_0}\right)\right)\right). \quad (3.40)$$

The value for ψ_f^{ch} varies with temperature, but the variation is sufficiently small that ψ_f^{ch} is often approximated as constant [16]. While Eq. 3.39 is derived using first principles, the expressions for the individual terms, such as the power produced by the turbine, can be derived either from first principles or from data. While there are many advantages of using purely physics-based models, these are not always available. However, by starting with Eq. 3.39 as the skeleton of the objective function, the overall metric to be minimized is based in fundamental thermodynamics regardless of whether an empirical or physics-based expression is used to characterize pump power, etc.

3.3 Defining the Constraints

There are three performance demands for the CCHP system which must be satisfied: an electricity demand, a hot water demand, and a cooling demand. The cooling and electricity demand profiles were generated based on [34]; the hot water demand was created based on water

use profiles in [38] and [39]. Each demand profile is defined over a 24-hour time horizon. The profiles are shown in Figure 3.4.

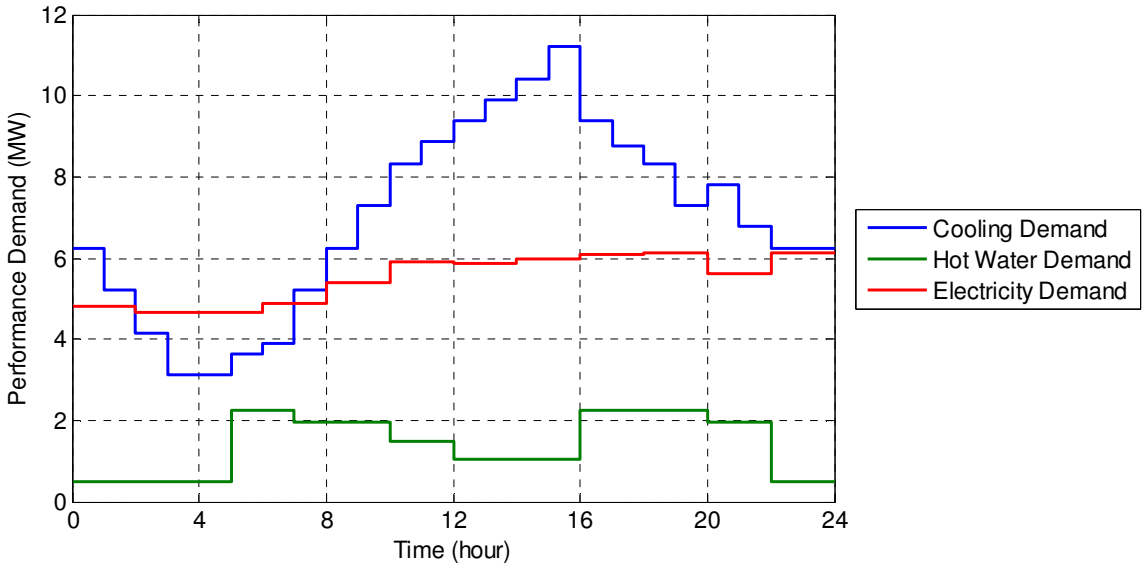

Figure 3.4: Performance constraints defined over 24-hour prediction horizon.

The performance demands must always be met; therefore, the following equality constraints are enforced in the optimization problem:

$$\begin{aligned} \dot{Q}_{C,dem}[k] &= \sum_{i=1}^{7} \dot{Q}_{C,i}[k] \;\forall\; k \\ \dot{Q}_{H,dem}[k] &= \dot{Q}_{H}[k] \;\forall\; k \\ \dot{W}_{elec,dem}[k] &= \left(\dot{W}_{GT}[k] + \dot{W}_{ST}[k] - \dot{W}_{p,1}[k] - \dot{W}_{p,2}[k] - \sum_{i=1}^{7} \dot{W}_{comp,ref,i}[k] \right) \;\forall\; k \;. \end{aligned} \tag{3.41}$$

Additionally, upper and lower bound constraints, shown in Table 3.5, are enforced on each of the decision variables.

Table 3.5 Upper and Lower Bound Constraints on Decision Variables

Decision Variable	Lower Bound	Upper Bound
$\dot{W}_{GT}$	1 MW	13.5 MW
$\dot{m}_f$	0.2 kg/s	0.85 kg/s
$f_{s,1}$	0.05	0.95
$\dot{m}_{CHW,1}$	1 kg/s	88.6 kg/s
$\dot{m}_{CHW,2}$	1 kg/s	126.6 kg/s
$\dot{m}_{CHW,3}$	1 kg/s	126.6 kg/s
$\dot{m}_{CHW,4}$	1 kg/s	284.8 kg/s
$\dot{m}_{CHW,5}$	1 kg/s	284.8 kg/s
$\dot{m}_{CHW,6}$	1 kg/s	316.5 kg/s
$\dot{m}_{CHW,7}$	1 kg/s	316.5 kg/s
$T_{CHWS,i} \forall i \in \{1,...,7\}$	3.33°C	5.55°C

3.4 Solution to EDM Problem

The static EDM problem was solved using the function *fmincon* in the MATLAB Optimization Toolbox [40] which used a sequential quadratic programming solver to find a local minimum for the nonlinear optimization problem. The optimal sequence of values for each decision variable is shown in the following figures.

The first three decision variables are the net power produced by the gas turbine, $\dot{W}_{GT}$, the mass flow rate of fuel (into the combustor), $\dot{m}_f$, and the fraction of steam sent to the steam turbine, f_1^s.

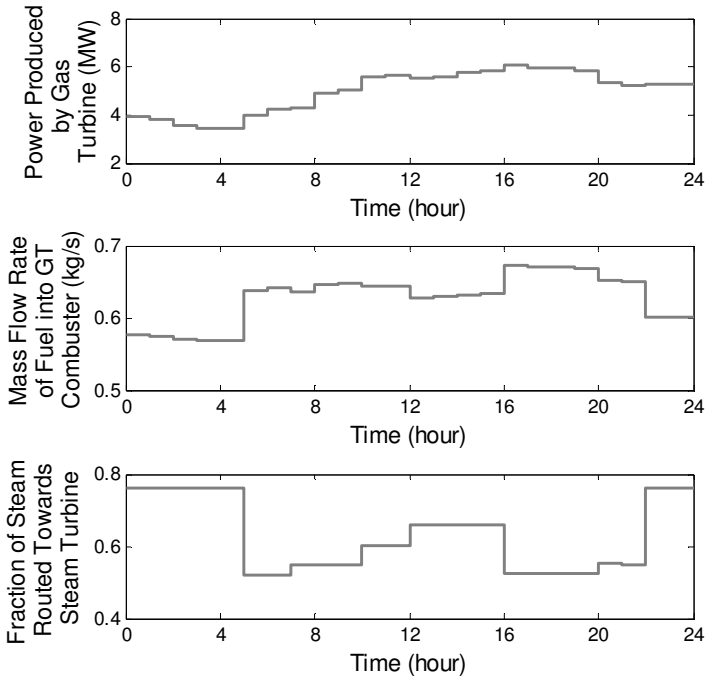

Figure 3.5: Optimal setpoints for $\dot{W}_{GT}$, $\dot{m}_f$, and f_1^s.

The remaining decision variables are associated with the electric chiller bank. The optimal water mass flow rates and supply water temperatures are shown in Figure 3.6 and Figure 3.7, respectively.

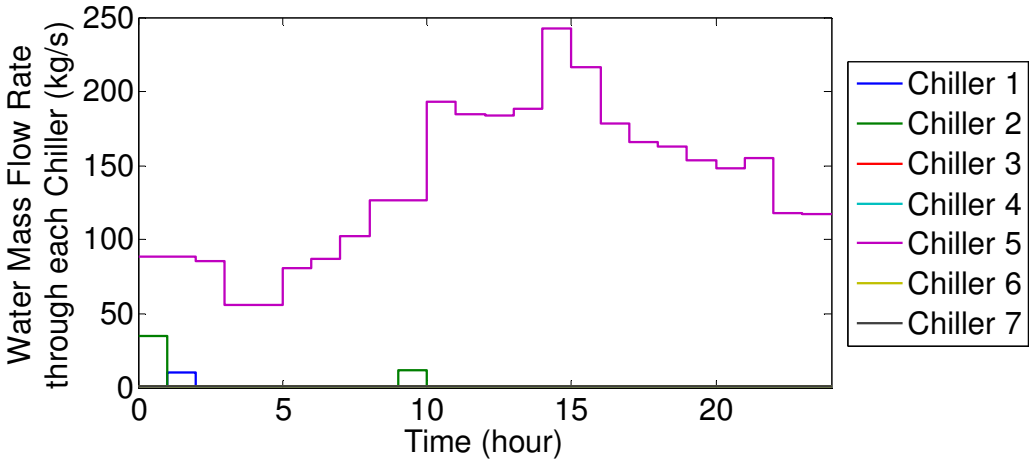

Figure 3.6: Optimal setpoints for water mass flow rate, $\dot{m}_{CHW,i}$, i={1,2,…,7}, through each chiller.

In this optimization problem, it is assumed that the chillers cannot be cycled on and off. Therefore, Chillers 3, 4, 6, and 7 operate with the minimum allowable flow rate of 1 kg/s whereas Chiller 5 is the primary chiller being used to meet the cooling demand. This is a result of the different power consumption characteristics between the individual chillers as described in Table 3.4. The optimal supply water temperature is held at the upper limit of 5.55°C for Chillers 3, 4, 6, and 7 indicating that they were being asked to provide the least amount of cooling allowed in the optimization. The supply water temperature fluctuates between the upper and lower bounds for Chillers 1, 2, and 5.

To explain this fluctuation, consider the chiller model equations, Eqs. 3.26 and 3.27, which describe $\dot{Q}_{c,i}$ and $\dot{W}_{CHW,i}$. The cooling capacity provided by the ith chiller is dependent upon both the mass flow rate of water and the temperature of the supply water of that chiller, both of which are decision variables in the optimization problem. However, the power consumed by the ith chiller only depends on the cooling capacity it is providing. Therefore, there are multiple combinations of $\dot{m}_{CHW,i}$ and $T_{CHWS,i}$ for the ith chiller which will result in the same power consumption for that chiller.

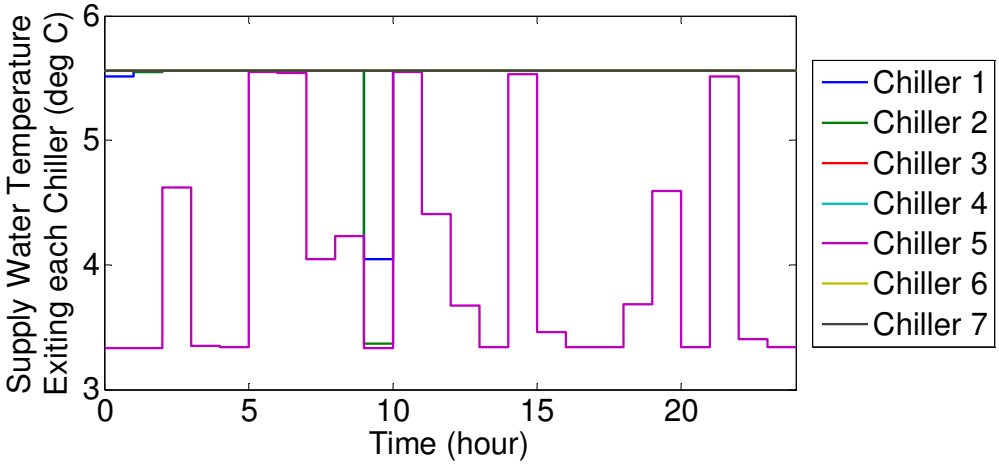

Figure 3.7: Optimal setpoints for supply water temperature, $T_{CHWS,i}$, i={1,2,…,7}, exiting each chiller.

3.5 Reversible Power

3.5.1 Reversible Power for Overall CCHP System

As discussed in Chapter 2, power minimization and exergy destruction rate minimization are related by the Gouy-Stodola theorem. Here we apply Eq. 2.8 to the entire CCHP system so that we can derive an expression for $\dot{W}_{rev}$:

$$\begin{aligned}&\dot{W}_{comp}-\dot{W}_{turb}+\dot{m}_f\psi_f^{\mathrm{ch}}-\dot{m}_{g,exhaust}\psi_{g,exhaust}+\left(1-\frac{T_0}{T_{HWR}}\right)\left(-\dot{Q}_H\right)\\&+\dot{W}_{p,1}+\dot{W}_{p,2}-\dot{W}_{ST}+\sum_{i=1}^{7}\left(\left(1-\frac{T_0}{T_{CHWR}}\right)\dot{Q}_{C,i}+\dot{W}_{comp,ref,i}\right)=\dot{W}-\dot{W}_{rev}\end{aligned} \tag{3.42}$$

where

$$\dot{W}=\dot{m}_f\mathrm{LHV}_{\mathrm{CH_4}}. \tag{3.43}$$

By virtue of the performance constraints imposed in the optimization problem, nearly all of the terms in $\dot{W}_{rev}$ are constant (with respect to the decision variables in the optimization problem):

$$\begin{aligned}\dot{W}_{rev}=&\underbrace{\left(\dot{W}_{turb}-\dot{W}_{comp}+\dot{W}_{ST}-\dot{W}_{p,1}-\dot{W}_{p,2}-\sum_{i=1}^{7}\dot{W}_{comp,ref,i}\right)}_{\text{constrained to be equal to the total campus electricity demand}}\\&-\underbrace{\left(1-\frac{T_0}{T_{HWR}}\right)}_{\substack{\text{specified}\\\text{in optimization}\\\text{problem}}}\underbrace{\left(-\dot{Q}_H\right)}_{\substack{\text{constrained to be}\\\text{equal to the total}\\\text{campus hot water}\\\text{demand}}}-\sum_{i=1}^{7}\underbrace{\left(1-\frac{T_0}{T_{CHWR}}\right)}_{\substack{\text{specified}\\\text{in optimization}\\\text{problem}}}\underbrace{\dot{Q}_{C,i}}_{\substack{\text{constrained to be}\\\text{equal to the total}\\\text{campus cooling}\\\text{demand}}}\\&+\dot{m}_{g,exhaust}\psi_{g,exhaust}+\dot{m}_f\left(\mathrm{LHV}_{\mathrm{CH_4}}-\psi_f^{\mathrm{ch}}\right).\end{aligned} \tag{3.44}$$

However, in this case, there are two terms which are not: $\dot{m}_{g,exhaust}\psi_{g,exhaust}$ is the amount of flow exergy that exits the HRSG, and $\dot{m}_f\left(\mathrm{LHV}_{\mathrm{CH_4}}-\psi_f^{\mathrm{ch}}\right)$ is the difference between the flow exergy entering the combustor, $\dot{m}_f\psi_f^{\mathrm{ch}}$, and the amount of energy released during the combustion reaction, $\dot{m}_f\mathrm{LHV}_{\mathrm{CH_4}}$. It is possible for the three performance constraints to be met for different values of $\dot{m}_{g,exhaust}\psi_{g,exhaust}$ and $\dot{m}_f\left(\mathrm{LHV}_{\mathrm{CH_4}}-\psi_f^{\mathrm{ch}}\right)$, suggesting that minimizing exergy

destruction has the potential to provide a different solution than minimizing power consumption (in terms of mass flow rate of fuel) for the overall system. A comparison between EDM and energy consumption minimization for the CCHP system is presented in Section 3.7.

3.5.2 Reversible Power for Electric Chiller Bank

Although the reversible power for the overall CCHP system is not constant with respect to the optimization problem, we can re-examine the reversible power for individual subsystems. In particular, we will show that the reversible power is constant for the electric chiller bank and introduce the concept of interchangeability wherein the exergy destruction rate and power consumption can be combined within the same objective function to be minimized and yield the same solution as EDM.

The exergy destruction rate for the electric chiller bank was given in Eq. 3.38 and is restated here:

$$\dot{X}_{dest,CHW} = \sum_{i=1}^{7}\left(\left(1-\frac{T_0}{T_{CHWR}}\right)\dot{Q}_{C,i} + \dot{W}_{comp,ref,i}\right). \qquad (3.45)$$

The actual power consumed by the electric chiller bank is described by

$$\dot{W}_{CHW} = \sum_{i=1}^{7}\left(\dot{W}_{comp,ref,i}\right). \qquad (3.46)$$

Applying Eq. 2.8 to the electric chiller bank yields

$$\dot{W}_{rev,CHW} = -\sum_{i=1}^{7}\left(1-\frac{T_0}{T_{CWR}}\right)\dot{Q}_{C,i}\,. \qquad (3.47)$$

Therefore the EDM objective function for the CCHP system can be redefined as

$$J_{EDM-INT} = \sum_{k=1}^{24}\left(\dot{X}_{dest,GT}[k] + \dot{X}_{dest,HRSG}[k] + \dot{X}_{dest,SL}[k] + \underbrace{\dot{W}_{CHW}[k] - \dot{W}_{rev,CHW}[k]}_{\dot{X}_{dest,CHW}}\right) \qquad (3.48)$$

where $\dot{X}_{dest,CHW}$ has been replaced by $\dot{W}_{CHW} - \dot{W}_{rev,CHW}$. However,

$$J_{EDM-INT} = \left(\sum_{k=1}^{24}\dot{X}_{dest,GT}[k] + \dot{X}_{dest,HRSG}[k] + \dot{X}_{dest,SL}[k] + \dot{W}_{CHW}[k]\right) - C \qquad (3.49)$$

where

$$C = \sum_{k=1}^{24} \dot{W}_{rev,CHW}[k] \qquad (3.50)$$

is constant with respect to the optimization problem because T_0 and T_{CWR} are specified in the optimization problem and $\dot{Q}_{C,i}$ is constrained to equal the specified cooling demand at each hour. Note that this does not imply that $\dot{W}_{rev,CHW}$ is constant as a function of time.

In general, if, for two objective functions J_1 and J_2, $J_1 = J_2 - C$ where C is a real number, then

$$\mathbf{v}^* = \arg\min\left(J_1\right) = \arg\min\left(J_1 + C\right) = \arg\min\left(J_2\right). \qquad (3.51)$$

Therefore, solving an optimization problem using $J_{EDM\text{-}INT}$ or J_{EDM} will yield the same solution. We call this additional layer of flexibility the 'interchangeability' between EDM and power minimization. While the equivalence between EDM and power minimization for certain systems has been described in [27], here we show that it can be used for individual subsystems in an optimization problem for a larger system comprised of many subsystems, some of which may need to be characterized in terms of exergy destruction rate as opposed to power consumption.

In Section 3.6, results characterizing the interchangeability of $\dot{X}_{dest,CHW}$ and $\dot{W}_{CHW}$ are presented.

3.6 EDM with Interchangeability

To demonstrate the interchangeability between power consumption and exergy destruction rate in the electric chiller bank, $J_{EDM\text{-}INT}$, given in Eq. 3.48, was used in place of Eq. 3.2 to find the optimal setpoints for the CCHP system. All model equations and constraints were identical to the case presented in Section 3.4. Figure 3.8 shows that the optimal setpoints for the power produced by the gas turbine, the fuel mass flow rate, and the fraction of steam used in the steam turbine, are identical between the two optimization problems (EDM and EDM with interchangeability). Moreover, the total power consumed by the electric chiller bank is also the same in both solutions.

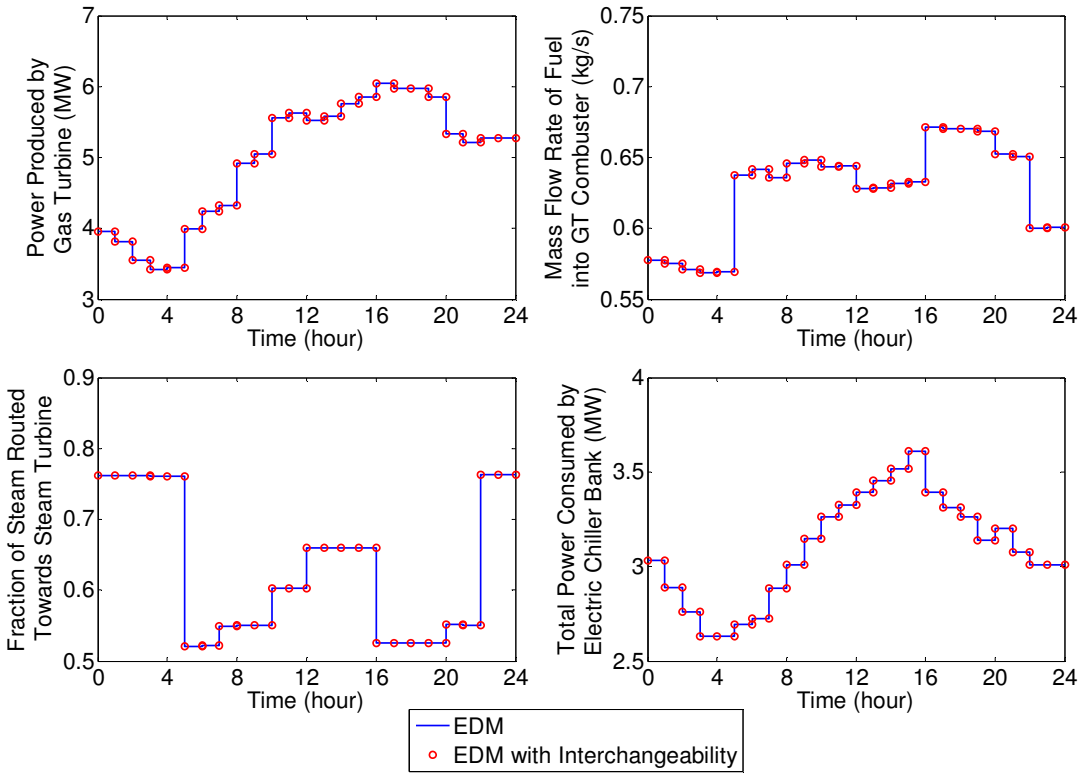

Figure 3.8: Optimal setpoints for $\dot{W}_{GT}$, $\dot{m}_f$, and f_1^s. Also pictured is the total power consumed by the electric chiller bank (lower right).

This feature is useful in simplifying the overall objective function for a particular IES by only requiring certain subsystems to be described in terms of their exergy destruction rate and allowing the others to be defined in terms of their power consumption (energy consumption rate) while still benefitting from an overall minimization of exergy destruction.

3.7 Comparison of EDM against Energy Consumption Minimization

In this section, comparisons are made between energy consumption minimization and exergy destruction minimization of the CCHP system. An energy consumption minimization of the CCHP system is defined as

$$J_{PM} = \sum_{k=1}^{24} \mathrm{LHV}_{\mathrm{CH_4}} \dot{m}_f[k] \cdot Ts \qquad (3.52)$$

where Ts = 3600 seconds and the subscript PM is used to denote energy consumption minimization. Again, the objective function can be simplified as

$$J_{PM} = \sum_{k=1}^{24} \mathrm{LHV}_{\mathrm{CH_4}} \dot{m}_f[k] \,. \qquad (3.53)$$

Two different cases based on η_{comp} (Eq. 3.4), η_{turb} (Eq. 3.12), and η_{ST} (Eq. 3.20), defined in Table 3.6, were considered to highlight the differences between the two optimization problems.

Table 3.6 Definitions of Case 1 and Case 2

	η_{comp}	η_{turb}	η_{ST}
Case 1	0.5	0.5	1.0
Case 2	1.0	1.0	0.5

The optimal solutions from the energy consumption minimization and the EDM for Case 1 are compared in the following figures.

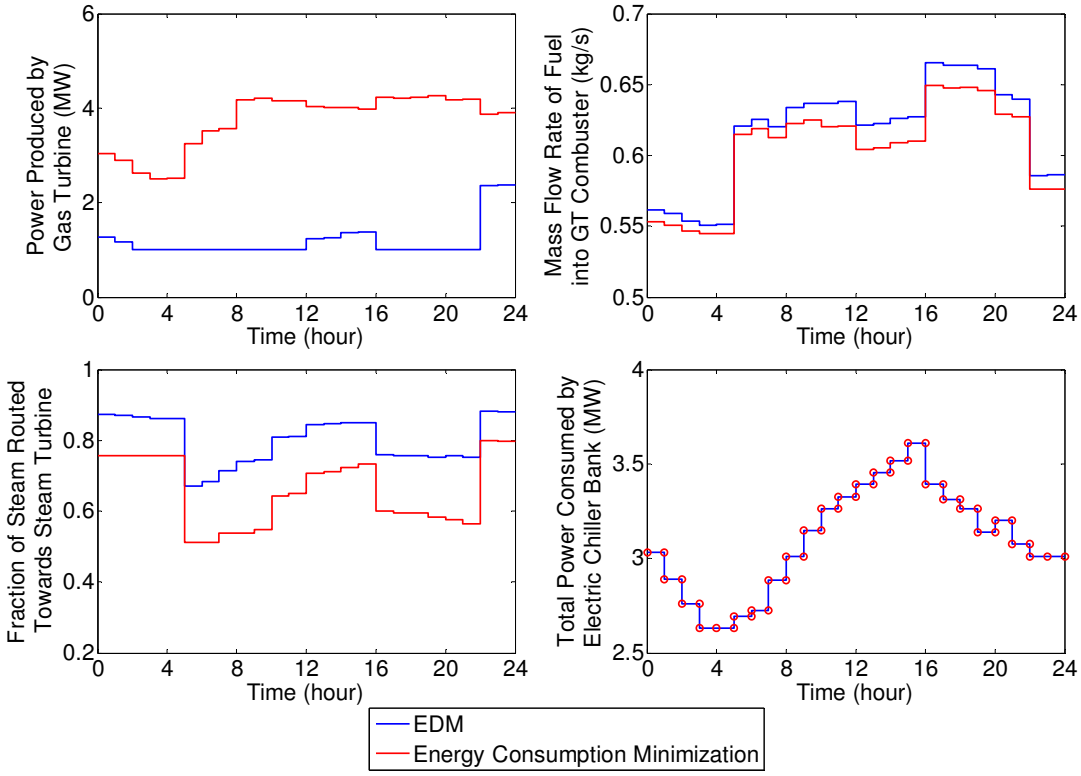

Figure 3.9: Optimal setpoints for $\dot{W}_{GT}$, $\dot{m}_f$, and f_1^s as produced by EDM and energy consumption minimization in Case 1. Also pictured is the total power consumed by the electric chiller bank (lower right) computed using the optimal solution of each optimization problem. Circle markers indicate that the two curves lie directly on top of one another

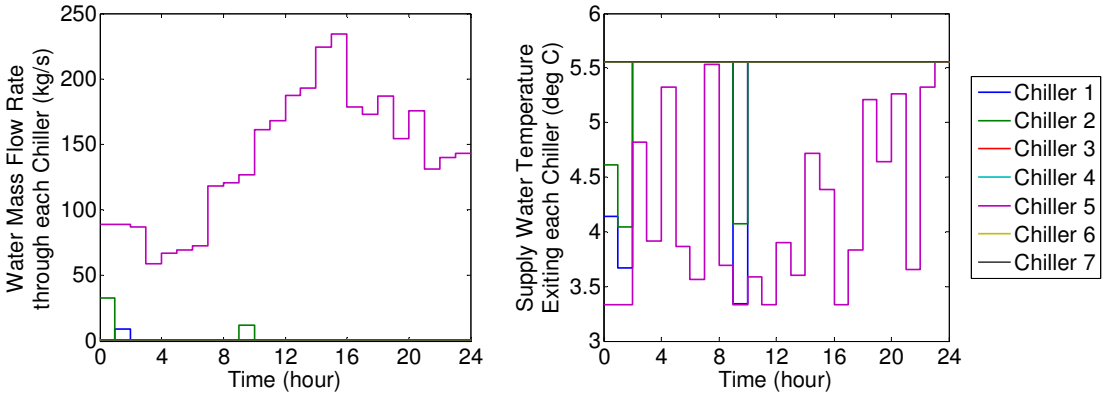

Figure 3.10: Optimal setpoints for $\dot{m}_{CHW,i}$ and $T_{CHWS,i}$, i={1,2,…,7}, using EDM in Case 1.

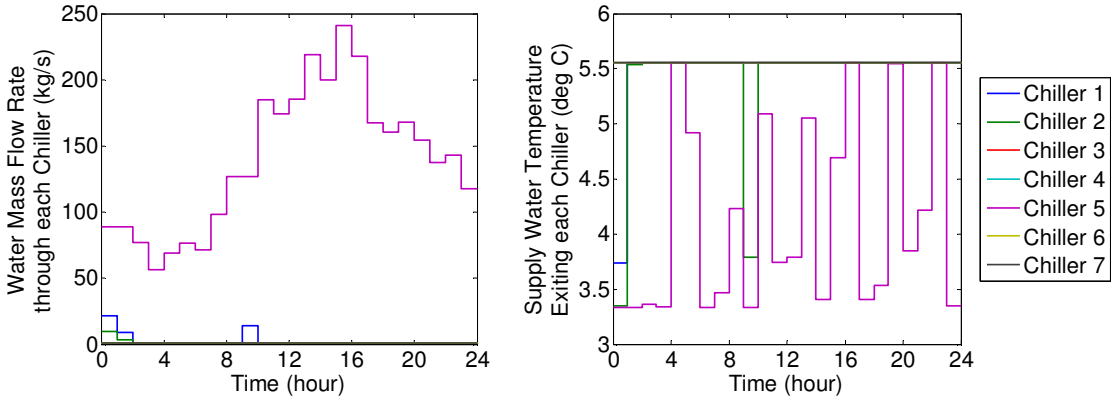

Figure 3.11: Optimal setpoints for $\dot{m}_{CHW,i}$ and $T_{CHWS,i}$, i={1,2,…,7}, using energy consumption minimization in Case 1.

Both objective functions, J_{EDM} and J_{PM}, were evaluated using the optimal solution from both the EDM and the energy consumption minimization. These results are shown in Table 3.7 where the percent difference is defined as

$$\%\ difference = 100 \times \frac{J\left(\mathbf{v}_{EDM}^{*}\right) - J\left(\mathbf{v}_{PM}^{*}\right)}{J\left(\mathbf{v}_{EDM}^{*}\right)} \ . \qquad (3.54)$$

Table 3.7 J_{EDM} and J_{PM} Evaluated Using Optimal Solutions from both EDM and PM in Case 1

Objective Function	Exergy Destruction Minimization (kW)	Energy Consumption Minimization (kW)	Percent Difference (%)
J_{EDM}	537,800	549420	-2.16
J_{PM}	739,940	725380	1.97

As expected, in Case 1, the EDM outperformed the energy consumption minimization with respect to exergy destruction whereas the energy consumption minimization outperformed the EDM with respect to energy consumption. Figure 3.9 shows that the EDM significantly favored producing power with the steam turbine over the gas turbine by choosing to operate the gas turbine at its lower bound of 1MW for a large portion of the 24-hour time horizon. This is consistent with the fact that the steam turbine was designed to be significantly more efficient than the gas turbine in Case 1. The effects of the difference between η_{comp}, η_{turb}, and η_{ST} manifest themselves explicitly in J_{EDM} via the terms $\dot{X}_{dest,GT}$ and $\dot{X}_{dest,SL}$. As mentioned in Chapter 2, these

two terms are naturally weighted against one another because they describe the same physical quantity, rate of exergy destruction, for two interacting systems. In J_{PM} the effects of the difference between η_{comp}, η_{turb}, and η_{ST} only manifest themselves through the equality constraints to meet the specified cooling, heating, and electricity demands.

Next we compare energy consumption minimization and EDM when the gas turbine is significantly more efficient than the steam turbine (described as Case 2 in Table 3.6).

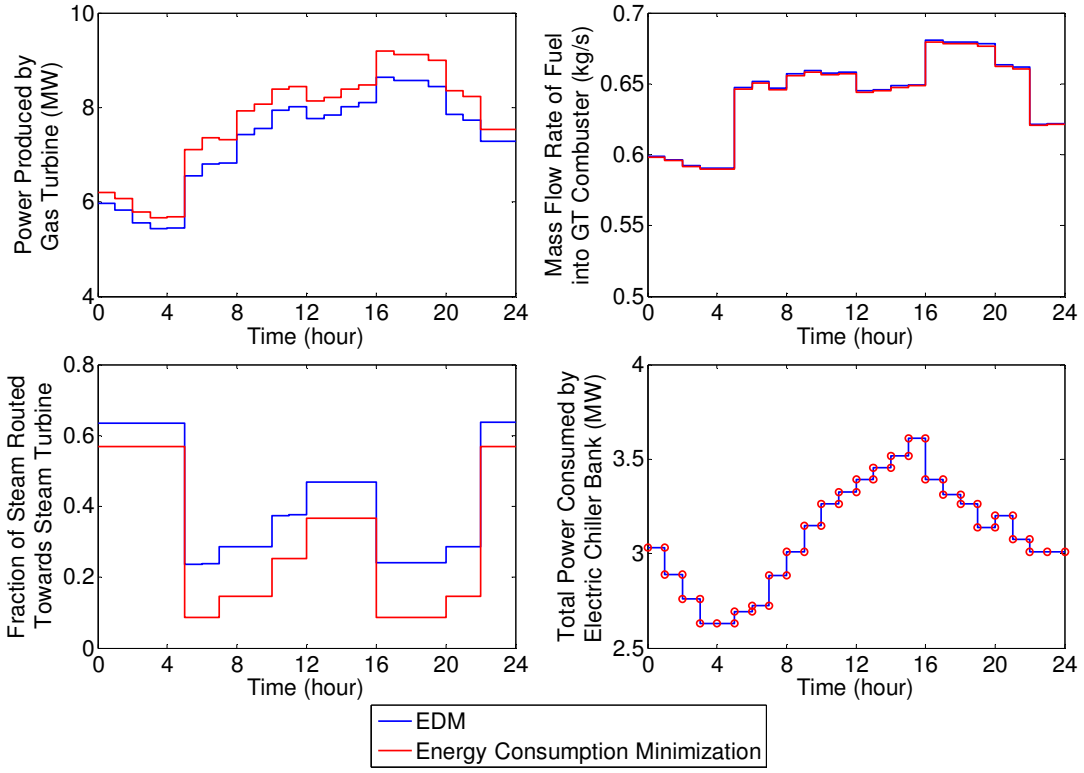

Figure 3.12: Optimal setpoints for $\dot{W}_{GT}$, $\dot{m}_f$, and f_1^s as produced by EDM and energy consumption minimization in Case 2. Also pictured is the total power consumed by the electric chiller bank (lower right) computed using the optimal solution of each optimization problem. Circle markers indicate that the two curves lie directly on top of one another.

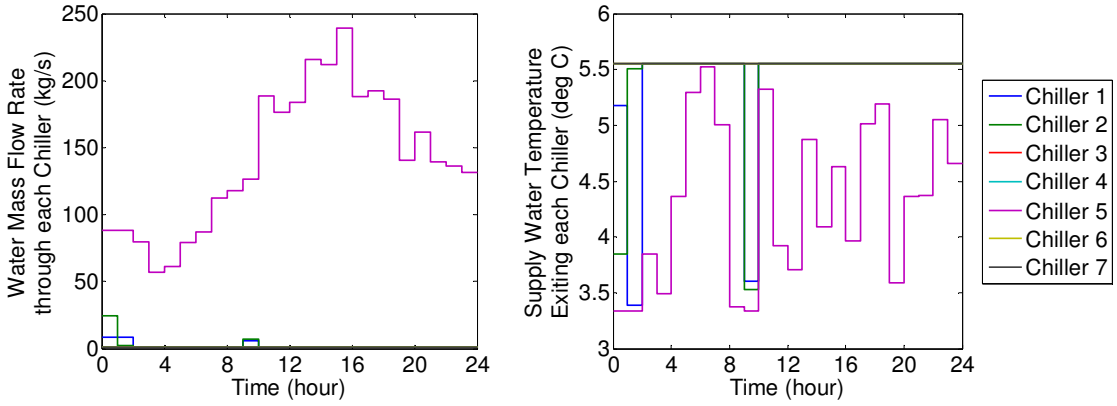

Figure 3.13: Optimal setpoints for $\dot{m}_{CHW,i}$ and $T_{CHWS,i}$, i={1,2,…,7}, using EDM in Case 2.

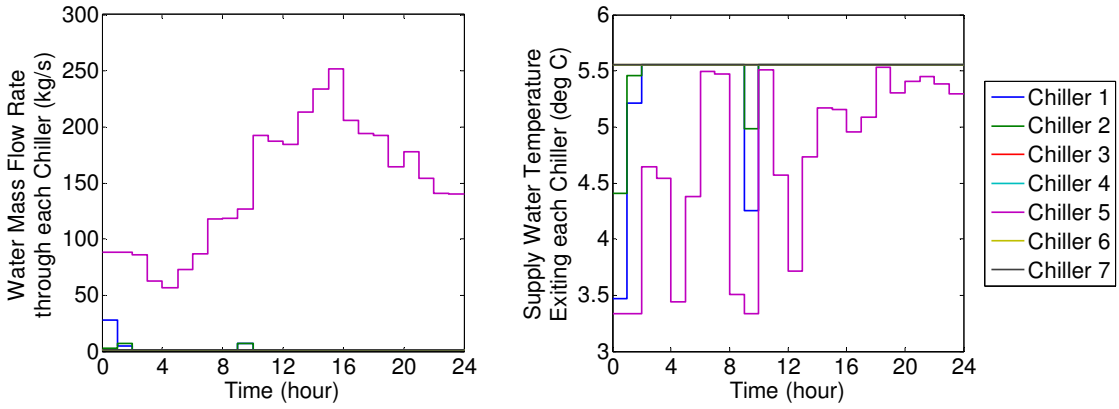

Figure 3.14: Optimal setpoints for $\dot{m}_{CHW,i}$ and $T_{CHWS,i}$, i={1,2,…,7}, using energy consumption minimization in Case 2.

Table 3.8 J_{EDM} and J_{PM} Evaluated Using Optimal Solutions from both EDM and PM in Case 2

Objective Function	Exergy Destruction Minimization (kW)	Energy Consumption Minimization (kW)	Percent Difference (%)
J_{EDM}	554,310	555380	-0.19
J_{PM}	771,380	770220	0.15

In Case 2, the solutions of the two optimization problems resulted in similar amounts of energy consumption and exergy destruction over the 24 hour time horizon. Moreover, the gas turbine and steam turbine were utilized in similar ways, although the EDM slightly favored the steam turbine over the gas turbine. It is important to note that the EDM made significantly

different decisions in response to the change in efficiencies from Case 1 to Case 2 whereas the energy consumption minimization did not do so.

The results of the two cases indicate that there are specific tradeoffs being made with respect to using EDM versus energy consumption minimization. In Case 1, the EDM was able to find a solution which destroyed about 2% less exergy as compared to the energy consumption minimization by specifically utilizing the steam turbine which had an isentropic efficiency of 1 as compared to the gas turbine isentropic efficiency of 0.5. In Case 2, where the quantitative tradeoff in exergy destruction and energy consumption was small between EDM and energy consumption minimization, the optimal solutions still chose to operate the gas turbine and steam turbine differently. This may have implications on additional optimization objectives, such as equipment wear, which can be alleviated if a system is operated with fewer irreversible losses such as friction.

3.8 Summary

In this chapter, exergy destruction minimization was used for setpoint optimization of a CCHP system for varying demand profiles. The differences between exergy destruction rate minimization and power minimization were characterized in the context of the reversible power. When the reversible power is not constant with respect to decision variables, the results presented in this chapter highlight that EDM offers an interesting alternative to energy consumption minimization, in the context of setpoint optimization, where the tradeoff between exergy destruction and energy consumption results in a different operation of individual components and/or subsystems. When the reversible power is constant (with respect to decision variables), the interchangeability between the exergy destruction rate and power consumption indicates that EDM will both minimize exergy destruction and energy consumption. Therefore, exergy destruction, as a minimization metric, expands the solution spaces typically considered in the operational optimization of IESs.

Chapter 4
EDM-Based Setpoint Optimization and Control of a VCC System

In this chapter, the exergy destruction minimization (EDM) framework outlined in Chapter 2 is applied to a vapor-compression cycle (VCC) system. After a brief introduction to VCC systems, a static setpoint optimization problem is formulated. In order to operate an experimental VCC system at the optimized setpoints, a feedforward plus feedback control approach is described and then implemented experimentally. The experimental results are also compared to design point operation of the same system to quantify how optimization and control of the VCC system can lead to improvements in efficiency.

4.1 Introduction to Vapor-Compression Cycle Systems

VCC systems are used to remove heat from a low-temperature (T_L) environment and reject it to a high-temperature (T_H) reservoir (typically ambient air). A standard VCC system contains four components – a compressor, a condenser, an expansion device, and an evaporator – and operates between high and low temperature reservoirs as shown in Figure 4.1.

The basic operation of a VCC system is as follows. Beginning at transition point 1, near-saturated refrigerant vapor is compressed to a higher temperature and pressure. The superheated refrigerant vapor enters the condenser at transition point 2 where it loses energy to ambient air (or another secondary fluid) passing over the condenser coil. The refrigerant leaves as a subcooled liquid and then enters an expansion device at transition point 3 (e.g. thermostatic expansion valve, electronic expansion valve, capillary tube, etc.) where it undergoes a rapid drop in pressure and temperature. At transition point 4, the refrigerant enters the evaporator as a two-

phase fluid and begins absorbing energy from air (or another secondary fluid) passing across the evaporator coil. The refrigerant leaves the evaporator as a superheated vapor and the cycle begins again at the inlet of the compressor.

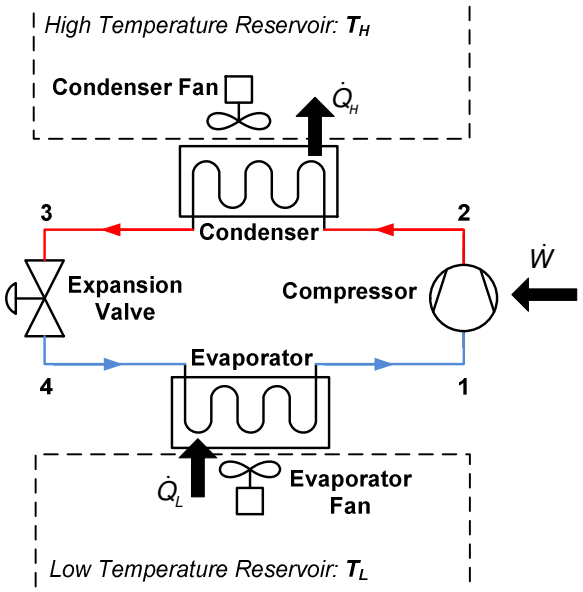

Figure 4.1: Schematic of a standard VCC system.

In the following sections, the thermodynamic cycle which governs the operation of VCC systems will be described in greater detail, along with standard first-law and second-law efficiency metrics for these systems.

4.1.1 Thermodynamic Cycles for Refrigeration

A standard refrigeration cycle consists of four processes acting on the refrigerant: compression (1 to 2), condensation (2 to 3), expansion (3 to 4), and evaporation (4 to 1), where 1, 2, 3, and 4 refer to the transition points of the cycle. The most efficient refrigeration cycle is the Carnot refrigeration cycle (CRC), shown in Figure 4.2, which assumes isentropic compression and expansion, and isothermal condensation and evaporation. Although a system governed by the CRC is not practically realizable, it provides a baseline for evaluating how "close to ideal" a real system is operating.

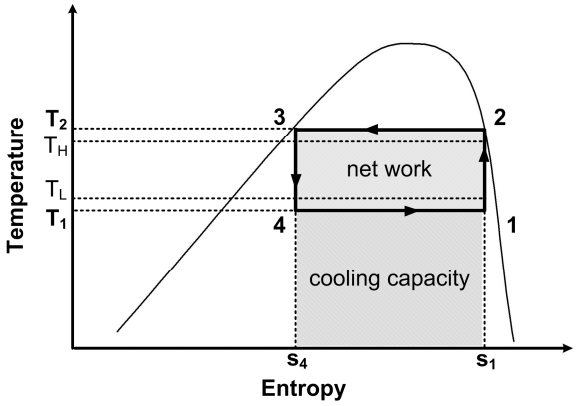

Figure 4.2: Temperature-entropy (*T*-*s*) diagram of the Carnot refrigeration cycle.

The standard vapor-compression cycle (VCC) is derived from the CRC. Since specific enthalpy is an important measurement in the VCC, the VCC is generally characterized on a pressure-enthalpy (*P*-*h*) diagram as shown in Figure 4.3.

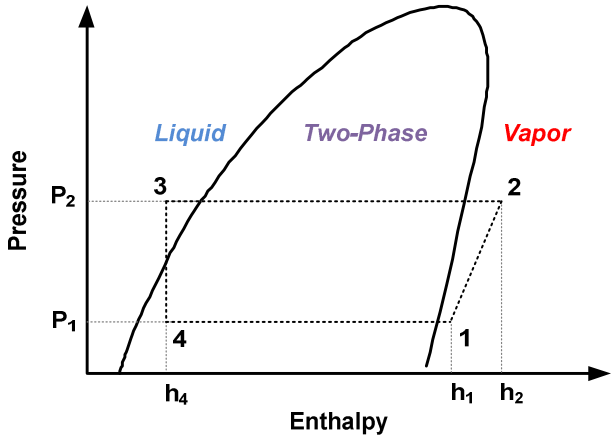

Figure 4.3: Pressure-enthalpy (*P*-*h*) diagram of a standard vapor-compression cycle.

The following assumptions on the refrigerant processes are made in the standard VCC:

1. isentropic compression ($s_1 = s_2$)
2. isobaric condensation ($P_2 = P_3$)
3. isenthalpic expansion ($h_3 = h_4$)
4. isobaric evaporation ($P_4 = P_1$)
5. evaporation of refrigerant to a superheated vapor state, ($T_1 > T_4$)
6. condensation of refrigerant to a subcooled liquid state ($T_{3,sat} > T_3$).

4.1.2 Efficiency Metrics

The standard first-law efficiency metric for refrigeration cycles is the coefficient of performance (COP). The COP for the CRC operating at steady-state, shown in Eq. 4.1, is solely a function of T_1 and T_2 [41] and is bounded above by virtue of Eq. 4.2 and Eq. 4.3 which maintain necessary temperature gradients during condensation and evaporation, respectively (see Figure 4.2). Recall that T_H is the ambient reservoir temperature and T_L is the temperature of the cooled environment. A higher COP corresponds to more efficient operation.

$$\mathrm{COP}_{Carnot} = \frac{\text{cooling capacity}}{\text{net work}} = \frac{T_1(s_1 - s_4)}{(T_2 - T_1)(s_1 - s_4)} = \frac{T_1}{T_2 - T_1} < \frac{T_L}{T_H - T_L} \tag{4.1}$$

$$T_2 > T_H \tag{4.2}$$

$$T_1 < T_L \tag{4.3}$$

The COP for the standard VCC operating at steady-state, given in Eq. 4.4, is bounded above by the Carnot COP [41].

$$\mathrm{COP} = \frac{\text{cooling capacity}}{\text{supplied power}} = \frac{\dot{Q}_L}{\dot{W}_{VCC}} = \frac{\dot{m}_r(h_1 - h_4)}{\dot{m}_r(h_2 - h_1)} < \mathrm{COP}_{Carnot} < \frac{T_L}{T_H - T_L} \tag{4.4}$$

Interestingly, the greatest upper bound of the COP, $T_L/(T_H - T_L)$, is solely dependent on the high and low reservoir temperatures rather than on any *physical* design parameters of a particular VCC system itself.

An additional metric, the second law or exergetic efficiency, defined earlier in Chapter 2, provides a more complete measure of the efficiency of the VCC. Intuitively, η_{II} is a measure of how effectively the exergy supplied to a system, in this case work done on the system by the compressor, is used. Unlike COP, the exergetic efficiency is defined such that $\eta_{II} \in [0,1]$ thereby making it consistent with the way in which most efficiencies are defined.

$$0 \le \eta_{\mathrm{II}} = \left\{1 - \frac{\text{exergy destroyed}}{\text{exergy supplied}}\right\} = \left\{1 - \frac{\dot{X}_{dest,VCC}}{\dot{W}_{VCC}}\right\} < 1 \tag{4.5}$$

For a standard VCC system operating at steady-state, η_{II} can be described as a function of COP by substituting Eq. 4.12 into Eq. 4.5 and simplifying:

$$0 \leq \eta_{\text{II}} = \frac{\text{COP}}{\left(\frac{T_L}{T_H - T_L}\right)} < 1. \qquad (4.6)$$

4.1.3 Control of VCC Systems

Electronic actuators, such as variable-speed compressors, electronic expansion valves (EEVs), and variable-speed fans, have long been advocated as integral to improving the efficiency of VCC systems [42] [43] [44]. Moreover, these actuators provide the control engineer with access to the various degrees of freedom (DOFs) of the system and consequently, the ability to operate the system without cycling the compressor. Therefore, there is significant potential for improving the partial-load operational efficiency of any given VCC system through optimization and control of these available DOFs.

Conducting a setpoint optimization relies on an understanding of the DOFs which are available to be optimized. As will be discussed in Section 4.2.1, the standard VCC has five optimization DOFs. However, research in setpoint optimization of VCC system operation has been characterized by the number of DOFs being constrained a priori [45] [46] [47]. In this chapter, we are specifically interested in considering all available DOFs of the VCC system.

Finally, beyond the optimization of operation setpoints, a control framework is necessary to ensure that the system does indeed operate optimally. The typical choice of feedback control variables for VCC systems are evaporator refrigerant pressure or saturation temperature, and evaporator superheat, controlled by the compressor and EEV, respectively [44] [48] [49] [50]. However, this particular choice of input-output control variables is rooted in the legacy of mechanical control of VCC systems. Before the advent of electronic control, mechanical control devices, such as the thermostatic expansion valve (TEV), were developed in which the sensor and actuator were mechanically coupled and only tunable manually offline. Today, with electronic sensing and actuation, the sensor and actuator are decoupled. In [51], the authors explored this flexibility and, using a different choice of input-output pairings for a standard VCC system, designed and implemented a decentralized controller which accurately tracked given reference commands. The control framework presented in this chapter is independent of a particular choice of input-output pairings, instead introducing a design variable Λ which allows

the user to specify his/her choice of input-output pairings for a particular system hardware configuration.

4.2 Optimization Problem Formulation

4.2.1 Determining the Decision Variables

Based on the constitutive relationships between pressure, temperature, entropy, etc., [16] the VCC has 8 thermodynamic degrees of freedom (DOFs) – two DOFs for each of the four transition points in the cycle. However, the four equality constraints (specified in the previous section) which arise from isentropic, isobaric, and isenthalpic assumptions constrain 4 of these DOFs. Therefore, the three specific enthalpies of the cycle, $\{h_1, h_2, h_3{=}h_4\}$, and any one of the following three quantities, $\{P_1, P_2, T_1\}$, uniquely define the remaining thermodynamic states at each of the transition points. Moreover, to actually compute critical quantities of interest, such as the amount of cooling that is achieved (Eq. 4.7) or the amount of power consumed by the compressor (Eq. 4.8), there is one additional DOF which must be considered: the refrigerant mass flow rate, $\dot{m}_r$. This DOF is a fluid dynamic variable, rather than a thermodynamic variable, and is not captured in the *P-h* diagram of the VCC.

$$\dot{Q}_L = \dot{m}_r(h_1 - h_4) \tag{4.7}$$

$$\dot{W}_{VCC} = \dot{W}_k = \dot{m}_r\left(h_2 - h_1\right) \tag{4.8}$$

4.2.2 Objective Function Development

For VCC system setpoint optimization, we will again consider two primary objectives: a performance objective and an efficiency objective. For a VCC system, the performance objective is to achieve some desired cooling capacity. Following the framework outlined in Chapter 2, the optimization problem will be formulated as an exergy destruction minimization (EDM) problem with the performance objective enforced as an equality constraint. Whereas in Chapter 3 the objective was to minimize the total exergy destroyed over a 24-hour time period, here we do not consider a time-varying performance objective. Therefore, the objective function J_{VCC} is defined as

$$J_{VCC} = \dot{X}_{dest,VCC} . \quad (4.9)$$

Since the VCC is a closed thermodynamic cycle, the exergy rate balance for a closed system (control mass) is used to derive an expression for the total rate of exergy destruction:

$$\frac{dX}{dt} = \sum_j \left(1 - \frac{T_0}{T_j}\right)\dot{Q}_j - \left(\dot{W} - P_0 \frac{dV}{dt}\right) + \dot{X}^{ch} - \dot{X}_{dest} . \quad (4.10)$$

During steady-state operation of the VCC system, the following simplifications can be made to Eq. 4.10:

$$\frac{\cancel{dX}}{\cancel{dt}} = \sum_j \left(1 - \frac{T_0}{T_j}\right)\dot{Q}_j - \left(\dot{W} - P_0 \frac{\cancel{dV}}{\cancel{dt}}\right) + \cancel{\dot{X}^{ch}} - \dot{X}_{dest} . \quad (4.11)$$

Moreover, by assuming the ambient temperature, T_H, is the reference temperature, T_0, Eq. 4.11 reduces to

$$\dot{X}_{dest,VCC} = -(-\dot{W}_{VCC}) + \left(1 - \frac{T_H}{T_L}\right)\dot{Q}_L \quad (4.12)$$

where T_j has been replaced by T_L. Equation 4.12 is evaluated with T_H and T_L in degrees Kelvin. Substituting Eq. 4.7 and Eq. 4.8 into Eq. 4.12 yields

$$\dot{X}_{dest,VCC} = \dot{m}_r (h_1 - h_4)\left(1 - \frac{T_H}{T_L}\right) + \dot{m}_r \left(h_2 - h_1\right) \geq 0 . \quad (4.13)$$

As discussed in Chapter 2, the exergy destruction rate is nonnegative by definition. Therefore, the theoretical minimum value of J_{VCC} is zero, and its solution is defined as

$$\mathbf{v}^* = \arg\min_{\mathbf{v}} \left(J_{VCC}\right) = \left(h_1^* \quad h_2^* \quad h_4^* \quad P_1^* \quad \dot{m}^*\right)^T \in \mathbb{R}^5 . \quad (4.14)$$

subject to a number of different constraints which will be defined in the next section.

4.2.3 Defining Constraints

There are a number of different constraints which need to be defined for this optimization problem. They include performance, thermodynamic, and design constraints, in addition to

upper and lower bound constraints on the individual decision variables. Each of these different constraints will be described in the following subsections.

4.2.3.1 Performance Constraint

In this optimization problem, the performance objective of achieving a desired cooling capacity is enforced as the following equality constraint:

$$C_{des} = \dot{Q}_L = \dot{m}_r (h_1 - h_4) . \quad (4.15)$$

Note that if some deviation away from the desired cooling capacity is allowed, the performance constraint can be defined as an inequality constraint of the form

$$\left| C_{des} - \dot{m}_r (h_1 - h_4) \right| \leq \gamma \quad (4.16)$$

where γ is the maximum allowable error between the desired and achieved cooling capacities.

4.2.3.2 Thermodynamic Constraints

The following thermodynamic constraints must be enforced in the optimization of a standard VCC system:

1. $h_1 < h_2$
2. $h_4 < h_1$
3. $T_1 < T_L$
4. $T_3 > T_H$
5. $T_1 - T_4 > 0$
6. $T_{3,sat} - T_3 > 0$

where $T_{3,sat}$ is the saturated refrigerant temperature at P_2. The first two constraints ensure that compression and evaporation, respectively, occur. The third and fourth constraints impose the correct temperature gradients during evaporation and condensation, respectively. Note that in the VCC, the refrigerant temperature at the outlet of the condenser is denoted T_3 whereas in the CRC it is T_2. The fifth constraint ensures that only refrigerant vapor is compressed. Finally, the sixth constraint ensures that only refrigerant liquid is expanded.

4.2.3.3 Design Constraints

The hardware in a particular VCC system constrains the setpoints achievable by that system when it is operated. The design constraints imposed by the two heat exchangers

(evaporator and condenser) as well as their corresponding fans are defined by the following inequalities:

$$\begin{aligned} \dot{Q}_L &\le \dot{Q}_{L,max} \\ \dot{m}_r(h_1 - h_4) &\le (UA)_{L,\max}(T_L - T_4) \ , \end{aligned} \qquad (4.17)$$

and

$$\begin{aligned} \dot{Q}_H &\le \dot{Q}_{H,max} \\ \dot{m}_r(h_2 - h_4) &\le (UA)_{H,\max}(T_3 - T_H) \ , \end{aligned} \qquad (4.18)$$

where $(UA)_{L,max}$ and $(UA)_{H,max}$ are the maximum overall heat transfer coefficients across the evaporator and condenser, respectively. These coefficients can be estimated using heat transfer correlations and a thermal resistance circuit as shown in Figure 4.4 [52]. In order to simplify the estimation of the maximum UA values for the evaporator and condenser, respectively, the following assumptions are made:

1. $\dot{m}_{a,e}$ and $\dot{m}_{a,c}$ are assumed to be their maximum possible values based on the design of the evaporator and condenser fans, respectively,
2. the refrigerant in each heat exchanger is entirely a two-phase fluid,
3. T_H and T_L are constant throughout the condenser and evaporator, respectively,
4. fin heat transfer is one-dimensional.

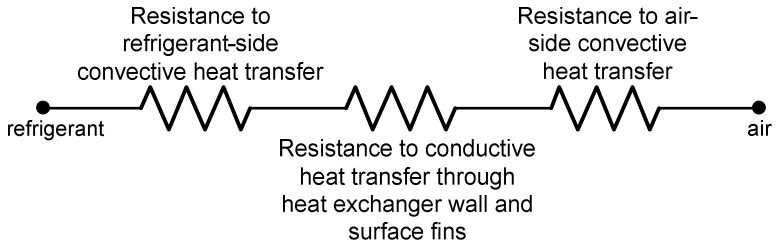

Figure 4.4: Thermal resistance circuit used to estimate overall heat transfer coefficients for the evaporator and condenser.

The correlations used to estimate the heat transfer coefficients α_r and α_a for the specific evaporator and condenser considered in the experimental case study are described in [53]. The fraction of the outer tube surface area covered by fins is denoted by F_a.

$$\frac{1}{UA} = \left(\frac{1}{\alpha_r A_i} + \frac{t}{kA_o(1-F_a)} + \frac{1}{\alpha_a A_o} \right) \quad (4.19)$$

4.2.3.4 Upper and Lower Bound Constraints

The final set of constraints which is enforced in the optimization problem consists of upper and lower bound constraints on the decision variables. The thermodynamic decision variables in the optimization of any VCC system will be bounded (above and below) by the fluid properties of the refrigerant used in that particular VCC system [54]. For the case study presented in this chapter, refrigerant R134a will be considered. The bound on the refrigerant mass flow rate, $\dot{m}_r$, is based on typical performance characteristics of R134a as reported in the ASHRAE Handbook [54] but will also depend on the physical hardware of the system being optimized.

Table 4.1: Upper and Lower Bound Constraints on Decision Variables for R134a

Decision Variable	Units	Lower Bound	Upper Bound
h_1	kJ/kg	220	350
h_2	kJ/kg	220	350
h_4	kJ/kg	20	220
P_1	kPa	150	550
$\dot{m}_r$	kg/s	0.00	0.00611

4.3 Control Synthesis

In this section, we characterize the steady-state behavior of a standard VCC system and create a control framework for realizing the optimized operation setpoints on an actual VCC system.

The control inputs for a standard VCC system are the electronic expansion valve (EEV) aperture, a_v, the compressor speed, ω_k and the evaporator and condenser fan speeds, $\omega_{f,e}$ and $\omega_{f,c}$ respectively. It is assumed that the compressor, and evaporator and condenser fans, are variable-speed. The vector of control input variables, **u**, is defined as

$$\mathbf{u} = \begin{pmatrix} a_v & \omega_k & \omega_{f,e} & \omega_{f,c} \end{pmatrix}^T \in \mathbb{R}^4. \quad (4.20)$$

The four thermodynamic optimization variables, h_1, h_2, h_4, and P_1, are rewritten via constitutive relationships [16] in terms of an equivalent set of pressures and temperatures which can be measured on a physical system. Therefore, the vector of decision variables is redefined as

$$\mathbf{v} = \begin{pmatrix} P_1 & P_2 & T_1 & T_3 & \dot{m}_r \end{pmatrix}^T \in \mathbb{R}^5 \tag{4.21}$$

where

$$\mathbf{v}^* = \arg\min_{\mathbf{v}} \left(J_{VCC} \right) = \begin{pmatrix} P_1^* & P_2^* & T_1^* & T_3^* & \dot{m}_r^* \end{pmatrix}^T \in \mathbb{R}^5 . \tag{4.22}$$

The decision variables and the control inputs are related during steady-state operation of the standard VCC system by the following 9 equations:

$$\hat{K}_v = f_1(a_v, P_1, P_2), \tag{4.23}$$

$$\hat{\eta}_{vol} = f_2(\omega_k, P_1, P_2), \tag{4.24}$$

$$\widehat{(UA)}_L = f_3(P_1, P_2, \dot{m}_r, \omega_{f,e}), \tag{4.25}$$

$$\widehat{(UA)}_H = f_4(P_2, \dot{m}_r, \omega_{f,c}), \tag{4.26}$$

$$\hat{\dot{Q}}_L = \widehat{(UA)}_L (T_L - T_4) = \dot{m}_r (h_1 - h_4), \tag{4.27}$$

$$\hat{\dot{Q}}_H = \widehat{(UA)}_H (T_3 - T_H) = \dot{m}_r (h_2 - h_4), \tag{4.28}$$

$$\hat{\dot{m}}_{r,v} = \hat{K}_v \sqrt{\rho_3 (P_2 - P_1)}, \tag{4.29}$$

$$\hat{\dot{m}}_{r,k} = \hat{\eta}_{vol} \delta_k \omega_k \rho_1, \tag{4.30}$$

$$\hat{\dot{m}}_{r,v} = \hat{\dot{m}}_{r,k}, \tag{4.31}$$

where K_v is the valve flow coefficient, η_{vol} is the compressor volumetric efficiency, and $(UA)_L$ and $(UA)_H$ are the overall heat transfer coefficients [52] at the low and high temperature reservoirs, respectively. The functions f_i, i={1,2,3,4} are empirically-derived nonlinear relationships; additional details are provided in [53].

Once $\mathbf{v}^*$ has been determined, $\hat{\mathbf{u}}^*$ can be determined by iteratively solving Eqs. 4.23 – 4.31. The hat notation is used to denote that $\hat{\mathbf{u}}^*$ is obtained based on the functions f_i, i={1,2,3,4} which have some associated uncertainty, defined as

$$\left| K_v - \hat{K}_v \right| = \tilde{K}_v \geq 0, \tag{4.32}$$

$$| \eta_{vol} - \hat{\eta}_{vol} | = \tilde{\eta}_{vol} \geq 0, \tag{4.33}$$

$$| (UA)_L - \widehat{(UA)}_L | = \widetilde{(UA)}_L \geq 0, \tag{4.34}$$

and

$$| (UA)_H - \widehat{(UA)}_H | = \widetilde{(UA)}_H \geq 0. \tag{4.35}$$

This uncertainty is further propagated to the calculation of $\hat{\dot{Q}}_L$, $\hat{\dot{Q}}_H$, $\hat{\dot{m}}_{r,v}$, and $\hat{\dot{m}}_{r,k}$. If the model uncertainty in Eq. 4.32 - 4.35 is zero, then $\hat{\mathbf{u}}^* = \mathbf{u}^*$, where $\mathbf{u}^*$ is the actual input vector required to achieve operation at the optimal set points, $\mathbf{v}^*$. Therefore, the elements of $\hat{\mathbf{u}}^*$ are analogous to model-based feedforward control input signals, denoted as $\mathbf{u}_{FF}$ in Figure 4.5.

However, when the model uncertainty is nonzero,

$$\mathbf{u}^* - \hat{\mathbf{u}}^* = \tilde{\mathbf{u}} \geq 0. \tag{4.36}$$

One method for compensating for $\tilde{\mathbf{u}}$ is through the use of feedback control. Even with some amount of model uncertainty, the feedforward control input signals, which are computed using *nonlinear* static models, move the system near the operation setpoints specified by $\mathbf{v}^*$. This allows for a *linear* feedback controller to locally augment the feedforward control input signals so that operation at $\mathbf{v}^*$ is achieved.

However, as a consequence of the fluid dynamics of the EEV, compressor, and heat exchanger fans, there are 5 optimization DOFs but only 4 control DOFs in a standard VCC system. As long as u_1 and u_2 and any two of the following three variables, $\{P_1, P_2, \dot{m}_r\}$, are specified, the third variable will be constrained by Eq. 4.29 – 4.31. Instead, one must project $\mathbf{v} \in \mathbb{R}^5$ from the 5-dimensional optimization space onto the 4-dimensional control space, resulting in a new vector $\mathbf{y} \in \mathbb{R}^4$ that is some linear combination of the original optimization variables:

$$\mathbf{y} = \Lambda \mathbf{v} \ . \qquad (4.37)$$

The matrix $\Lambda \in \mathbb{R}^{4\times5}$ in Eq. 4.37 is a design variable that can be chosen based on a variety of factors, including sensor cost, sensor accuracy, or sensitivities in the nonlinear empirically-derived functions f_i, i={1,2,3,4}. A schematic of the complete optimization and control architecture is shown in Figure 4.5.

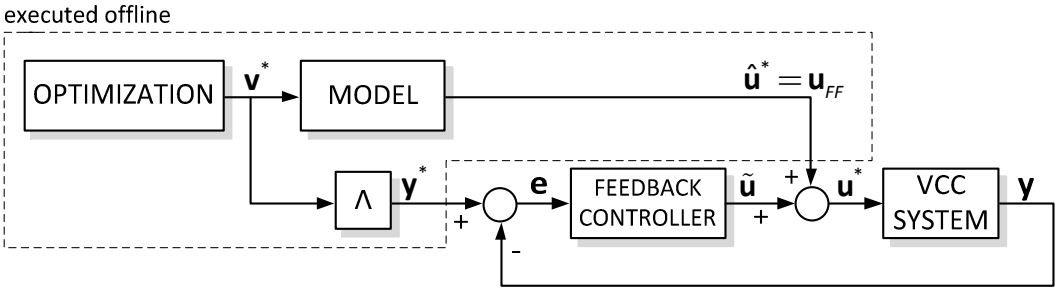

Figure 4.5: Schematic of feedforward plus feedback optimization and control architecture.

4.4 Experimental Case Study

The previous section described a feedforward plus feedback control framework to be used for operating a VCC system at an optimal choice of operation setpoints as determined by EDM. To validate the efficacy of this approach, an experimental case study will be presented in which the objective is to track the cooling load profile shown in Figure 4.6. The load profile begins with a desired capacity of 0.70kW (Case 1) and then increases to 0.85kW (Case 2).

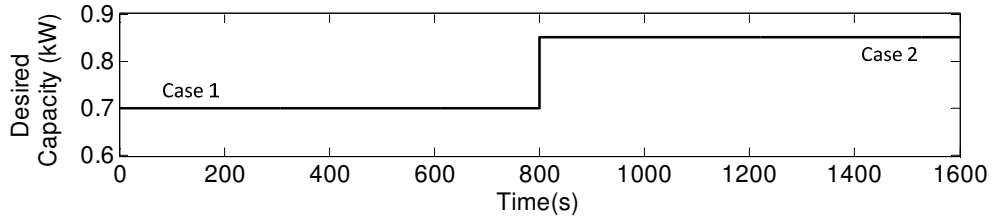

Figure 4.6: Cooling capacity load profile.

The experimental system considered in this case study contains a receiver tank at the outlet of the condenser, thereby constraining the condenser outlet refrigerant condition to be saturated liquid (Eq. 4.38).

$$T_3 = T_{3,sat} \qquad (4.38)$$

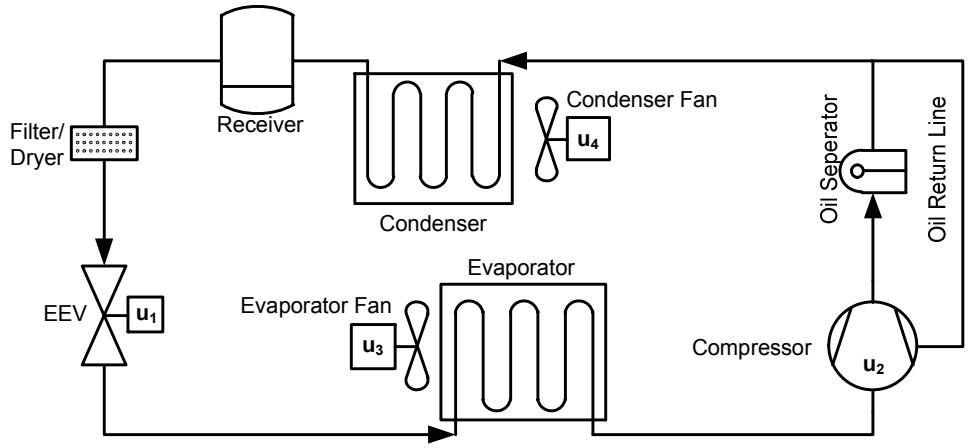

Figure 4.7: Schematic of experimental system.

Furthermore, for clarity of exposition, we assume that the heat transfer across each heat exchanger is maximized. This is equivalent to imposing the following constraints:

$$\begin{aligned} \dot{Q}_{L,max} &= \dot{Q}_L \\ (UA)_{L,max}(T_L - T_4) &= \dot{m}_r(h_1 - h_4) \ , \end{aligned} \qquad (4.39)$$

$$\begin{aligned} \dot{Q}_{H,max} &= \dot{Q}_H \\ (UA)_{H,max}(T_3 - T_H) &= \dot{m}_r(h_2 - h_4) \ . \end{aligned} \qquad (4.40)$$

From a control perspective, these constraints are satisfied by operating the evaporator and condenser fans, respectively, at their maximum fan speed such that the overall heat transfer coefficients of the evaporator and condenser, $(UA)_L$ and $(UA)_H$, are maximized. Therefore, the control space is constrained to be 2-dimensional: $\mathbf{u} = \begin{pmatrix} a_v & \omega_k \end{pmatrix}^T$

4.4.1 Offline Setpoint Optimization

Two separate static setpoint optimization problems were solved to determine the optimal setpoints at each of the two desired cooling capacities. In each optimization problem, the values of the high and low temperature reservoirs were specified as T_H = 24°C and T_L = 12°C. The function *fmincon* in the MATLAB Optimization Toolbox [40] was used to solve each optimization problem with an interior-point search algorithm. The optimal operation setpoints are presented in Table 4.2.

Table 4.2 Optimal Setpoints for Steady-State Operation

Decision Variable	Units	Desired Cooling Capacity	
		Case 1: 0.7kW	Case 2: 0.85 kW
P_1	kPa	265	239
P_2	kPa	837	887
T_1	°C	3.35	0.214
T_3	°C	32.9	35.0
$\dot{m}_r$	kg/s	0.00449	0.00565

The feedforward control inputs were determined by iteratively solving Eqs. 4.23 - 4.31 and are shown in Table 4.3. The empirical models for K_v and η_{vol} for the particular EEV and compressor on the experimental system are described in Appendix A. The feedforward control inputs for $u_3 = \omega_{f,e}$ and $u_4 = \omega_{f,c}$ are constrained to their maximum possible values.

Table 4.3 Model-based Feedforward Control Inputs

Control Input	Units	Desired Cooling Capacity	
		Case 1: 0.7 kW	Case 2: 0.85 kW
$u_1 = a_v$	% open	9.5	11
$u_2 = \omega_k$	rpm	950	1300
$u_3 = \omega_{f,e}$	% of max rpm	100	100
$u_4 = \omega_{f,c}$	% of max rpm	100	100

4.4.2 Feedback Control Design

By virtue of the constraints described by Eqs. 4.38 – 4.40, only two variables in $\mathbf{v}$ can be independently controlled. Therefore, $\mathbf{v} \in \mathbb{R}^5$ will be projected onto $\mathbf{y} \in \mathbb{R}^2$. The particular choice of Λ, shown in Eq. 4.41, was based on the superior time response and accuracy of pressure transducers as compared to that of thermocouples and mass flow sensors on the experimental system considered in this case study.

$$\mathbf{y} = \begin{pmatrix} y_1 \\ y_2 \end{pmatrix} = \begin{pmatrix} 0.5 & 0.5 & 0 & 0 & 0 \\ -1 & 1 & 0 & 0 & 0 \end{pmatrix} \begin{pmatrix} P_1 \\ P_2 \\ T_1 \\ T_3 \\ \dot{m}_r \end{pmatrix} \tag{4.41}$$

A feedback controller will be used to compensate for $\tilde{\mathbf{u}} = \mathbf{u}^* - \mathbf{u}_{FF}$ to regulate $\mathbf{y}$. The desire to regulate the system to optimal operation setpoints with minimal root-mean-square (RMS) error leads to the choice of a 2-norm based optimal controller such as a linear quadratic regulator (LQR). However, this is just one of many possible feedback controllers that could be used here.

A standard prediction error/maximum likelihood system identification (ID) algorithm in the MATLAB System ID Toolbox [55] was used to identify a second-order, 2-input 2-output linear state space mapping between $\mathbf{u}$ and $\mathbf{y}$. Details of the identification are given in Appendix B. Since the identified system order is the same as the number of inputs and outputs, the original state space realization of the plant (given in Eq. B.6 in Appendix B) is transformed by replacing $\mathbf{x}$ with $\bar{\mathbf{C}}^{-1}\bar{\mathbf{y}}$, as shown in Eq. 4.42, such that the output vector, $\bar{\mathbf{y}}$ is the new state vector of the system. Note that $\bar{\mathbf{y}}$ and $\bar{\mathbf{u}}$ represent scaled vectors; $\mathbf{x}$ was not scaled during the system ID process. Moreover, all variables represent deviation variables from a nominal operation condition.

$$\begin{gathered} \dot{\bar{\mathbf{y}}} = \tilde{\mathbf{A}}\bar{\mathbf{y}} + \tilde{\mathbf{B}}\bar{\mathbf{u}} \\ \bar{\mathbf{y}} = \tilde{\mathbf{C}}\bar{\mathbf{y}} \\ \tilde{\mathbf{A}} = \bar{\mathbf{C}}\bar{\mathbf{A}}\bar{\mathbf{C}}^{-1},\ \tilde{\mathbf{B}} = \bar{\mathbf{C}}\bar{\mathbf{B}},\ \tilde{\mathbf{C}} = \mathbf{I}_2 \end{gathered} \tag{4.42}$$

The original system is Type 0 and will therefore only track step reference inputs with a non-zero static error constant [56]. Consequently, the scaled identified plant model is augmented with 2 integrators to ensure zero steady-state error when the system is required to track step references, as shown in Eq. 4.43, where $\bar{\mathbf{e}} \in \mathbb{R}^2$ represents the tracking error, $\bar{\mathbf{z}} \in \mathbb{R}^2$ represents the additional integrator states, and $\bar{\mathbf{u}} \in \mathbb{R}^4$ represents the input vector.

$$\begin{pmatrix} \dot{\bar{\mathbf{e}}} \\ \dot{\bar{\mathbf{z}}} \end{pmatrix} = \begin{pmatrix} \tilde{\mathbf{A}} & 0 \\ \mathbf{I} & 0 \end{pmatrix} \begin{pmatrix} \bar{\mathbf{e}} \\ \bar{\mathbf{z}} \end{pmatrix} + \begin{pmatrix} \tilde{\mathbf{B}} \\ 0 \end{pmatrix} \bar{\mathbf{u}} + \begin{pmatrix} \tilde{\mathbf{A}} \\ 0 \end{pmatrix} \bar{\mathbf{r}}$$
$$\bar{\mathbf{e}} = \bar{\mathbf{y}} - \bar{\mathbf{r}} \qquad . \qquad (4.43)$$
$$\dot{\bar{\mathbf{z}}} = \bar{\mathbf{e}}$$

The linear quadratic cost function, J_{LQR}, is shown in Eq. 4.44. The weighting matrices, $\mathbf{Q_I}$ and $\mathbf{Q_{II}}$, were tuned to improve the transient performance of the controller; $\mathbf{R}$ was tuned to ensure that the actuation did not cause excessive wear on the individual actuators (Eq. 4.45). The resulting gain matrix, $\mathbf{K}$, is given in Eq. 4.46.

$$J_{\mathrm{LQR}} = \int_0^\infty \left(\bar{\mathbf{e}}^{\mathrm{T}} \mathbf{Q_I} \bar{\mathbf{e}} + \bar{\mathbf{z}}^{\mathrm{T}} \mathbf{Q_{II}} \bar{\mathbf{z}} + \bar{\mathbf{u}}^{\mathrm{T}} \mathbf{R} \bar{\mathbf{u}} \right) dt \, . \qquad (4.44)$$

$$\mathbf{Q_I} = \begin{pmatrix} 50 & 0 \\ 0 & 50 \end{pmatrix}, \mathbf{Q_{II}} \begin{pmatrix} 2 & 0 \\ 0 & 1 \end{pmatrix}, \mathbf{R} = \begin{pmatrix} 250 & 0 \\ 0 & 200 \end{pmatrix}. \qquad (4.45)$$

$$\mathbf{K} = \begin{pmatrix} 4.49 & -0.794 & 0.0848 & -0.0202 \\ 3.02 & 3.27 & 0.0319 & 0.0670 \end{pmatrix}. \qquad (4.46)$$

4.4.3 Experimental Implementation

The feedforward plus feedback control architecture was implemented on the experimental VCC system to achieve operation at the optimal setpoints determined in the offline optimization in Section 4.4.1. Figure 4.8 shows the cooling capacity achieved on the system compared to the desired cooling capacity profile. Figure 4.9 shows the regulation of the optimized set points; recall that only linear combinations of P_1 and P_2 were regulated with the feedback controller based on the choice of Λ.

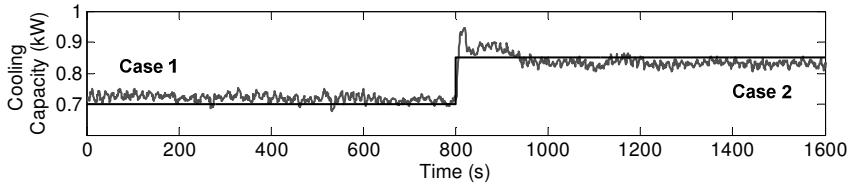

Figure 4.8: Cooling capacity achieved on experimental system.

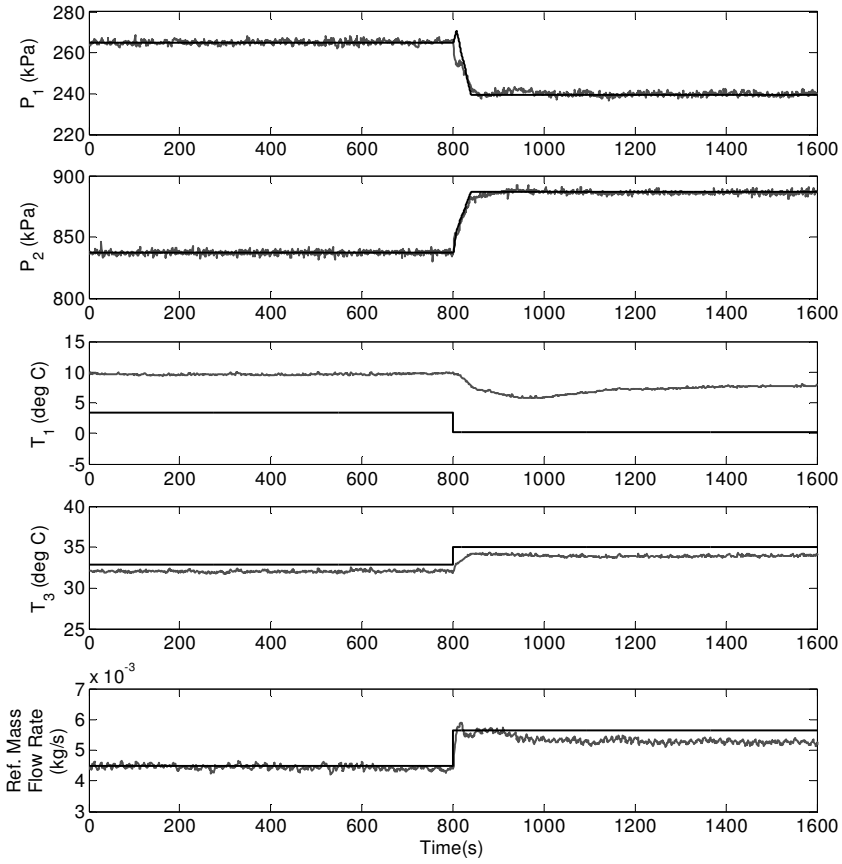

Figure 4.9: Optimized variables plotted as a function of time.

Figure 4.10 shows the control inputs of the feedback plus feedforward control architecture as compared to feedforward alone.

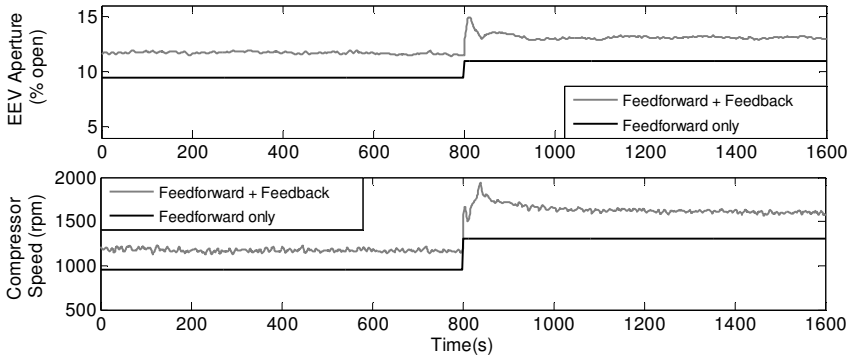

Figure 4.10: Control inputs plotted as a function of time.

4.4.4 Discussion

4.4.4.1 Comparison of Predicted and Experimental Results

The experimental results are quantitatively compared against the predicted optimal operation in Table 4.4 and Table 4.5 for Case 1 and Case 2, respectively. For each case, the experimental data was averaged to obtain the steady-state values shown below.

Table 4.4 Predicted versus Experimental Results: Case 1

	Units	Prediction	Experiment
Achieved Capacity	kW	0.700	0.720
P_1	kPa	265	265
P_2	kPa	837	837
T_1	°C	3.35	9.64
T_3	°C	32.9	32.1
$\dot{m}_r$	kg/s	0.00449	0.00444
COP	N/A	6.34	2.31
η_{II}	%	26.7	8.21
T_H	°C	24	24.8
T_L	°C	12	14.6

Table 4.5 Predicted versus Experimental Results: Case 2

	Units	Prediction	Experiment
Achieved Capacity	kW	0.850	0.830
P_1	kPa	239	241
P_2	kPa	887	885
T_1	°C	0.214	7.19
T_3	°C	35.0	33.9
$\dot{m}_r$	kg/s	0.00565	0.00533
COP	N/A	5.39	1.99
η_{II}	%	22.7	7.84
T_H	°C	24	24.9
T_L	°C	12	13.7

As expected, there is some discrepancy between the predicted optimal operation and the actual system operation due to differences between the static model equations and experimental system. Moreover, the exact temperatures of the high and low-temperature reservoirs (T_H and T_L) were not known during the offline optimization; the inputs used for the optimization were T_H = 24°C and T_L = 12°C whereas the actual values differed by 1–3°C (see Table 4.4 and Table 4.5).

Given that Λ was chosen so that linear combinations of P_1 and P_2 were regulated using a feedback controller, it is not surprising that the optimal values of P_1 and P_2 were achieved during operation of the experimental system. The largest error is observed between T_1 and T_1^* in both Case 1 and Case 2. This is a result of the model uncertainty and assumptions associated with the estimation of $(\widehat{UA})_{L,max}$. Finally, the discrepancy in the values of COP and η_{II} between the predicted optimal operation and actual operation of the system is due to the fact that in the offline optimization, the compressor isentropic efficiency was assumed to be 100% although in actuality, the isentropic efficiency is less than 100% and varies as a function of operating condition.

4.4.4.2 Comparison of Experimental Results against Design Point Operation

Despite the potential for discrepancy, the experimental results illustrate that there is a significant benefit to the approach being advocated here. Now we examine the results in the context of current industrial operation in which the operation set points are not optimized for varying cooling capacity but are instead chosen on or near the design point of the system.

In order to provide a reasonable condition for comparison, the experimental VCC system was operated as it might be if it were a commercial system - with a fixed speed chosen close to the maximum rated speed of the compressor and a constant evaporator superheat of 8°C, typically regulated via a TEV. This can be considered the most efficient the system would be operated in industry as it is near the design point of the system. A proportional-integral controller tuned for the experimental VCC system [57] was used to regulate evaporator superheat via an EEV, as shown in Figure 4.11, to mimic superheat regulation via a TEV. The compressor was operated at a fixed speed of 2000 rpm, and the evaporator and condenser fans were operated at 100% of their maximum speeds. The COP and second-law efficiency of the system operating at this condition are given in Table 4.6.

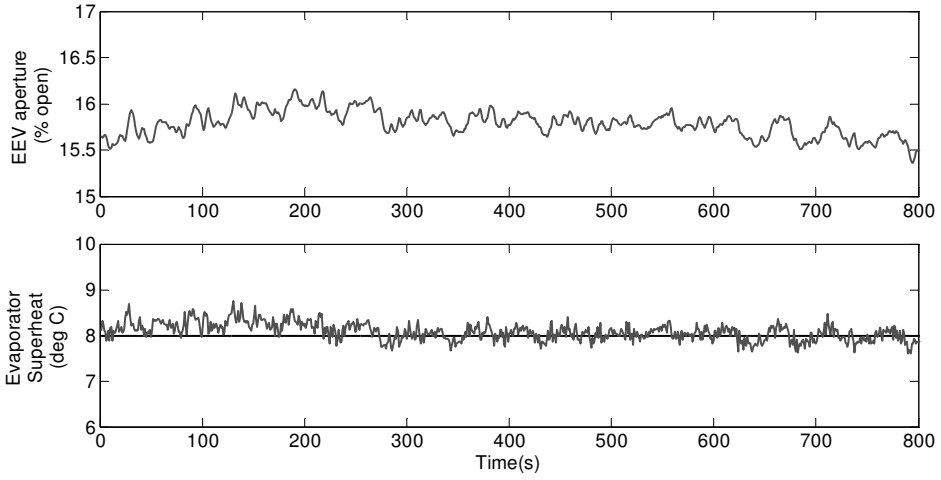

Figure 4.11: EEV control signal and evaporator superheat plotted as a function of time for ω_k = 2000 rpm.

In Case 1, the system was optimized to achieve 0.7kW of cooling capacity. The optimization results show a 25.5% increase in COP and a 5.80% increase in η_{II} over the system operating at its design point (Table 4.6). This demonstrates that when operated off the design

point, the system achieved a higher system efficiency with the use of optimized operation setpoints and flexible system control.

Table 4.6 Comparison of Optimization Case 1 with Design Point Operation

Parameter	Units	Design Point	Case 1	% Improvement
Achieved Capacity	kW	0.981	0.720	--
COP	N/A	1.84	2.31	25.5
η_{II}	%	7.76	8.21	5.80
T_H	°C	24.9	24.8	--
T_L	°C	12.8	14.6	--

In Case 2, the system was optimized to achieve 0.85 kW of cooling capacity, thereby operating closer to the design point of the system. Table 4.7 shows that when operated at optimized setpoints, an 8.15% increase in COP and a 1.03% increase in η_{II} were achieved. Therefore, even as the operation of the system approached the design point operating capacity, the optimized setpoints in conjunction with the feedforward plus feedback control scheme enabled more efficient operation of the system. However, as evidenced by the results in the two cases, the benefits are greater with greater deviation from the design point.

Table 4.7 Comparison of Optimization Case 2 with Design Point Operation

Parameter	Units	Design Point	Case 2	% Improvement
Achieved Capacity	kW	0.981	0.830	--
COP	N/A	1.84	1.99	8.15
η_{II}	%	7.76	7.84	1.03
T_H	°C	24.9	24.9	--
T_L	°C	12.8	13.7	--

These results highlight that optimization at the design stage alone is insufficient to ensure efficient operation of VCC systems. A particular feature of the exergy-based objective function is that it explicitly accounts for T_H and T_L, parameters that are often variable during system operation. Regardless of how optimally a system is designed to provide a given amount of cooling, conventional system design can only account for nominal values of T_H and T_L at best.

On the other hand, an optimization of the system that monitors environmental conditions and adjusts system operation will likely lead to more efficient operation.

Finally, it is important to recognize the role of control in achieving efficiency improvements during VCC system operation. The optimal operation setpoints can only be achieved through regulation of the optimized variables, highlighting a fundamental tradeoff in the control of VCC systems. While adding a variable frequency drive (VFD) to the compressor and fans, and/or replacing a TEV with an EEV, requires an initial monetary investment, an improvement in efficiency is then achievable. These results quantify, for steady-state operation, an increase in COP that is achievable in the case of multivariable control of the VCC via a variable-speed compressor and EEV. The results also provide concrete motivation for further research in developing optimization and control strategies which specifically utilize all available DOFs of the VCC.

Chapter 5
Optimal Control of a VCC System using EDM

In this chapter, exergy destruction minimization will be used to optimize the control inputs for a VCC system in an optimal control framework. First, a dynamic expression for the exergy destruction rate in a standard VCC system will be derived. Next, a finite-horizon optimal control problem is solved to determine the control input sequences which minimize the total exergy destroyed over the specified time horizon while tracking a desired cooling capacity reference trajectory. The results are compared to an energy consumption minimization over the same time horizon and highlight that the EDM chooses to actuate the system so as to consume more energy, but operate the system with significantly higher exergetic efficiency, than the energy consumption minimization.

5.1 Dynamic Modeling of VCC Systems

In order to use EDM with an optimal control algorithm, such as model predictive control, it is necessary to have a dynamic model of the system to be optimized. In a four component VCC system (compressor, condenser, expansion device, and evaporator), the compressor and expansion device are typically modeled statically because their dynamics are significantly faster than the dynamics of the heat exchangers. For dynamic modeling of the heat exchangers, two different approaches have been primarily used: a finite-volume approach and a lumped parameter moving boundary approach. Although commercial modeling packages such as e-Thermal [58], Modelica [59], and SINDA/FLUENT [60] use a discretized modeling approach for detailed and accurate models, this is done at the expense of model complexity, resulting in models that are not suitable for control design. In the lumped parameter moving boundary modeling approach, the heat exchanger is modeled with a fixed number of fluid regions (defined by fluid phase), and the

location of the boundary between each fluid region is a dynamic variable, allowing the length of the fluid regions to vary. Fluid properties such as temperature, density, etc., are lumped in each region, and an average is used for model computations. Although this approach results in some loss in accuracy, the resulting models are of low dynamic order, making them very well suited for control design. A review of the literature shows that this approach has been applied to a variety of VCC systems, often with variations in the details of the modeling approach [61].

The condenser and evaporator models that are used in this chapter are described in detail in [62] and [63]. For the purpose of control design in Section 5.3, the nonlinear models are linearized; see Appendix C for details.

5.2 Derivation of Dynamic Rate of Exergy Destruction

To develop a dynamic expression for the total rate of exergy destruction in a standard VCC system, it is necessary to consider each component individually as a control volume, as shown in Figure 5.1 . The total rate of exergy destruction in the VCC system (assuming a four-component system) is a sum of the rates of exergy destruction in each individual component:

$$\dot{X}_{dest,VCC} = \dot{X}_{dest,k} + \dot{X}_{dest,v} + \dot{X}_{dest,c} + \dot{X}_{dest,e}\,. \qquad (5.1)$$

Note that the evaporator and condenser fans are not considered in this analysis for the purpose of illustrative clarity. They could be added if needed, but the refrigerant-focused construct here is sufficient for illustrating the primary contributions of the EDM approach.

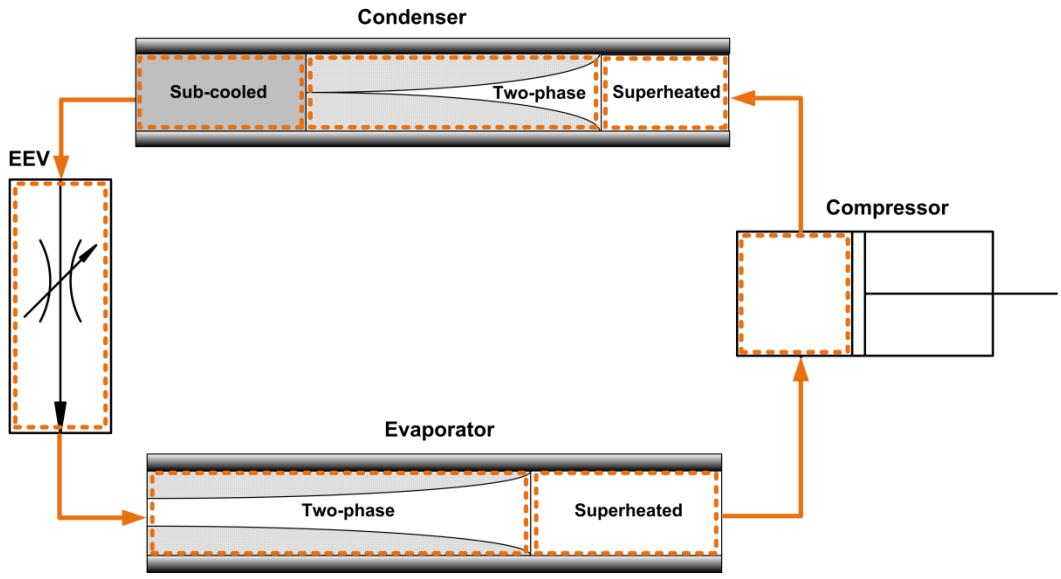

Figure 5.1: Schematic depicting control volumes drawn inside each component of the VCC system. Each control volume contains only the refrigerant flowing through that component.

As in Chapters 3 and 4, the following exergy rate balance can be applied to each component:

$$\frac{dX_{cv}}{dt} = \sum_j \left(1 - \frac{T_0}{T_j}\right)\dot{Q}_j - \left(\dot{W}_{cv} - P_0 \frac{dV_{cv}}{dt}\right) + \sum_i \dot{m}_i \psi_i - \sum_o \dot{m}_o \psi_o - \dot{X}_{dest} \qquad (5.2)$$

where $\dot{Q}_j$ is the heat transfer rate at the location on the control volume boundary where the instantaneous temperature is T_j. An alternative method for deriving the exergy destruction rate is to perform an entropy balance on the control volume using Eq. 5.3, solve for the rate of entropy generation, and then scale $\dot{S}_{gen}$ by the reference environment temperature, T_0, as shown in Eq. 5.4.

$$\frac{dS_{cv}}{dt} = \sum_j \frac{\dot{Q}_j}{T_j} + \sum_i \dot{m}_i s_i - \sum_o \dot{m}_o s_o + \dot{S}_{gen} \qquad (5.3)$$

$$\dot{X}_{dest} = T_0 \dot{S}_{gen} \qquad (5.4)$$

Since transient operation is being considered, the differentials $\frac{dX_{cv}}{dt}$ and $\frac{dV_{cv}}{dt}$ (Eq. 5.2) are no longer equal to zero. This increases the difficulty of finding a dynamic expression for the

exergy destruction rate of the system. However, *s*, specific entropy, is a thermodynamic property, whereas specific exergy is not. This suggests that it will be easier to find an expression for a differential in entropy, $\frac{dS_{cv}}{dt}$, rather than the differential in exergy. This will be described in more detail in Section 5.2.3.

In the following sections, the exergy destruction rate for each component in a standard VCC system will be derived. The reference temperature, T_0, for the exergy calculation is again assumed to be the temperature of the high-temperature reservoir (i.e. ambient environment), T_H.

5.2.1 Static Components

In VCC system modeling, both the compressor and expansion device, assumed here to be an electronic expansion valve (EEV), are typically modeled using quasi-steady assumptions. Therefore, the compressor and EEV control volumes can be analyzed assuming that they are operating at steady-state.

5.2.1.1 Compressor

The compressor is assumed to be adiabatic but not isentropic. Therefore, there is no exergy transfer by heat. A control volume is defined around the refrigerant inside the compressor; the inlet and outlet mass flow rates are equal to the refrigerant mass flow rate through the compressor. Assuming steady state operation, Eq. 5.2 reduces to

$$-\left(-\dot{W}_k\right)+\dot{m}_{r,k}\left(\psi_{k,i}-\psi_{k,o}\right)-\dot{X}_{dest,k}=0. \qquad (5.5)$$

Recall that the change in flow exergy between two states, denoted arbitrarily as 1 and 2 in Eq. 5.6, is given by

$$\psi_1-\psi_2=\left(h_1-h_2\right)-T_0\left(s_1-s_2\right)+\frac{v_1^2-v_2^2}{2}+g\left(z_1-z_2\right). \qquad (5.6)$$

The effects of kinetic and potential energy are assumed negligible. Substituting Eq. 5.6 into Eq. 5.5 and simplifying yields

$$\dot{X}_{dest,k}=-\left(-\dot{W}_k\right)+\dot{m}_{r,k}\left[\left(h_{k,ri}-h_{k,ro}\right)-T_H\left(s_{k,ri}-s_{k,ro}\right)\right]. \qquad (5.7)$$

Note that the work transfer rate term in Eq. 5.7 must be a positive quantity because if the compressor was isentropic, then the rate of exergy destruction would equal zero (and $h_{k,ri} - h_{k,ro}$ is a negative quantity). Therefore, we write $-\left(-\dot{W}_k\right)$ to emphasize the fact that the sign convention for work done *on* the system is negative (work done *by* the system is taken to be positive). The expression for $-\left(-\dot{W}_k\right)$ is

$$\dot{W}_k = \dot{m}_{r,k}\left(h_{k,ro} - h_{k,ri}\right). \qquad (5.8)$$

The rate of exergy destruction in the compressor is determined by substituting Eq. 5.8 into Eq. 5.7 and simplifying:

$$\dot{X}_{dest,k} = -T_H \dot{m}_{r,k}\left(s_{k,ri} - s_{k,ro}\right). \qquad (5.9)$$

5.2.1.2 Expansion Device

A control volume is defined around the refrigerant in the EEV, and the expansion of the refrigerant is assumed to be isenthalpic (i.e. $h_{v,ri} = h_{v,ro}$). There is only exergy transfer by mass transfer, and the inlet and outlet mass flow rates are equal to the refrigerant mass flow rate through the EEV. Assuming steady-state operation, Eq. 5.2 reduces to

$$\dot{m}_{r,v}\left(\psi_{v,i} - \psi_{v,o}\right) - \dot{X}_{dest,v} = 0. \qquad (5.10)$$

Again, the effects of kinetic and potential energy are considered negligible. Substituting Eq. 5.6 into Eq. 5.10 and simplifying results in the following expression for the exergy destruction rate through the valve:

$$\dot{X}_{dest,v} = -T_H \dot{m}_{r,v}\left(s_{v,ri} - s_{v,ro}\right). \qquad (5.11)$$

5.2.2 Dynamic Components

The remaining components are the two heat exchangers: the evaporator and the condenser. The dynamics of these components drive the overall dynamics of the cycle, and therefore dynamic rates of exergy destruction through each of these components will be derived.

5.2.2.1 Evaporator

In the lumped parameter moving boundary modeling approach, the evaporator is typically modeled with two fluid regions: a two-phase refrigerant fluid region and a superheated refrigerant fluid region. In this way, separate lumped parameters are used to estimate the fluid properties in each of the fluid regions, thereby improving the accuracy of the estimates. Similarly, two separate control volumes are used to derive the total exergy destruction rate through the evaporator as shown in Figure 5.2. Additional advantages of this multiple control volume approach will be discussed in Section 5.2.3.

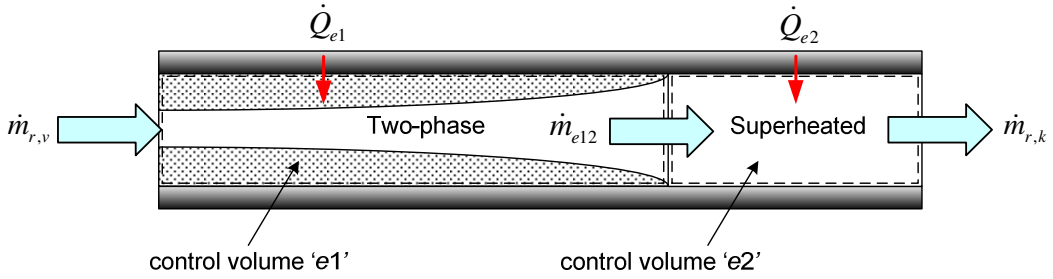

Figure 5.2: Individual control volumes drawn around each fluid region in an evaporator.

For the two-phase refrigerant fluid region, denoted by the subscript *e*1, Eq. 5.2 reduces to

$$\frac{dX_{e1}}{dt} = \left(1 - \frac{T_H}{T_{w,e1}}\right)\dot{Q}_{e1} + P_0\frac{dV_{e1}}{dt} + \dot{m}_{r,v}\left(h_{e,ri} - T_H s_{e,ri}\right) - \dot{m}_{e12}\left(h_{e,g} - T_H s_{e,g}\right) - \dot{X}_{dest,e1} \quad (5.12)$$

where T_j is replaced with $T_{w,e1}$, the lumped tube wall temperature in the two-phase fluid region, and $\dot{m}_{e12}$ is the refrigerant mass flow rate between the two control volumes pictured in Figure 5.2. Similarly, for the superheated refrigerant fluid region, denoted by the subscript *e2*, Eq. 5.2 reduces to

$$\frac{dX_{e2}}{dt} = \left(1 - \frac{T_H}{T_{w,e2}}\right)\dot{Q}_{e2} + P_0\frac{dV_{e2}}{dt} + \dot{m}_{e12}\left(h_{e,g} - T_H s_g\right) - \dot{m}_{r,k}\left(h_{e,ro} - T_H s_{e,ro}\right) - \dot{X}_{dest,e2} \quad (5.13)$$

where T_j is replaced with $T_{w,e2}$, the lumped tube wall temperature in the superheated fluid region. Applying superposition allows us to express $\dot{X}_{dest,e}$ as

$$\dot{X}_{dest,e} = \dot{X}_{dest,e1} + \dot{X}_{dest,e2}\,. \quad (5.14)$$

Therefore, the total exergy destruction rate through the evaporator is

$$\dot{X}_{dest,e} = \left(1-\frac{T_H}{T_{w,e1}}\right)\dot{Q}_{e1} + \left(1-\frac{T_H}{T_{w,e2}}\right)\dot{Q}_{e2} + P_0\left(\frac{dV_{e1}}{dt}+\frac{dV_{e2}}{dt}\right) + \dot{m}_{r,v}\left(h_{e,ri}-T_H s_{e,ri}\right) - \dot{m}_{r,k}\left(h_{e,ro}-T_H s_{e,ro}\right) - \left(\frac{dX_{e1}}{dt}+\frac{dX_{e2}}{dt}\right) \quad (5.15)$$

where it is assumed that

$$\begin{aligned}\dot{Q}_e &= \dot{Q}_{e1} + \dot{Q}_{e2} \\ &= (UA)_{e1}\left(T_{w,e1}-T_{r,e1}\right) + (UA)_{e2}\left(T_{w,e2}-T_{r,e2}\right)\ .\end{aligned} \quad (5.16)$$

In other words, it is assumed that there is no heat transfer between the refrigerant in control volume $e1$ and the refrigerant in control volume $e2$. In Eq. 5.16, $T_{r,e1}$ and $T_{r,e2}$ refer to the lumped refrigerant temperature in each fluid region, and $(UA)_{e1}$ and $(UA)_{e2}$ are the overall heat transfer coefficients between the refrigerant and tube wall in each fluid region.

As described earlier in this chapter, it is difficult to evaluate $\frac{dX_{cv}}{dt}$. Fortunately, the entropy rate balance (Eq. 5.3) can be used to derive an expression for the exergy destruction rate in terms of $\frac{dS_{cv}}{dt}$ instead of $\frac{dX_{cv}}{dt}$. Applying Eq. 5.3 to each control volume of the evaporator yields

$$\frac{dS_{e1}}{dt} = \frac{\dot{Q}_{e1}}{T_{w,e1}} + \left(\dot{m}_{r,v}s_{e,ri} - \dot{m}_{e12}s_{e,g}\right) + \dot{S}_{gen,e1}, \quad (5.17)$$

$$\frac{dS_{e2}}{dt} = \frac{\dot{Q}_{e2}}{T_{w,e2}} + \left(\dot{m}_{e12}s_{e,g} - \dot{m}_{r,k}s_{e,ro}\right) + \dot{S}_{gen,e2}, \quad (5.18)$$

where

$$\dot{S}_{gen,e} = \dot{S}_{gen,e1} + \dot{S}_{gen,e2}\,. \quad (5.19)$$

Substituting Eq. 5.17 and Eq. 5.18 into Eq. 5.19 and rearranging yields the following alternative expression for the exergy destruction rate in the evaporator:

$$\dot{X}_{dest,e} = T_H\dot{S}_{gen,e} = -T_H\left(\frac{\dot{Q}_{e1}}{T_{w,e1}}+\frac{\dot{Q}_{e2}}{T_{w,e2}}\right) - \left(\dot{m}_{r,v}T_H s_{e,ri} - \dot{m}_{r,k}T_H s_{e,ro}\right) + T_H\left(\frac{dS_{e1}}{dt}+\frac{dS_{e2}}{dt}\right). \quad (5.20)$$

Furthermore, the equivalence between the two approaches for deriving $\dot{X}_{dest,e}$ can be verified by setting Eq. 5.20 equal to Eq. 5.15. This yields

$$\underbrace{\left(\frac{dX_{e1}}{dt}+\frac{dX_{e2}}{dt}\right)}_{\frac{dX_e}{dt}}=\underbrace{\dot{Q}_{e1}+\dot{Q}_{e2}+P_0\left(\frac{dV_{e1}}{dt}+\frac{dV_{e2}}{dt}\right)+\left(\dot{m}_{r,v}h_{e,ri}-\dot{m}_{r,k}h_{e,ro}\right)}_{\frac{dE_e}{dt}}-T_H\underbrace{\left(\frac{dS_{e1}}{dt}+\frac{dS_{e2}}{dt}\right)}_{\frac{dS_e}{dt}} \quad (5.21)$$

which is the definition of exergy (recall Eq. 2.12.1). Expressions for $\frac{dS_{e1}}{dt}$ and $\frac{dS_{e2}}{dt}$ will be derived in Section 5.2.3.

5.2.2.2 Condenser

In the lumped parameter moving boundary modeling approach, the condenser is typically modeled with 3 refrigerant fluid regions: a superheated fluid region, a two-phase fluid region, and a subcooled fluid region. Therefore, separate lumped parameters are used to estimate the fluid properties in each of the fluid regions, thereby improving the accuracy of the estimates. To remain consistent with the modeling approach, three separate control volumes are used to derive the total exergy destruction rate through the condenser as shown in Figure 5.3.

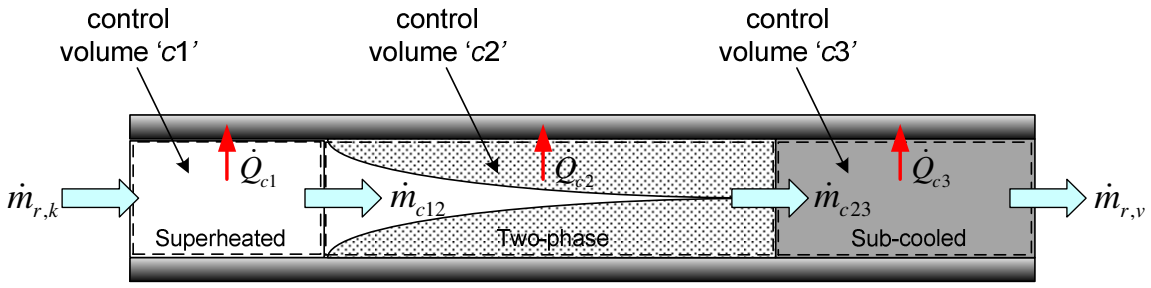

Figure 5.3: Individual control volumes drawn around each fluid region in a condenser.

Although at steady-state it can be assumed that the heat transfer out of the condenser is occurring at the reference temperature, T_H, the control volumes defined in Figure 5.3 for the condenser only contain the refrigerant flowing through the condenser tube. Therefore, the transfer of heat away from the refrigerant is occurring at the tube wall temperatures of each fluid region.

For the superheated refrigerant fluid region, denoted by the subscript $c1$, Eq. 5.2 reduces to

$$\frac{dX_{c1}}{dt}=\left(1-\frac{T_H}{T_{w,c1}}\right)\left(-\dot{Q}_{c1}\right)+P_0\frac{dV_{c1}}{dt}+\dot{m}_{r,k}\left(h_{c,ri}-T_H s_{c,ri}\right)-\dot{m}_{c12}\left(h_{c,g}-T_H s_{c,g}\right)-\dot{X}_{dest,c1}. \quad (5.22)$$

Similarly, for the two-phase refrigerant fluid region, denoted by the subscript $c2$, Eq. 5.2 reduces to

$$\frac{dX_{c2}}{dt}=\left(1-\frac{T_H}{T_{w,c2}}\right)\left(-\dot{Q}_{c2}\right)+P_0\frac{dV_{c2}}{dt}+\dot{m}_{c12}\left(h_{c,g}-T_H s_{c,g}\right)-\dot{m}_{c23}\left(h_{c,l}-T_H s_{c,l}\right)-\dot{X}_{dest,c2}. \quad (5.23)$$

Finally, for the subcooled refrigerant fluid region, denoted by the subscript $c3$, Eq. 5.2 reduces to

$$\begin{aligned}\frac{dX_{c3}}{dt}=&\left(1-\frac{T_H}{T_{w,c3}}\right)\left(-\dot{Q}_{c3}\right)+P_0\frac{dV_{c3}}{dt}+\dot{m}_{c23}\left(h_{c,l}-T_H s_{c,l}\right)\\&-\dot{m}_{r,v}\left(h_{c,ro}-T_H s_{c,ro}\right)-\dot{X}_{dest,c3}.\end{aligned} \quad (5.24)$$

As in the case of the evaporator,

$$\dot{X}_{dest,c}=\dot{X}_{dest,c1}+\dot{X}_{dest,c2}+\dot{X}_{dest,c3}. \quad (5.25)$$

Therefore, the total exergy destruction rate through the condenser is

$$\begin{aligned}\dot{X}_{dest,c}=&\left(1-\frac{T_H}{T_{w,c1}}\right)\left(-\dot{Q}_{c1}\right)+\left(1-\frac{T_H}{T_{w,c2}}\right)\left(-\dot{Q}_{c2}\right)+\left(1-\frac{T_H}{T_{w,c3}}\right)\left(-\dot{Q}_{c3}\right)\\&+P_0\left(\frac{dV_{c1}}{dt}+\frac{dV_{c2}}{dt}+\frac{dV_{c3}}{dt}\right)+\dot{m}_{r,k}\left(h_{c,ri}-T_H s_{c,ri}\right)-\dot{m}_{r,v}\left(h_{c,ro}-T_H s_{c,ro}\right)\\&-\left(\frac{dX_{c1}}{dt}+\frac{dX_{c2}}{dt}+\frac{dX_{c3}}{dt}\right).\end{aligned} \quad (5.26)$$

The entropy rate balance shown in Eq. 5.3 can again be applied to each control volume in the condenser:

$$\frac{dS_{c1}}{dt}=\frac{-\dot{Q}_{c1}}{T_{w,c1}}+\left[\dot{m}_{r,k}s_{c,ri}-\dot{m}_{c12}s_{c,g}\right]+\dot{S}_{gen,c1}, \quad (5.27)$$

$$\frac{dS_{c2}}{dt}=\frac{-\dot{Q}_{c2}}{T_{w,c2}}+\left[\dot{m}_{c12}s_{c,g}-\dot{m}_{c23}s_{c,l}\right]+\dot{S}_{gen,c2}, \quad (5.28)$$

and

$$\frac{dS_{c3}}{dt} = \frac{-\dot{Q}_{c3}}{T_{w,c3}} + \left[\dot{m}_{c23} s_{c,l} - \dot{m}_{r,v} s_{c,ro} \right] + \dot{S}_{gen,c3} \qquad (5.29)$$

where

$$\dot{S}_{gen,c} = \dot{S}_{gen,c1} + \dot{S}_{gen,c2} + \dot{S}_{gen,c3}. \qquad (5.30)$$

Substituting Eqs. 5.27 – 5.29 into Eq. 5.30 and rearranging yields the following alternative expression for the exergy destruction rate in the condenser:

$$\begin{aligned} \dot{X}_{dest,c} = T_H \dot{S}_{gen,c} = T_H \left(\frac{\dot{Q}_{c1}}{T_{w,c1}} + \frac{\dot{Q}_{c2}}{T_{w,c2}} + \frac{\dot{Q}_{c3}}{T_{w,c3}} \right) - \left(\dot{m}_{r,k} T_H s_{c,ri} - \dot{m}_{r,v} T_H s_{c,ro} \right) \\ + T_H \left(\frac{dS_{c1}}{dt} + \frac{dS_{c2}}{dt} + \frac{dS_{c3}}{dt} \right) \end{aligned} \qquad (5.31)$$

where it is assumed that

$$\dot{Q}_c = \dot{Q}_{c1} + \dot{Q}_{c2} + \dot{Q}_{c3}. \qquad (5.32)$$

Again, Eq. 5.32 relies on the assumption that there is no heat transfer between the refrigerant in control volumes $c1$, $c2$, and $c3$.

Expressions for $\frac{dS_{ci}}{dt}$, $i=\{1,2,3\}$, will be derived in the next section.

5.2.3 Evaluating the Entropy Differential

In order to express $\frac{dS_{cv}}{dt}$ in terms of thermodynamic variables, the method proposed in [64], described in Eqs. 5.33 – 5.36, is used.

$$\frac{dS_{cv}}{dt} = \frac{d}{dt}\left\{ m_{cv} s(var1, var2) \right\} = \frac{dm_{cv}}{dt}\left\{ s_{cv}(var1, var2) \right\} + \frac{ds_{cv}}{dt}\left\{ m_{cv} \right\} \qquad (5.33)$$

$$\frac{ds_{cv}}{dt} = \frac{\partial(s_{cv})}{\partial(var1)}\left\{ \frac{d(var1)}{dt} \right\} + \frac{\partial(s_{cv})}{\partial(var2)}\left\{ \frac{d(var2)}{dt} \right\} \qquad (5.34)$$

$$\frac{ds_{cv}}{dt} = \frac{d}{dt}\left\{ s(h,P) \right\} = \left. \frac{(\partial s_{cv})}{\partial h} \right|_P \frac{dh}{dt} + \left. \frac{(\partial s_{cv})}{\partial P} \right|_h \frac{dP}{dt} \qquad (5.35)$$

$$\frac{dS_{cv}}{dt} = s_{cv}\frac{dm_{cv}}{dt} + m_{cv}\left(\left.\frac{(\partial s_{cv})}{\partial h}\right|_{P}\frac{dh}{dt} + \left.\frac{(\partial s_{cv})}{\partial P}\right|_{h}\frac{dP}{dt}\right) \quad (5.36)$$

In Eq. 5.35 the dependent variables were chosen as specific enthalpy and pressure, but they can be chosen as any two independent thermodynamic state variables. Equation 5.36 highlights why it is helpful to define multiple control volumes for the heat exchangers in which a separate control volume is drawn around each fluid region (recall Figure 5.2). *This formulation allows for lumped parameters to be used to approximate s_{cv} and m_{cv} for each control volume as is done in the lumped parameter moving boundary dynamic modeling approach.*

The expression for $\frac{dm_{cv}}{dt}$ can be derived in the lumped parameter moving boundary framework for each control volume as described in [65].

5.2.3.1 Entropy Rate of Change in Evaporator

For the two-phase fluid region of the evaporator, refrigerant mean void fraction, rather than specific enthalpy, and pressure will be used to describe specific entropy. Mean void fraction is related to mean quality, $\overline{x}$, by the following relationship:

$$\overline{x} = \overline{\gamma}\frac{\rho_g}{\rho}. \quad (5.37)$$

Evaluating Eq. 5.36 for the two-phase fluid region of the evaporator yields

$$\frac{dS_{e1}}{dt} = s_{e1}\frac{dm_{e1}}{dt} + m_{e1}\left(\left.\frac{(\partial s_{e1})}{\partial \overline{\gamma}_e}\right|_{P}\frac{d\overline{\gamma}_e}{dt} + \left.\frac{(\partial s_{e1})}{\partial P_e}\right|_{\overline{\gamma}}\frac{dP_e}{dt}\right) \quad (5.38)$$

which can be further simplified as

$$\frac{dS_{e1}}{dt} = s_{e1}\frac{dm_{e1}}{dt} + \rho_{e1}\zeta_{e1}L_{R,e}A_{CR,e}\left(\left.\frac{(\partial s_{e1})}{\partial \overline{\gamma}_e}\right|_{P}\frac{d\overline{\gamma}_e}{dt} + \left.\frac{(\partial s_{e1})}{\partial P_e}\right|_{\overline{\gamma}}\frac{dP_e}{dt}\right) \quad (5.39)$$

where

$$\frac{dm_{e1}}{dt} = \left(\dot{m}_{r,v} - \dot{m}_{e12}\right) + \rho_{e1}A_{CR,e}L_{R,e}\frac{d\zeta_{e1}}{dt} \quad (5.40)$$

and

$$s_{e1} = \overline{x}_e s_{e,g} + \left(1-\overline{x}_e\right) s_{e,l} = \frac{\overline{\gamma}_e \rho_{e,g} s_{e,g} + \left(1-\overline{\gamma}_e\right) \rho_{e,l} s_{e,l}}{\overline{\gamma}_e \rho_{e,g} + \left(1-\overline{\gamma}_e\right) \rho_{e,l}} \ . \qquad (5.41)$$

The variables $\rho_{e,l}$, $\rho_{e,g}$, $s_{e,l}$, and $s_{e,g}$ are all solely functions of pressure. The partial derivatives $\left.\frac{\partial s_{e1}}{\partial \overline{\gamma}_e}\right|_P$ and $\left.\frac{\partial s_{e1}}{\partial P_e}\right|_{\overline{\gamma}}$, shown in Eq. 5.42 and Eq. 5.43 respectively, are derived using Eq. 5.41.

$$\left.\frac{\partial s_{e1}}{\partial \overline{\gamma}_e}\right|_P = \frac{\left(\overline{\gamma}_e \rho_{e,g} + \left(1-\overline{\gamma}_e\right)\rho_{e,l}\right)\left(\rho_{e,g} s_{e,g} - \rho_{e,l} s_{e,l}\right) - \left(\overline{\gamma}_e \rho_{e,g} s_{e,g} + \left(1-\overline{\gamma}_e\right)\rho_{e,l} s_{e,l}\right)\left(\rho_{e,g} - \rho_{e,l}\right)}{\left(\overline{\gamma}_e \rho_{e,g} + \left(1-\overline{\gamma}_e\right)\rho_{e,l}\right)^2} \qquad (5.42)$$

$$\left.\frac{\partial s_{e1}}{\partial P_e}\right|_{\overline{\gamma}} = \frac{\beta_1 - \beta_2}{\beta_3} \qquad (5.43)$$

$$\begin{aligned}
\beta_1 &= \left(\overline{\gamma}_e \rho_{e,g} + \left(1-\overline{\gamma}_e\right)\rho_{e,l}\right)\left(\overline{\gamma}_e \rho_{e,g} \frac{ds_{e,g}}{dP_e} + s_{e,g}\overline{\gamma}_e \frac{d\rho_{e,g}}{dP_e} + \left(1-\overline{\gamma}_e\right)\rho_{e,l}\frac{ds_{e,l}}{dP_e} + s_{e,l}\left(1-\overline{\gamma}_e\right)\frac{d\rho_{e,l}}{dP_e}\right) \\
\beta_2 &= \left(\overline{\gamma}_e \rho_{e,g} s_{e,g} + \left(1-\overline{\gamma}_e\right)\rho_{e,l} s_{e,l}\right)\left(\overline{\gamma}_e \frac{d\rho_{e,g}}{dP_e} + \left(1-\overline{\gamma}_e\right)\frac{d\rho_{e,l}}{dP_e}\right) \qquad (5.44) \\
\beta_3 &= \left(\overline{\gamma}_e \rho_{e,g} + \left(1-\overline{\gamma}_e\right)\rho_{e,l}\right)^2
\end{aligned}$$

Evaluating Eq. 5.36 for the superheated fluid region of the evaporator yields

$$\frac{dS_{e2}}{dt} = s_{e2}\frac{dm_{e2}}{dt} + \rho_{e2}\zeta_{e2}L_{R,e}A_{CR,e}\left(\left.\frac{(\partial s_{e2})}{\partial h_{e2}}\right|_P \frac{dh_{e2}}{dt} + \left.\frac{(\partial s_{e2})}{\partial P_e}\right|_h \frac{dP_e}{dt}\right) \qquad (5.45)$$

where

$$\frac{dm_{e2}}{dt} = \left(\dot{m}_{e12} - \dot{m}_{r,k}\right) + \rho_{g,e}A_{CR,e}L_{R,e}\frac{d\zeta_{e1}}{dt} \ . \qquad (5.46)$$

5.2.3.2 Entropy Rate of Change in Condenser

The procedure described in the previous section can be applied to the rate of change of entropy in each of the condenser control volumes. It is assumed that the outlet refrigerant condition of the condenser is subcooled liquid; therefore, the condenser is characterized using three fluid regions. As in the case of the evaporator, specific enthalpy and pressure are used to describe specific entropy in the superheated and subcooled fluid regions, and mean void fraction and pressure are used in the two-phase fluid region.

The expressions for $\frac{dS_{c1}}{dt}$, $\frac{dS_{c2}}{dt}$, and $\frac{dS_{c3}}{dt}$ are given in Eqs. 5.47 – 5.52, respectively.

$$\frac{dS_{c1}}{dt} = s_{c1}\frac{dm_{c1}}{dt} + \rho_{c1}\zeta_{c1}L_{R,c}A_{CR,c}\left(\left.\frac{(\partial s_{c1})}{\partial h_{c1}}\right|_P \frac{dh_{c1}}{dt} + \left.\frac{(\partial s_{c1})}{\partial P_c}\right|_h \frac{dP_c}{dt}\right) \quad (5.47)$$

$$\frac{dm_{c1}}{dt} = \left(\dot{m}_{r,k} - \dot{m}_{c12}\right) + \rho_{g,c}A_{CR,c}L_{R,c}\frac{d\zeta_{c1}}{dt} \quad (5.48)$$

$$\frac{dS_{c2}}{dt} = s_{c2}\frac{dm_{c2}}{dt} + \rho_{c2}\zeta_{c2}L_{R,c}A_{CR,c}\left(\left.\frac{(\partial s_{c,2})}{\partial \overline{\gamma}_c}\right|_P \frac{d\overline{\gamma}_c}{dt} + \left.\frac{(\partial s_{c,2})}{\partial P_c}\right|_{\overline{\gamma}} \frac{dP_c}{dt}\right) \quad (5.49)$$

$$\frac{dm_{c2}}{dt} = \left(\dot{m}_{c12} - \dot{m}_{c23}\right) + \rho_{l,c}A_{CR,c}L_{R,c}\left(\frac{d\zeta_{c1}}{dt} + \frac{d\zeta_{c2}}{dt}\right) - \rho_{g,c}A_{CR,c}L_{R,c}\frac{d\zeta_{c1}}{dt} \quad (5.50)$$

$$\frac{dS_{c3}}{dt} = s_{c3}\frac{dm_{c3}}{dt} + \rho_{c3}\zeta_{c3}L_{R,c}A_{CR,c}\left(\left.\frac{(\partial s_{c3})}{\partial h_{c3}}\right|_P \frac{dh_{c3}}{dt} + \left.\frac{(\partial s_{c3})}{\partial P_c}\right|_h \frac{dP_c}{dt}\right) \quad (5.51)$$

$$\frac{dm_{c3}}{dt} = \left(\dot{m}_{c23} - \dot{m}_{r,v}\right) - \rho_{l,c}A_{CR,c}L_{R,c}\left(\frac{d\zeta_{c1}}{dt} + \frac{d\zeta_{c2}}{dt}\right) \quad (5.52)$$

5.2.4 Dynamic Rate of Exergy Destruction for Complete VCC System

Substituting Eqs. 5.9, 5.11, 5.20, and 5.31 into Eq. 5.1 and simplifying results in $\dot{X}_{dest,VCC}$, the instantaneous exergy destruction rate in the standard VCC system:

$$\begin{aligned}\dot{X}_{dest,VCC} = {} & T_H\left(\frac{\dot{Q}_{c1}}{T_{w,c1}} + \frac{\dot{Q}_{c2}}{T_{w,c2}} + \frac{\dot{Q}_{c3}}{T_{w,c3}} - \frac{\dot{Q}_{e1}}{T_{w,e1}} - \frac{\dot{Q}_{e2}}{T_{w,e2}}\right) \\ & + T_H\left(\frac{dS_{e1}}{dt} + \frac{dS_{e2}}{dt} + \frac{dS_{c1}}{dt} + \frac{dS_{c2}}{dt} + \frac{dS_{c3}}{dt}\right)\end{aligned} \quad (5.53)$$

where

$$\frac{dS_{e1}}{dt} = s_{e1}\frac{dm_{e1}}{dt} + \rho_{e1}\zeta_{e1}L_{R,e}A_{CR,e}\left(\left.\frac{(\partial s_{e1})}{\partial \overline{\gamma}_e}\right|_P \frac{d\overline{\gamma}_e}{dt} + \left.\frac{(\partial s_{e1})}{\partial P_e}\right|_{\overline{\gamma}} \frac{dP_e}{dt}\right), \quad (5.54)$$

$$\frac{dS_{e2}}{dt} = s_{e2}\frac{dm_{e2}}{dt} + \rho_{e2}\zeta_{e2}L_{R,e}A_{CR,e}\left(\left.\frac{(\partial s_{e2})}{\partial h_{e2}}\right|_P \frac{dh_{e2}}{dt} + \left.\frac{(\partial s_{e2})}{\partial P_e}\right|_h \frac{dP_e}{dt}\right), \quad (5.55)$$

$$\frac{dS_{c1}}{dt} = s_{c1}\frac{dm_{c1}}{dt} + \rho_{c1}\zeta_{c1}L_{R,c}A_{CR,c}\left(\left.\frac{(\partial s_{c1})}{\partial h_{c1}}\right|_{P}\frac{dh_{c1}}{dt} + \left.\frac{(\partial s_{c1})}{\partial P_c}\right|_{h}\frac{dP_c}{dt}\right), \quad (5.56)$$

$$\frac{dS_{c2}}{dt} = s_{c2}\frac{dm_{c2}}{dt} + \rho_{c2}\zeta_{c2}L_{R,c}A_{CR,c}\left(\left.\frac{(\partial s_{c,2})}{\partial \overline{\gamma}_c}\right|_{P}\frac{d\overline{\gamma}_c}{dt} + \left.\frac{(\partial s_{c,2})}{\partial P_c}\right|_{\overline{\gamma}}\frac{dP_c}{dt}\right), \quad (5.57)$$

and

$$\frac{dS_{c3}}{dt} = s_{c3}\frac{dm_{c3}}{dt} + \rho_{c3}\zeta_{c3}L_{R,c}A_{CR,c}\left(\left.\frac{(\partial s_{c3})}{\partial h_{c3}}\right|_{P}\frac{dh_{c3}}{dt} + \left.\frac{(\partial s_{c3})}{\partial P_c}\right|_{h}\frac{dP_c}{dt}\right). \quad (5.58)$$

5.3 Optimal Control Problem Formulation

In this section, an optimal control problem is formulated using total exergy destruction as the minimization metric. Rather than optimizing operational setpoints as was done in Chapters 3 and 4, the decision variables in the optimal control problem formulated in this section are the control inputs themselves. Additionally, the optimization is a dynamic one in the sense that dynamic model information about how the system will behave at future time steps is used to influence control decisions at the current time step.

In Section 5.3.1, model predictive control (MPC) is introduced. In Section 5.3.2, an objective function is defined based on the dynamic exergy destruction rate derived in Section 5.2. Finally, in Section 5.3.3, the constraints enforced in the optimal control problem are defined.

5.3.1 Model Predictive Control

There are many different optimal control algorithms. However, all of them are used to find optimal control decisions by minimizing some objective function. Here, model predictive control (MPC), a receding-horizon optimal control framework, will be used. MPC uses a dynamic model to predict how a system will behave in response to a particular sequence of control decisions over a specified prediction horizon.

The prediction horizon, n_p, is the number of discrete time steps over which the system behavior is predicted. It is defined as

$$n_p = \frac{t_{horizon}}{\Delta t}. \quad (5.59)$$

where Δt is the length of the discrete time step and $t_{horizon}$ is the length of time over which the algorithm predicts the system behavior. The control horizon, n_u, is the number of discrete time steps for which control decisions are optimized, where $n_u \leq n_p$.

A linearized discrete model of the system dynamics of the form

$$\delta\mathbf{x}[k+1] = \mathbf{A}\delta\mathbf{x}[k] + \mathbf{B}_1\delta\mathbf{u}[k] + \mathbf{B}_2\delta\mathbf{d}[k] \quad (5.60)$$

is used to predict the system behavior over the prediction horizon. Since the model is linearized about some equilibrium condition of the system, $\delta\mathbf{x}$, $\delta\mathbf{u}$, and $\delta\mathbf{d}$ represent deviations from the equilibrium condition. The state, input, and disturbance vectors are described in Eqs. 5.61, 5.62, and 5.63, respectively. Note that instead of treating the evaporator and condenser fan speeds as the decision variables, the air mass flow rates produced by each fan, $\dot{m}_{a,e}$ and $\dot{m}_{a,c}$, are the decision variables. Details of the model linearization are provided in Appendix C. To simplify the notation, the use of δ will be dropped since it is understood that we are discussing deviations about some nominal operating condition when referring to state, input, and disturbance variables.

$$\mathbf{x} = \begin{bmatrix} \zeta_{e1} & P_e & h_{e2} & T_{w,e1} & T_{w,e2} & \bar{\gamma}_e & \zeta_{c1} & \zeta_{c1} & P_c & h_{c1} & h_{c3} & T_{w,c1} & T_{w,c2} & T_{w,c3} & \bar{\gamma}_c \end{bmatrix}^T \in \mathbb{R}^{15} \quad (5.61)$$

$$\mathbf{u} = \begin{bmatrix} a_v & \omega_k & \dot{m}_{a,e} & \dot{m}_{a,c} \end{bmatrix}^T \in \mathbb{R}^4 \quad (5.62)$$

$$\mathbf{d} = \begin{bmatrix} T_{e,ai} & T_{c,ai} \end{bmatrix}^T \in \mathbb{R}^2 \quad (5.63)$$

One can constrain the rate of change in control decisions over the control horizon by augmenting the system with additional states defined as

$$\mathbf{x}_\mathbf{u}[k] = \mathbf{u}[k-1] \quad (5.64)$$

where

$$\mathbf{u}[k] = \mathbf{u}[k-1] + \Delta\mathbf{u}[k]. \quad (5.65)$$

Therefore,

$$\mathbf{x}_\mathbf{u}[k+1] = \mathbf{x}_\mathbf{u}[k] + \Delta\mathbf{u}[k] \tag{5.66}$$

and the augmented state-space representation of the system is given by

$$\begin{pmatrix} \mathbf{x}[k+1] \\ \mathbf{x}_\mathbf{u}[k+1] \end{pmatrix} = \begin{pmatrix} \mathbf{A} & \mathbf{B}_1 \\ \mathbf{0} & \mathbf{I} \end{pmatrix} \begin{pmatrix} \mathbf{x}[k] \\ \mathbf{x}_\mathbf{u}[k] \end{pmatrix} + \begin{pmatrix} \mathbf{B}_1 \\ \mathbf{I} \end{pmatrix} \Delta\mathbf{u}[k] + \begin{pmatrix} \mathbf{B}_2 \\ \mathbf{0} \end{pmatrix} \mathbf{d}[k] \tag{5.67}$$

which is represented with the simplified notation shown in Eq. 5.68.

$$\bar{\mathbf{x}}[k+1] = \bar{\mathbf{A}}\bar{\mathbf{x}}[k] + \bar{\mathbf{B}}_1\Delta\mathbf{u}[k] + \bar{\mathbf{B}}_2\mathbf{d}[k] \tag{5.68}$$

$$\bar{\mathbf{x}} = \begin{pmatrix} \mathbf{x} \\ \mathbf{x}_\mathbf{u} \end{pmatrix},\ \bar{\mathbf{A}} = \begin{pmatrix} \mathbf{A} & \mathbf{B}_1 \\ \mathbf{0} & \mathbf{I} \end{pmatrix},\ \bar{\mathbf{B}}_1 = \begin{pmatrix} \mathbf{B}_1 \\ \mathbf{I} \end{pmatrix},\ \bar{\mathbf{B}}_2 \begin{pmatrix} \mathbf{B}_2 \\ \mathbf{0} \end{pmatrix} \tag{5.69}$$

For a numerical optimization, it is convenient to define the input vector in its lifted form,

$$\Delta\mathbf{U} = \begin{bmatrix} \Delta\mathbf{u}[k] & \Delta\mathbf{u}[k+1] & \cdots & \Delta\mathbf{u}[k+n_u-1] \end{bmatrix}^T. \tag{5.70}$$

Using the lifted input vector, $\Delta\mathbf{U}$, and the initial value of the state vector, $\bar{\mathbf{x}}[0]$, the evolution of all of the states can be quickly evaluated in the lifted vector $\bar{\mathbf{X}}$ using the lifted matrix equation

$$\bar{\mathbf{X}} = \mathbf{T}\bar{\mathbf{x}}[k] + \mathbf{S}_1\Delta\mathbf{U} + \mathbf{S}_2\mathbf{D} \tag{5.71}$$

where

$$\bar{\mathbf{X}} = \begin{bmatrix} \bar{\mathbf{x}}[k] & \bar{\mathbf{x}}[k+1] & \cdots & \bar{\mathbf{x}}[k+n_p-1] \end{bmatrix}^T. \tag{5.72}$$

The expressions for $\mathbf{T}$, $\mathbf{S}_1$, and $\mathbf{S}_2$ are given by

$$\mathbf{T} = \begin{bmatrix} \bar{\mathbf{A}} \\ \bar{\mathbf{A}}^2 \\ \vdots \\ \bar{\mathbf{A}}^{n_p} \end{bmatrix}, \tag{5.73}$$

$$\mathbf{S}_1 = \begin{bmatrix} \bar{\mathbf{B}}_1 & 0 & \cdots & 0 \\ \bar{\mathbf{A}}\bar{\mathbf{B}}_1 & \ddots & \ddots & \vdots \\ \vdots & \ddots & \bar{\mathbf{B}}_1 & 0 \\ \bar{\mathbf{A}}^{n_u-1}\bar{\mathbf{B}}_1 & \cdots & \bar{\mathbf{A}}\bar{\mathbf{B}}_1 & \bar{\mathbf{B}}_1 \\ \vdots & \vdots & \vdots & \vdots \\ \bar{\mathbf{A}}^{n_p-2}\bar{\mathbf{B}}_1 & \ddots & \ddots & \bar{\mathbf{A}}^{n_p-n_u-1}\bar{\mathbf{B}}_1 \\ \bar{\mathbf{A}}^{n_p-1}\bar{\mathbf{B}}_1 & \cdots & \bar{\mathbf{A}}^{n_p-n_u-1}\bar{\mathbf{B}}_1 & \bar{\mathbf{A}}^{n_p-n_u}\bar{\mathbf{B}}_1 \end{bmatrix}, \qquad (5.74)$$

and

$$\mathbf{S}_2 = \begin{bmatrix} \bar{\mathbf{B}}_2 & 0 & \cdots & 0 \\ \bar{\mathbf{A}}\bar{\mathbf{B}}_2 & \ddots & \ddots & \vdots \\ \vdots & \ddots & \bar{\mathbf{B}}_2 & 0 \\ \bar{\mathbf{A}}^{n_u-1}\bar{\mathbf{B}}_2 & \cdots & \bar{\mathbf{A}}\bar{\mathbf{B}}_2 & \bar{\mathbf{B}}_2 \\ \vdots & \vdots & \vdots & \vdots \\ \bar{\mathbf{A}}^{n_p-2}\bar{\mathbf{B}}_2 & \ddots & \ddots & \bar{\mathbf{A}}^{n_p-n_u-1}\bar{\mathbf{B}}_2 \\ \bar{\mathbf{A}}^{n_p-1}\bar{\mathbf{B}}_2 & \cdots & \bar{\mathbf{A}}^{n_p-n_u-1}\bar{\mathbf{B}}_2 & \bar{\mathbf{A}}^{n_p-n_u}\bar{\mathbf{B}}_2 \end{bmatrix}. \qquad (5.75)$$

The objective function $J_{EDM,VCC}$, which will be defined in the next section, is a function of $\bar{\mathbf{X}}$.

5.3.2 Objective Function

Since the optimal control framework that will be used considers a finite time horizon, the total exergy destroyed over the time horizon, as opposed to the exergy destruction rate at each time instant, will be minimized. Additionally, for robustness considerations, the performance objective of achieving a specified cooling capacity is included in the objective function rather than as an equality constraint, and a weighting parameter, λ, is used to emphasize the importance of one objective over the other. Finally, in order to numerically solve this type of optimization problem, the cost function must be evaluated in discrete time. Therefore, numerical integration will be used to approximate the total exergy destroyed over the finite time horizon.

The complete objective function is expressed as

$$J_{EDM,VCC} = \underbrace{\left(\left\| C_{des} - C_{ach} \right\|_2\right)}_{\substack{Performance \\ Objective}} + \lambda \underbrace{\left(\sum_{k=1}^{n_p} \dot{X}_{dest,VCC}[k] \right) \Delta t}_{\substack{Efficiency \\ Objective}} \qquad (5.76)$$

where $C_{des} \in \mathbb{R}^{n_p}$ is specified in the optimization problem and $C_{ach} \in \mathbb{R}^{n_p}$ is calculated using the expression

$$C_{ach} = \dot{Q}_e = (UA)_{e1}\left(T_{w,e1} - T_{r,e1}\right) + (UA)_{e2}\left(T_{w,e2} - T_{r,e2}\right) . \tag{5.77}$$

The efficiency objective can be expanded as

$$\begin{aligned}\left(\sum_{k=1}^{n_p} \dot{X}_{dest,VCC}[k]\right)\Delta t = T_H \sum_{k=1}^{n_p}\left(\frac{\dot{Q}_{c1}[k]}{T_{w,c1}[k]} + \frac{\dot{Q}_{c2}[k]}{T_{w,c2}[k]} + \frac{\dot{Q}_{c3}[k]}{T_{w,c3}[k]} - \frac{\dot{Q}_{e1}[k]}{T_{w,e1}[k]} - \frac{\dot{Q}_{e2}[k]}{T_{w,e2}[k]}\right)\Delta t \\ + T_H \sum_{k=1}^{n_p}\left(g_{e1}[k] + g_{e2}[k] + g_{c1}[k] + g_{c2}[k] + g_{c3}[k]\right)\Delta t\end{aligned} \tag{5.78}$$

where

$$\dot{Q}_{ei}[k] = (UA)_{ei}[k]\cdot\left(T_{w,ei}[k] - T_{r,ei}[k]\right),\ i \in \{1,2\}, \tag{5.79}$$

$$\dot{Q}_{ci}[k] = (UA)_{ci}[k]\cdot\left(T_{r,ci}[k] - T_{w,ci}[k]\right),\ i \in \{1,2,3\}, \tag{5.80}$$

$$\begin{aligned}g_{e1}[k] = {} & s_{e1}[k]\left(\dot{m}_{r,v}[k] - \dot{m}_{e12}[k] + L_{R,e}A_{CR,e}\rho_{e1}[k]\left(\frac{\zeta_{e1}[k] - \zeta_{e1}[k-1]}{\Delta t}\right)\right) \\ & + L_{R,e}A_{CR,e}\rho_{e1}[k]\zeta_{e1}[k]\left(\frac{(\partial s_{e1})}{\partial \overline{\gamma}_e}[k]\left(\frac{\overline{\gamma}_e[k] - \overline{\gamma}_e[k-1]}{\Delta t}\right) + \frac{(\partial s_{e1})}{\partial P_e}[k]\left(\frac{P_e[k] - P_e[k-1]}{\Delta t}\right)\right),\end{aligned} \tag{5.81}$$

$$\begin{aligned}g_{e2}[k] = {} & s_{e2}[k]\left(\dot{m}_{e12}[k] - \dot{m}_{r,k}[k] + L_{R,e}A_{CR,e}\rho_{g,e}[k]\left(\frac{\zeta_{e1}[k] - \zeta_{e1}[k-1]}{\Delta t}\right)\right) \\ & + L_{R,e}A_{CR,e}\rho_{e2}[k]\zeta_{e2}[k]\left(\frac{(\partial s_{e2})}{\partial h_{e2}}[k]\left(\frac{h_{e2}[k] - h_{e2}[k-1]}{\Delta t}\right) + \frac{(\partial s_{e2})}{\partial P_e}[k]\left(\frac{P_e[k] - P_e[k-1]}{\Delta t}\right)\right),\end{aligned} \tag{5.82}$$

$$\begin{aligned}g_{c1}[k] = {} & s_{c1}[k]\left(\dot{m}_{r,k}[k] - \dot{m}_{c12}[k] + L_{R,c}A_{CR,c}\rho_{g,c}[k]\left(\frac{\zeta_{c1}[k] - \zeta_{c1}[k-1]}{\Delta t}\right)\right) \\ & + L_{R,c}A_{CR,c}\rho_{c1}[k]\zeta_{c1}[k]\left(\frac{(\partial s_{c1})}{\partial h_{c1}}[k]\left(\frac{h_{c1}[k] - h_{c1}[k-1]}{\Delta t}\right) + \frac{(\partial s_{c1})}{\partial P_c}[k]\left(\frac{P_c[k] - P_c[k-1]}{\Delta t}\right)\right),\end{aligned} \tag{5.83}$$

$$\begin{aligned}g_{c2}[k] = {} & s_{c2}[k]\left(\dot{m}_{c12}[k] - \dot{m}_{c23}[k] + L_{R,c}A_{CR,c}\rho_{l,c}[k]\left(\frac{\zeta_{c1}[k] - \zeta_{c1}[k-1]}{\Delta t} + \frac{\zeta_{c2}[k] - \zeta_{c2}[k-1]}{\Delta t}\right)\right) \\ & - s_{c2}[k]\left(L_{R,c}A_{CR,c}\rho_{g,c}[k]\left(\frac{\zeta_{c1}[k] - \zeta_{c1}[k-1]}{\Delta t}\right)\right) \\ & + L_{R,c}A_{CR,c}\rho_{c2}[k]\zeta_{c2}[k]\left(\frac{(\partial s_{c2})}{\partial \overline{\gamma}_c}[k]\left(\frac{\overline{\gamma}_c[k] - \overline{\gamma}_c[k-1]}{\Delta t}\right) + \frac{(\partial s_{c2})}{\partial P_c}[k]\left(\frac{P_c[k] - P_c[k-1]}{\Delta t}\right)\right),\end{aligned} \tag{5.84}$$

and

$$g_{c3}[k] = s_{c3}[k]\left(\dot{m}_{c23}[k] - \dot{m}_{r,v}[k] - L_{R,c}A_{CR,c}\rho_{l,c}[k]\left(\frac{\zeta_{c1}[k]-\zeta_{c1}[k-1]}{\Delta t} + \frac{\zeta_{c2}[k]-\zeta_{c2}[k-1]}{\Delta t}\right)\right)$$
$$+L_{R,c}A_{CR,c}\rho_{c3}[k]\zeta_{c3}[k]\left(\frac{(\partial s_{c3})}{\partial h_{c3}}[k]\left(\frac{h_{c3}[k]-h_{c3}[k-1]}{\Delta t}\right) + \frac{(\partial s_{c3})}{\partial P_c}[k]\left(\frac{P_c[k]-P_c[k-1]}{\Delta t}\right)\right). \quad (5.85)$$

For clarity of notation, the rate of change of entropy in each evaporator control volume is denoted by the function g_{ei} where $i = \{1,2\}$. Similarly, in each condenser control volume, the rate of change of entropy is denoted by the function g_{ci} where $i = \{1,2,3\}$. It should also be noted that $J_{EDM,VCC}$ is not only a function of the states of the dynamical system representation of the VCC system, but also a function of variables such as $T_{r,c1}$ and $\frac{(\partial s_{e2})}{\partial h}$ which are nonlinear functions of the states. These variables are typically evaluated using data-based refrigerant look-up tables [65].

5.3.3 Constraints

In the MPC framework, upper and lower bound constraints can easily be placed on the values of the control decisions at each time instant. These are detailed in Section 5.4.1 for the specific VCC system considered in the case study. Additionally, upper and/or lower bound constraints can be enforced on specific state variables in the dynamical system. The constraints enforced in the case study are

$$\zeta_{e1}[k] \leq 0.95 \ \forall \ k \quad (5.86)$$

and

$$\zeta_{c1}[k] + \zeta_{c2}[k] \leq 0.95 \ \forall \ k \ . \quad (5.87)$$

Equations 5.86 and 5.87 ensure that the normalized lengths of the superheated fluid region in the evaporator and subcooled region in the condenser, respectively, are maintained at some minimum fraction of the total tube length in each heat exchanger. These constraints are necessary for the purpose of this discussion since the linearized model assumes that the evaporator is operating with 2 fluid regions and that the condenser is operating with 3 fluid regions.

Finally, the following three nonlinear thermodynamic constraints are introduced to satisfy the second law of thermodynamics:

$$\dot{W}_{VCC}[k] - \dot{X}_{dest,VCC}[k] \geq 0 \ \forall \ k \tag{5.88}$$

where $\dot{W}_{VCC}$ is equal to the power (energy consumption rate) of the compressor, $\dot{W}_k$, and

$$\begin{aligned} \dot{X}_{dest,k}[k] &\geq 0 \ \forall \ k \\ \dot{X}_{dest,v}[k] &\geq 0 \ \forall \ k \\ \dot{X}_{dest,e}[k] &\geq 0 \ \forall \ k \\ \dot{X}_{dest,c}[k] &\geq 0 \ \forall \ k \ . \end{aligned} \tag{5.89}$$

Equation 5.88 ensures that the reversible power is always nonnegative, and the inequalities shown in Eq. 5.89 ensure that the exergy destruction rate for each individual component of the VCC system is always nonnegative.

5.4 Simulated Case Study

In this section, a case study will be presented in which the exergy destruction minimization (EDM) optimal control problem is solved for a particular VCC system and specified cooling capacity demand profile. In Section 5.4.1 the solution of the EDM optimal control problem will be presented. In Section 5.4.2, a second optimal control problem minimizing energy consumption over a finite time horizon will be formulated and solved, and the solution will be compared against the results presented in Section 5.4.1. The tradeoffs between minimizing energy consumption and minimizing exergy destruction will discussed, specifically in the context of transient VCC system operation.

5.4.1 Solution of EDM Optimal Control Problem

The exergy destruction minimization (EDM) optimal control problem formulated in the previous section is solved offline as a finite-horizon optimization problem and then validated on the corresponding nonlinear VCC system model in the ATTMO Toolbox [66]. The function *fmincon* in the MATLAB Optimization Toolbox was used with a sequential quadratic programming algorithm to find the solution, defined as

$$\mathbf{u}^{*}_{EDM} = \arg\min_{\mathbf{u}} \left(J_{EDM,VCC} \right) \tag{5.90}$$

where

$$J_{EDM,VCC} = \left\| C_{des} - C_{ach} \right\|_2 + \lambda \cdot \sum_{k=1}^{n_p} \dot{X}_{dest,VCC}[k] \cdot \Delta t \ . \tag{5.91}$$

The desired cooling capacity, C_{des}, is shown in Figure 5.4. This reference trajectory was chosen to elicit the transient behavior that results from high frequency loading in cooling applications such as refrigerated food transport.

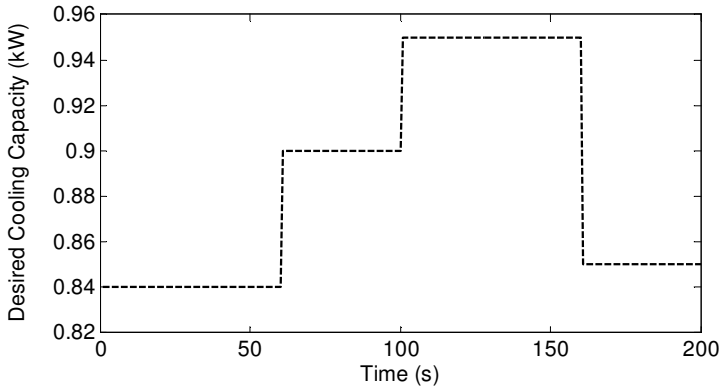

Figure 5.4: Cooling capacity reference trajectory.

The time horizon, $t_{horizon}$, is chosen as 200 seconds to match the total length of the cooling capacity reference trajectory shown in Figure 5.4. The sample time, Δt, was chosen as 1 second. Therefore, the prediction and control horizons, n_p and n_u, consist of 200 discrete time steps. The weighting factor λ was chosen heuristically as 1×10^{-2} to sufficiently weight the performance objective and achieve reasonable reference tracking performance. The constant disturbances (Eq. 5.63) were specified as $T_{e,ai}$ = 18°C and $T_{c,ai}$ = 26°C. Finally, the upper and lower bound constraints on the decision variables are given in Table 5.1 where a_v is the EEV aperture, ω_k is the compressor speed, and $\dot{m}_{a,e}$ and $\dot{m}_{a,c}$ are the evaporator and condenser air mass flow rates.

Table 5.1: Upper and Lower Bound Constraints on Decision Variables

Decision Variable	Units	Lower Bound	Upper Bound
a_v	% open	8	11
ω_k	rpm	900	1100
$\dot{m}_{a,e}$	kg/s	0.1	0.3
$\dot{m}_{a,e}$	kg/s	0.3	0.6

The optimal control input signals are shown in Figure 5.5. The exergy destruction rate and the exergetic efficiency are plotted as a function of time in Figure 5.6.

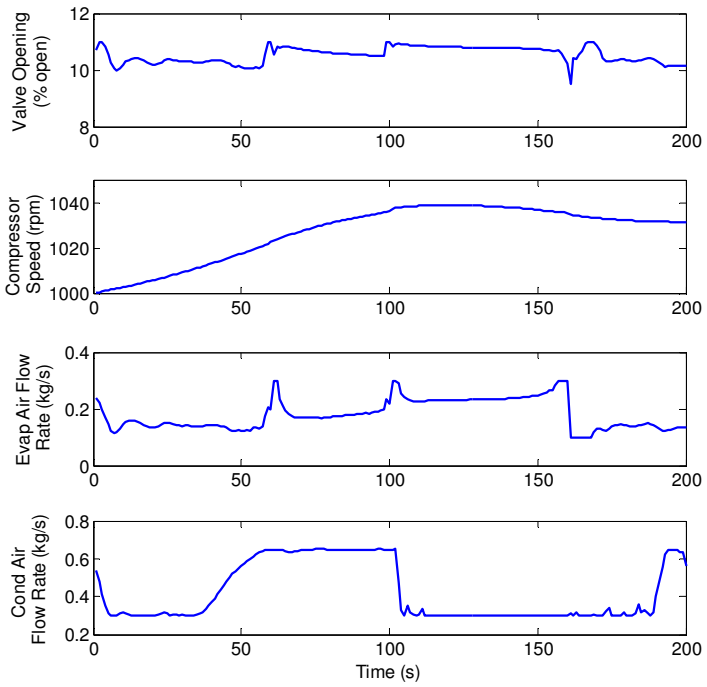

Figure 5.5: Optimal control input signals, $\mathbf{u}^*_{EDM}$.

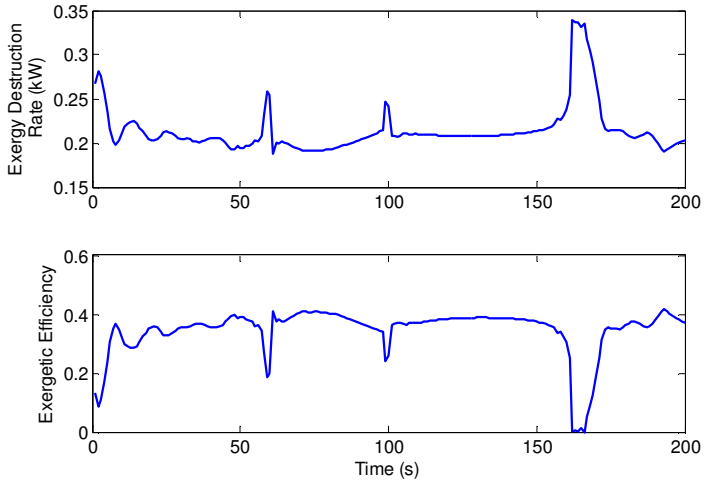

Figure 5.6: Simulated exergy destruction rate and exergetic efficiency using $\mathbf{u}^{*}_{EDM}$ using the linearized system model.

When solved offline, the optimization problem is relying on the accuracy of the linearized prediction model to determine the optimal control decisions for meeting both the performance and efficiency objectives. To validate the accuracy of the solution, the optimal control input signals were fed as inputs to the original nonlinear VCC system model. The cooling capacity achieved based on the offline optimization is compared to the achieved cooling capacity in the nonlinear system model in Figure 5.7. For the interested reader, additional plots comparing the individual dynamic state variables from both the linear and nonlinear simulations are presented in Appendix D.

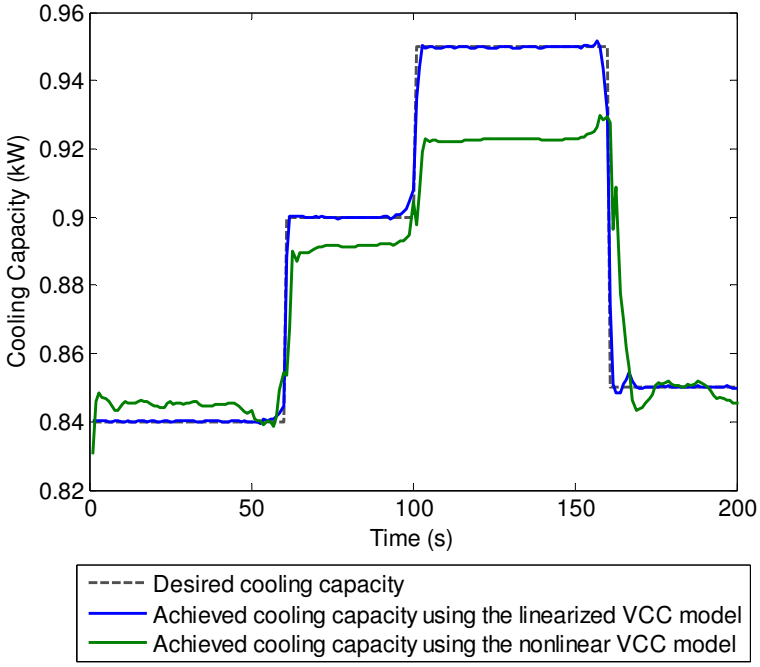

Figure 5.7: Comparison of simulated cooling capacity using the linearized system model with simulated cooling capacity using nonlinear system model.

As expected, there is some discrepancy between the curves shown in Figure 5.7, particularly when the system is trying to track the highest cooling capacity of 0.95kW between t =100 seconds and t =160 seconds. The nominal operating condition of the linearized prediction model produces about 0.83kW of cooling. Therefore, operation at 0.95kW represents a deviation away from the nominal operating condition greater than 10% which may account for the discrepancy.

5.4.2 Comparison between EDM and Energy Consumption Minimization

5.4.2.1 Reversible Power Analysis

During steady-state operation, power minimization and exergy destruction (rate) minimization are equivalent for a standard VCC system as was shown in the case of the electric chiller bank in Chapter 3. However, during transient operation, this is not necessarily true. Recall Eq. 2.8 written here in non-rate form:

$$X_{dest} = W - W_{rev} \ . \qquad (5.92)$$

Using Eq. 5.92, the reversible work during a finite time horizon assuming transient operation of the VCC system is

$$\begin{aligned} W_{rev} &= W - X_{dest} \\ &= \sum_{k=1}^{n_p}\left(\dot{m}_{r,k}[k]\left(h_{k,ro}[k]-h_{k,ri}[k]\right)\right) - T_H \sum_{k=1}^{n_p}\left(\frac{\dot{Q}_{c1}[k]}{T_{w,c1}[k]}+\frac{\dot{Q}_{c2}[k]}{T_{w,c2}[k]}+\frac{\dot{Q}_{c3}[k]}{T_{w,c3}[k]}-\frac{\dot{Q}_{e1}[k]}{T_{w,e1}[k]}-\frac{\dot{Q}_{e2}[k]}{T_{w,e2}[k]}\right) \\ &\quad -T_H \sum_{k=1}^{n_p}\left(g_{e1}[k]+g_{e2}[k]+g_{c1}[k]+g_{c2}[k]+g_{c3}[k]\right) \end{aligned} \quad (5.93)$$

which will not be constant with respect to the decision variables in the optimization problem. Therefore, we expect that the optimal control problem formulated with a power minimization metric will produce a different optimal solution than was presented in the previous section.

We will now define a second optimal control problem where the objective function, $J_{PM,VCC}$, is formulated to minimize the total *energy* consumed over the time horizon:

$$\begin{aligned} J_{PM,VCC} &= \left(\left\|C_{des}-C_{ach}\right\|_2\right) + \lambda\cdot\left(\sum_{k=1}^{n_p}\dot{W}_k[k]\right)\Delta t \\ &= \left(\left\|C_{des}-C_{ach}\right\|_2\right) + \lambda\cdot\left(\sum_{k=1}^{n_p}\dot{m}_k[k]\left(h_{k,ro}[k]-h_{k,ri}[k]\right)\right)\Delta t \end{aligned} \quad (5.94)$$

where $\dot{W}_k$ is the instantaneous power consumption (i.e. energy consumption rate) in the VCC system. The optimal solution is defined as

$$\mathbf{u}^*_{PM} = \arg\min_{\mathbf{u}}\left(J_{PM,VCC}\right) . \quad (5.95)$$

Using an abuse of notation, the subscript *PM*, signifying power minimization, will be used to represent *energy consumption* minimization, rather than using the abbreviation ECM which can be easily confused with EDM.

The energy consumption minimization optimal control problem was formulated with the same constraints, weighting factor λ, and constant disturbances that were specified in the optimal control problem designed to minimize total exergy destruction. The solutions of the two optimal control problems will be compared in the following figures. Note that all of the figures contain simulated results using the *linearized* model.

First the tracking of the desired cooling capacity by each optimal controller is compared in Figure 5.8. Both optimal solutions produce very similar results.

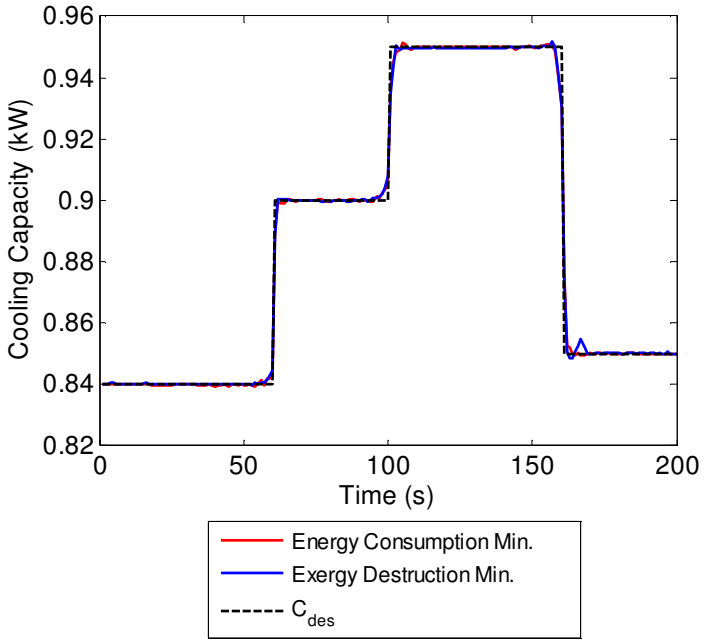

Figure 5.8: Comparison of cooling capacity tracking performance using $\mathbf{u}^*_{EDM}$ and $\mathbf{u}^*_{PM}$.

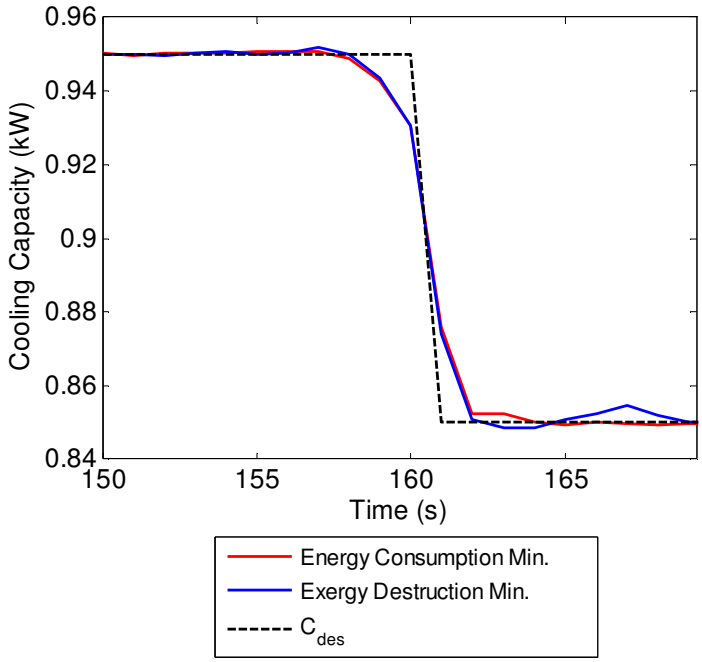

Figure 5.9: Closer view of Figure 5.8.

The optimal control input signals which achieve this reference tracking performance are compared in Figure 5.10. The primary difference is seen in the optimal control input signal for the condenser air mass flow rate; the energy consumption minimization chose the maximum

allowable air mass flow rate for most of the 200-second time horizon whereas the EDM primarily chose the minimum allowable air mass flow rate.

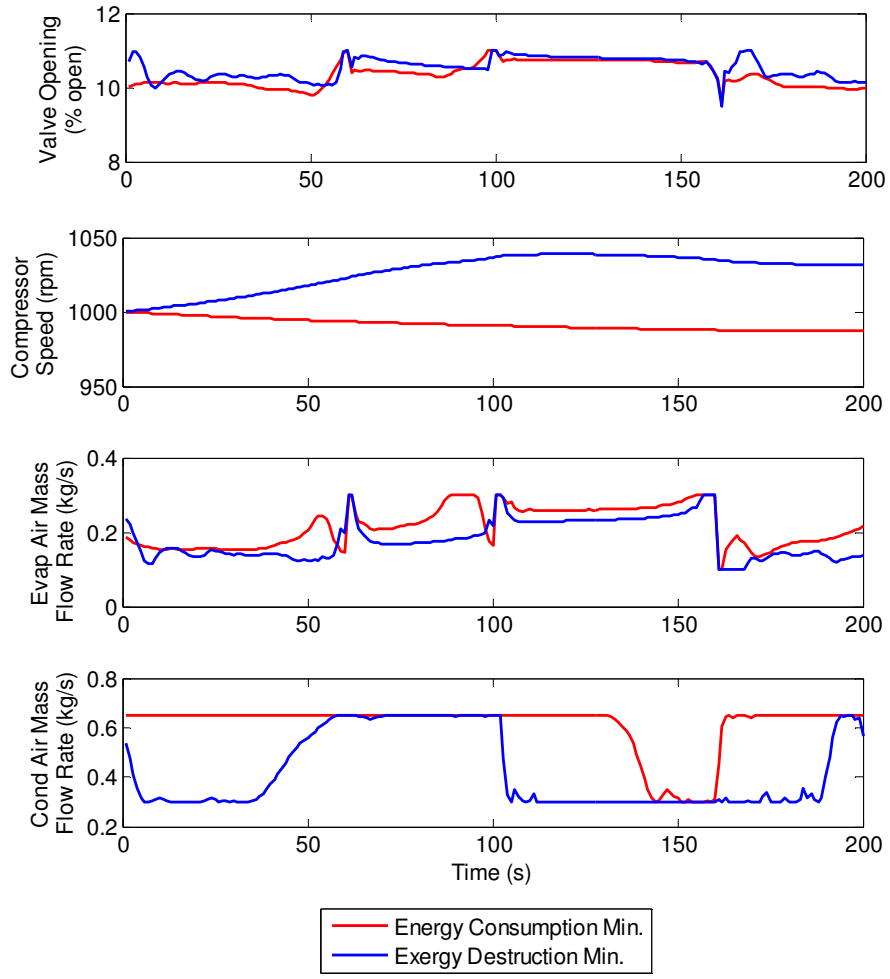

Figure 5.10: Comparison between $\mathbf{u}^*_{EDM}$ and $\mathbf{u}^*_{PM}$.

Remark 1. Only the refrigerant side dynamics of the VCC system are considered in the derivation of the dynamic rate of exergy destruction. Therefore the power consumption of the heat exchanger fans was not considered in the derivation of either objective function, implying that there was no penalty, from an energy perspective, of choosing a very high condenser air mass flow rate. This can explain why the energy consumption minimization chose to operate the system with a very high condenser air mass flow rate, and in some cases high evaporator air mass flow rate as well. However, this control decision will have consequences with regards to the exergy destruction in the condenser, to be highlighted in Figure 5.12. ■

The exergy destruction rate, energy consumption rate, and reversible power resulting from each of the two optimal solutions are shown in Figure 5.11.

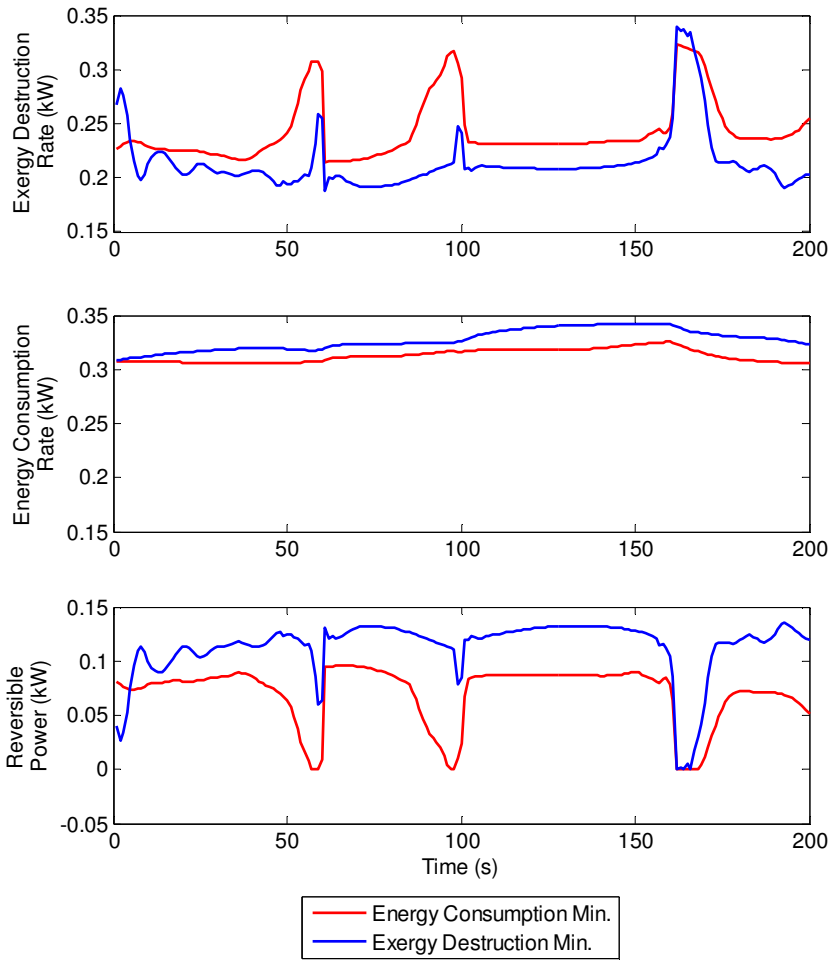

Figure 5.11: Comparison of exergy destruction rate, energy consumption rate, and reversible power over 200 second time horizon using $\mathbf{u}^*_{EDM}$ and $\mathbf{u}^*_{PM}$. The same range is used for each plot.

First, it is important to highlight that the reversible work is not equivalent between the two optimal control problems, verifying the statement made earlier regarding the expected difference in the two optimal control solutions. This is particularly important because transient exergy analyses are not typically applied to VCC systems nor is EDM typically conducted using a dynamic exergy destruction rate. These results show that when considering transient operation of a VCC system, EDM has the potential to make different decisions about how to operate the

system than a conventional power or energy minimization will, to meet the same performance demand.

Also as expected, EDM produced a solution which destroys less exergy over the 200-second time horizon whereas the energy consumption minimization produced a solution which consumes less energy over the same time horizon. The total exergy destroyed and total energy consumed using each optimal solution is compared in Table 5.2. Note that the percent differences were calculated relative to the EDM solution.

Table 5.2 Total Exergy Destruction and Energy Consumption Evaluated Using $\mathbf{u}^*_{EDM}$ and $\mathbf{u}^*_{PM}$

	Exergy Destruction Minimization (kJ)	Energy Consumption Minimization (kJ)	Percent Difference (%)
Total Exergy Destroyed	42.85	48.45	-13.05
Total Energy Consumed	65.48	62.54	4.49

Although the EDM optimal solution results in 4.49% greater energy consumption than the energy consumption minimization optimal solution, it destroys 13.05% less exergy. Therefore, the tradeoff between energy consumption and exergy destruction is not necessarily 1:1. To analyze this more closely, the exergy destruction rate for each individual VCC component is compared in Figure 5.12 The total exergy destroyed and energy consumed in each component using both optimal solutions is shown in Table 5.3.

Table 5.3 Total Exergy Destruction Evaluated for each Component Using Optimal Solutions from both EDM and Energy Consumption Minimization

Total Exergy Destruction by Component	Exergy Destruction Minimization (kJ)	Energy Consumption Minimization (kJ)	Percent Difference (%)
EEV	3.11	2.82	9.42
Compressor	33.7	31.9	5.34
Evaporator	2.77	2.36	14.6
Condenser	3.24	11.3	-250

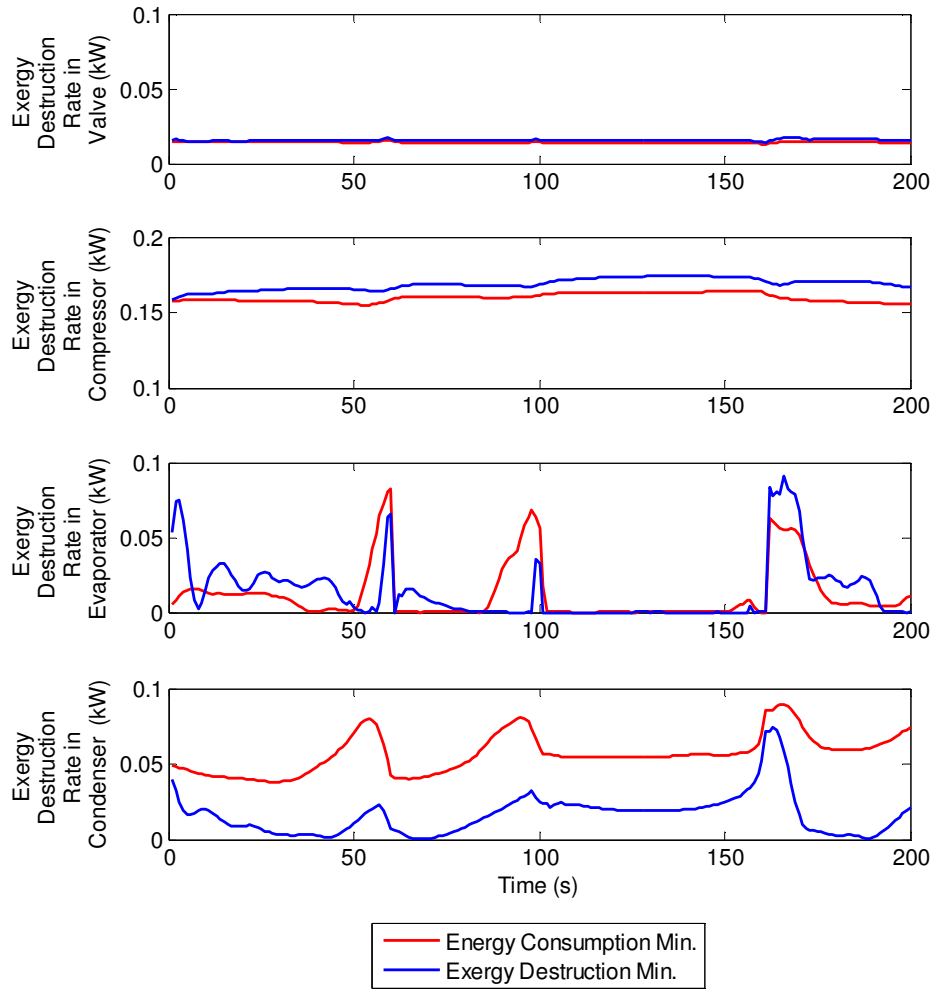

Figure 5.12: Exergy destruction rate comparison by VCC system component for $\mathbf{u}^*_{EDM}$ and $\mathbf{u}^*_{PM}$. The same range is used for each plot.

Surprisingly, the energy consumption minimization produced a set of optimal control inputs which destroyed *less* exergy in the EEV, compressor, and evaporator. However, in the condenser, the energy consumption minimization destroyed 250% *more* exergy than was destroyed using the optimal solution $\mathbf{u}^*_{EDM}$. Despite the fact that the energy consumption minimization "outperformed" the EDM in the EEV, compressor, and evaporator, the difference in exergy destruction in the condenser was so significant as to overcome the differences in the other three components.

Remark 2. It has long been cited that the greatest exergy destruction site in a VCC system is the compressor [19]. This is still the case as shown in Table 5.3. However, these results show

that it is possible for exergy to be destroyed on the same order of magnitude in other components, in this case the condenser, when all four control inputs are being modulated. As variable-speed fans become more common in commercial VCC systems, the effect of air mass flow rate on the overall efficiency of the system can be quite significant, particularly during transient operation. What is more, the irreversibilities being characterized here are not of the fan (which is omitted from this analysis) but from heat transfer and mass transfer occurring inside the condenser. These irreversibilities are inherently not taken into account in an energy consumption minimization, which would only be able to account for losses in the fan which is responsible for producing the air mass flow rate. ■

Finally, it is useful to consider efficiency metrics for VCC systems – the COP and the exergetic efficiency – computed for transient operation as shown in Eq. 5.96 and Eq. 5.97 respectively.

$$\mathrm{COP}[k] = \frac{\dot{Q}_e[k]}{\dot{W}_k[k]} \tag{5.96}$$

$$\eta_{II}[k] = 1 - \frac{\dot{X}_{dest,VCC}[k]}{\dot{W}_k[k]} \tag{5.97}$$

COP is a measure of the rate at which cooling is achieved by the VCC system, relative to the rate at which work is done on the system. By virtue of how VCC systems work, the COP is generally greater than one, with a higher COP indicating greater efficiency. A major downside of COP as a metric, however, is that it is inherently not normalized, so it cannot be used to characterize how well a system is performing relative to a baseline measure of performance. Alternatively, the exergetic efficiency measures the rate at which exergy is destroyed relative to the rate at which exergy is supplied to the VCC system. This metric is defined between 0 and 1 and tells us how effectively the exergy supplied to this system, in this case work done on the compressor, is used in the VCC system in an absolute sense.

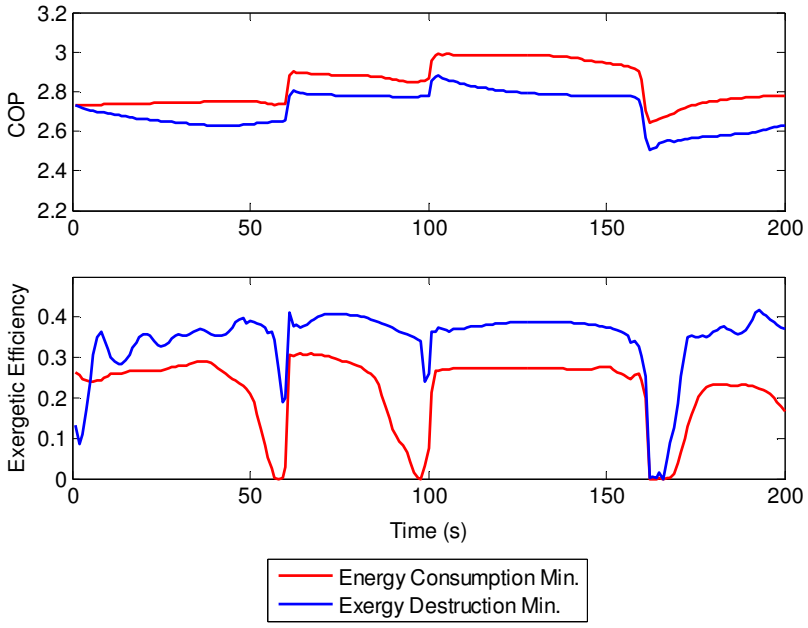

Figure 5.13: Instantaneous COP and exergetic efficiency resulting from operating the system with $\mathbf{u}^*_{EDM}$ and $\mathbf{u}^*_{PM}$.

Figure 5.13 shows that the energy consumption minimization operates the system at a higher COP but with a lower exergetic efficiency. On average, the COP achieved by minimizing exergy destruction was 4.68% lower than that achieved by minimizing energy consumption. On the other hand, on average, the exergetic efficiency achieved by minimizing exergy destruction was 36.6% greater than that achieved by minimizing energy consumption. These results indicate that although the EDM optimal solution would operate the system in such a way as to consume more energy, that energy is being used by the system more "effectively". To be more precise, this means operating the system with fewer irreversibilities, such as friction in refrigerant flow and losses in heat transfer across finite temperature differences. Operating the system in this way can have implications on the wear of the physical components themselves, a longer term objective for the operation of thermal systems which was not explicitly accounted for in either objective function considered in this case study.

5.4.3 Summary

To summarize, the results in this section showed that during transient operation of a VCC system, there exists a distinct tradeoff in system operation based on minimization of exergy destruction versus minimization of energy consumption. Major conclusions are reiterated below.

- Exergy destruction minimization and energy consumption minimization are not equivalent when the dynamic exergy destruction rate for a VCC system is considered.
- The dynamic EDM objective function specifically accounted for irreversibilities in each component of the VCC whereas the energy consumption minimization did not.
- The distribution of exergy destruction across the components of the VCC system changes as a function of the control inputs, demonstrating not only the importance of considering the dynamic exergy destruction rate but also of optimal control of VCC systems with full actuation.
- Minimizing total exergy destruction leads to operation with a higher exergetic efficiency which may result in less component wear over time.

Chapter 6
Conclusion

6.1 Summary of Research Contributions

Integrated energy systems (IESs) are complex systems which operate across multiple energy domains and offer a reliable and efficient way to generate both electrical power and thermal energy to meet multiple end requirements. In order to operate these systems effectively, setpoint optimization and/or optimal control is needed. In this thesis, an optimization and control framework for the operation of IESs was developed with a specific emphasis on providing a systematic method for obtaining a physics-based, generalizable, and modular objective function.

We have proposed the use of exergy destruction as the metric for obtaining such a versatile objective function. Exergy destruction minimization (EDM) is a tool which has primarily been used for design optimization but not for real-time optimization and control of thermodynamic and other energy systems. Nevertheless, it is well suited for IESs because it can fully characterize irreversibilities across multiple energy domains. Moreover, the exergy destruction rate for a complex system can be derived by analyzing subsystems and/or components individually and then summing these rates for the overall system.

The generalizability and modularity of the framework was demonstrated through its application to a combined cooling, heating, and power (CCHP) system. The CCHP system was easily divided into 4 subsystems which were analyzed individually, thereby greatly simplifying the derivation of the complete objective function. An additional layer of flexibility was introduced as the "interchangeability" between power minimization and exergy destruction rate minimization for those subsystems in which the reversible power is constant with respect to the decision variables. Interchangeability allows the user to only derive the exergy destruction rate

for those systems in which the equivalence does not hold and construct an objective function which would result in the same solution as minimizing the rate of exergy destruction in every subsystem.

Exergy analyses have long been used to better understand the behavior of a variety of thermodynamic systems, primarily from a static design and operation point of view. However, as the complexity of integrated energy systems grows, for example as a result of intermittent grid power from renewable energy technologies such as wind and solar, an understanding of transient behavior is needed. As a case study, a detailed derivation of the dynamic exergy destruction rate in a standard VCC system was derived for the refrigerant-side dynamics assuming a lumped parameter moving boundary model framework for the heat exchanger dynamics. The dynamic rate of exergy destruction was then used in formulating an EDM optimal control problem for a VCC system wherein the decision variables were the control inputs to the system. Moreover, the VCC system was assumed to be fully actuated with an electronic expansion valve (EEV), and variable-speed compressor, evaporator fan, and condenser fan. The results highlighted how time-varying control decisions can affect the distribution of irreversibilities throughout the overall system, particularly in the heat exchangers which are typically considered to have fewer irreversibilities compared to the compressor and EEV.

The relationship between exergy destruction rate, power consumption, and reversible power was utilized throughout this work to specifically characterize when tradeoffs exists between the minimization of energy consumption versus exergy destruction. During both steady-state operation of the CCHP system and transient operation of the VCC system, it was shown that minimizing exergy destruction increases exergetic efficiency at some expense of energy consumption, but that the decrease in exergy destruction can possibly outweigh the increases in energy consumption.

As electrification of individual and integrated energy systems continues to increase, model-based optimization and control techniques offer many tools for improving the efficiency of such systems during many different modes of operation. This thesis showed that an exergy destruction minimization has the potential to uncover a different set of solutions than those produced by an energy or power minimization, and should therefore be considered as a valuable tool for *operational* optimization of IESs. Moving forward, increased complexity and a greater

diversity of systems can be analyzed to ensure that this potential does indeed scale across a wide class of IESs. Specific areas of future investigation are detailed in the next section.

6.2 Future Work

The generalizability and modularity of the approach are key features which are needed for widespread applicability of this framework to IESs. Further investigation should include consideration of irreversibilities in non-thermodynamic energy systems, such as wind turbines, and in storage devices, such as chemical batteries or chilled water storage tanks. These subsystems are becoming integral parts of IESs. Energy storage devices particularly lend themselves to the EDM approach because they neither produce nor consume energy but instead are used for the transfer of energy from one medium to another (and also often one form of energy to another). The storage and discharge processes are inherently irreversible, and these losses affect the overall efficiency of a given system.

Exergy destruction minimization has not previously been combined with optimal control algorithms for online control of energy systems. Based on the results of this work, further complexity can be addressed. The dynamic exergy destruction rate derived for the standard VCC system currently does not account for irreversibilities on the secondary fluid side of the heat exchangers, nor the two components which act solely on the secondary fluid – the heat exchanger fans. An augmentation of the dynamic exergy rate to include these features will offer further insight into the distribution of irreversibilities in the system during transient operation, particularly during high frequency actuation of the system.

It is also important to validate the ideas proposed in this work on physical hardware to gain a deeper understanding of the benefits of EDM for operational optimization of energy systems. To make the dynamic EDM metric more viable for experimental implementation, additional investigation should consider alternative nonlinear search algorithms which may increase the speed of solving the optimal control problem. Moreover, in the specific case of VCC systems, alternative formulations of the control architecture, such as a time-scale separation of the fast and slow dynamics, can be considered.

List of References

[1] D. Wu and R. Wang, "Combined cooling, heating and power: A review," *Progress in Energy and Combustion Science,* vol. 32, no. 5-6, pp. 459-495, 2006.

[2] "Combined heat and power partnership," U.S. Environmental Protection Agency, 12 September 2012. [Online]. Available: http://epa.gov/chp/index.html.

[3] P. LeMar, "Integrated Energy Systems (IES) for Buildings: A Market Assessment," Resource Dynamics Corporation, 2002.

[4] "White House Announces Executive Order on Industrial Energy Efficiency, including Combined Heat and Power," Federal Energy Management Program, 30 August 2012. [Online]. Available: http://www1.eere.energy.gov/femp/news/news_detail.html?news_id=18599.

[5] M. Hosseini, I. Dincer and M. A. Rosen, "Hybrid solar-fuel cell combined heat and power systems for residential applications: Energy and exergy analyses," *Journal of Power Sources,* vol. 221, pp. 372-380, 2013.

[6] X. P. Chen, Y. D. Wang, H. D. Yu, D. W. Wu, Y. Li and A. P. Roskilly, "A domestic CHP system with hybrid electrical energy storage," *Energy and Buildings,* 2012.

[7] "Combined heat and power technology fills an important energy niche," U.S. Energy Information Administration, 4 October 2012. [Online]. Available: http://www.eia.gov/todayinenergy/detail.cfm?id=8250#.

[8] O. A. Shaneb, P. C. Taylor and G. Coates, "Optimal online operation of residential mu systems using linear programming," *Energy and Buildings,* vol. 44, pp. 17-25, 2012.

[9] H. Cho, R. Luck and L. M. Chamra, "Supervisory Feed-Forward Control for Real-Time Topping Cycle CHP Operation," *Journal of Energy Resources Technology,* 2010.

[10] V. Tsourapas, A. Stefanopoulou and J. Sun, "Dynamics, optimization and control of a fuel cell based combined heat power (chp) system for shipboard applications," in *Proceedings of the 2005*

American Control Conference, 2005.

[11] A. Y. Petrov, A. Zaltash, S. D. Labinov, D. T. Rizy and R. L. Linkous, "Dynamic performance of a 30-kW microturbine-based CHP system," *ASHRAE Transactions,* vol. 111, no. 1, 2005.

[12] X. Q. Kong, R. Z. Wang and X. H. Huang, "Energy optimization model for a CCHP system with available gas turbines," *Applied Thermal Engineering,* vol. 25, no. 2, pp. 377-391, 2005.

[13] T. A. Reddy and I. Maor, "Cost penalties of near optimal scheduling control of BCHP systems: part II - modeling, optimization, and analysis results," *ASHRAE Transactions,* vol. 115, no. 1, pp. 287-307, 2009.

[14] H. Cho, R. Luck, S. D. Eksioglu and L. M. Chamra, "Cost-optimized real-time operation of CHP systems," *Energy and Buildings,* vol. 41, no. 4, pp. 445-451, 2009.

[15] E. Thorin, H. Brand and C. Weber, "Long-term optimization of cogeneration systems in a competitive market environment," *Applied Energy,* vol. 81, no. 2, pp. 152-169, 2005.

[16] M. J. Moran and H. N. Shapiro, Fundamentals of Engineering Thermodynamics, John Wiley & Sons, Inc., 2004.

[17] A. Bejan, Entropy Generation Minimization, Boca Raton: CRC Press LLC, 1996q.

[18] Y. A. Cengel and M. A. Boles, Thermodynamics: An Engineering Approach, 6th ed., Boston: The McGraw-Hill Companies, Inc., 2008.

[19] T. J. Kotas, The Exergy Method of Thermal Plant Analysis, London: Butterworths, 1985.

[20] J. U. Ahamed, R. Saidur and H. H. Masjuki, "A review on exergy analysis of vapor compression refrigeration system," *Renewable and Sustainable Energy Reviews,* vol. 15, no. 3, pp. 1593-1600, 2011.

[21] H. Mahabadipour and H. Ghaebi, "Development and comparison of two expander cycles used in refrigeration system of olefin plant based on exergy analysis," *Applied Thermal Engineering,* vol. 50, no. 1, pp. 771-780, 2012.

[22] A. Cihan, O. Hachafzoglu and K. Kahveci, "Energy-exergy analysis and modernization suggestions for a combined-cycle power plant," *International Journal of Energy Research,* vol. 30, no. 2, pp. 115-126, 2006.

[23] G. Tsatsaronis, "Thermoeconomic Analysis and Optimization of Energy Systems," *Progress in Energy and Combustion Science,* vol. 19, no. 3, pp. 227-257, 1993.

[24] G. Tsatsaronis and M. J. Moran, "Exergy-Aided Cost Minimization," *Energy Conversion and Management,* vol. 38, no. 15-17, pp. 1535-1542, 1997.

[25] A. Abusoglu and M. Kanoglu, "Exergoeconomic analysis and optimization of combined heat and power production: A review," *Renewable and Sustainable Energy Reviews,* vol. 13, pp. 2295-2308, 2009.

[26] A. Lazzaretto and G. Tsatsaronis, "SPECO: A systematic and general methodology for calculating efficiencies and costs in thermal systems," *Energy,* vol. 31, no. 8-9, pp. 1257-1289, 2006.

[27] A. Bejan, "Fundamentals of exergy analysis, entropy generation minimization, and the generation of flow architecture," *International Journal of Energy Research,* vol. 26, pp. 545-565, 2002.

[28] R. J. Krane, "A Second Law analysis of the optimum design and operation of thermal energy storage systems," *International Journal of Heat and Mass Transfer,* vol. 30, no. 1, pp. 43-57, 1987.

[29] W. G. le Roux, T. Bello-Ochende and J. P. Meyer, "Thermodynamic optimisation of the integrated design of a small-scale solar thermal Brayton cycle," *International Journal of Energy Research,* vol. 36, pp. 1088-1104, 2012.

[30] P. K. Nag and S. De, "Design and Operation of a Heat Recovery Steam Generator with Minimum Irreversibility," *Applied Thermal Engineering,* vol. 17, no. 4, pp. 385-391, 1997.

[31] J. Vargas and A. Bejan, "Thermodynamic optimization of finned crossflow heat exchangers for aircraft environmental control systems," *International Journal of Heat and Fluid Flow,* vol. 22, pp. 657-665, 2001.

[32] B. David, J. Ramousse and L. Luo, "Optimization of thermoelectric heat pumps by operating condition management and heat exchanger design," *Energy Conversion and Management,* vol. 60, pp. 125-133, 2012.

[33] N. Jain and A. G. Alleyne, "A framework for the optimization of integrated energy systems," *Applied Thermal Engineering,* vol. 48, pp. 495-505, 2012.

[34] V. Chandan, A.-T. Do, B. Jin, F. Jabbari, J. Brouwer, I. Akrotirianakis, A. Chakraborty and A. Alleyne, "Modeling and Optimization of a Combined Cooling, Heating and Power Plant System," in *Proceedings of ACC 2012, the 31st American Control Conference*, Montreal, 2012.

[35] V. Chandan and A. Torzhkov, "Gray-Box Model Formulation of a Cogenerating Microgrid, Part 1: Physical Formulation," 2011. [Online]. Available: http://mechse.illinois.edu/media/uploads/web_sites/104/files/cchp_modeling_chandan_vikas_2011.20121117.50a84437378641.65743102.pdf. [Accessed September 2012].

[36] A. H. Harvey, A. P. Peskin and S. A. Klein, *NIST Standard Reference Database 10,* Boulder: National Institute of Standards and Technology, 1997.

[37] M. Pidwirny, "Chapter 7: Introduction to the Atmosphere," May 2009. [Online]. Available:

http://www.physicalgeography.net/fundamentals/7l.html. [Accessed September 2012].

[38] X. Li and J. M. Ogden, "Understanding the design and economics of distributed tri-generation systems," *Journal of Power Sources,* no. 197, pp. 186-195, 2012.

[39] L. Ni, S. K. Lau, H. Li, T. Zhang, J. S. Stansbury, J. Shi and J. Neal, "Feasibility study of a localized residential grey water energy-recovery system," *Applied Thermal Engineering,* no. 39, pp. 53-62, 2012.

[40] Toolbox, MATLAB Optimization, *The Mathworks Inc.,* Natick, MA, 2002.

[41] W. Stoecker and J. Jones, Refrigeration and Air-Conditioning, New York: McGraw-Hill Book Company, 1983.

[42] T. Q. Qureshi and S. A. Tassou, "Variable-speed capacity control in refrigeration systems," *Applied Thermal Engineering,* vol. 16, no. 2, pp. 103-113, 1996.

[43] Braven, K. D, Penoncello, S., Herold, K., et. al., "Improving heat pumps and air conditioning," *Mechanical Engineering,* vol. 115, no. 9, 1993.

[44] X. D. He, S. Liu, H. H. Asada and H. Itoh, "Multivariable Control of Vapor Compression Systems," *HVAC&R Research,* vol. 4, no. 3, pp. 205-230, 1998.

[45] L. S. Larsen, C. Thybo, J. Stoustrup and H. Rasmussen, "Control methods utilizing energy optimizing schemes in refrigeration systems," in *European Control Conference*, 2003.

[46] L. F. S. Larsen and C. Thybo, "Potential energy savings in refrigeration systems using optimal setpoints," in *Conference on Control Applications*, 2002.

[47] J. B. Jensen and S. Skogestad, "Optimal operation of simple refrigeration cycles; Part I: Degrees of freedom and optimality of sub-cooling," *Computers and Chemical Engineering,* vol. 31, no. 5-6, pp. 712-721, 2007.

[48] M. S. Elliott and B. P. Rasmussen, "A Model-Based Predictive Supervisory Controller for Multi-Evaporator HVAC Systems," in *Proceedings of the American Control Conference*, 2009.

[49] R. Shah, B. P. Rasmussen and A. G. Alleyne, "Application of a Multivariable Adaptive Control Strategy to Automotive Air Conditioning Systems," *International Journal of Adaptive Control and Signal Processing,* vol. 18, no. 2, pp. 199-221, 2004.

[50] L. F. S. Larsen, C. Thybo, J. Stoustrup and H. Rasmussen, "A Method for Online Steady State Energy Minimization with Application to Refrigeration Systems," in *Proceedings of the 43rd IEEE Conference on Decision and Control*, 2004.

[51] N. Jain, B. Li, M. Keir, B. Hencey and A. Alleyne, "Decentralized Feedback Structures of a Vapor

Compression Cycle System," *IEEE Transactions on Control Systems Technology,* vol. 18, no. 1, pp. 185-193, 2010.

[52] F. P. Incropera and D. P. DeWitt, Fundamentals of Heat and Mass Transfer, New York: John Wiley and Sons Inc., 1985.

[53] B. Eldredge, *Improving the Accuracy and Scope of Control-Oriented Vapor Compression Cycle System Models,* Master's thesis, University of Illinois at Urbana-Champaign, 2006.

[54] ASHRAE Handbook: Fundamentals, American Society of Heating, Refrigeration, and Air-Conditioning Engineers, Inc., 2009.

[55] L. Ljung, *System Identification Toolbox for Use with MATLAB,* 2007.

[56] K. Ogata, Modern Control Engineering, 4th ed., Prentice Hall, 2002.

[57] R. Otten, *Superheat Control for Air Conditioning and Refrigeration Systems: Simulation and Experiments,* Master's Thesis: University of Illinois at Urbana-Champaign, 2010.

[58] G. Anand, M. Mahajan, N. Jain, B. Maniam and T. M. Tumas, "e-Thermal: Automobile Air Conditioning Module," in *Society of Automotive Engineers 2004 World Congress*, Detroit, 2004.

[59] H. Tummescheit and J. Eborn, "Design of a Thermo-Hydraulic Model Library in Modelica," in *12th European Simulation Multiconference*, San Diego.

[60] B. A. Cullimore and T. J. Hendricks, "Design and Transient Simulation of Vehicle Air Conditioning Systems," in *Society of Automotive Engineers 2004 World Congress*, Detroit, 2004.

[61] S. Bendapudi and J. E. Braun, "A Review of Literature on Dynamic Models of Vapor Compression Equipment," ASHRAE Report #4036-5, May 2002.

[62] T. L. McKinley and A. G. Alleyne, "An advanced nonlinear switched heat exchanger model for vapor compression cycles using the moving-boundary method," *International Journal of Refrigeration,* vol. 31, no. 7, pp. 1253-1264, 2008.

[63] B. Li and A. G. Alleyne, "A dynamic model of a vapor compression cycle with shut-down and start-up operations," *International Journal of Refrigeration,* vol. 33, no. 3, pp. 538-552, 2010.

[64] J. H. Doty, J. A. Camberos and K. L. Yerkes, "Approximate Approach for Direct Calculation of Unsteady Entropy Generation Rate for Engineering Applications," in *Proceedings of the 50th AIAA Aersopace Sciences Meeting*, Nashville, 2012.

[65] B. P. Rasmussen, *Control-Oriented Modeling of Transcritical Vapor Compression Systems,* Urbana, IL: University of Illinois at Urbana-Champaign, M.S. Thesis, 2000.

[66] M. Kania, J. Koeln, A. Alleyne, K. McCarthy , N. Wu and S. Patnaik, "A Dynamic Modeling

Toolbox for Air Vehicle Vapor Cycle Systems," in *SAE Power Systems International*, Phoenix, AZ, 2012.

[67] B. P. Rasmussen, *Dynamic Modeling and Advanced Control of Air Conditioning and Refrigeration Systems,* Urbana, IL: University of Illinois at Urbana-Champaign, Ph.D. Thesis, 2005.

[68] J. Nocedal and S. J. Wright, Numerical Optimization, New York: Springer Science+Business Media, LLC., 2006.

Appendix A

Nonlinear Parameter Models for Experimental VCC System

This appendix contains nonlinear parameter models for the EEV and compressor on an experimental air-conditioning and refrigeration test stand at the University of Illinois at Urbana-Champaign [67]. The models for valve flow coefficient and compressor volumetric efficiency, shown in Eqs. A.1 and A.2 respectively, were developed in [53] and are shown here for the reader's reference.

$$\begin{aligned}\hat{K}_v = f_1(a_v, P_1, P_2) &= (-9.5984\times10^{-6}) + (2.0481\times10^{-6})a_v \\ &+(5.4106\times10^{-9})(P_2 - P_1) + (-7.4909\times10^{-10})a_v(P_2 - P_1) + (-3.7775\times10^{-8})a_v{}^2\end{aligned} \quad (A.1)$$

$$\begin{aligned}\hat{\eta}_{vol} = f_2(\omega_k, P_1, P_2) &= (0.65127) + (0.00027681)\omega_k + (-0.031338)\frac{P_2}{P_1} \\ &+(3.0221\times10^{-5})\omega_k\frac{P_2}{P_1} + (-1.1905\times10^{-7})\omega_k^2 + (-0.0081256)\left(\frac{P_2}{P_1}\right)^2\end{aligned} \quad (A.2)$$

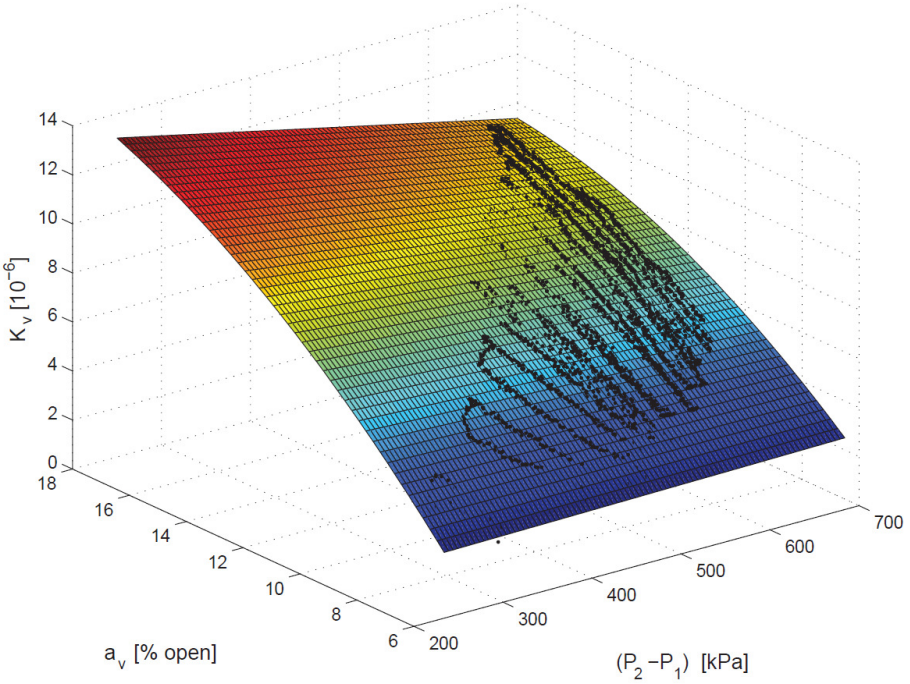

Figure A.1: Flow coefficient map for an EEV. Black points represent experimental data used for map generation.

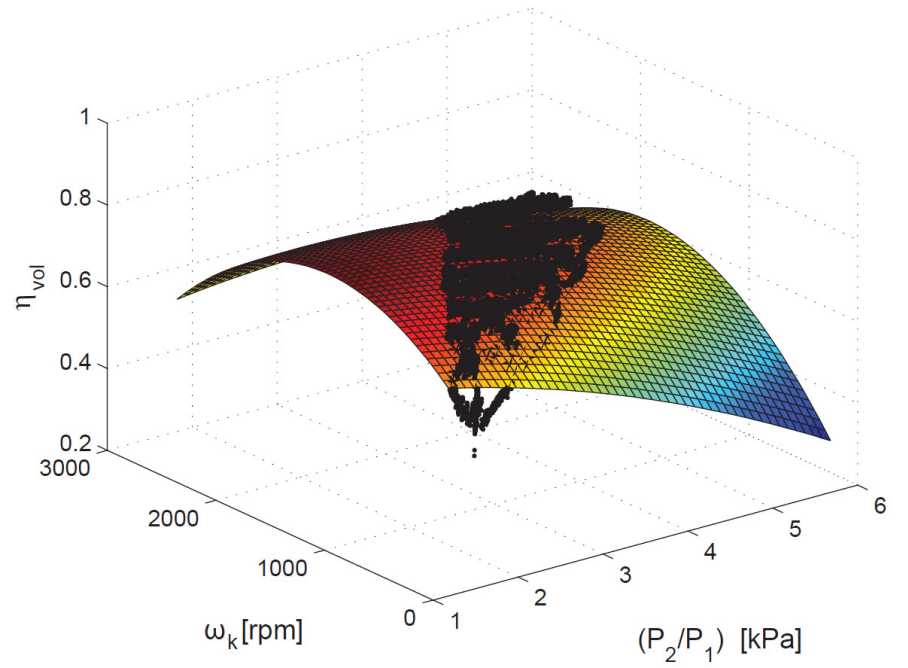

Figure A.2: Volumetric efficiency map for a semi-hermetic reciprocating compressor. Black points represent experimental data used for map generation.

Appendix B
System Identification of Experimental VCC System

This appendix contains the details of a 2-input 2-output system identification of an experimental air-conditioning and refrigeration test stand at the University of Illinois at Urbana-Champaign [67]. The open-loop data was detrended prior to identification; consequently all input and output variables are deviation variables with respect to the nominal operating condition of $u_1 = a_v = 11\%$ and $u_2 = \omega_k = 1200$ rpm. Additionally, the input and output data sets were scaled such that

$$\bar{u} = N_u u \tag{B.1}$$

and

$$\bar{y} = N_y^{-1} y \tag{B.2}$$

where

$$N_u = \begin{pmatrix} 1.87 & 0 \\ 0 & 0.0178 \end{pmatrix}, \tag{B.3}$$

$$N_y = \begin{pmatrix} 18.7 & 0 \\ 0 & 9.93 \end{pmatrix}, \tag{B.4}$$

and $\bar{u} \in \mathbb{R}^{N\times 2}$ and $\bar{y} \in \mathbb{R}^{N\times 2}$ represent the scaled input and output data sets, respectively. N is the number of data points collected for the identification. The diagonal elements of N_u and N_y, respectively, are defined as

$$\begin{aligned} N_u(i,i) &= \sigma(u_i) \\ N_y(i,i) &= \sigma(y_i) \end{aligned} \tag{B.5}$$

for $u_i \in \mathbb{R}^N$, $y_i \in \mathbb{R}^N$, $i = \{1,2\}$ where σ is the standard deviation.

The model was identified with approximately half of the input and output data sets, with the remaining data used for cross validation of the identified model. The scaled identified state space [A,B,C,D] system model is given in Eq. B.6. Again, a bar denotes a scaled quantity.

$$\bar{A} = \begin{pmatrix} -0.0128 & 0.00587 \\ 0.0237 & -0.0322 \end{pmatrix}, \bar{B} = \begin{pmatrix} 0.000832 & -0.000445 \\ -0.00225 & 0.00185 \end{pmatrix}$$
$$\bar{C} = \begin{pmatrix} 28.9 & 3.02 \\ 12.4 & 22.0 \end{pmatrix}, \bar{D} = \begin{pmatrix} 0 & 0 \\ 0 & 0 \end{pmatrix} \qquad \text{(B.6)}$$

The identified model is compared with the identification data in Figure B.1. The cross-validation of the identified model is shown in Figure B.2.

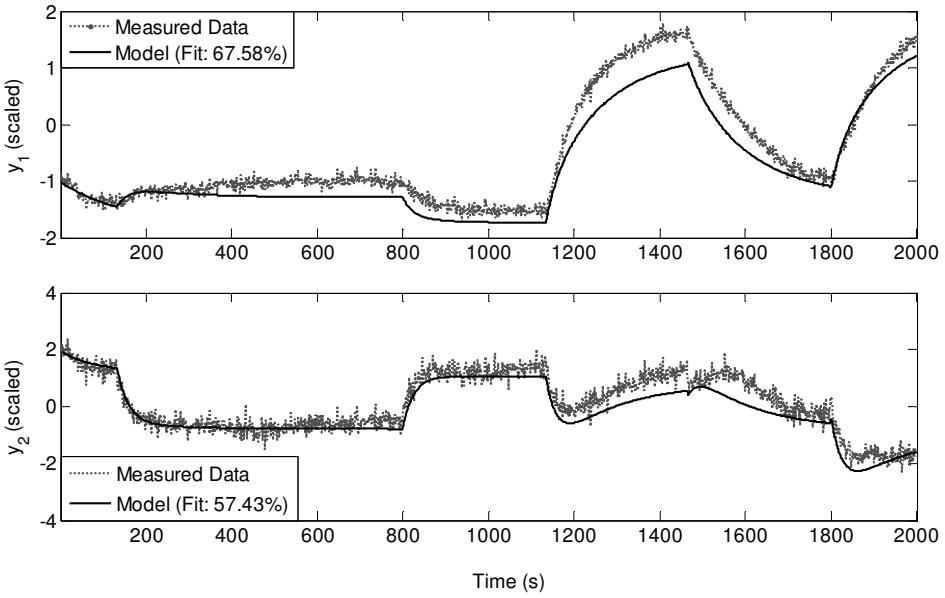

Figure B.1: Validation of identified model; $y_1 = 0.5(P_1 + P_2)$ and $y_2 = P_2 - P_1$.

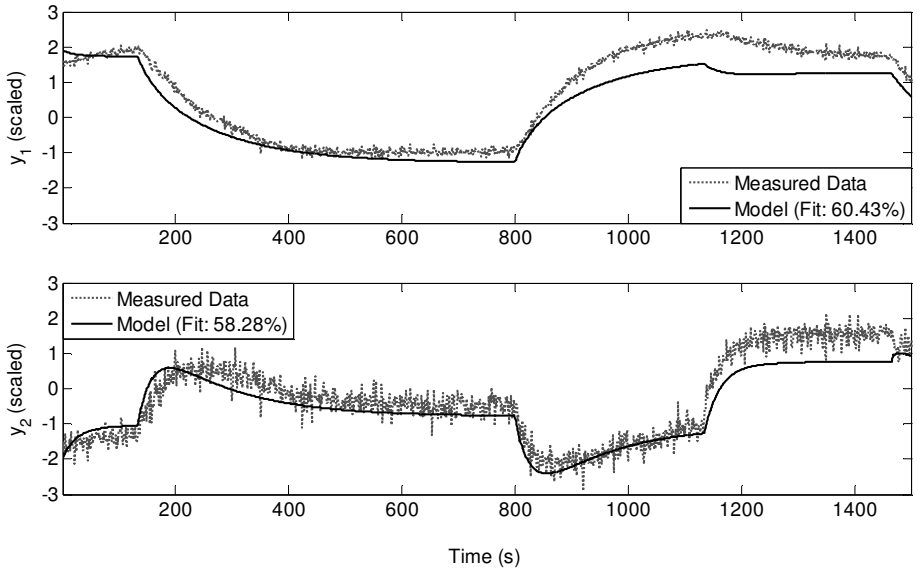

Figure B.2: Cross validation of the identified model.

Appendix C
VCC System Model Linearization

This appendix describes the linearization procedure used to obtain a first-principles linearized model of a standard VCC system in the lumped parameter moving boundary modeling framework.

C.1 Individual Component Linearization

C.1.1 Linearization of Heat Exchanger Models

The linearization procedure for the lumped parameter moving boundary heat exchanger models is described in detail in [67]. The procedure is summarized here for the benefit of the reader. The governing equations for a given heat exchanger model in the lumped parameter moving boundary framework can be written in the form

$$Z(\mathbf{x},\mathbf{u})\cdot\dot{\mathbf{x}} = f(\mathbf{x},\mathbf{u}) \qquad (C.1)$$

where Z can be assumed to be invertible. Then the state derivative vector can be expressed as

$$\begin{aligned}\dot{\mathbf{x}} &= Z(\mathbf{x},\mathbf{u})^{-1}\cdot f(\mathbf{x},\mathbf{u}) \\ &= g(\mathbf{x},\mathbf{u})\ .\end{aligned} \qquad (C.2)$$

Linearizing the system about some operating condition ($\mathbf{x_0}$,$\mathbf{u_0}$) where $\boldsymbol{\delta}\mathbf{x} = \mathbf{x} - \mathbf{x_0}$ and $\boldsymbol{\delta}\mathbf{u} = \mathbf{u} - \mathbf{u_0}$ yields

$$\delta\dot{\mathbf{x}} = \left(\left.\frac{\partial g}{\partial \mathbf{x}}\right|_{\mathbf{x_0},\mathbf{u_0}}\right)\delta\mathbf{x} + \left(\left.\frac{\partial g}{\partial \mathbf{u}}\right|_{\mathbf{x_0},\mathbf{u_0}}\right)\delta\mathbf{u} \qquad (C.3)$$

which can be rewritten as

$$\dot{\mathbf{x}} = \left(\left. \frac{\partial g}{\partial \mathbf{x}} \right|_{\mathbf{x_0},\mathbf{u_0}} \right) (\mathbf{x} - \mathbf{x_0}) + \left(\left. \frac{\partial g}{\partial \mathbf{u}} \right|_{\mathbf{x_0},\mathbf{u_0}} \right) (\mathbf{u} - \mathbf{u_0}) \ . \qquad (C.4)$$

Expanding the first term in Eq. C.4 results in

$$\left. \frac{\partial g}{\partial \mathbf{x}} \right|_{\mathbf{x_0},\mathbf{u_0}} = \left(Z|_{\mathbf{x_0},\mathbf{u_0}} \right)^{-1} \cdot \left. \frac{\partial f}{\partial \mathbf{x}} \right|_{\mathbf{x_0},\mathbf{u_0}} - \left(Z|_{\mathbf{x_0},\mathbf{u_0}} \right)^{-2} \left(\left. \frac{\partial Z}{\partial \mathbf{x}} \right|_{\mathbf{x_0},\mathbf{u_0}} \right)^{-1} \cdot f|_{\mathbf{x_0},\mathbf{u_0}} \ . \qquad (C.5)$$

If the linearization point is chosen to be an equilibrium point of the system, then

$$f|_{\mathbf{x_0},\mathbf{u_0}} = f(\mathbf{x_0}, \mathbf{u_0}) = 0 \qquad (C.6)$$

thereby simplifying Eq. C.5 to

$$\left. \frac{\partial g}{\partial \mathbf{x}} \right|_{\mathbf{x_0},\mathbf{u_0}} = \left(Z|_{\mathbf{x_0},\mathbf{u_0}} \right)^{-1} \cdot \left. \frac{\partial f}{\partial \mathbf{x}} \right|_{\mathbf{x_0},\mathbf{u_0}} . \qquad (C.7)$$

Similarly, for the second term in Eq. C.4, choosing ($\mathbf{x_0}$,$\mathbf{u_0}$) to be an equilibrium point of the system results in

$$\left. \frac{\partial g}{\partial \mathbf{u}} \right|_{\mathbf{x_0},\mathbf{u_0}} = \left(Z|_{\mathbf{x_0},\mathbf{u_0}} \right)^{-1} \cdot \left. \frac{\partial f}{\partial \mathbf{u}} \right|_{\mathbf{x_0},\mathbf{u_0}} . \qquad (C.8)$$

Substituting Eq. C.7 and Eq. C.8 into Eq. C.4 yields

$$\dot{\mathbf{x}} = \left(Z|_{\mathbf{x_0},\mathbf{u_0}} \right)^{-1} \cdot \left(\left. \frac{\partial f}{\partial \mathbf{x}} \right|_{\mathbf{x_0},\mathbf{u_0}} \right) (\mathbf{x} - \mathbf{x_0}) + \left(Z|_{\mathbf{x_0},\mathbf{u_0}} \right)^{-1} \cdot \left(\left. \frac{\partial f}{\partial \mathbf{u}} \right|_{\mathbf{x_0},\mathbf{u_0}} \right) (\mathbf{u} - \mathbf{u_0}) \qquad (C.9)$$

which is in the familiar state space form of

$$\dot{\mathbf{x}} = \mathbf{A}\,\delta\mathbf{x} + \mathbf{B}\,\delta\mathbf{u} \qquad (C.10)$$

where

$$\mathbf{A} = \left(Z|_{\mathbf{x_0},\mathbf{u_0}} \right)^{-1} \cdot \left. \frac{\partial f}{\partial \mathbf{x}} \right|_{\mathbf{x_0},\mathbf{u_0}} = Z^{-1} F_x \qquad (C.11)$$

and

$$\mathbf{B} = \left(Z\big|_{\mathbf{x_0},\mathbf{u_0}} \right)^{-1} \cdot \frac{\partial f}{\partial \mathbf{u}}\bigg|_{\mathbf{x_0},\mathbf{u_0}} = Z^{-1} F_u \ . \qquad \text{(C.12)}$$

In the next section, this procedure is demonstrated for the evaporator model with two refrigerant fluid regions. Since the linearization procedure is analogous for the condenser model with three refrigerant fluid regions, details of that linearization will not be provided in this appendix. The governing equations for the condenser model are provided in [66].

C.1.1.1 Evaporator Model with Two Refrigerant Fluid Regions

The mass and energy conservation equations for the two-phase refrigerant fluid region in the evaporator are given in Eq. C.13 and Eq. C.14, respectively.

$$\frac{d\zeta_{e1}}{dt} + \frac{\zeta_{e1}}{\rho_{e1}} \frac{\partial \rho_{e1}}{\partial P_e} \frac{dP_e}{dt} + \frac{\zeta_{e1}}{\rho_{e1}} \frac{\partial \rho_{e1}}{\partial \overline{\gamma}_e} \frac{d\overline{\gamma}_e}{dt} + \frac{\dot{m}_{e12}}{\rho_{e1} V_e} = \frac{\dot{m}_{e,in}}{\rho_{e1} V_e} \qquad \text{(C.13)}$$

$$\left[\frac{\partial h_{e1}}{\partial P_e} - \frac{1}{\rho_{e1}} \right] \frac{dP_e}{dt} + \frac{\partial h_{e1}}{\partial \overline{\gamma}_e} \frac{d\overline{\gamma}_e}{dt} + \frac{h_{e,g} - h_{e1}}{\rho_{e1} V_e \zeta_{e1}} \dot{m}_{e12} = \frac{\dot{Q}_{e1} + \dot{m}_{e,in}(h_{e,in} - h_{e1})}{\rho_{e1} V_e \zeta_{e1}} \qquad \text{(C.14)}$$

The mass and energy conservation equations for the superheated refrigerant fluid region in the evaporator are given in Eq. C.15 and Eq. C.16, respectively.

$$\frac{d\zeta_{e1}}{dt} - \frac{\zeta_{e2}}{\rho_{e2}} \frac{\partial \rho_{e2}}{\partial P_e} \frac{dP_e}{dt} - \frac{\zeta_{e2}}{\rho_{e2}} \frac{\partial \rho_{e2}}{\partial h_{e2}} \frac{dh_{e2}}{dt} + \frac{\dot{m}_{e12}}{\rho_{e2} V_e} = \frac{\dot{m}_{e,out}}{\rho_{e2} V_e} \qquad \text{(C.15)}$$

$$-\frac{1}{\rho_{e2}} \frac{dP_e}{dt} + \frac{dh_{e2}}{dt} - \frac{h_{e,g} - h_{e2}}{\rho_{e2} V_e \zeta_{e2}} \dot{m}_{e12} = \frac{\dot{Q}_{e2} - \dot{m}_{e,out}(h_{e2} - h_{e,g})}{\rho_{e2} V_e \zeta_{e2}} \qquad \text{(C.16)}$$

The governing equation for mean-void fraction is given in Eq. C.17.

$$\frac{\partial \overline{\gamma}_{tot,e}}{\partial P_e} \frac{dP_e}{dt} - \frac{d\overline{\gamma}_e}{dt} = K_{e,\gamma} \left(\overline{\gamma}_e - \overline{\gamma}_{e,tot} \right) \qquad \text{(C.17)}$$

The governing equations for the tube wall in the two-phase and superheated regions respectively are

$$(mc)_{ew} \zeta_{e1} \frac{dT_{w,e1}}{dt} - (mc)_{ew} \left(T_{wt,e1} - T_{w,e1} \right) \frac{d\zeta_{e1}}{dt} = -\dot{Q}_{e1,r} - \dot{Q}_{e1,a} \qquad \text{(C.18)}$$

and

$$(mc)_{ew}\zeta_{e2}\frac{dT_{w,e2}}{dt}-(mc)_{ew}\left(T_{w,e2}-T_{wt,e1}\right)\frac{d\zeta_{e1}}{dt}=-\dot{Q}_{e2,r}-\dot{Q}_{e2,a}\ . \qquad (C.19)$$

These 6 nonlinear equations can written in the matrix form $Z_e\dot{\mathbf{x}}_e = f_e$ where

$$Z_e=\begin{bmatrix}
[\rho_{e1}-\rho_{e2}]V_e & \left[\zeta_{e1}\frac{\partial\rho_{e1}}{\partial P_e}+\zeta_{e2}\frac{\partial\rho_{e2}}{\partial P_e}\right]V_e & V_e\zeta_{e2}\frac{\partial\rho_{e2}}{\partial h_{e2}} & 0 & 0 & V_e\zeta_{e1}\frac{\partial\rho_{e1}}{\partial\overline{\gamma}_e}\\
\left(h_{e,g}-h_{e2}\right)\rho_{e2}V_e & -\zeta_{e2}V_e\left[1+\left(h_{e,g}-h_{e2}\right)\frac{\partial\rho_{e2}}{\partial P_e}\right] & \zeta_{e2}V_e\left[\rho_{e2}-\left(h_{e,g}-h_{e2}\right)\frac{\partial\rho_{e2}}{\partial h_{e2}}\right] & 0 & 0 & 0\\
-\left[\rho_{e1}V_e\left(h_{e,g}-h_{e1}\right)\right] & \zeta_{e1}V_e\left[\rho_{e1}\left(\frac{\partial h_{e1}}{\partial P_e}-\frac{1}{\rho_{e1}}\right)-\left(h_{e,g}-h_{e1}\right)\frac{\partial\rho_{e1}}{\partial P_e}\right] & 0 & 0 & 0 & \zeta_{e1}V_e\left[\rho_{e1}\frac{\partial h_{e1}}{\partial\overline{\gamma}_e}-\left(h_{e,g}-h_{e1}\right)\frac{\partial\rho_{e1}}{\partial\overline{\gamma}_e}\right]\\
-(mc)_{ew}\left(T_{wt,e1}-T_{w,e1}\right) & 0 & 0 & (mc)_{ew}\zeta_{e1} & 0 & 0\\
-(mc)_{ew}\left(T_{w,e2}-T_{wt,e1}\right) & 0 & 0 & 0 & (mc)_{ew}\zeta_{e2} & 0\\
0 & \frac{\partial\overline{\gamma}_{e,tot}}{\partial P_e} & 0 & 0 & 0 & -1
\end{bmatrix}, \qquad (C.20)$$

$$\dot{\mathbf{x}}_e=\begin{bmatrix}\dot{\zeta}_{e1}\\ \dot{P}_e\\ \dot{h}_{e2}\\ \dot{T}_{w,e1}\\ \dot{T}_{w,e2}\\ \dot{\overline{\gamma}}_e\end{bmatrix}, \qquad (C.21)$$

and

$$f_e=\begin{bmatrix}
\dot{m}_{e,in}-\dot{m}_{e,out}\\
\dot{Q}_{e2,r}+2\dot{m}_{e,out}\left(h_{e,g}-h_{e2}\right)\\
\dot{Q}_{e1,r}+\dot{m}_{e,in}\left(h_{e,in}-h_{e,g}\right)\\
-\dot{Q}_{e1,r}-\dot{Q}_{e1,a}\\
-\dot{Q}_{e2,r}-\dot{Q}_{e2,a}\\
K_{e,\gamma}\left(\overline{\gamma}_e-\overline{\gamma}_{e,tot}\right)
\end{bmatrix}. \qquad (C.22)$$

Detailed expressions for the heat transfer rates $\dot{Q}_{e1,r}$, $\dot{Q}_{e2,r}$, $\dot{Q}_{e1,a}$, and $\dot{Q}_{e2,a}$, are given in Eq. C.23.

$$\begin{aligned}
\dot{Q}_{e1,r}&=\zeta_{e1}A_e\alpha_{e1}\left(T_{w,e1}-T_{r,e1}\right)\\
\dot{Q}_{e2,r}&=\zeta_{e2}A_e\alpha_{e2}\left(T_{w,e2}-T_{r,e2}\right)\\
\dot{Q}_{e1,a}&=\zeta_{e1}\dot{m}_{a,e}c_{p,a}\left(T_{e1,ao}-T_{e,ai}\right)\\
\dot{Q}_{e2,a}&=\zeta_{e2}\dot{m}_{a,e}c_{p,a}\left(T_{e2,ao}-T_{e,ai}\right)
\end{aligned} \qquad (C.23)$$

Substituting Eq. C.23 into Eq. C.22 as well as applying the equalities $\dot{m}_{e,in} = \dot{m}_{r,v}$ and $\dot{m}_{e,out} = \dot{m}_{r,k}$ results in

$$f_e = \begin{bmatrix} \dot{m}_{r,v} - \dot{m}_{r,k} \\ (1-\zeta_{e1}) A_e \alpha_{r,e2} \left(T_{w,e2} - T_{r,e2}\right) + 2\dot{m}_{r,k} \left(h_{e,g} - h_{e2}\right) \\ \zeta_{e1} A_e \alpha_{r,e1} \left(T_{w,e1} - T_{r,e1}\right) + \dot{m}_{r,v} \left(h_{e,in} - h_{e,g}\right) \\ -\zeta_{e1} A_e \alpha_{r,e1} \left(T_{w,e1} - T_{r,e1}\right) - \zeta_{e1} \dot{m}_{a,e} c_{p,a} \left(T_{e1,ao} - T_{e,ai}\right) \\ -(1-\zeta_{e1}) A_e \alpha_{r,e2} \left(T_{w,e2} - T_{r,e2}\right) - (1-\zeta_{e1}) \dot{m}_{a,e} c_{p,a} \left(T_{e2,ao} - T_{e,ai}\right) \\ K_{\gamma,e} \left(\overline{\gamma}_e - \overline{\gamma}_{e,tot}\right) \end{bmatrix}. \quad \text{(C.24)}$$

The columns of $\frac{\partial f_e}{\partial x}$ are shown individually in Eqs. C.25 through C.30.

$$\frac{\partial f_e}{\partial x_1} = \begin{bmatrix} 0 \\ -A_e \alpha_{r,e2} \left(T_{w,e2} - T_{r,e2}\right) \\ A_e \alpha_{r,e1} \left(T_{w,e1} - T_{r,e1}\right) \\ -A_e \alpha_{r,e1} \left(T_{w,e1} - T_{r,e1}\right) - \dot{m}_{a,e} c_{p,a} \left(T_{e1,ao} - T_{e,ai}\right) \\ A_e \alpha_{r,e2} \left(T_{w,e2} - T_{r,e2}\right) + \dot{m}_{a,e} c_{p,a} \left(T_{e2,ao} - T_{e,ai}\right) \\ 0 \end{bmatrix} \quad \text{(C.25)}$$

$$\frac{\partial f_e}{\partial x_2} = \begin{bmatrix} \frac{\partial \dot{m}_{r,v}}{\partial P_e} - \frac{\partial \dot{m}_{r,k}}{\partial P_e} \\ -\zeta_{e2} A_e \alpha_{r,e2} \frac{\partial T_{r,e2}}{\partial P_e} + 2\dot{m}_k \frac{\partial h_{e,g}}{\partial P_e} + 2h_{e,g} \frac{\partial \dot{m}_{r,k}}{\partial P_e} \\ -\zeta_{e1} A_e \alpha_{r,e1} \frac{\partial T_{r,e1}}{\partial P_e} - \dot{m}_v \frac{\partial h_{e,g}}{\partial P_e} - h_{e,g} \frac{\partial \dot{m}_{r,v}}{\partial P_e} \\ \zeta_{e1} A_e \alpha_{r,e1} \frac{\partial T_{r,e1}}{\partial P_e} \\ \zeta_{e2} A_e \alpha_{r,e2} \frac{\partial T_{r,e2}}{\partial P_e} \\ -K_{\overline{\gamma},e} \frac{\partial \overline{\gamma}_{e,tot}}{\partial P_e} \end{bmatrix} \quad \text{(C.26)}$$

$$\frac{\partial f_e}{\partial x_3} = \begin{bmatrix} \dfrac{\partial \dot{m}_{r,v}}{\partial P_e} - \dfrac{\partial \dot{m}_{r,k}}{\partial P_e} \\ -\zeta_{e2} A_e \alpha_{r,e2} \dfrac{\partial T_{r,e2}}{\partial h_{e2}} - 2\dot{m}_k + 4\left(h_{e,g} - h_{e2}\right) \dfrac{\partial \dot{m}_{r,k}}{\partial h_{e,out}} \\ 0 \\ 0 \\ \zeta_{e2} A_e \alpha_{r,e2} \dfrac{\partial T_{r,e2}}{\partial P_e} \\ 0 \end{bmatrix} \qquad (C.27)$$

$$\frac{\partial f_e}{\partial x_4} = \begin{bmatrix} 0 \\ 0 \\ \zeta_{e1} A_e \alpha_{r,e1} \\ -\zeta_{e1} A_e \alpha_{r,e1} - \zeta_{e1} \dot{m}_{a,e} c_{p,a} \dfrac{\partial T_{e1,ao}}{\partial T_{w,e1}} \\ 0 \\ 0 \end{bmatrix} \qquad (C.28)$$

$$\frac{\partial f_e}{\partial x_5} = \begin{bmatrix} 0 \\ \zeta_{e2} A_e \alpha_{r,e2} \\ 0 \\ 0 \\ -\zeta_{e2} A_e \alpha_{r,e2} - \zeta_{e2} \dot{m}_{a,e} c_{p,a} \dfrac{\partial T_{e2,ao}}{\partial T_{w,e2}} \\ 0 \end{bmatrix} \qquad (C.29)$$

$$\frac{\partial f_e}{\partial x_6} = \begin{bmatrix} 0 \\ 0 \\ 0 \\ 0 \\ 0 \\ K_{\bar{\gamma},e} \end{bmatrix} \qquad \text{(C.30)}$$

The final expression for $\frac{\partial f_e}{\partial u}$ is

$$\frac{\partial f_e}{\partial u} = \begin{bmatrix} \frac{\partial \dot{m}_{r,v}}{\partial a_v} & -\frac{\partial \dot{m}_{r,k}}{\partial \omega_k} & 0 & 0 & 0 & 0 \\ 0 & 2\left(h_{e,g} - h_{e2}\right)\frac{\partial \dot{m}_{r,k}}{\partial \omega_k} & 0 & 0 & 0 & 0 \\ \left(h_{e,in} - h_{e,g}\right)\frac{\partial \dot{m}_{r,v}}{\partial a_v} & 0 & 0 & 0 & 0 & 0 \\ 0 & 0 & -\zeta_{e1} c_{p,a}\left(T_{e1,ao} - T_{e,ai}\right) & 0 & \zeta_{e1}\dot{m}_{a,e} c_{p,a} & 0 \\ 0 & 0 & -\zeta_{e2} c_{p,a}\left(T_{e2,ao} - T_{e,ai}\right) & 0 & \zeta_{e2}\dot{m}_{a,e} c_{p,a} & 0 \\ 0 & 0 & 0 & 0 & 0 & 0 \end{bmatrix}. \qquad \text{(C.31)}$$

The **A** and **B** matrices for the linearized evaporator model can then be obtained by evaluating Eq. C.11 and Eq. C.12 for some equilibrium condition ($\mathbf{x_0}$,$\mathbf{u_0}$) using the symbolic expressions derived for $\frac{\partial f_e}{\partial x}$, $\frac{\partial f_e}{\partial u}$, and Z.

C.1.2 Linearization of Mass Flow Device Models

The EEV and compressor are described by nonlinear static models. The nonlinear models, as well as details of the linearization of these models, are described in [65].

C.2 Integration of Individual Linearized Component Models

Once each of the four component models (EEV, compressor, evaporator, and condenser) has been linearized, a single state space representation of the complete system can be obtained. Since the linearized compressor and EEV models are static, they do not contribute any new state information to the model. However, they are incorporated into the complete system model via

terms such as $\frac{\partial \dot{m}_{r,v}}{\partial a_v}$ which appear in the derivation of the linearized evaporator and condenser models. After a considerable amount of algebra, symbolic expressions for the final **A** and **B** matrices can be obtained with the following state and input vectors:

$$\mathbf{x} = \begin{bmatrix} \zeta_{e1} & P_e & h_{e2} & T_{w,e1} & T_{w,e2} & \bar{\gamma}_e & \zeta_{c1} & \zeta_{c1} & P_c & h_{c1} & h_{c3} & T_{w,c1} & T_{w,c2} & T_{w,c3} & \bar{\gamma}_c \end{bmatrix}^T \in \mathbb{R}^{15} \qquad (C.32)$$

and

$$\mathbf{u} = \begin{bmatrix} a_v & \omega_k & \dot{m}_{a,e} & \dot{m}_{a,c} & T_{e,ai} & T_{c,ai} \end{bmatrix}^T \in \mathbb{R}^6 \ . \qquad (C.33)$$

Due to their size and complexity, the symbolic representations of **A** and **B** are not shown here.

C.3 Linearized Model Validation

The operating condition about which the system was linearized for the case study presented in Chapter 5 is given in Eqs. C.34 and C.35.

$$\mathbf{x_0} = \begin{bmatrix} 0.860 & 290 & 256 & 2.32 & 12.2 & 0.979 & 0.148 & 0.688 & 910 & 295 & 93.5 & 37.0 & 33.7 & 27.7 & 0.852 \end{bmatrix}^T \qquad (C.34)$$

$$\mathbf{u_0} = \begin{bmatrix} 10 & 1000 & 0.15 & 0.6 & 18 & 26 \end{bmatrix}^T \qquad (C.35)$$

Note that the linearized model contains six inputs, where $\mathbf{u_0}(5)$ and $\mathbf{u_0}(6)$ are the evaporator and condenser air inlet temperatures. In the optimal control problem formulation used in Chapter 5, these two inputs are treated as disturbances because they are not controllable.

The continuous-time **A** and **B** matrices of the linearized model are shown in Eq. C.37 and Eq. C.36 which are located at the end of this appendix because of the size of the matrices. For the case study presented in Chapter 5, the continuous-time state space representation was converted to discrete time with a sample time of 1 second using the *c2d* command in MATLAB. The linearization is first done in continuous time because the moving boundary model governing equations are derived in continuous time. Then for a given control methodology, the user can choose to convert the linearized state-space representation into the most appropriate form.

The nonlinear VCC system model, simulated using the ATTMO Toolbox [66], and the linearized model, were both perturbed using pseudo-random binary signals generated in MATLAB. The nonlinear model inputs are shown in Figure C.1.

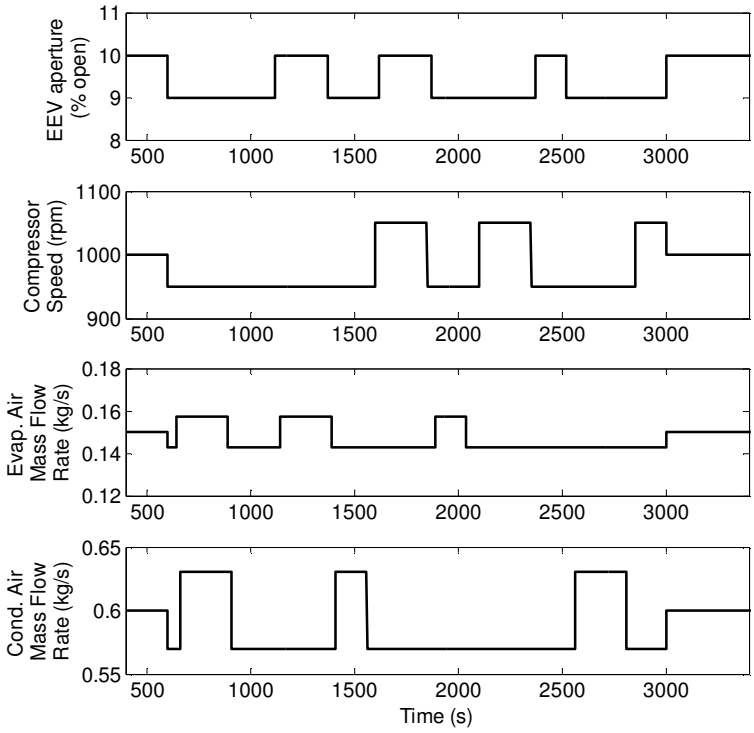

Figure C.1: Model validation perturbation signals.

The dynamic response of the fifteen model states in both the linearized and nonlinear models are compared in the following figures. Note that they are *not* presented in the same order in which they appear in Eq. C.34.

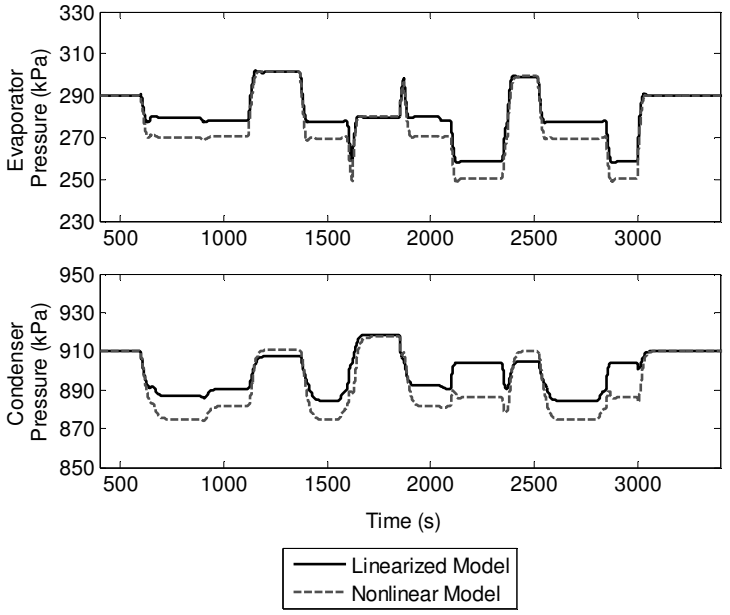

Figure C.2: Linearized model validation of P_c and P_e.

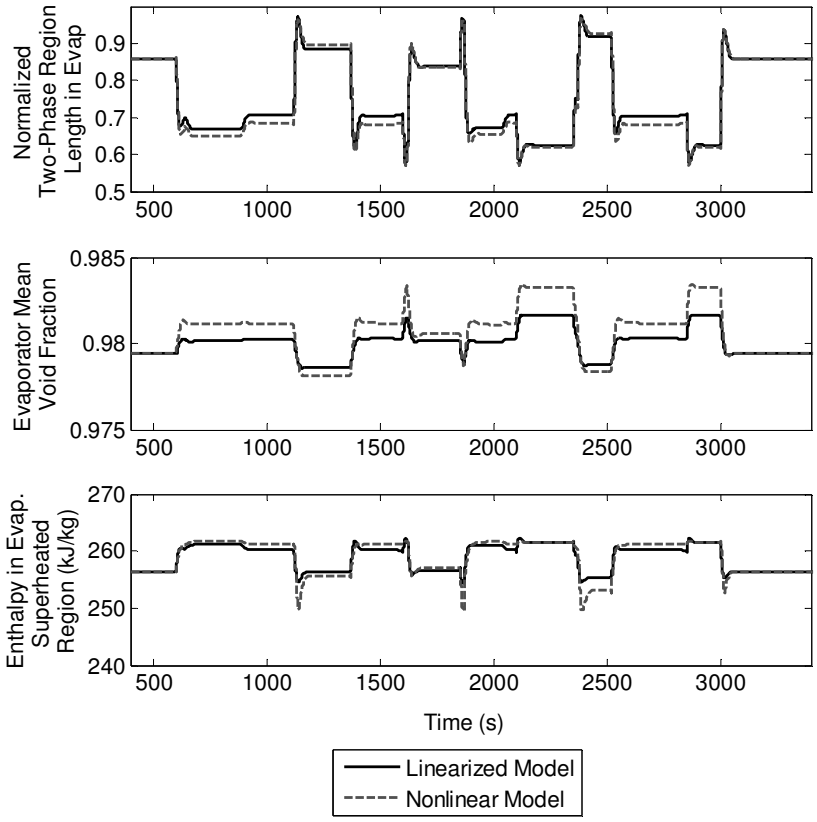

Figure C.3: Linearized model validation of ζ_{e1}, $\bar{\gamma}_e$, and h_{e2}.

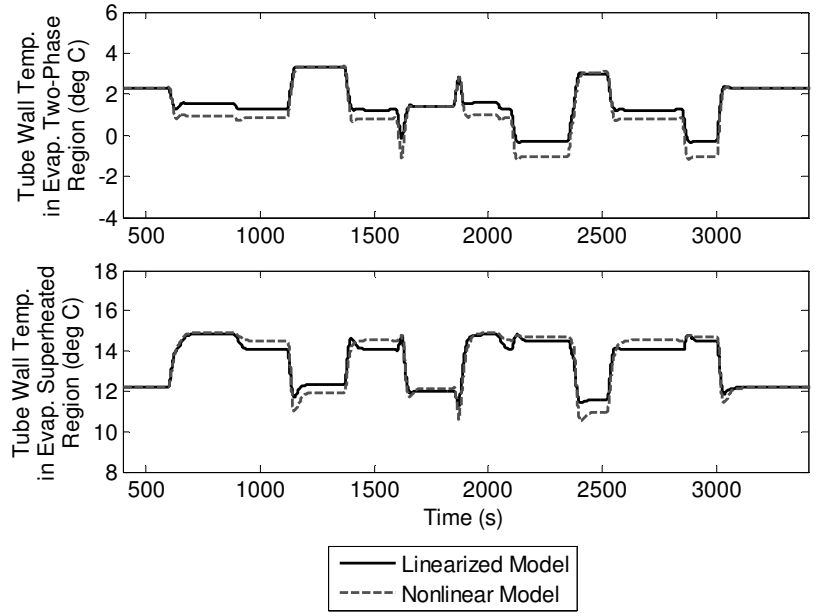

Figure C.4: Linearized model validation of $T_{w,e1}$ and $T_{w,e2}$.

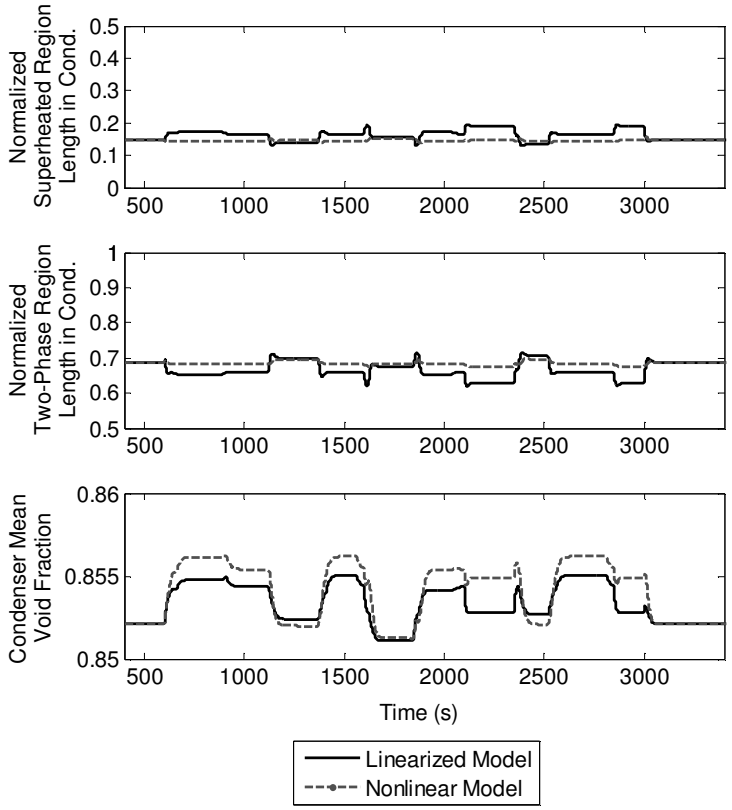

Figure C.5: Linearized model validation of ζ_{c1}, ζ_{c2}, and $\bar{\gamma}_c$.

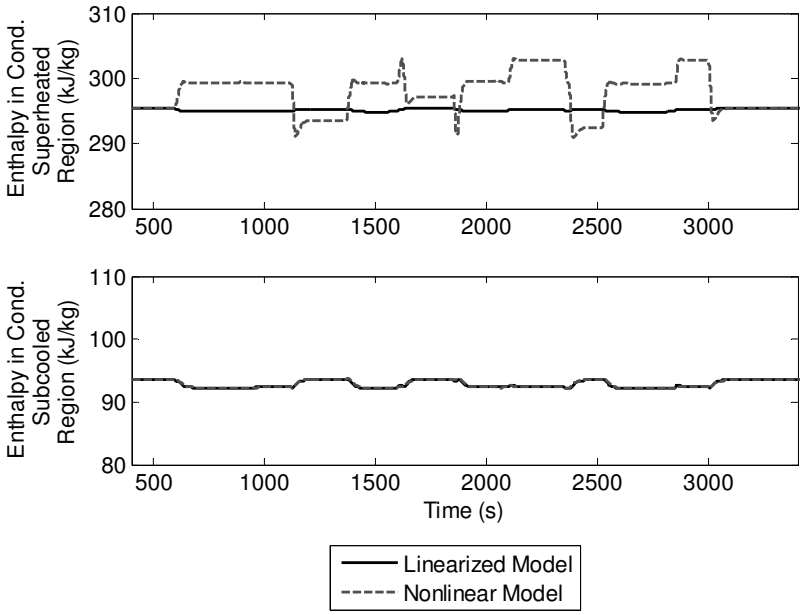

Figure C.6: Linearized model validation of h_{c1} and h_{c3}.

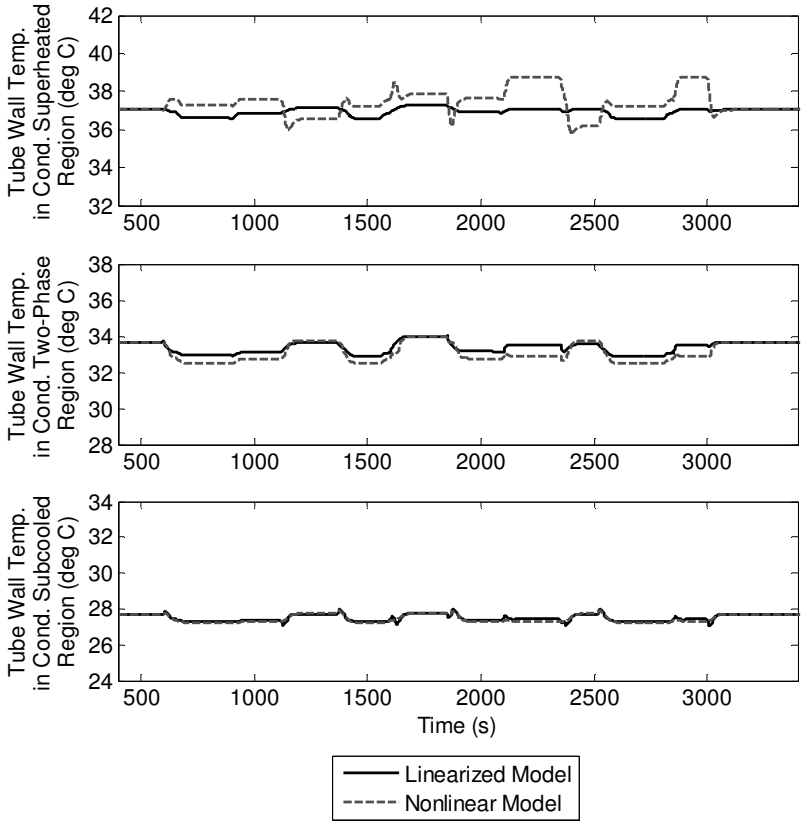

Figure C.7: Linearized model validation of $T_{w,c1}$, $T_{w,c2}$, and $T_{w,c3}$.

$$\mathbf{B} = \begin{bmatrix} 0.0257 & 4.00\times10^{-4} & 0 & 0 & 0 & 0 \\ 4.39 & -0.171 & 0 & 0 & 0 & 0 \\ 1.40 & -0.0547 & 0 & 0 & 0 & 0 \\ 0 & 0 & 2.78 & 0 & 0.0434 & 0 \\ 0 & 0 & 1.03 & 0 & 0.0434 & 0 \\ -0.00030 & 0 & 0 & 0 & 0 & 0 \\ 0.0001 & 5.00\times10^{-4} & 0 & 0 & 0 & 0 \\ 0.00120 & -6.00\times10^{-4} & 0 & 0 & 0 & 0 \\ -0.642 & 0.178 & 0 & 0 & 0 & 0 \\ -0.0117 & 0.00320 & 0 & 0 & 0 & 0 \\ -0.00850 & 0.00450 & 0 & 0 & 0 & 0 \\ 0 & 0 & 0 & -0.421 & 0 & 0.0726 \\ -4.00\times10^{-4} & -0.00250 & 0 & -0.293 & 0 & 0.0726 \\ -0.454 & 0.0030 & 0 & -0.0645 & 0 & 0.0726 \\ 1.00\times10^{-4} & 0 & 0 & 0 & 0 & 0 \end{bmatrix} \quad \text{(C.36)}$$

$$\mathbf{A} = \begin{bmatrix}
-0.46 & 0.00460 & 0.00340 & -0.189 & -0.00290 & -209 & 0 & 0 & 0 & 0 & -0.00130 & 0 & 0 & 0 & 0 \\
76.5 & -4.63 & -1.54 & 42.1 & 1.30 & 78.6 & 0 & 0 & 0.0611 & 0 & -0.215 & 0 & 0 & 0 & 0 \\
-321 & -0.00160 & -17.1 & -6.42 & 7.67 & -9482 & 0 & 0 & 0.0196 & 0 & -0.0684 & 0 & 0 & 0 & 0 \\
0 & 0.0247 & 0 & -0.304 & 0 & 0 & 0 & 0 & 0 & 0 & 0 & 0 & 0 & 0 & 0 \\
0 & 0.00130 & 0.0516 & 0 & -0.0892 & 0 & 0 & 0 & 0 & 0 & 0 & 0 & 0 & 0 & 0 \\
-0.00540 & 0 & 1.00\times10^{-4} & -0.00300 & -1.00\times10^{-4} & -5.00 & 0 & 0 & 0 & 0 & 0 & 0 & 0 & 0 & 0 \\
0 & 0 & 0.0197 & 0 & 0 & 0 & -3.12 & 0.0207 & 0 & -0.0193 & 0 & 0.0198 & -0.00640 & 0 & -2.00\times10^{-4} \\
0 & 0 & -0.0232 & 0 & 0 & 0 & 3.65 & -0.0445 & 2.00\times10^{-4} & 0.0226 & 0 & -0.0232 & 0.0134 & -1.00\times10^{-4} & 4.04 \\
0 & 0.523 & 0.406 & 0 & 0 & 0 & -246 & -167 & -2.16 & -1.53 & -0.00700 & 1.57 & 51.9 & 0.0403 & 1.59 \\
0 & 0.00950 & 0.00740 & 0 & 0 & 0 & -4.49 & -3.05 & -0.0393 & -0.0278 & -1.00\times10^{-4} & 0.0286 & 0.946 & 0.000700 & 0.0289 \\
0 & -6.00\times10^{-4} & 0.179 & 0 & 0 & 0 & -25.6 & 3.55 & -0.0106 & -0.174 & -0.174 & 0.179 & -0.325 & 0.183 & -212 \\
0 & 0 & 0 & 0 & 0 & 0 & -0.00420 & 0 & 9.00\times10^{-4} & 0.0334 & 0 & -0.107 & 0 & 0 & 0 \\
0 & 0.000100 & -0.0962 & 0 & 0 & 0 & 15.2 & -0.101 & 0.00990 & 0.0939 & 0 & -0.0970 & -0.292 & 0 & 0.00100 \\
0 & -6.00\times10^{-4} & 0.125 & 0 & 0 & 0 & -19.5 & 0.873 & -0.00820 & -0.121 & 0.0380 & 0.124 & -0.258 & -0.125 & -148 \\
0 & -1.00\times10^{-4} & 0 & 0 & 0 & 0 & 0.0283 & 0.0192 & -3.00\times10^{-4} & 2.00\times10^{-4} & 0 & -2.00\times10^{-4} & -0.00600 & -0.00600 & -5.00
\end{bmatrix} \quad \text{(C.37)}$$

Appendix D

Nonlinear Model Validation of EDM Optimal Control Solution

This appendix contains additional plots comparing the linear and nonlinear VCC model simulations of the optimal control inputs $\mathbf{u}^*_{EDM}$.

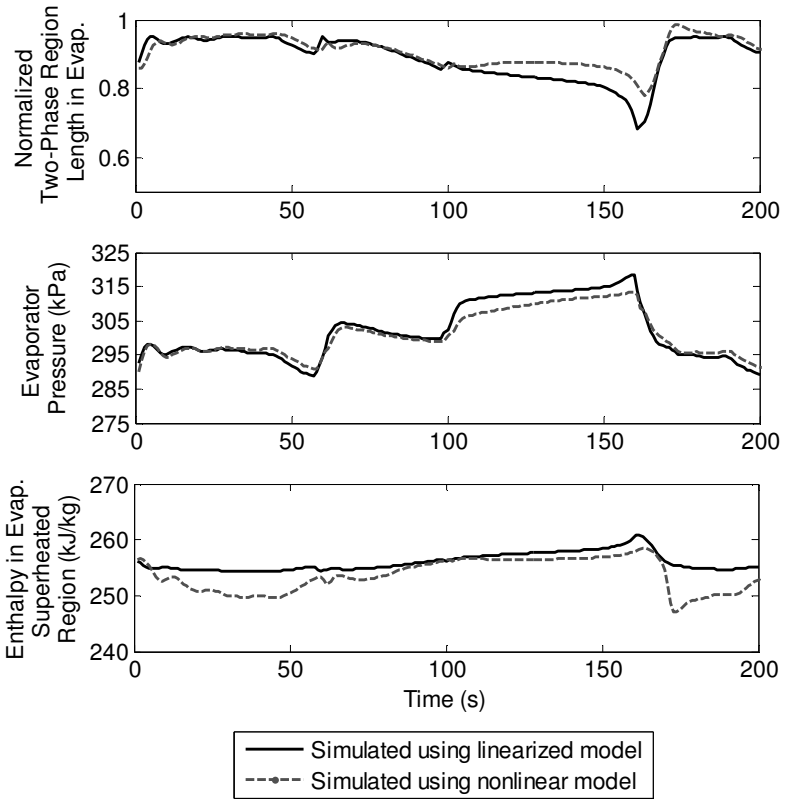

Figure D.1: Comparison of evaporator model states ζ_{e1}, P_e, and h_{e2} simulated using the linearized system model versus using the nonlinear system model for $\mathbf{u} = \mathbf{u}^*_{EDM}$.

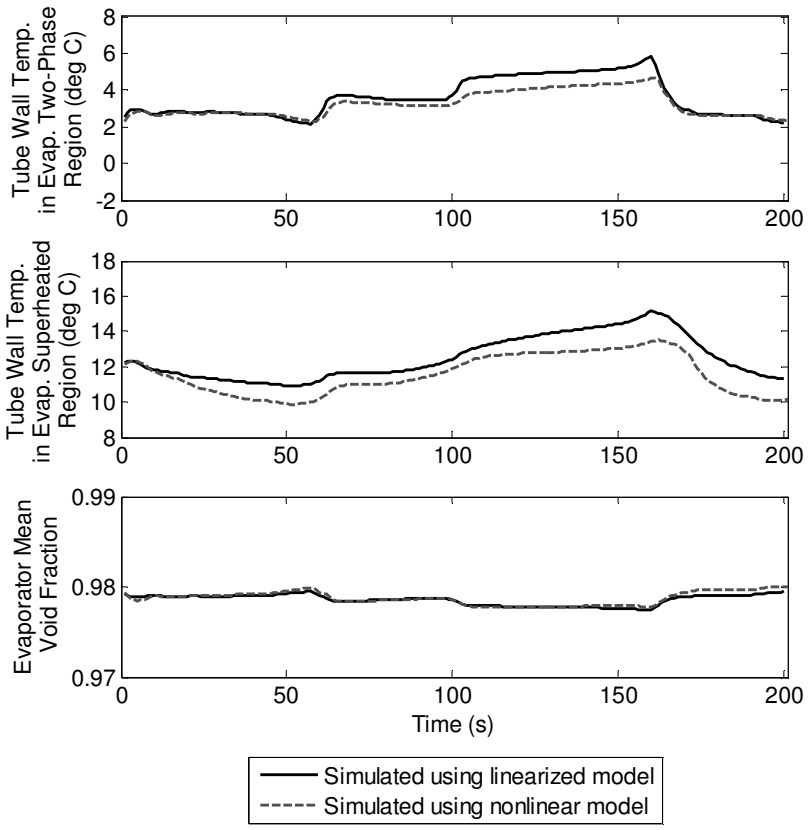

Figure D.2: Comparison of evaporator model states $T_{w,e1}$, $T_{w,e2}$, and $\bar{\gamma}_e$ simulated using the linearized system model versus using the nonlinear system model for $\mathbf{u} = \mathbf{u}^*_{EDM}$.

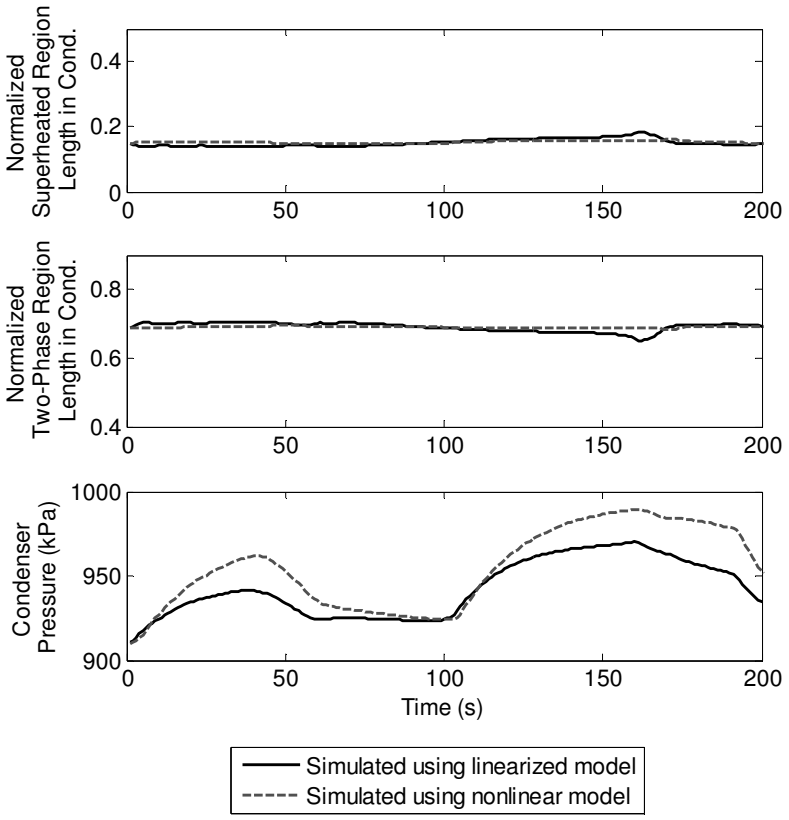

Figure D.3: Comparison of condenser model states ζ_{c1}, ζ_{c2}, and P_c simulated using the linearized system model versus using the nonlinear system model for $\mathbf{u} = \mathbf{u}^*_{EDM}$.

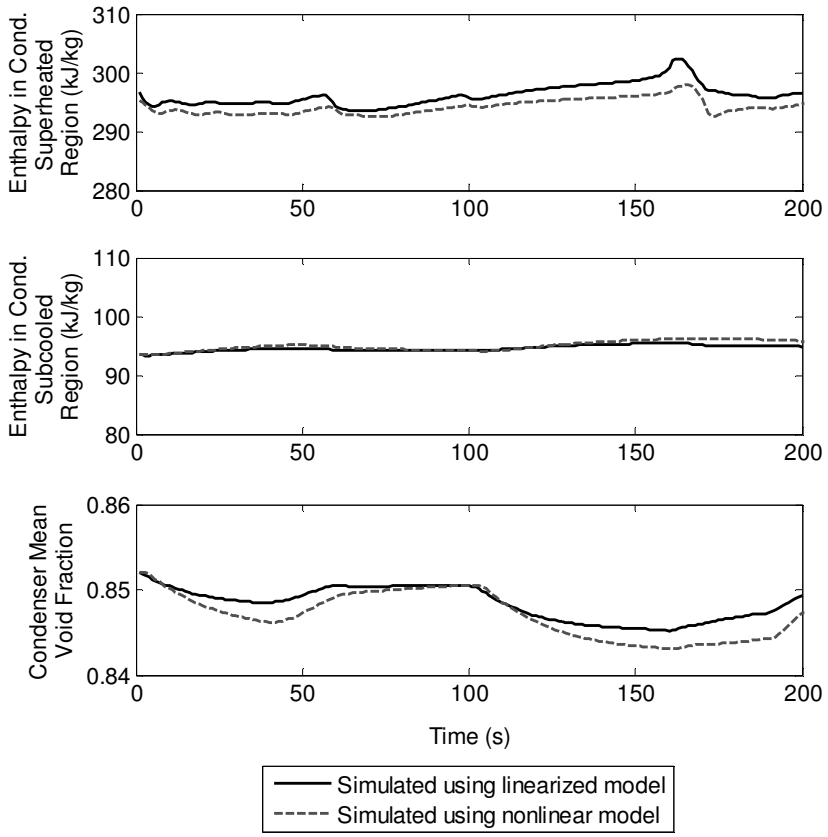

Figure D.4: Comparison of condenser model states h_{c1}, h_{c3}, and $\bar{\gamma}_c$ simulated using the linearized system model versus using the nonlinear system model for $\mathbf{u} = \mathbf{u}^{*}_{EDM}$.

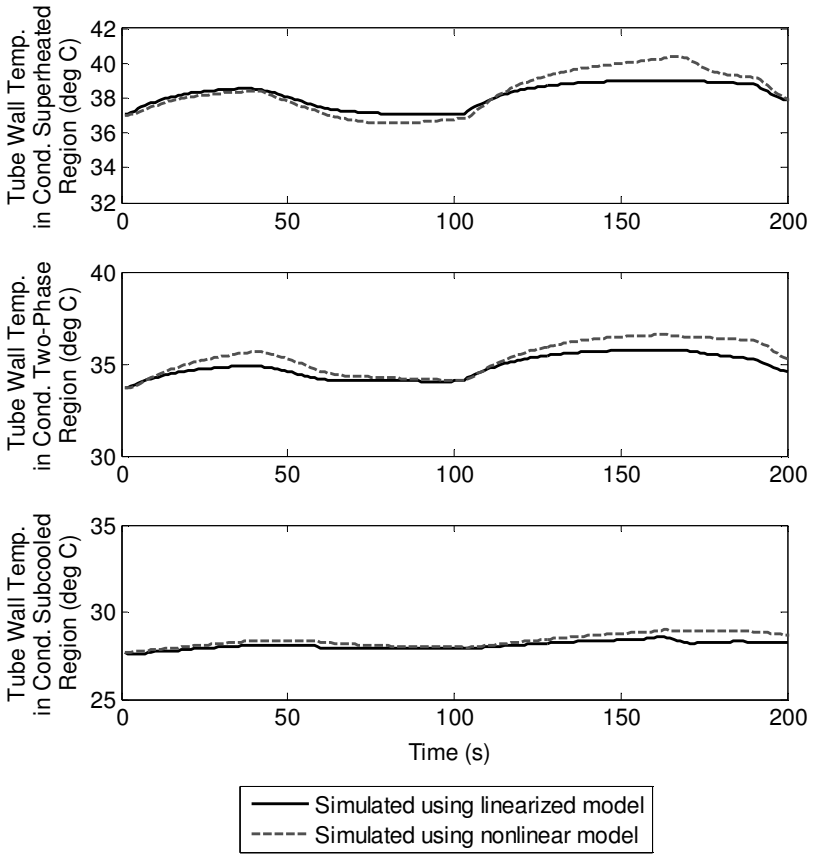

Figure D.5: Comparison of evaporator model states $T_{w,c1}$, $T_{w,c2}$, and $T_{w,c3}$ simulated using the linearized system model versus using the nonlinear system model for $\mathbf{u} = \mathbf{u}^{*}_{EDM}$.

Appendix E
MATLAB Code

E.1 CCHP Static Setpoint Optimization

The MATLAB code presented below is divided into three separate blocks; the first block of code calls the function *fmincon* which in turn calls two other functions: *CCHP_NJmod_objective_function_3* and *CCHP_NJmod_constraints_3*. The code for these two functions is provided below the first block of code.

```
% This is the main program for CCHP Optimization

% Essential constants
N  = 24;     % Number of time samples in prediction horizon (each sample is 1 Hr)
nc = 7;      % Number of chillers%
Ts = 3600;   % Prediction window step size (seconds) (1 hour = 3600 seconds)

% Demand data
Qc_dem      = zeros(N,1); %Campus cooling demand at times 1,2,..N
Elec_dem    = zeros(N,1); %Campus electricity demand at times 1,2,..N
Qh_dem      = zeros(N,1); %Campus hot water demand at times 1,2,...,N

% Ambient conditions
P0          = ones(N,1)*101.325; % kPa
T0          = zeros(N,1); %Ambient temperature at times 1,2,...,N in deg Kelvin

T0(1) = 19 + 273.15;
T0(2) = 18 + 273.15;
T0(3) = 16 + 273.15;
T0(4) = 15 + 273.15;
T0(5) = 16 + 273.15;
T0(6) = 17 + 273.15;
T0(7) = 18 + 273.15;
T0(8) = 19 + 273.15;
T0(9) = 20 + 273.15;
T0(10) = 21 + 273.15;
T0(11) = 22 + 273.15;
T0(12) = 23 + 273.15;
T0(13) = 24 + 273.15;
T0(14) = 25 + 273.15;
T0(15) = 26 + 273.15;
T0(16) = 28 + 273.15;
T0(17) = 28.5 + 273.15;
T0(18) = 29 + 273.15;
T0(19) = 28 + 273.15;
T0(20) = 26 + 273.15;
T0(21) = 24.5 + 273.15;
T0(22) = 23 + 273.15;
T0(23) = 22 + 273.15;
T0(24) = 20 + 273.15;
```

```
% Predicted campus hot water demand at times 1,2,...,N (in units of MW)

Qh_dem(1) = 1.2;
Qh_dem(2) = 1.2;
Qh_dem(3) = 1.2;
Qh_dem(4) = 1.2;
Qh_dem(5) = 1.2;
Qh_dem(6) = 5.64;
Qh_dem(7) = 5.64;
Qh_dem(8) = 4.92;
Qh_dem(9) = 4.92;
Qh_dem(10) = 4.92;
Qh_dem(11) = 3.72;
Qh_dem(12) = 3.72;
Qh_dem(13) = 2.64;
Qh_dem(14) = 2.64;
Qh_dem(15) = 2.64;
Qh_dem(16) = 2.64;
Qh_dem(17) = 5.64;
Qh_dem(18) = 5.64;
Qh_dem(19) = 5.64;
Qh_dem(20) = 5.64;
Qh_dem(21) = 4.92;
Qh_dem(22) = 4.92;
Qh_dem(23) = 1.2;
Qh_dem(24) = 1.2;

Qh_dem = 1000*Qh_dem/2.5; % Convert campus hot water demand into units of kW and scale down

%Predicted campus cooling demands at times 1,2,...N (in units of kW)
Qc_dem(1) = 26260;
Qc_dem(2) = 21883;
Qc_dem(3) = 17506;
Qc_dem(4) = 13130;
Qc_dem(5) = 13130;
Qc_dem(6) = 15318;
Qc_dem(7) = 16412;
Qc_dem(8) = 21883;
Qc_dem(9) = 26260;
Qc_dem(10) = 30637;
Qc_dem(11) = 35014;
Qc_dem(12) = 37202;
Qc_dem(13) = 39390;
Qc_dem(14) = 41579;
Qc_dem(15) = 43767;
Qc_dem(16) = 47049;
Qc_dem(17) = 0.8*49238;
Qc_dem(18) = 0.8*45955;
Qc_dem(19) = 0.8*43767;
Qc_dem(20) = 0.8*38296;
Qc_dem(21) = 32825;
Qc_dem(22) = 28448;
Qc_dem(23) = 26260;
Qc_dem(24) = 26260;

Qc_dem     = Qc_dem/4.2; % Scale down hot water load

%Predicted campus electricity demands at times 1,2,...N based on real data
%in units of MW
Elec_dem(1) = 12.0;
Elec_dem(2) = 12.0;
Elec_dem(3) = 11.65;
Elec_dem(4) = 11.65;
Elec_dem(5) = 11.70;
Elec_dem(6) = 11.70;
Elec_dem(7) = 12.25;
Elec_dem(8) = 12.25;
Elec_dem(9) = 13.45;
Elec_dem(10) = 13.45;
Elec_dem(11) = 14.77;
Elec_dem(12) = 14.77;
Elec_dem(13) = 14.65;
Elec_dem(14) = 14.65;
Elec_dem(15) = 14.93;
Elec_dem(16) = 14.93;
Elec_dem(17) = 15.21;
Elec_dem(18) = 15.21;
Elec_dem(19) = 15.33;
Elec_dem(20) = 15.33;
Elec_dem(21) = 14.05;
```

```
Elec_dem(22) = 14.05;
Elec_dem(23) = 15.35;
Elec_dem(24) = 15.35;

Elec_dem = 1000*Elec_dem/2.5; % Convert campus electricity demand into units of kW and scale down

%************************************************************************
%**Set Initial values to optimization variables for passing into fmincon**
%************************************************************************

m_L_init = 9*Qc_dem/(4.18*5*(60-40)); % Initial values of mass flow rate supplied to campus at times 1,2,..N
calculated based on predicted cooling loads and design campus supply and return loads

%Initial values of overall stream mass flow rates through chillers are set
%below.
m_CHW_init(1,1) = m_L_init(1);
m_CHW_init(2,1) = m_L_init(2);
m_CHW_init(3,1) = m_L_init(3);
m_CHW_init(4,1) = m_L_init(4);
m_CHW_init(5,1) = m_L_init(5);
m_CHW_init(6,1) = m_L_init(6);
m_CHW_init(7,1) = m_L_init(7);
m_CHW_init(8,1) = m_L_init(8);
m_CHW_init(9,1) = m_L_init(9);
m_CHW_init(10,1) = m_L_init(10);
m_CHW_init(11,1) = m_L_init(11);
m_CHW_init(12,1) = m_L_init(12);
m_CHW_init(13,1) = m_L_init(13);
m_CHW_init(14,1) = m_L_init(14);
m_CHW_init(15,1) = m_L_init(15);
m_CHW_init(16,1) = m_L_init(16);
m_CHW_init(17,1) = m_L_init(17);
m_CHW_init(18,1) = m_L_init(18);
m_CHW_init(19,1) = m_L_init(19);
m_CHW_init(20,1) = m_L_init(20);
m_CHW_init(21,1) = m_L_init(21);
m_CHW_init(22,1) = m_L_init(22);
m_CHW_init(23,1) = m_L_init(23);
m_CHW_init(24,1) = m_L_init(24);

m_CHW_mat_init = zeros(N,nc); % Initial values of individual chiller mass flow rates expressed as a matrix

for k = 1:N
    for i = 1:nc
        m_CHW_mat_init(k,i) = (m_CHW_init(k,1))/nc; % Overall stream mass flow rate uniformly distributed among
% individual chillers
    end
end

T_CHWS_mat_init = ones(N,nc)*(273.15+5*(40-32)/9);  % Initial values of Chiller supply water temperatures
% expressed as a matrix
m_CHW_vec_init = reshape(m_CHW_mat_init',N*nc,1);   % Reshaping of initial values of individual chiller mass
% flow rates
T_CHWS_vec_init = reshape(T_CHWS_mat_init',N*nc,1); % Reshaping of initial values of individual chiller supply
% water temperatures

m_f_vec_init    = ones(N,1)*0.7;       % arbitrarily chosen
f_s_1_vec_init  = ones(N,1)*0.5;       % arbitrarily chosen
W_GT_vec_init   = ones(N,1)*6000;      % arbitrarily chosen

x0 = [m_CHW_vec_init; m_f_vec_init; T_CHWS_vec_init; f_s_1_vec_init; W_GT_vec_init]; %Expression for overall
% vector for initial values for passing to fmicon

%************************************************************************
%**********************Call Optimization Solver**************************
%************************************************************************

% Minimum mass flow permitted through each chiller
    m_CHW_mat_min(1) = 1;
    m_CHW_mat_min(2) = 1;
    m_CHW_mat_min(3) = 1;
    m_CHW_mat_min(4) = 1;
    m_CHW_mat_min(5) = 1;
    m_CHW_mat_min(6) = 1;
    m_CHW_mat_min(7) = 1;

% Maximum mass flow permitted through each chiller
    m_CHW_mat_max(1) = 88.6;
    m_CHW_mat_max(2) = 126.6;
    m_CHW_mat_max(3) = 126.6;
    m_CHW_mat_max(4) = 284.8;
```

```
    m_CHW_mat_max(5) = 284.8;
    m_CHW_mat_max(6) = 316.5;
    m_CHW_mat_max(7) = 316.5;

m_CHW_min   = 5;        % Minimum total water mass flow rate through chillers (not set to zero to avoid
% division by zero later on)
m_CHW_max   = 1582.3;   % Maximum total water mass flow rate through chillers

m_f_min     = 0.2;      % Minimum fuel flow rate through combustor (kg/s)
m_f_max     = 0.8322;   % Maximum fuel flow rate through combustor (kg/s)

f_s_1_min   = 0.05;   % Minimum fraction
f_s_1_max   = 0.95;   % Maximum fraction

T_CHWS_max  = (273.15+5*(42-32)/9); %Maximum allowed temperature of overall supply stream from chillers at at
% all times
T_CHWS_min  = (273.15+5*(38-32)/9); %Minimum allowed temperature of overall supply stream from chillers at at
% all times

W_GT_min    = 1000;     % Minimum allowed power to be generated from Gas Turbine
W_GT_max    = 13500;    % Maximum allowed power to be generated from Gas Turbine

% Define Upper and Lower Bound Constraints

UB = zeros(17*N,1);
LB = zeros(17*N,1);

UB(1:N)         = m_CHW_mat_max(1);
UB(N+1:2*N)     = m_CHW_mat_max(2);
UB(2*N+1:3*N)   = m_CHW_mat_max(3);
UB(3*N+1:4*N)   = m_CHW_mat_max(4);
UB(4*N+1:5*N)   = m_CHW_mat_max(5);
UB(5*N+1:6*N)   = m_CHW_mat_max(6);
UB(6*N+1:7*N)   = m_CHW_mat_max(7);
UB(7*N+1:8*N)   = m_f_max;
UB(8*N+1:9*N)   = T_CHWS_max;
UB(9*N+1:10*N)    = T_CHWS_max;
UB(10*N+1:11*N)   = T_CHWS_max;
UB(11*N+1:12*N)   = T_CHWS_max;
UB(12*N+1:13*N)   = T_CHWS_max;
UB(13*N+1:14*N)   = T_CHWS_max;
UB(14*N+1:15*N)   = T_CHWS_max;
UB(15*N+1:16*N)   = f_s_1_max;
UB(16*N+1:17*N)   = W_GT_max;

LB(1:N)         = m_CHW_mat_min(1);
LB(N+1:2*N)     = m_CHW_mat_min(2);
LB(2*N+1:3*N)   = m_CHW_mat_min(3);
LB(3*N+1:4*N)   = m_CHW_mat_min(4);
LB(4*N+1:5*N)   = m_CHW_mat_min(5);
LB(5*N+1:6*N)   = m_CHW_mat_min(6);
LB(6*N+1:7*N)   = m_CHW_mat_min(7);
LB(7*N+1:8*N)   = m_f_min;
LB(8*N+1:9*N)   = T_CHWS_min;
LB(9*N+1:10*N)    = T_CHWS_min;
LB(10*N+1:11*N)   = T_CHWS_min;
LB(11*N+1:12*N)   = T_CHWS_min;
LB(12*N+1:13*N)   = T_CHWS_min;
LB(13*N+1:14*N)   = T_CHWS_min;
LB(14*N+1:15*N)   = T_CHWS_min;
LB(15*N+1:16*N)   = f_s_1_min;
LB(16*N+1:17*N)   = W_GT_min;

%Perform optimization
tic;

OPTIONS =
optimset('FunValCheck','on','UseParallel','always','Display','iter','MaxFunEvals',100000000,'MaxIter',...
        100000,'Algorithm','interior-point','Diagnostics','on','TolX',1e-10,'TolCon',1e-4,'TolFun',1e-10);
[x_star,fstar] =
fmincon(@CCHP_NJmod_objective_function_3,x0,[],[],[],[],LB,UB,@CCHP_NJmod_constraints_3,OPTIONS,T0,P0,Qc_dem,Qh
_dem,Elec_dem,N,nc,Ts);%xstar stores optimal variables, fstar is optimal objective function at xstar

m_CHW_mat   = vec2mat(x_star(1:N*nc),nc);           % (kg/s) Chilled water mass flows stored in a matrix (rows
% denote time sample (1,2,...N) and columns denote chiller number (1,2,...nc))
m_f         = x_star(N*nc+1:N*nc+N);                % (kg/s) Mass flow rate of fuel supplied to gas turbine at
% times 1,2,..N
T_CHWS_mat  = vec2mat(x_star(N*nc+N+1:2*N*nc+N),nc);% (deg K) Chilled water supply temperatures stored in a
% matrix (rows denote time sample (1,2,...N) and columns denote chiller number (1,2,...nc))
f_s_1       = x_star(2*N*nc+N+1:2*N*nc+2*N);        % (unitless) Fraction of mass flow rate diverted to steam
% turbine at times 1,2,..N
```

```
W_GT        = x_star(2*N*nc+2*N+1:2*N*nc+3*N);      % (kW) Power supplied by Gas Turbine at times 1,2,..N

T = toc

~~~~~~~~~~~~~~~~~~~~~~~~~~~~~~~~~~~~~~~~~~~~~~~~~~~~~~~~~~~~~~~~~~~~~~~~~~~~~~~~~~~~~~~~~~~~~~~~~~~~~~~~~~~~~~~~~~~

function J = CCHP_NJmod_objective_function_3(x,T0,P0,Qc_dem,Qh_dem,Elec_dem,N,nc,Ts)

% Nomenclature

% m - mass flow rate
% Q - heat transfer rate
% W - work transfer rate (power)
% T - temperature
% P - pressure
% psi - specific exergy
% ndv - number of decision variables
% np - length of prediction window

% Decision Variables

m_CHW_mat   = vec2mat(x(1:N*nc),nc);               % Chilled water mass flows stored in a matrix (rows denote
% time sample (1,2,...N) and columns denote chiller number (1,2,...nc))
m_f         = x(N*nc+1:N*nc+N);                    % Mass flow rate of fuel supplied to gas turbine at times
% 1,2,..N
T_CHWS_mat  = vec2mat(x(N*nc+N+1:2*N*nc+N),nc);    % Chilled water supply temperatures stored in a matrix (rows
% denote time sample (1,2,...N) and columns denote chiller number (1,2,...nc))
f_s_1       = x(2*N*nc+N+1:2*N*nc+2*N);            % Fraction of mass flow rate diverted to steam turbine at
% times 1,2,..N
W_GT        = x(2*N*nc+2*N+1:2*N*nc+3*N);          % Power supplied by Gas Turbine at times 1,2,..N

% Fluid Properties (constants wrt optimization)

% Specific heat capacities (kJ/kg-K) at times 1,2,..N
c_pa = ones(N,1)*1.01;  % air
c_pg = ones(N,1)*1.1;   % natural gas (CH4) exhaust gas
c_pw = ones(N,1)*4.186; % water

R    = 0.287*ones(N,1);          % kJ/kg-K (value for air used for exhaust gas)
rho_w= 1000*ones(N,1);           % kg/m^3
LHV  = 50.020*1000*ones(N,1);    % kJ/kg Corrected on 04/03/2013 by Neera Jain
psi_f= 51.849*1000*ones(N,1);    % kJ/kg Corrected on 04/03/2013 by Neera Jain

% Operating Parameters (specified by user and constant wrt optimization)

% Pressures (kPa)
P_dae       = (101.325 + 9*6.894)*ones(N,1);    % Deaerator pressure in steam loop at times 1,2,..N
P_cond1     = (0.6203*101.325)*ones(N,1);       % Condensor 1 pressure in steam loop at times 1,2,..N
P_w_in      = (101.325 + 285*6.894)*ones(N,1);  % Inlet water pressure to HRSG at times 1,2,..N

% Temperatures (deg Kelvin)
T_w_in      = (5*(240-32)/9 + 273.15)*ones(N,1);    % Inlet water temperatures to HRSG at times 1,2,..N in deg
% Kelvin
T_hw_sink   = (5*(224-32)/9 + 273.15)*ones(N,1);    % Hot water return temperature from campus hot water loop
% at times 1,2,..N in deg Kelvin
T_chwr      = ( (60-32)*(5/9) + 273.15 )*ones(N,1); % 60F converted into deg Kelvin

% Enthalpy (kJ/kg)
h_w_in      = 462.8*ones(N,1); % Inlet water enthalpy to HRSG in kJ/kg for specified value of P_w_in;

% 3 different cases - only one should be uncommented at any given time

% Case 1:
% Component efficiencies at times 1,2,..N
eta_compair = ones(N,1)*0.5;
eta_GT      = ones(N,1)*0.5;
eta_ST      = ones(N,1)*1.0;

% Case 2:
% Component efficiencies at times 1,2,..N
eta_compair = ones(N,1)*1.0;
eta_GT      = ones(N,1)*1.0;
eta_ST      = ones(N,1)*0.5; % based on Vikas' code

% Case 0:
% Component efficiencies at times 1,2,..N
eta_compair = ones(N,1)*0.85; % based on data
eta_GT      = ones(N,1)*0.95;
eta_ST      = ones(N,1)*0.80; % based on Vikas' code

% Other
Pr_compair  = (16)*ones(N,1);  % Chosen based on pressure ratio of 16 from UC Irvine slides
```

```
epsil       = 0.8455;        % HRSG overall effectiveness
f_SG_pw     = 0.95;          % Water stream pressure loss factor in HRSG
m_w        = ( 1/1 )*( 122.6*0.001196/15.8/0.001 )*ones(N,1); % Water mass flow rate through HRSG at times
% 1,2,..N

theta_T1 = 0.0249*ones(N,1); %Defined in Eq. (22)
theta_T2 = 435.47*ones(N,1); %Defined in Eq. (22)
theta_cp1= 0.0006*ones(N,1); %Defined in Excel File created by Neera
theta_cp2= 1.6599*ones(N,1); %Defined in Excel File created by Neera
theta_Ts1= 0.4445*ones(N,1); %Theta "Steam Temp" 1
theta_Ts2= 1041.6*ones(N,1); %Theta "Steam Temp" 2

% Control Volume 1 - Gas Turbine and Generator

m_a             = ( 22.0 )*m_f;         % based on non-stoichiometric combustion of methane
m_g             = 1.02*m_a;             % based on non-stoichiometric combustion of methane

T_air_in        = T0;
T_compair_out   = T_air_in.*( ones(N,1) + ( 1./eta_compair ).*( Pr_compair.^(0.4/1.4) - ones(N,1) ) );  % Units
% Kelvin
P_compair_out   = P0.*Pr_compair;
W_compair       = ( m_a.*c_pa.*( T_compair_out - T_air_in ) );

W_turb = W_compair + W_GT; % W_GT is the net power produced by the gas turbine; W_turb is the amount produced
% just by the turbine.

T_comb_out      = ( m_f.*psi_f )./( m_a.*c_pa ) + T_compair_out;
P_comb_out      = P_compair_out; % Corrected 4/3/2013 by Neera Jain

T_turb_out      = T_comb_out - W_turb./( m_g.*c_pg );
P_turb_out      = P_comb_out.*( ( -( 1 - T_turb_out./T_comb_out )./( eta_GT ) + 1 ).^(1.4/0.4) );

% Control Volume 2 - Heat Recovery Steam Generator (HRSG)

% Assumptions
% 1. The pressure and temperature of water exiting the steam loop ( P_w_in and T_w_in ) are controlled to be
% constant
% 2. There is no pressure drop in the gas stream from inlet to outlet ( P_g_in = P_g_out )*
% 3. The pressure in the steam/water stream drops by a constant factor f_SG_pw from inlet to outlet

T_g_in      = T_turb_out; % Exhaust gas from turbine becomes inlet gas to HRSG
P_g_in      = P_turb_out; % Exhaust gas from turbine becomes inlet gas to HRSG

T_g_out     = T_g_in - epsil.*( T_g_in - T_w_in );
P_g_out     = P_g_in;     % See assumption (2)

h_s_out     = h_w_in + ( m_g ./ m_w ).*c_pg.*( T_turb_out - T_g_out );

%constraint: h_s_out > hg_sat = 2797.27 kJ/kg (Tsat = 210C)
T_w_out     = ( theta_Ts1.*h_s_out - theta_Ts2 ) + 273.15*ones(N,1);
P_w_out     = f_SG_pw.*P_w_in;

psi_g       = c_pg.*( T_g_out - T0 ) - T0.*( c_pg.*log(T_g_out./T0) - R.*log(P_g_out./P0) );

% Control Volume 3 - Steam Loop (Steam Turbine and Heating Load)

% Assumptions
% 1. The deaerator and condensers operate at constant pressures, i.e. P_cond1, P_cond2, P_dae are controlled to
% be constant
% 2. The pressure and temperature of water exiting the steam loop ( P_w_out and T_hwr ) are controlled to be
% constant
% 3. Stream driving the steam turbine behaves like an ideal gas

m_s       = m_w;        % The mass flow rate of water/steam is constant throughout the entire loop
m_s1      = f_s_1.*m_s;
m_s2      = m_s - m_s1;
T_s_in    = T_w_out;    % The hot water vapor exiting the HRSG is the steam which enters the steam loop
P_s_in    = P_w_out;    % The hot water vapor exiting the HRSG is the steam which enters the steam loop
T_hwr     = T_w_in;     % The hot water into the HRSG is the same as the hot water return wrt the steam loop
P_hwr     = P_w_in;     % The hot water into the HRSG is the same as the hot water return wrt the steam loop

c_ps      = theta_cp1.*T_s_in + theta_cp2; %kJ/kg-K

Qh        = m_s2.*c_ps.*( T_s_in - (theta_T1.*P_s_in + theta_T2) ); % The heat transferred out of the control
volume to meet the heating load

W_p1      = ( m_s1./rho_w ).*( P_dae - P_cond1 ); % Power consumed by Pump 1
W_p2      = ( m_s./rho_w ).*( P_hwr - P_dae );    % Power consumed by Pump 2
W_ST      = m_s1.*c_ps.*eta_ST.*T_s_in.*( 1 - ( P_cond1./P_s_in ).^0.25 ); % Power generated by the Steam
Turbine
```

```
% Control Volume 4

% Assumptions
% 1. The chilled water return temperature is uniform for each chiller ( T_chwr ) and is controlled to be
% constant
% 2. The chilled water supply temperatures are allowed to vary within a small band around 40 deg F
% 3. Stream driving the steam turbine behaves like an ideal gas

coeff1 = [0.1357;0.1357;0.1716;0.1604;0.1213;0.3683;0.3127]; %First Regression coefficients in Eq. (2)
coeff2 = [204.91;204.91;99.453;686.29;454.94;151.29;427.63]; %Second Regression coefficients in Eq. (2)

Qc_1 = m_CHW_mat(:,1).*c_pw.*( T_chwr - T_CHWS_mat(:,1) );
Qc_2 = m_CHW_mat(:,2).*c_pw.*( T_chwr - T_CHWS_mat(:,2) );
Qc_3 = m_CHW_mat(:,3).*c_pw.*( T_chwr - T_CHWS_mat(:,3) );
Qc_4 = m_CHW_mat(:,4).*c_pw.*( T_chwr - T_CHWS_mat(:,4) );
Qc_5 = m_CHW_mat(:,5).*c_pw.*( T_chwr - T_CHWS_mat(:,5) );
Qc_6 = m_CHW_mat(:,6).*c_pw.*( T_chwr - T_CHWS_mat(:,6) );
Qc_7 = m_CHW_mat(:,7).*c_pw.*( T_chwr - T_CHWS_mat(:,7) );

W_compref1 = coeff1(1)*Qc_1 + coeff2(1)*ones(N,1);
W_compref2 = coeff1(2)*Qc_2 + coeff2(2)*ones(N,1);
W_compref3 = coeff1(3)*Qc_3 + coeff2(3)*ones(N,1);
W_compref4 = coeff1(4)*Qc_4 + coeff2(4)*ones(N,1);
W_compref5 = coeff1(5)*Qc_5 + coeff2(5)*ones(N,1);
W_compref6 = coeff1(6)*Qc_6 + coeff2(6)*ones(N,1);
W_compref7 = coeff1(7)*Qc_7 + coeff2(7)*ones(N,1);

X_d_ch_1 = (ones(N,1) - T0./T_chwr).*(Qc_1) + W_compref1;
X_d_ch_2 = (ones(N,1) - T0./T_chwr).*(Qc_2) + W_compref2;
X_d_ch_3 = (ones(N,1) - T0./T_chwr).*(Qc_3) + W_compref3;
X_d_ch_4 = (ones(N,1) - T0./T_chwr).*(Qc_4) + W_compref4;
X_d_ch_5 = (ones(N,1) - T0./T_chwr).*(Qc_5) + W_compref5;
X_d_ch_6 = (ones(N,1) - T0./T_chwr).*(Qc_6) + W_compref6;
X_d_ch_7 = (ones(N,1) - T0./T_chwr).*(Qc_7) + W_compref7;

%Objective Function - only one should be uncommented at any given time

% J - exergy

J = 0;

for k = 1:N
    J = J + ( W_compair(k) - W_turb(k) + m_f(k)*psi_f(k) - m_g(k)*psi_g(k) ) + ( (1 - T0(k)/T_hwr(k))*(-Qh(k))
+ W_p1(k) + W_p2(k) - W_ST(k) ) ...
          + ( X_d_ch_1(k) + X_d_ch_2(k) + X_d_ch_3(k) + X_d_ch_4(k) + X_d_ch_5(k) + X_d_ch_6(k) + X_d_ch_7(k)
);
end

% J - exergy + energy
    J = 0;

    for k = 1:N
        J = J + (W_compair(k) - W_turb(k) + m_f(k)*psi_f(k) - m_g(k)*psi_g(k) ) + ( (1 - T0(k)/T_hwr(k))*(-
Qh(k)) + W_p1(k) + W_p2(k) - W_ST(k) ) ...
              + ( W_compref1(k) + W_compref2(k) + W_compref3(k) + W_compref4(k) + W_compref5(k) + W_compref6(k)
+ W_compref7(k) );
    end

% J - fuel

    J = 0;

    for k = 1:N
        J = J + LHV(k)*m_f(k);
    end

end

~~~~~~~~~~~~~~~~~~~~~~~~~~~~~~~~~~~~~~~~~~~~~~~~~~~~~~~~~~~~~~~~~~~~~~~~~~~~~~~~~~~~~~~~~~~~~~~~~~~~~~~~~~~~~~~~~~~~~~~~~~~~~

function [c,ceq] = CCHP_NJmod_constraints_3(x,T0,P0,Qc_dem,Qh_dem,Elec_dem,N,nc,Ts)

% This Function Expresses all the Equality and Inequality Constraints in the Optimization

% Nomenclature

% m - mass flow rate
% Q - heat transfer rate
% W - work transfer rate (power)
% T - temperature
% P - pressure
```

```
% psi - specific exergy
% ndv - number of decision variables
% np - length of prediction window

% Decision Variables

m_CHW_mat   = vec2mat(x(1:N*nc),nc);               % Chilled water mass flows stored in a matrix (rows denote
% time sample (1,2,...N) and columns denote chiller number (1,2,...nc))
m_f         = x(N*nc+1:N*nc+N);                    % Mass flow rate of fuel supplied to gas turbine at times
% 1,2,..N
T_CHWS_mat  = vec2mat(x(N*nc+N+1:2*N*nc+N),nc);    % Chilled water supply temperatures stored in a matrix (rows
% denote time sample (1,2,...N) and columns denote chiller number (1,2,...nc))
f_s_1       = x(2*N*nc+N+1:2*N*nc+2*N);            % Fraction of mass flow rate diverted to steam turbine at
% times 1,2,..N
W_GT        = x(2*N*nc+2*N+1:2*N*nc+3*N);          % Power supplied by Gas Turbine at times 1,2,..N

% Fluid Properties (constants wrt optimization)

% Specific heat capacities (kJ/kg-K) at times 1,2,..N
c_pa = ones(N,1)*1.01;  % air
c_pg = ones(N,1)*1.1;   % natural gas (CH4) exhaust gas
c_pw = ones(N,1)*4.186; % water

R    = 0.287*ones(N,1);          % kJ/kg-K (value for air used for exhaust gas)
rho_w= 1000*ones(N,1);           % kg/m^3
LHV  = 50.020*1000*ones(N,1);    % kJ/kg Corrected on 04/03/2013 by Neera Jain
psi_f= 51.849*1000*ones(N,1);    % kJ/kg Corrected on 04/03/2013 by Neera Jain

% Operating Parameters (specified by user and constant wrt optimization)

% Pressures (kPa)
P_dae       = (101.325 + 9*6.894)*ones(N,1);    % Deaerator pressure in steam loop at times 1,2,..N
P_cond1     = (0.6203*101.325)*ones(N,1);       % Condensor 1 pressure in steam loop at times 1,2,..N
P_w_in      = (101.325 + 285*6.894)*ones(N,1);  % Inlet water pressure to HRSG at times 1,2,..N

% Temperatures (deg Kelvin)
T_w_in      = (5*(240-32)/9 + 273.15)*ones(N,1);    % Inlet water temperatures to HRSG at times 1,2,..N in deg
% Kelvin
T_hw_sink   = (5*(224-32)/9 + 273.15)*ones(N,1);    % Hot water return temperature from campus hot water loop
% at times 1,2,..N in deg Kelvin
T_chwr      = ( (60-32)*(5/9) + 273.15 )*ones(N,1); % 60F converted into deg Kelvin

% Enthalpy (kJ/kg)
h_w_in      = 462.8*ones(N,1); % Inlet water enthalpy to HRSG in kJ/kg for specified value of P_w_in;

% Case 1:
% Component efficiencies at times 1,2,..N
eta_compair = ones(N,1)*0.5; % based on data
eta_GT      = ones(N,1)*0.5;
eta_ST      = ones(N,1)*1.0; % based on Vikas' code

% Case 2:
% Component efficiencies at times 1,2,..N
eta_compair = ones(N,1)*1.0; % based on data
eta_GT      = ones(N,1)*1.0;
eta_ST      = ones(N,1)*0.5; % based on Vikas' code

% Case 0:
% Component efficiencies at times 1,2,..N
eta_compair = ones(N,1)*0.85; % based on data
eta_GT      = ones(N,1)*0.95;
eta_ST      = ones(N,1)*0.80; % based on Vikas' code

% Other
Pr_compair  = (16)*ones(N,1);  % Chosen based on pressure ratio of 16 from UC Irvine slides
epsil       = 0.8455;        % HRSG overall effectiveness
f_SG_pw     = 0.95;          % Water stream pressure loss factor in HRSG
m_w        = ( 1/1 )*( 122.6*0.001196/15.8/0.001 )*ones(N,1); % Water mass flow rate through HRSG at times
% 1,2,..N

theta_T1 = 0.0249*ones(N,1); %Defined in Eq. (22)
theta_T2 = 435.47*ones(N,1); %Defined in Eq. (22)
theta_cp1= 0.0006*ones(N,1); %Defined in Excel File created by Neera
theta_cp2= 1.6599*ones(N,1); %Defined in Excel File created by Neera
theta_Ts1= 0.4445*ones(N,1); %Theta "Steam Temp" 1
theta_Ts2= 1041.6*ones(N,1); %Theta "Steam Temp" 2

% Control Volume 1 - Gas Turbine and Generator

m_a             = ( 22.0 )*m_f;         % based on non-stoichiometric combustion of methane
m_g             = 1.02*m_a;             % based on non-stoichiometric combustion of methane
```

```
T_air_in        = T0;
T_compair_out   = T_air_in.*( ones(N,1) + ( 1./eta_compair ).*( Pr_compair.^(0.4/1.4) - ones(N,1) ) );  % Units
Kelvin

P_compair_out   = P0.*Pr_compair;
W_compair       = ( m_a.*c_pa.*( T_compair_out - T_air_in ) );

W_turb = W_compair + W_GT;

T_comb_out      = ( m_f.*psi_f )./( m_a.*c_pa ) + T_compair_out;
P_comb_out      = P_compair_out;

T_turb_out      = T_comb_out - W_turb./( m_g.*c_pg );
P_turb_out      = P_comb_out.*( ( -( 1 - T_turb_out./T_comb_out )./( eta_GT ) + 1 ).^(1.4/0.4) );

% Control Volume 2 - Heat Recovery Steam Generator (HRSG)

% Assumptions
% 1. The pressure and temperature of water exiting the steam loop ( P_w_in and T_w_in ) are controlled to be
% constant
% 2. There is no pressure drop in the gas stream from inlet to outlet ( P_g_in = P_g_out )*
% 3. The pressure in the steam/water stream drops by a constant factor f_SG_pw from inlet to outlet

T_g_in      = T_turb_out; % Exhaust gas from turbine becomes inlet gas to HRSG
P_g_in      = P_turb_out; % Exhaust gas from turbine becomes inlet gas to HRSG

T_g_out     = T_g_in - epsil.*( T_g_in - T_w_in );
P_g_out     = P_g_in;     % See assumption (2)

h_s_out     = h_w_in + ( m_g ./ m_w ).*c_pg.*( T_turb_out - T_g_out );

%constraint: h_s_out > hg_sat = 2797.27 kJ/kg (Tsat = 210C)
T_w_out     = ( theta_Ts1.*h_s_out - theta_Ts2 ) + 273.15*ones(N,1);
P_w_out     = f_SG_pw.*P_w_in;

psi_g       = c_pg.*( T_g_out - T0 ) - T0.*( c_pg.*log(T_g_out./T0) - R.*log(P_g_out./P0) );

% Control Volume 3 - Steam Loop (Steam Turbine and Heating Load)

% Assumptions
% 1. The deaerator and condensers operate at constant pressures, i.e. P_cond1, P_cond2, P_dae are controlled to
% be constant
% 2. The pressure and temperature of water exiting the steam loop ( P_w_out and T_hwr ) are controlled to be
% constant
% 3. Stream driving the steam turbine behaves like an ideal gas

m_s       = m_w;        % The mass flow rate of water/steam is constant throughout the entire loop
m_s1      = f_s_1.*m_s;
m_s2      = m_s - m_s1;
T_s_in    = T_w_out;    % The hot water vapor exiting the HRSG is the steam which enters the steam loop
P_s_in    = P_w_out;    % The hot water vapor exiting the HRSG is the steam which enters the steam loop
T_hwr     = T_w_in;     % The hot water into the HRSG is the same as the hot water return wrt the steam loop
P_hwr     = P_w_in;     % The hot water into the HRSG is the same as the hot water return wrt the steam loop

c_ps      = theta_cp1.*T_s_in + theta_cp2; %kJ/kg-K

Qh        = m_s2.*c_ps.*( T_s_in - (theta_T1.*P_s_in + theta_T2) ); % The heat transfered out of the control
volume to meet the heating load

W_p1      = ( m_s1./rho_w ).*( P_dae - P_cond1 ); % Power consumed by Pump 1
W_p2      = ( m_s./rho_w ).*( P_hwr - P_dae );    % Power consumed by Pump 2
W_ST      = m_s1.*c_ps.*eta_ST.*T_s_in.*( 1 - ( P_cond1./P_s_in ).^0.25 ); % Power generated by the Steam
Turbine

% Control Volume 4

% Assumptions
% 1. The chilled water return temperature is uniform for each chiller ( T_chwr ) and is controlled to be
% constant
% 2. The chilled water supply temperatures are allowed to vary within a small band around 40 deg F
% 3. Stream driving the steam turbine behaves like an ideal gas

coeff1 = [0.1357;0.1357;0.1716;0.1604;0.1213;0.3683;0.3127]; %First Regression coefficients in Eq. (2)
coeff2 = [204.91;204.91;99.453;686.29;454.94;151.29;427.63]; %Second Regression coefficients in Eq. (2)

Qc_1 = m_CHW_mat(:,1).*c_pw.*( T_chwr - T_CHWS_mat(:,1) );
Qc_2 = m_CHW_mat(:,2).*c_pw.*( T_chwr - T_CHWS_mat(:,2) );
Qc_3 = m_CHW_mat(:,3).*c_pw.*( T_chwr - T_CHWS_mat(:,3) );
Qc_4 = m_CHW_mat(:,4).*c_pw.*( T_chwr - T_CHWS_mat(:,4) );
Qc_5 = m_CHW_mat(:,5).*c_pw.*( T_chwr - T_CHWS_mat(:,5) );
```

```
Qc_6 = m_CHW_mat(:,6).*c_pw.*( T_chwr - T_CHWS_mat(:,6) );
Qc_7 = m_CHW_mat(:,7).*c_pw.*( T_chwr - T_CHWS_mat(:,7) );

W_compref1 = coeff1(1)*Qc_1 + coeff2(1)*ones(N,1);
W_compref2 = coeff1(2)*Qc_2 + coeff2(2)*ones(N,1);
W_compref3 = coeff1(3)*Qc_3 + coeff2(3)*ones(N,1);
W_compref4 = coeff1(4)*Qc_4 + coeff2(4)*ones(N,1);
W_compref5 = coeff1(5)*Qc_5 + coeff2(5)*ones(N,1);
W_compref6 = coeff1(6)*Qc_6 + coeff2(6)*ones(N,1);
W_compref7 = coeff1(7)*Qc_7 + coeff2(7)*ones(N,1);

Qc_Total = Qc_1 + Qc_2 + Qc_3 + Qc_4 + Qc_5 + Qc_6 + Qc_7;

W_compref_Total = W_compref1 + W_compref2 + W_compref3 + W_compref4 + W_compref5 + W_compref6 + W_compref7;

%************************************************************************
%******COOLING PLUS POWER PLANT EQUALITY AND INEQUALITY CONSTRAINTS*******
%************************************************************************

%Equality constraints

ceq = zeros(3*N,1); %Pre-allocation for equality constraints

ceq(1:N,1)         = Qc_dem - Qc_Total;    % kW
ceq(N+1:2*N,1)     = Qh_dem - Qh;          % kW
ceq(2*N+1:3*N,1)   = W_GT + W_ST - Elec_dem - W_compref_Total - (W_p1 + W_p2); % kW

%Inequality constraints

c = zeros(2*N,1);

c(1:N,1)         = 2797.27*ones(N,1) - h_s_out;
c(N+1:2*N,1)     = P0 - P_g_out;

end
```

E.2 EDM-based Optimal Control of a VCC System

The MATLAB code presented below is divided into 4 separate blocks; the first block of code calls is an initialization script which loads various parameters to the workspace. This script calls the function *Dynamic_Optim_Exergy_R134a_Offline* which in turn calls two other functions: *Dynamic_Solver_Exergy_R134a_offline*, *Dynamic_Nonlcon_Exergy_R134a_offline*.

```
% Initialization File for Offline Optimization

clear all;clc;

%Updated 11-23-12
load dnom_112312
load xnom_112312
load unom_112312

X0 = xnom;
U0 = unom;

Ts      = 1;        % sampling time
nu      = 200;      % control horizon
np      = 200;      % prediction horizon
n       = 15;       % number of states
u       = 4;        % number of control inputs
nd      = 2;        % number of disturbances

%% Load Desired Capacity and Ambient Temperature Profiles

load C_des_400_pt_84_2

C_des = C_desired(1:200);
T_H   = ones(np,1)*26;
```

```
T_L   = ones(np,1)*18;

%% Define optim_input

optim_input = [X0; U0; xnom; unom; dnom];

clear xnom unom dnom X0 U0 C_desired

%% Load Heat Transfer Coefficients

load UA_values_112312
U_guess = zeros(u*np,1);

%% Load System Model

A  = eye(n);
B1 = zeros(n,u);
B2 = zeros(n,nd);

load VCC_A_matrix_discrete_point83_nonIScomp_TS1
load VCC_B1_matrix_discrete_point83_nonIScomp_TS1
load VCC_B2_matrix_discrete_point83_nonIScomp_TS1

% Load these but they will not be used
load E_matrix
load D_matrix

D_matrix = D;
E_matrix = E;

A  = VCC_A;
B1 = VCC_B1;
B2 = VCC_B2;

clear VCC_A VCC_B1 VCC_B2

%% Define Max and Min bounds on U

Mins = [8; 900; 0.10; 0.30];

Maxs = [11; 1100; 0.3; 0.65];

%%

output = Dynamic_Optim_Exergy_R134a_Offline(optim_input, C_des, T_L, T_H, Ts, nu, np, n, u, nd, UA, A, B1, B2,
D_matrix, E_matrix, Mins, Maxs, U_guess)

~~~~~~~~~~~~~~~~~~~~~~~~~~~~~~~~~~~~~~~~~~~~~~~~~~~~~~~~~~~~~~~~~~~~~~~~~~~~~~~~~~~~~~~~~~~~~~~~~~~~~~~~~~~~~~~~~~~~~~~~~

function [output] = Dynamic_Optim_Exergy_R134a_Offline(optim_input, C_des, T_L, T_H, Ts, nu, np, n, u, nd, UA,
A, B1, B2, D_matrix, E_matrix, Mins, Maxs, U_guess)

tic;

X0      = optim_input(1:15);  % absolute X0
U0      = optim_input(16:19); % absolute U0
xnom    = optim_input(20:34); % nominal x
unom    = optim_input(35:38); % nominal u
dnom    = optim_input(39:40); % nominal d

% Create lifted nominal vectors for U, X, and D

    Unom_Lifted = zeros(nu*u,1);

    for i = 1:u:u*nu
        Unom_Lifted(i:i+u-1) = unom;
    end
    clear i

    Xnom_Lifted = zeros(np*n,1);

    for i = 1:n:n*np
        Xnom_Lifted(i:i+n-1) = xnom;
    end
    clear i

    Dnom_Lifted = zeros(np*nd,1);

    for i = 1:nd:nd*np
        Dnom_Lifted(i:i+nd-1) = dnom;
    end
    clear i
```

```
% Create lifted D and D_delta vectors

    D = zeros(np*nd,1);

    k = 1;
    for i = 1:nd:nd*np
        D(i:i+nd-1) = [T_L(k); T_H(k)];
        k = k + 1;
    end
    clear i k

    D_delta = D - Dnom_Lifted;

% Define Augmented x vector (not lifted yet)

    X0_delta = X0 - xnom;
    U0_delta = U0 - unom;

    X_bar0_delta = [X0_delta;U0_delta];

% State Space System Representation

    C1 = eye(n);
    C2 = eye(u);

% Define Augmented System [x x_u]

    A_bar  = [A B1; zeros(u,n) eye(u)];
    B1_bar = [B1;eye(u)];
    B2_bar = [B2;zeros(u,nd)];
    % c_bar  = [C1 zeros(n,u); zeros(u,n) C2];

    c_bar  = [C1 zeros(n,u)];
    c2_bar = [zeros(u,n) C2];

    C_bar = zeros(n*np,(n+u)*np);
    for i = 1:np
        C_bar((i-1)*n+1:i*n,(i-1)*(n+u)+1:i*(n+u)) = c_bar;
    end

    C2_bar = zeros(u*np, (n+u)*np);
    for i = 1:np
        C2_bar((i-1)*u+1:i*u,(i-1)*(n+u)+1:i*(n+u)) = c2_bar;
    end

% Define Lifted Matrices for Determining X_bar

    T = zeros((n+u)*np,n+u);
    for i = 1:np
        T((i-1)*(n+u)+1:i*(n+u),:) = A_bar^i;
    end

    S1 = zeros((n+u)*np,u*nu);
    for i = 1:np
        for j = 1:nu
            if i-j < 0
                S1((i-1)*(n+u)+1:i*(n+u),(j-1)*u+1:j*u) = zeros((n+u),u);
            elseif i-j == 0
                S1((i-1)*(n+u)+1:i*(n+u),(j-1)*u+1:j*u) = B1_bar;
            elseif i-j > 0
                S1((i-1)*(n+u)+1:i*(n+u),(j-1)*u+1:j*u) = A_bar^(i-j)*B1_bar;
            end
        end
    end

    S2 = zeros((n+u)*np,nd*np);
    for i = 1:np
        for j = 1:nu
            if i-j < 0
                S2((i-1)*(n+u)+1:i*(n+u),(j-1)*nd+1:j*nd) = zeros((n+u),nd);
            elseif i-j == 0
                S2((i-1)*(n+u)+1:i*(n+u),(j-1)*nd+1:j*nd) = B2_bar;
            elseif i-j > 0
                S2((i-1)*(n+u)+1:i*(n+u),(j-1)*nd+1:j*nd) = A_bar^(i-j)*B2_bar;
            end
        end
    end

% Define Matrices for Linear Constraints
```

```
% Linear constraints on 'Zeta_e1' and 'Zeta_c1+Zeta_c2'
m       = zeros(2,n);
m(1,1)  = 1;
m(2,7)  = 1;
m(2,8)  = 1;

M = zeros(2*np,n*np);
for i = 1:np
    M((i-1)*2+1:i*2,(i-1)*n+1:i*n) = m;
end

zmax = [(1-0.05);(1-0.05)];
znom = [xnom(1);(xnom(7)+xnom(8))];
Zmax = zeros(2*np,1);
Znom = zeros(2*np,1);
for i = 1:np
    Zmax((i-1)*2+1:i*2) = zmax;
    Znom((i-1)*2+1:i*2) = znom;
end

bZETAmax   = (Zmax - Znom) - M*C_bar*T*X_bar0_delta - M*C_bar*S2*D_delta;
aZETAmax   = M*C_bar*S1;

clear M m znom zmax Znom Zmax

% Linear constraints on 'Tw3c'
m       = zeros(1,n);
m(1,14) = 1;

M = zeros(1*np,n*np);
for i = 1:np
    M((i-1)*1+1:i*1,(i-1)*n+1:i*n) = m;
end

Zmax = T_H + 0.2;
znom = [xnom(14)];
Znom = zeros(1*np,1);
for i = 1:np
    Znom((i-1)*1+1:i*1) = znom;
end

bTwmax   = -Zmax + Znom + M*C_bar*T*X_bar0_delta + M*C_bar*S2*D_delta;
aTwmax   = -M*C_bar*S1;

% Upper and Lower Bound Constraints on U

bmin = zeros(u*nu,1);
for i = 1:nu;
    bmin((i-1)*u+1:i*u,1) = -Mins+U0;
end

bmax = zeros(u*nu,1);
for i = 1:nu;
    bmax((i-1)*u+1:i*u,1) = Maxs-U0;
end

amin = zeros(u*nu);
for i = 1:nu
    for j = 1:nu
        if i-j >= 0
            amin((i-1)*u+1:i*u,(j-1)*u+1:j*u)=-1*eye(u);
        else
            amin((i-1)*u+1:i*u,(j-1)*u+1:j*u)=zeros(u);
        end
    end
end

amax = zeros(u*nu);
for i = 1:nu
    for j = 1:nu
        if i-j >= 0
            amax((i-1)*u+1:i*u,(j-1)*u+1:j*u)=eye(u);
        else
            amax((i-1)*u+1:i*u,(j-1)*u+1:j*u)=zeros(u);
        end
    end
end

a = [amin;amax;aZETAmax;aTwmax];
b = [bmin;bmax;bZETAmax;bTwmax];
```

```
%%%%%%%%%%%%%%%%%%%%%%%%%%%%%%%%%%%%%%%%%%%%%%%%%%%%%%%%%%%%%%%%%%%%%%%%%%%%
% Stage 2: Optimization
%%%%%%%%%%%%%%%%%%%%%%%%%%%%%%%%%%%%%%%%%%%%%%%%%%%%%%%%%%%%%%%%%%%%%%%%%%%%

I_L = amax;

OPTIONS =
optimset('FunValCheck','on','UseParallel','always','Display','iter','MaxFunEvals',2000000,'MaxIter',...
2000000,'Algorithm','sqp','Diagnostics','on','TolX',1e-3,'TolCon',5e-4,'TolFun',1e-3);

% Call FMINCON
[U,J_fval,Exitflag] = fmincon(@Dynamic_Solver_Exergy_R134a_offline,U_guess,a,b,[],[],[],[],...
@Dynamic_Nonlcon_Exergy_R134a_offline,OPTIONS,T,S1,S2,X0_delta,U0_delta,D_delta,Xnom_Lifted,Unom_Lifted,C_bar,C
2_bar,C_des,T_L,T_H,Ts,nu,np,n,u,nd,I_L,UA,D_matrix,E_matrix);

T = toc

%%%%%%%%%%%%%%%%%%%%%%%%%%%%%%%%%%%%%%%%%%%%%%%%%%%%%%%%%%%%%%%%%%%%%%%%%%%%
% Stage 3: Create output vector
%%%%%%%%%%%%%%%%%%%%%%%%%%%%%%%%%%%%%%%%%%%%%%%%%%%%%%%%%%%%%%%%%%%%%%%%%%%%

output  = [U; J_fval; Exitflag; T];

end

~~~~~~~~~~~~~~~~~~~~~~~~~~~~~~~~~~~~~~~~~~~~~~~~~~~~~~~~~~~~~~~~~~~~~~~~~~~~~~~~~~~~~~~~~~~~~~~~~~~~~~~~~~~~~~~~~~

function J =
Dynamic_Solver_Exergy_R134a_offline(U,T,S1,S2,X0_delta,U0_delta,D_delta,Xnom_Lifted,Unom_Lifted,C_bar,C2_bar,C_
des,T_L,T_H,Ts,nu,np,n,u,nd,I_L,UA,D_matrix,E_matrix)

load FluidProp_R134a_Thermosys

% Assign values to physical parameters of HX's

L_ref_e     = 11.45;
Ac_ref_e    = 5.165e-5;
L_ref_c     = 10.6895;
Ac_ref_c    = 5.156e-5;

% Convert T_H and T_L to Kelvin

Tcai_K = T_H + ones(np,1)*273;
Teai_K = T_L + ones(np,1)*273;

% Initial State Vector - X0_delta (dimension: 15 x 1) - delta away from nominal

% Initial Input Vector - U0_delta (dimension: 4 x 1) - delta away from nominal

% Define X_bar0

X_bar0_delta = [X0_delta;U0_delta];

X_bar_delta  = T*X_bar0_delta + S1*U + S2*D_delta; % delta away from nominal

X_delta      = C_bar*X_bar_delta;  % (separating X from X_bar)
Xu_delta     = C2_bar*X_bar_delta; % (separating Xu from X_bar)

X            = X_delta + Xnom_Lifted; % column vector of states
X_0          = X0_delta + Xnom_Lifted(1:n); % column vector

% Separate lifted state vector X_bar into individual state sequences:

zeta_e1 = zeros(np+1,1);
Pe      = zeros(np+1,1);
He2     = zeros(np+1,1);
Tw1e    = zeros(np+1,1);
Tw2e    = zeros(np+1,1);
GammaE  = zeros(np+1,1);
zeta_c1 = zeros(np+1,1);
zeta_c2 = zeros(np+1,1);
Pc      = zeros(np+1,1);
Hc1     = zeros(np+1,1);
Hc3     = zeros(np+1,1);
Tw1c    = zeros(np+1,1);
Tw2c    = zeros(np+1,1);
Tw3c    = zeros(np+1,1);
GammaC  = zeros(np+1,1);

i = 1;
zeta_e1(i) = X_0(1);
```

```
Pe(i)       = X_0(2);
He2(i)      = X_0(3);
Tw1e(i)     = X_0(4);
Tw2e(i)     = X_0(5);
GammaE(i)   = X_0(6);
zeta_c1(i)  = X_0(7);
zeta_c2(i)  = X_0(8);
Pc(i)       = X_0(9);
Hc1(i)      = X_0(10);
Hc3(i)      = X_0(11);
Tw1c(i)     = X_0(12);
Tw2c(i)     = X_0(13);
Tw3c(i)     = X_0(14);
GammaC(i)   = X_0(15);
clear i

zeta_e1(2:end) = X(1:n:end);
Pe(2:end)      = X(2:n:end);
He2(2:end)     = X(3:n:end);
Tw1e(2:end)    = X(4:n:end);
Tw2e(2:end)    = X(5:n:end);
GammaE(2:end)  = X(6:n:end);
zeta_c1(2:end) = X(7:n:end);
zeta_c2(2:end) = X(8:n:end);
Pc(2:end)      = X(9:n:end);
Hc1(2:end)     = X(10:n:end);
Hc3(2:end)     = X(11:n:end);
Tw1c(2:end)    = X(12:n:end);
Tw2c(2:end)    = X(13:n:end);
Tw3c(2:end)    = X(14:n:end);
GammaC(2:end)  = X(15:n:end);

zeta_e2 = ones(np+1,1) - zeta_e1;
zeta_c3 = ones(np+1,1) - zeta_c1 - zeta_c2;

U0_Lifted = zeros(np*u,1);

U_MPC = U0_Lifted + I_L*U + Unom_Lifted;

a_v     = zeros(np,1);
omega_k = zeros(np,1);
me_air  = zeros(np,1);
mc_air  = zeros(np,1);

a_v     = U_MPC(1:u:end);
omega_k = U_MPC(2:u:end);
me_air  = U_MPC(3:u:end);
mc_air  = U_MPC(4:u:end);

U_MPC2 = U0_Lifted + I_L*U + Unom_Lifted;

omega_k2 = U_MPC2(2:u:end);

%%%%%%%%%%%%%%%%%%%%%%%%%%%%%%%%%%%%%%%%%%%%%%%%%%%%%%%%%%%%%%%%%%%%%%%%%%%%%%%
%%%%%%%%%%%%%%%%%%%%%%%%%%%%%%%%%%%%%%%%%%%%%%%%%%%%%%%%%%%%%%%%%%%%%%%%%%%%%%%

% Determing necessary refrigerant properties via interpolation

% Evaporator

% Two-Phase Zone (Evaporator)
Tr1e        = interp1(FluidProp.Psat, FluidProp.Tsat, Pe);
H1g         = interp1(FluidProp.Psat, FluidProp.Hg, Pe);

rho1g       = interp1(FluidProp.Psat, FluidProp.Rhog, Pe);
rho1f       = interp1(FluidProp.Psat, FluidProp.Rhof, Pe);
drho1g_dP   = interp1(FluidProp.Psat, FluidProp.dRhog_dP, Pe);
drho1f_dP   = interp1(FluidProp.Psat, FluidProp.dRhof_dP, Pe);

rho_e1      = GammaE.*rho1g+(ones(np+1,1)-GammaE).*rho1f;
drho_e1_dP  = GammaE.*drho1g_dP+(ones(np+1,1)-GammaE).*drho1f_dP;

s1g         = interp1(FluidProp.Psat, FluidProp.sg, Pe);
s1f         = interp1(FluidProp.Psat, FluidProp.sf, Pe);
ds1g_dP     = interp1(FluidProp.Psat, FluidProp.dsg_dP, Pe);
ds1f_dP     = interp1(FluidProp.Psat, FluidProp.dsf_dP, Pe);

xbar_e      = (rho1g./rho_e1).*GammaE;
s_e1        = xbar_e.*s1g+(ones(np+1,1)-xbar_e).*s1f;

ds1_dGamma_P = ((GammaE.*rho1g + (ones(np+1,1)-GammaE).*rho1f).*(rho1g.*s1g - rho1f.*s1f) - ...
```

```
    (GammaE.*rho1g.*s1g + rho1f.*s1f - GammaE.*rho1f.*s1f).*(rho1g - rho1f))./((GammaE.*rho1g + (ones(np+1,1)-
GammaE).*rho1f).^2);

ds1_dP_Gamma = (rho_e1.*((GammaE.*rho1g.*ds1g_dP + GammaE.*s1g.*drho1g_dP)+(rho1g.*ds1f_dP +
s1f.*drho_e1_dP)+...
    (GammaE.*rho1g.*ds1f_dP + GammaE.*s1f.*drho1g_dP)) - (GammaE.*rho1g.*s1g + rho_e1.*s1f -
GammaE.*rho1g.*s1f).*drho_e1_dP) ./ (rho_e1.^2);

% Superheated Zone (Evaporator)
Tr2e        = interp2(FluidProp.H, FluidProp.P, FluidProp.T_ph, He2, Pe);
rho_e2      = interp2(FluidProp.H, FluidProp.P, FluidProp.Rho_ph, He2, Pe);
s_e2        = interp2(FluidProp.H, FluidProp.P, FluidProp.S_ph, He2, Pe);
ds2_dH_P    = interp2(FluidProp.H, FluidProp.P, FluidProp.dS_dH_P_ph, He2, Pe);
ds2_dP_H    = interp2(FluidProp.H, FluidProp.P, FluidProp.dS_dP_H_ph, He2, Pe);
drho2_dH_P  = interp2(FluidProp.H, FluidProp.P, FluidProp.dRho_dH_P_ph, He2, Pc);
drho2_dP_H  = interp2(FluidProp.H, FluidProp.P, FluidProp.dRho_dP_H_ph, He2, Pc);

He_out      = 2.*He2 - H1g;

s_k_in      = interp2(FluidProp.H, FluidProp.P, FluidProp.S_ph, He_out, Pe);
Xe          = GammaE.*(rho1g./rho_e1);

%%%%%%%%%%%%%%%%%%%%%%%%%%%%%%%%%%%%%%%%%%%%%%%%%%%%%%%%%%%%%%%%%%%%%%%%%%%%%%%

% Calculate valve mass flow rate
Pdelta      = Pc(2:np+1)-Pe(2:np+1);
Cd          = (-9.5984e-6) + (2.0481e-6).*a_v + (5.4106e-9).*Pdelta + (-7.4909e-10).*a_v.*Pdelta + ...
                    (-3.7775e-8).*(a_v.^2);
rho_c3      = interp2(FluidProp.H, FluidProp.P, FluidProp.Rho_ph, Hc3, Pc);
mdot_v        = zeros(np+1,1);
mdot_v(2:np+1) = Cd.*sqrt(rho_c3(2:np+1).*Pdelta);

% Calculate compressor mass flow rate
rho_k_in    = interp2(FluidProp.H_mg_ph,FluidProp.P_mg_ph,FluidProp.Rho_ph,He_out,Pe);
rps         = omega_k./60;
P_ratio     = Pc(2:np+1)./Pe(2:np+1);
eta_v       = 0.65127 + 0.00027681.*omega_k - 0.031338.*P_ratio + 3.0221e-5.*omega_k.*P_ratio...
    - 1.1905e-7.*(omega_k.^2) - 0.0081256.*(P_ratio.^2);
volume      = 3.042e-5;

mdot_k       = zeros(np+1,1);
mdot_k(2:np+1)= rps.*volume.*rho_k_in(2:np+1).*eta_v;

Hk_out_s     = interp2(FluidProp.S, FluidProp.P, FluidProp.H_ps, s_k_in, Pc);

eta_is       = ( (0.054812149750754) + (0.220895407941643).*P_ratio + (0.000034670672050).*omega_k2.*P_ratio +
...
                (-0.000000036818854).*omega_k2.^2 + (-0.041677058377446).*P_ratio.^2 );
Hk_out(2:np+1)= (Hk_out_s(2:np+1) - He_out(2:np+1))./eta_is + He_out(2:np+1);
Hc_in(2:np+1) = Hk_out(2:np+1);
H2g          = interp1(FluidProp.Psat, FluidProp.Hg, Pc);
Hc1(2:np+1)   = 0.5*(H2g(2:np+1) + Hc_in(2:np+1)');

s_k_out(2:np+1) = interp2(FluidProp.H, FluidProp.P, FluidProp.S_ph, Hc_in(2:np+1)', Pc(2:np+1));

%%%%%%%%%%%%%%%%%%%%%%%%%%%%%%%%%%%%%%%%%%%%%%%%%%%%%%%%%%%%%%%%%%%%%%%%%%%%%%%

% Determing necessary refrigerant properties via interpolation

% Condenser

% Superheated Zone (Condenser)
Tr1c        = interp2(FluidProp.H, FluidProp.P, FluidProp.T_ph, Hc1, Pc);
rho_c1      = interp2(FluidProp.H, FluidProp.P, FluidProp.Rho_ph, Hc1, Pc);
s_c1        = interp2(FluidProp.H, FluidProp.P, FluidProp.S_ph, Hc1, Pc);
ds1_dH_P    = interp2(FluidProp.H, FluidProp.P, FluidProp.dS_dH_P_ph, Hc1, Pc);
ds1_dP_H    = interp2(FluidProp.H, FluidProp.P, FluidProp.dS_dP_H_ph, Hc1, Pc);
drho1_dH_P  = interp2(FluidProp.H, FluidProp.P, FluidProp.dRho_dH_P_ph, Hc1, Pc);
drho1_dP_H  = interp2(FluidProp.H, FluidProp.P, FluidProp.dRho_dP_H_ph, Hc1, Pc);

% Two-Phase Zone (Condenser)
Tr2c        = interp1(FluidProp.Psat, FluidProp.Tsat, Pc);
H2f         = interp1(FluidProp.Psat, FluidProp.Hf, Pc);

rho2g       = interp1(FluidProp.Psat, FluidProp.Rhog, Pc);
rho2f       = interp1(FluidProp.Psat, FluidProp.Rhof, Pc);
drho2g_dP   = interp1(FluidProp.Psat, FluidProp.dRhog_dP, Pc);
drho2f_dP   = interp1(FluidProp.Psat, FluidProp.dRhof_dP, Pc);

rho_c2      = GammaC.*rho2g+(ones(np+1,1)-GammaC).*rho2f;
drho_c2_dP  = GammaC.*drho2g_dP+(ones(np+1,1)-GammaC).*drho2f_dP;
```

```
s2g         = interp1(FluidProp.Psat, FluidProp.sg, Pc);
s2f         = interp1(FluidProp.Psat, FluidProp.sf, Pc);
ds2g_dP     = interp1(FluidProp.Psat, FluidProp.dsg_dP, Pc);
ds2f_dP     = interp1(FluidProp.Psat, FluidProp.dsf_dP, Pc);

xbar_c      = (rho2g./rho_c2).*GammaC;
s_c2        = xbar_c.*s2g+(ones(np+1,1)-xbar_c).*s2f;

ds2_dGamma_P = ((GammaC.*rho2g + (ones(np+1,1)-GammaC).*rho2f).*(rho2g.*s2g - rho2f.*s2f) - ...
    (GammaC.*rho2g.*s2g + rho2f.*s2f - GammaC.*rho2f.*s2f).*(rho2g - rho2f))./((GammaC.*rho2g + (ones(np+1,1)-
GammaC).*rho2f).^2);

ds2_dP_Gamma = (rho_c2.*((GammaC.*rho2g.*ds2g_dP + GammaC.*s2g.*drho2g_dP)+(rho2g.*ds2f_dP +
s2f.*drho_c2_dP)+...
    (GammaC.*rho2g.*ds2f_dP + GammaC.*s2f.*drho2g_dP)) - (GammaC.*rho2g.*s2g + rho_c2.*s2f -
GammaC.*rho2g.*s2f).*drho_c2_dP) ./ (rho_c2.^2);

Xc           = GammaC.*(rho2g./rho_c2);

% Subcooled Zone (Condenser)
Tr3c        = interp2(FluidProp.H, FluidProp.P, FluidProp.T_ph, Hc3, Pc);
s_c3        = interp2(FluidProp.H, FluidProp.P, FluidProp.S_ph, Hc3, Pc);
ds3_dH_P    = interp2(FluidProp.H, FluidProp.P, FluidProp.dS_dH_P_ph, Hc3, Pc);
ds3_dP_H    = interp2(FluidProp.H, FluidProp.P, FluidProp.dS_dP_H_ph, Hc3, Pc);
Hc_out      = 2.*Hc3 - H2f;
drho3_dH_P    = interp2(FluidProp.H, FluidProp.P, FluidProp.dRho_dH_P_ph, Hc3, Pc);


%%%%%%%%%%%%%%%%%%%%%%%%%%%%%%%%%%%%%%%%%%%%%%%%%%%%%%%%%%%%%%%%%%%%%%%%%%%%%%%

Ae_i    = 0.29166;          %m^2
Ac_i    = 0.275;            %m^2
UAe1    = (UA(1)*Ae_i).*zeta_e1;
UAe2    = (UA(2)*Ae_i).*zeta_e2;
UAc1    = (UA(4)*Ac_i).*zeta_c1;
UAc2    = (UA(3)*Ac_i).*zeta_c2;
UAc3    = (UA(5)*Ac_i).*zeta_c3;

Tw1e_k = Tw1e + ones(np+1,1)*273;
Tw2e_k = Tw2e + ones(np+1,1)*273;
Tw1c_k = Tw1c + ones(np+1,1)*273;
Tw2c_k = Tw2c + ones(np+1,1)*273;
Tw3c_k = Tw3c + ones(np+1,1)*273;

%%%%%%%%%%%%%%%%%%%%%%%%%%%%%%%%%%%%%%%%%%%%%%%%%%%%%%%%%%%%%%%%%%%%%%%%%%%%%%%
%%%%%%%%%%%%%%%%%%%%%%%%%%%%%%%%%%%%%%%%%%%%%%%%%%%%%%%%%%%%%%%%%%%%%%%%%%%%%%%

% Evaluating J_VCC (first for-loop calculates exergy based cost function and second for-loop calculates energy
based cost function; only evaluate one at a time)

% Initialize SUM
SUM     = 0;  % scalar
delta_t = Ts;
for i = 2:np+1

  % Condenser Entropy Terms

    mc_12   = mdot_k(i) - L_ref_c*Ac_ref_c*( ( rho_c1(i) - rho2g(i) )*( zeta_c1(i)-zeta_c1(i-1) )/delta_t +
zeta_c1(i)*drho1_dP_H(i)*( Pc(i)-Pc(i-1) )/delta_t ...
        + zeta_c1(i)*drho1_dH_P(i)*( Hc1(i)-Hc1(i-1) )/delta_t );

    mc_23   = mdot_v(i) + L_ref_c*Ac_ref_c*( rho2f(i) - rho_c3(i) )*( ( zeta_c1(i)-zeta_c1(i-1) )/delta_t + (
zeta_c2(i)-zeta_c2(i-1) )/delta_t ) ...
        + L_ref_c*Ac_ref_c*zeta_c3(i)*drho3_dH_P(i)*( Hc3(i)-Hc3(i-1) )/delta_t;

    dmc1_dt = ( mdot_k(i) - mc_12 ) + L_ref_c*Ac_ref_c*rho2g(i)*( ( zeta_c1(i)-zeta_c1(i-1) )/delta_t );
    dmc2_dt = ( mc_12 - mc_23 ) + L_ref_c*Ac_ref_c*rho2f(i)*( ( zeta_c1(i)-zeta_c1(i-1) )/delta_t + (
zeta_c2(i)-zeta_c2(i-1) )/delta_t ) - ...
        L_ref_c*Ac_ref_c*rho2g(i)*( ( zeta_c1(i)-zeta_c1(i-1) )/delta_t );
    dmc3_dt = ( mc_23 - mdot_v(i) ) - L_ref_c*Ac_ref_c*rho2f(i)*( ( zeta_c1(i)-zeta_c1(i-1) )/delta_t + (
zeta_c2(i)-zeta_c2(i-1) )/delta_t );

    Term_2  = s_c1(i)*dmc1_dt  + L_ref_c*Ac_ref_c*rho_c1(i)*zeta_c1(i)*( ds1_dH_P(i)*( Hc1(i)-Hc1(i-1)
)/delta_t + ds1_dP_H(i)*( Pc(i)-Pc(i-1) )/delta_t );
    Term_3  = s_c2(i)*dmc2_dt  + L_ref_c*Ac_ref_c*rho_c2(i)*zeta_c2(i)*( ds2_dGamma_P(i)*( GammaC(i)-GammaC(i-
1) )/delta_t + ds2_dP_Gamma(i)*( Pc(i)-Pc(i-1) )/delta_t );
    Term_4  = s_c3(i)*dmc3_dt  + L_ref_c*Ac_ref_c*rho_c3(i)*zeta_c3(i)*( ds3_dH_P(i)*( Hc3(i)-Hc3(i-1)
)/delta_t + ds3_dP_H(i)*( Pc(i)-Pc(i-1) )/delta_t );

  % Evaporator Entropy Terms
```

```
    me_12  = mdot_k(i) + L_ref_e*Ac_ref_e*( rho1g(i) - rho_e2(i) )*( zeta_e1(i)-zeta_e1(i-1) )/delta_t + ...
        L_ref_e*Ac_ref_e*zeta_e2(i)*( drho2_dP_H(i)*( Pe(i)-Pe(i-1) )/delta_t + drho2_dH_P(i)*( He2(i)-He2(i-1)
)/delta_t );

    dme1_dt = ( mdot_v(i) - me_12 ) + L_ref_e*Ac_ref_e*rho_e1(i)*( zeta_e1(i)-zeta_e1(i-1) )/delta_t;
    dme2_dt = ( me_12 - mdot_k(i) ) - L_ref_e*Ac_ref_e*rho1g(i)*( zeta_e1(i)-zeta_e1(i-1) )/delta_t;

    Term_5   = s_e1(i)*dme1_dt + L_ref_e*Ac_ref_e*rho_e1(i)*zeta_e1(i)*( ds1_dGamma_P(i)*( GammaE(i)-GammaE(i-
1) )/delta_t + ds1_dP_Gamma(i)*( Pe(i)-Pe(i-1) )/delta_t );
    Term_6   = s_e2(i)*dme2_dt + L_ref_e*Ac_ref_e*rho_e2(i)*zeta_e2(i)*( ds2_dH_P(i)*( He2(i)-He2(i-1)
)/delta_t + ds2_dP_H(i)*( Pe(i)-Pe(i-1) )/delta_t );

    Term_1    =  ((-Tcai_K(i-1)/Tw1e_k(i))*( UAe1(i)*(Tw1e(i) - Tr1e(i)) ) + (-Tcai_K(i-1)/Tw2e_k(i))*(
UAe2(i)*(Tw2e(i) - Tr2e(i)) ));
    Term_2a   =  ((-Tcai_K(i-1)/Tw1c_k(i))*( UAc1(i)*(Tw1c(i) - Tr1c(i)) ) + (-Tcai_K(i-1)/Tw2c_k(i))*(
UAc2(i)*(Tw2c(i) - Tr2c(i)) ) + (-Tcai_K(i-1)/Tw3c_k(i))*( UAc3(i)*(Tw3c(i) - Tr3c(i)) ));

SUM    = SUM + (Term_1 + Term_2a + Tcai_K(i-1)*Term_2 + Tcai_K(i-1)*Term_3 + Tcai_K(i-1)*Term_4 + Tcai_K(i-
1)*Term_5 + Tcai_K(i-1)*Term_6)*delta_t;

end


%  Initialize Cost 2
SUM     = 0;  % scalar
delta_t = Ts;
Wdot    = zeros(np,1);
k = 1;
for i = 2:np+1
    Wdot(k) = mdot_k(i)*(Hc_in(i) - He_out(i));
    SUM = SUM + Wdot(k)*delta_t;
    k = k + 1;
end

% Calculate J_VCC

J_VCC = SUM;

C_ach      = zeros(np,1);
C_ach      = UAe1(2:np+1).*(Tw1e(2:np+1) - Tr1e(2:np+1)) + UAe2(2:np+1).*(Tw2e(2:np+1) - Tr2e(2:np+1));
J_Capacity = norm(C_des - C_ach);

%%%%%%%%%%%%%%%%%%%%%%%%%%%%%%%%%%%%%%%%%%%%%%%%%%%%%%%%%%%%%%%%%%%%%%%%%%%%%%
%%%%%%%%%%%%%%%%%%%%%%%%%%%%%%%%%%%%%%%%%%%%%%%%%%%%%%%%%%%%%%%%%%%%%%%%%%%%%%

% Complete Objective Function

lambda = 1e-2;
J = lambda*J_VCC + J_Capacity;

~~~~~~~~~~~~~~~~~~~~~~~~~~~~~~~~~~~~~~~~~~~~~~~~~~~~~~~~~~~~~~~~~~~~~~~~~~~~~~~~~~~~~~~~~~~~~~~~~~~~~~~~~~~~~~~

function [c,ceq] =
Dynamic_Nonlcon_Exergy_R134a_offline(U,T,S1,S2,X0_delta,U0_delta,D_delta,Xnom_Lifted,Unom_Lifted,C_bar,C2_bar,C
_des,T_L,T_H,Ts,nu,np,n,u,nd,I_L,UA,D_matrix,E_matrix)

load FluidProp_R134a_Thermosys

% Assign values to physical parameters of HX's

L_ref_e     = 11.45;
Ac_ref_e    = 5.165e-5;
L_ref_c     = 10.6895;
Ac_ref_c    = 5.156e-5;

% Convert T_H and T_L to Kelvin

Tcai_K = T_H + ones(np,1)*273;
Teai_K = T_L + ones(np,1)*273;

% Initial State Vector - X0_delta (dimension: 15 x 1) - delta away from nominal

% Initial Input Vector - U0_delta (dimension: 4 x 1) - delta away from nominal

% Define X_bar0

X_bar0_delta = [X0_delta;U0_delta];

X_bar_delta  = T*X_bar0_delta + S1*U + S2*D_delta; % delta away from nominal

X_delta      = C_bar*X_bar_delta;  % (separating X from X_bar)
```

```
Xu_delta     = C2_bar*X_bar_delta; % (separating Xu from X_bar)

X            = X_delta + Xnom_Lifted; % column vector of states
X_0          = X0_delta + Xnom_Lifted(1:n); % column vector

% Separate lifted state vector X_bar into individual state sequences:

zeta_e1 = zeros(np+1,1);
Pe      = zeros(np+1,1);
He2     = zeros(np+1,1);
Tw1e    = zeros(np+1,1);
Tw2e    = zeros(np+1,1);
GammaE  = zeros(np+1,1);
zeta_c1 = zeros(np+1,1);
zeta_c2 = zeros(np+1,1);
Pc      = zeros(np+1,1);
Hc1     = zeros(np+1,1);
Hc3     = zeros(np+1,1);
Tw1c    = zeros(np+1,1);
Tw2c    = zeros(np+1,1);
Tw3c    = zeros(np+1,1);
GammaC  = zeros(np+1,1);

i = 1;
zeta_e1(i) = X_0(1);
Pe(i)      = X_0(2);
He2(i)     = X_0(3);
Tw1e(i)    = X_0(4);
Tw2e(i)    = X_0(5);
GammaE(i)  = X_0(6);
zeta_c1(i) = X_0(7);
zeta_c2(i) = X_0(8);
Pc(i)      = X_0(9);
Hc1(i)     = X_0(10);
Hc3(i)     = X_0(11);
Tw1c(i)    = X_0(12);
Tw2c(i)    = X_0(13);
Tw3c(i)    = X_0(14);
GammaC(i)  = X_0(15);
clear i

zeta_e1(2:end) = X(1:n:end);
Pe(2:end)      = X(2:n:end);
He2(2:end)     = X(3:n:end);
Tw1e(2:end)    = X(4:n:end);
Tw2e(2:end)    = X(5:n:end);
GammaE(2:end)  = X(6:n:end);
zeta_c1(2:end) = X(7:n:end);
zeta_c2(2:end) = X(8:n:end);
Pc(2:end)      = X(9:n:end);
Hc1(2:end)     = X(10:n:end);
Hc3(2:end)     = X(11:n:end);
Tw1c(2:end)    = X(12:n:end);
Tw2c(2:end)    = X(13:n:end);
Tw3c(2:end)    = X(14:n:end);
GammaC(2:end)  = X(15:n:end);

zeta_e2 = ones(np+1,1) - zeta_e1;
zeta_c3 = ones(np+1,1) - zeta_c1 - zeta_c2;

U0_Lifted = zeros(np*u,1);

U_MPC = U0_Lifted + I_L*U + Unom_Lifted;

a_v     = zeros(np,1);
omega_k = zeros(np,1);
me_air  = zeros(np,1);
mc_air  = zeros(np,1);

a_v     = U_MPC(1:u:end);
omega_k = U_MPC(2:u:end);
me_air  = U_MPC(3:u:end);
mc_air  = U_MPC(4:u:end);

U_MPC2 = U0_Lifted + I_L*U + Unom_Lifted;

omega_k2 = U_MPC2(2:u:end);

%%%%%%%%%%%%%%%%%%%%%%%%%%%%%%%%%%%%%%%%%%%%%%%%%%%%%%%%%%%%%%%%%%%%%%%%%%%%%%%
%%%%%%%%%%%%%%%%%%%%%%%%%%%%%%%%%%%%%%%%%%%%%%%%%%%%%%%%%%%%%%%%%%%%%%%%%%%%%%%
```

```
% Determing necessary refrigerant properties via interpolation

% Evaporator

% Two-Phase Zone (Evaporator)
Tr1e        = interp1(FluidProp.Psat, FluidProp.Tsat, Pe);
H1g         = interp1(FluidProp.Psat, FluidProp.Hg, Pe);

rho1g       = interp1(FluidProp.Psat, FluidProp.Rhog, Pe);
rho1f       = interp1(FluidProp.Psat, FluidProp.Rhof, Pe);
drho1g_dP   = interp1(FluidProp.Psat, FluidProp.dRhog_dP, Pe);
drho1f_dP   = interp1(FluidProp.Psat, FluidProp.dRhof_dP, Pe);

rho_e1      = GammaE.*rho1g+(ones(np+1,1)-GammaE).*rho1f;
drho_e1_dP  = GammaE.*drho1g_dP+(ones(np+1,1)-GammaE).*drho1f_dP;

s1g         = interp1(FluidProp.Psat, FluidProp.sg, Pe);
s1f         = interp1(FluidProp.Psat, FluidProp.sf, Pe);
ds1g_dP     = interp1(FluidProp.Psat, FluidProp.dsg_dP, Pe);
ds1f_dP     = interp1(FluidProp.Psat, FluidProp.dsf_dP, Pe);

xbar_e      = (rho1g./rho_e1).*GammaE;
s_e1        = xbar_e.*s1g+(ones(np+1,1)-xbar_e).*s1f;

ds1_dGamma_P = ((GammaE.*rho1g + (ones(np+1,1)-GammaE).*rho1f).*(rho1g.*s1g - rho1f.*s1f) - ...
    (GammaE.*rho1g.*s1g + rho1f.*s1f - GammaE.*rho1f.*s1f).*(rho1g - rho1f))./((GammaE.*rho1g + (ones(np+1,1)-
GammaE).*rho1f).^2);

ds1_dP_Gamma = (rho_e1.*((GammaE.*rho1g.*ds1g_dP + GammaE.*s1g.*drho1g_dP)+(rho1g.*ds1f_dP +
s1f.*drho_e1_dP)+...
    (GammaE.*rho1g.*ds1f_dP + GammaE.*s1f.*drho1g_dP)) - (GammaE.*rho1g.*s1g + rho_e1.*s1f -
GammaE.*rho1g.*s1f).*drho_e1_dP) ./ (rho_e1.^2);

% Superheated Zone (Evaporator)
Tr2e        = interp2(FluidProp.H, FluidProp.P, FluidProp.T_ph, He2, Pe);
rho_e2      = interp2(FluidProp.H, FluidProp.P, FluidProp.Rho_ph, He2, Pe);
s_e2        = interp2(FluidProp.H, FluidProp.P, FluidProp.S_ph, He2, Pe);
ds2_dH_P    = interp2(FluidProp.H, FluidProp.P, FluidProp.dS_dH_P_ph, He2, Pe);
ds2_dP_H    = interp2(FluidProp.H, FluidProp.P, FluidProp.dS_dP_H_ph, He2, Pe);
drho2_dH_P  = interp2(FluidProp.H, FluidProp.P, FluidProp.dRho_dH_P_ph, He2, Pc);
drho2_dP_H  = interp2(FluidProp.H, FluidProp.P, FluidProp.dRho_dP_H_ph, He2, Pc);

He_out      = 2.*He2 - H1g;

s_k_in      = interp2(FluidProp.H, FluidProp.P, FluidProp.S_ph, He_out, Pe);
Xe          = GammaE.*(rho1g./rho_e1);

%%%%%%%%%%%%%%%%%%%%%%%%%%%%%%%%%%%%%%%%%%%%%%%%%%%%%%%%%%%%%%%%%%%%%%%%%%%%%%%

% Calculate valve mass flow rate
Pdelta      = Pc(2:np+1)-Pe(2:np+1);
Cd          = (-9.5984e-6) + (2.0481e-6).*a_v + (5.4106e-9).*Pdelta + (-7.4909e-10).*a_v.*Pdelta + ...
                    (-3.7775e-8).*(a_v.^2);
rho_c3      = interp2(FluidProp.H, FluidProp.P, FluidProp.Rho_ph, Hc3, Pc);
mdot_v        = zeros(np+1,1);
mdot_v(2:np+1) = Cd.*sqrt(rho_c3(2:np+1).*Pdelta);

% Calculate compressor mass flow rate
rho_k_in    = interp2(FluidProp.H_mg_ph,FluidProp.P_mg_ph,FluidProp.Rho_ph,He_out,Pe);
rps         = omega_k./60;
P_ratio     = Pc(2:np+1)./Pe(2:np+1);
eta_v       = 0.65127 + 0.00027681.*omega_k - 0.031338.*P_ratio + 3.0221e-5.*omega_k.*P_ratio...
    - 1.1905e-7.*(omega_k.^2) - 0.0081256.*(P_ratio.^2);
volume      = 3.042e-5;

mdot_k       = zeros(np+1,1);
mdot_k(2:np+1)= rps.*volume.*rho_k_in(2:np+1).*eta_v;

Hk_out_s     = interp2(FluidProp.S, FluidProp.P, FluidProp.H_ps, s_k_in, Pc);

eta_is       = ( (0.054812149750754) + (0.220895407941643).*P_ratio + (0.000034670672050).*omega_k2.*P_ratio +
...
               (-0.000000036818854).*omega_k2.^2 + (-0.041677058377446).*P_ratio.^2 );
Hk_out(2:np+1)= (Hk_out_s(2:np+1) - He_out(2:np+1))./eta_is + He_out(2:np+1);
Hc_in(2:np+1) = Hk_out(2:np+1);
H2g          = interp1(FluidProp.Psat, FluidProp.Hg, Pc);
Hc1(2:np+1)   = 0.5*(H2g(2:np+1) + Hc_in(2:np+1)');

s_k_out(2:np+1) = interp2(FluidProp.H, FluidProp.P, FluidProp.S_ph, Hc_in(2:np+1)', Pc(2:np+1));

%%%%%%%%%%%%%%%%%%%%%%%%%%%%%%%%%%%%%%%%%%%%%%%%%%%%%%%%%%%%%%%%%%%%%%%%%%%%%%%
```

```
% Determing necessary refrigerant properties via interpolation

% Condenser

% Superheated Zone (Condenser)
Tr1c        = interp2(FluidProp.H, FluidProp.P, FluidProp.T_ph, Hc1, Pc);
rho_c1      = interp2(FluidProp.H, FluidProp.P, FluidProp.Rho_ph, Hc1, Pc);
s_c1        = interp2(FluidProp.H, FluidProp.P, FluidProp.S_ph, Hc1, Pc);
ds1_dH_P    = interp2(FluidProp.H, FluidProp.P, FluidProp.dS_dH_P_ph, Hc1, Pc);
ds1_dP_H    = interp2(FluidProp.H, FluidProp.P, FluidProp.dS_dP_H_ph, Hc1, Pc);
drho1_dH_P    = interp2(FluidProp.H, FluidProp.P, FluidProp.dRho_dH_P_ph, Hc1, Pc);
drho1_dP_H    = interp2(FluidProp.H, FluidProp.P, FluidProp.dRho_dP_H_ph, Hc1, Pc);

% Two-Phase Zone (Condenser)
Tr2c        = interp1(FluidProp.Psat, FluidProp.Tsat, Pc);
H2f         = interp1(FluidProp.Psat, FluidProp.Hf, Pc);

rho2g       = interp1(FluidProp.Psat, FluidProp.Rhog, Pc);
rho2f       = interp1(FluidProp.Psat, FluidProp.Rhof, Pc);
drho2g_dP   = interp1(FluidProp.Psat, FluidProp.dRhog_dP, Pc);
drho2f_dP   = interp1(FluidProp.Psat, FluidProp.dRhof_dP, Pc);

rho_c2      = GammaC.*rho2g+(ones(np+1,1)-GammaC).*rho2f;
drho_c2_dP  = GammaC.*drho2g_dP+(ones(np+1,1)-GammaC).*drho2f_dP;

s2g         = interp1(FluidProp.Psat, FluidProp.sg, Pc);
s2f         = interp1(FluidProp.Psat, FluidProp.sf, Pc);
ds2g_dP     = interp1(FluidProp.Psat, FluidProp.dsg_dP, Pc);
ds2f_dP     = interp1(FluidProp.Psat, FluidProp.dsf_dP, Pc);

xbar_c      = (rho2g./rho_c2).*GammaC;
s_c2        = xbar_c.*s2g+(ones(np+1,1)-xbar_c).*s2f;

ds2_dGamma_P = ((GammaC.*rho2g + (ones(np+1,1)-GammaC).*rho2f).*(rho2g.*s2g - rho2f.*s2f) - ...
    (GammaC.*rho2g.*s2g + rho2f.*s2f - GammaC.*rho2f.*s2f).*(rho2g - rho2f))./((GammaC.*rho2g + (ones(np+1,1)-
GammaC).*rho2f).^2);

ds2_dP_Gamma = (rho_c2.*((GammaC.*rho2g.*ds2g_dP + GammaC.*s2g.*drho2g_dP)+(rho2g.*ds2f_dP +
s2f.*drho_c2_dP)+...
    (GammaC.*rho2g.*ds2f_dP + GammaC.*s2f.*drho2g_dP)) - (GammaC.*rho2g.*s2g + rho_c2.*s2f -
GammaC.*rho2g.*s2f).*drho_c2_dP) ./ (rho_c2.^2);

Xc           = GammaC.*(rho2g./rho_c2);

% Subcooled Zone (Condenser)
Tr3c        = interp2(FluidProp.H, FluidProp.P, FluidProp.T_ph, Hc3, Pc);
s_c3        = interp2(FluidProp.H, FluidProp.P, FluidProp.S_ph, Hc3, Pc);
ds3_dH_P    = interp2(FluidProp.H, FluidProp.P, FluidProp.dS_dH_P_ph, Hc3, Pc);
ds3_dP_H    = interp2(FluidProp.H, FluidProp.P, FluidProp.dS_dP_H_ph, Hc3, Pc);
Hc_out      = 2.*Hc3 - H2f;
drho3_dH_P    = interp2(FluidProp.H, FluidProp.P, FluidProp.dRho_dH_P_ph, Hc3, Pc);

Ae_i    = 0.29166;          %m^2
Ac_i    = 0.275;            %m^2

UAe1    = (UA(1)*Ae_i).*zeta_e1;
UAe2    = (UA(2)*Ae_i).*zeta_e2;
UAc1    = (UA(4)*Ac_i).*zeta_c1;
UAc2    = (UA(3)*Ac_i).*zeta_c2;
UAc3    = (UA(5)*Ac_i).*zeta_c3;

Tw1e_k = Tw1e + ones(np+1,1)*273;
Tw2e_k = Tw2e + ones(np+1,1)*273;
Tw1c_k = Tw1c + ones(np+1,1)*273;
Tw2c_k = Tw2c + ones(np+1,1)*273;
Tw3c_k = Tw3c + ones(np+1,1)*273;

%%%%%%%%%%%%%%%%%%%%%%%%%%%%%%%%%%%%%%%%%%%%%%%%%%%%%%%%%%%%%%%%%%%%%%%%%%%%%%%
%%%%%%%%%%%%%%%%%%%%%%%%%%%%%%%%%%%%%%%%%%%%%%%%%%%%%%%%%%%%%%%%%%%%%%%%%%%%%%%

% Evaluating J_VCC

% Initialize SUM
Xdot_dest   = zeros(np,1);
dSedt       = zeros(np,1);
dScdt       = zeros(np,1);
delta_t = Ts;
k = 1;
for i = 2:np+1
```

```
  % Condenser Entropy Terms

    mc_12   = mdot_k(i) - L_ref_c*Ac_ref_c*( ( rho_c1(i) - rho2g(i) )*( zeta_c1(i)-zeta_c1(i-1) )/delta_t +
zeta_c1(i)*drho1_dP_H(i)*( Pc(i)-Pc(i-1) )/delta_t ...
        + zeta_c1(i)*drho1_dH_P(i)*( Hc1(i)-Hc1(i-1) )/delta_t );

    mc_23   = mdot_v(i) + L_ref_c*Ac_ref_c*( rho2f(i) - rho_c3(i) )*( ( zeta_c1(i)-zeta_c1(i-1) )/delta_t + (
zeta_c2(i)-zeta_c2(i-1) )/delta_t ) ...
        + L_ref_c*Ac_ref_c*zeta_c3(i)*drho3_dH_P(i)*( Hc3(i)-Hc3(i-1) )/delta_t;

    dmc1_dt = ( mdot_k(i) - mc_12 ) + L_ref_c*Ac_ref_c*rho2g(i)*( ( zeta_c1(i)-zeta_c1(i-1) )/delta_t );
    dmc2_dt = ( mc_12 - mc_23 ) + L_ref_c*Ac_ref_c*rho2f(i)*( ( zeta_c1(i)-zeta_c1(i-1) )/delta_t + (
zeta_c2(i)-zeta_c2(i-1) )/delta_t ) - ...
        L_ref_c*Ac_ref_c*rho2g(i)*( ( zeta_c1(i)-zeta_c1(i-1) )/delta_t );
    dmc3_dt = ( mc_23 - mdot_v(i) ) - L_ref_c*Ac_ref_c*rho2f(i)*( ( zeta_c1(i)-zeta_c1(i-1) )/delta_t + (
zeta_c2(i)-zeta_c2(i-1) )/delta_t );

    Term_2  = s_c1(i)*dmc1_dt  + L_ref_c*Ac_ref_c*rho_c1(i)*zeta_c1(i)*( ds1_dH_P(i)*( Hc1(i)-Hc1(i-1)
)/delta_t + ds1_dP_H(i)*( Pc(i)-Pc(i-1) )/delta_t );
    Term_3  = s_c2(i)*dmc2_dt  + L_ref_c*Ac_ref_c*rho_c2(i)*zeta_c2(i)*( ds2_dGamma_P(i)*( GammaC(i)-GammaC(i-
1) )/delta_t + ds2_dP_Gamma(i)*( Pc(i)-Pc(i-1) )/delta_t );
    Term_4  = s_c3(i)*dmc3_dt  + L_ref_c*Ac_ref_c*rho_c3(i)*zeta_c3(i)*( ds3_dH_P(i)*( Hc3(i)-Hc3(i-1)
)/delta_t + ds3_dP_H(i)*( Pc(i)-Pc(i-1) )/delta_t );

  % Evaporator Entropy Terms

    me_12  = mdot_k(i) + L_ref_e*Ac_ref_e*( rho1g(i) - rho_e2(i) )*( zeta_e1(i)-zeta_e1(i-1) )/delta_t + ...
        L_ref_e*Ac_ref_e*zeta_e2(i)*( drho2_dP_H(i)*( Pe(i)-Pe(i-1) )/delta_t + drho2_dH_P(i)*( He2(i)-He2(i-1)
)/delta_t );

    dme1_dt = ( mdot_v(i) - me_12 ) + L_ref_e*Ac_ref_e*rho_e1(i)*( zeta_e1(i)-zeta_e1(i-1) )/delta_t;
    dme2_dt = ( me_12 - mdot_k(i) ) - L_ref_e*Ac_ref_e*rho1g(i)*( zeta_e1(i)-zeta_e1(i-1) )/delta_t;

    Term_5   = s_e1(i)*dme1_dt + L_ref_e*Ac_ref_e*rho_e1(i)*zeta_e1(i)*( ds1_dGamma_P(i)*( GammaE(i)-GammaE(i-
1) )/delta_t + ds1_dP_Gamma(i)*( Pe(i)-Pe(i-1) )/delta_t );
    Term_6   = s_e2(i)*dme2_dt + L_ref_e*Ac_ref_e*rho_e2(i)*zeta_e2(i)*( ds2_dH_P(i)*( He2(i)-He2(i-1)
)/delta_t + ds2_dP_H(i)*( Pe(i)-Pe(i-1) )/delta_t );

    dScdt(k) = Term_2 + Term_3 + Term_4;
    dSedt(k) = Term_5 + Term_6;

    Term_1    =  ((-Tcai_K(i-1)/Tw1e_k(i))*( UAe1(i)*(Tw1e(i) - Tr1e(i)) ) + (-Tcai_K(i-1)/Tw2e_k(i))*(
UAe2(i)*(Tw2e(i) - Tr2e(i)) ));
    Term_2a   =  ((-Tcai_K(i-1)/Tw1c_k(i))*( UAc1(i)*(Tw1c(i) - Tr1c(i)) ) + (-Tcai_K(i-1)/Tw2c_k(i))*(
UAc2(i)*(Tw2c(i) - Tr2c(i)) ) + (-Tcai_K(i-1)/Tw3c_k(i))*( UAc3(i)*(Tw3c(i) - Tr3c(i)) ));

    Xdot_dest(k) = (Term_1 + Term_2a + Tcai_K(i-1)*Term_2 + Tcai_K(i-1)*Term_3 + Tcai_K(i-1)*Term_4 + Tcai_K(i-
1)*Term_5 + Tcai_K(i-1)*Term_6);

    k = k + 1;

end

Wdot_k = mdot_k(2:np+1).*( Hc_in(2:np+1)' - He_out(2:np+1) );

sv_ri = interp2(FluidProp.H, FluidProp.P, FluidProp.S_ph, Hc3(2:np+1), Pc(2:np+1));
sv_ro = interp2(FluidProp.H, FluidProp.P, FluidProp.S_ph, Hc3(2:np+1), Pe(2:np+1));

sk_ri = s_k_in(2:np+1);
sk_ro = s_k_out(2:np+1)';

se_ri = sv_ro;
se_ro = sk_ri;
sc_ri = sk_ro;
sc_ro = sv_ri;

% % Evaporator
Xdest_e = ((-Tcai_K./Tw1e_k(2:np+1)).*( UAe1(2:np+1).*(Tw1e(2:np+1) - Tr1e(2:np+1)) ) + (-
Tcai_K./Tw2e_k(2:np+1)).*( UAe2(2:np+1).*(Tw2e(2:np+1) - Tr2e(2:np+1)) )) - ...
Tcai_K.*( mdot_v(2:np+1).*se_ri - mdot_k(2:np+1).*se_ro ) + Tcai_K.*(dSedt);

% Condenser
Xdest_c = ((-Tcai_K./Tw1c_k(2:np+1)).*( UAc1(2:np+1).*(Tw1c(2:np+1) - Tr1c(2:np+1)) ) + (-
Tcai_K./Tw2c_k(2:np+1)).*( UAc2(2:np+1).*(Tw2c(2:np+1) - Tr2c(2:np+1)) ) + ...
(-Tcai_K./Tw3c_k(2:np+1)).*( UAc3(2:np+1).*(Tw3c(2:np+1) - Tr3c(2:np+1)) )) - ...
Tcai_K.*( mdot_k(2:np+1).*sc_ri - mdot_v(2:np+1).*sc_ro ) + Tcai_K.*(dScdt);


% Define nonlinear inequality constraints

c = zeros(3*np,1);
```

```
c(1:np)          = Xdot_dest - Wdot_k;
c(np+1:2*np)     = -Xdest_e;
c(2*np+1:3*np)   = -Xdest_c;

ceq = [];
```